THE UNIVERSITY OF ADELAIDE AUSTRALIA

Investigation of Single and Multiple Faults Under Varying Load Conditions Using Multiple Sensor Types to Improve Condition Monitoring of Induction Machines

PhD Thesis

Intesar Ahmed

A Thesis Presented for the Degree of Doctor of Philosophy

September 2007

Abstract

Condition monitoring involves taking measurements on an induction motor while it is operating in order to detect faults. For this purpose normally a single sensor type, for example current is used to detect broken rotor bar using fault frequency components only under the full-load condition or a limited number of load cases. The correlations among the different types of sensors and their ability to diagnose single and multiple faults over a wide range of loads have not been the focused in previous research.

Furthermore, to detect different faults in machines using any fault frequency components, it is important to investigate the variability in its amplitude to other effects apart from fault severity and load. This area has also often been neglected in the literature on condition monitoring.

The stator current and axial flux have been widely used as suitable sensors for detecting different faults i.e. broken rotor bar and eccentricity faults in motors. Apart from detecting the broken rotor bar faults in generalized form, the use of instantaneous power signal has often been neglected in the literature condition monitoring.

This thesis aims to improve machine condition monitoring and includes accurate and reliable detection of single and multiple faults (faults in the presence of other faults) in induction machines over a wide range of loads of rated output by using current, flux and instantaneous power as the best diagnostic medium.

The research presents the following specific tasks:

A comprehensive real database from non–invasive sensor measurements, i.e. vibration measurements, axial flux, 3-phase voltage, 3-phase current and speed measurements of induction motor is obtained by using laboratory testing on a large set of identical motors with different single and multiple faults. Means for introducing these faults of varying severity have been developed for this study.

The collected data from the studied machines has been analysed using a custom-written analysis programme to detect the severity of different faults in the machines. This helps to improve the accuracy and reliability in detecting of single and multiple faults in motors using fault frequency components from current, axial flux and instantaneous power spectra.

This research emphasises the importance of instantaneous power as a medium of detecting different single and multiple faults in induction motor under varying load conditions. This enables the possibility of obtaining accurate and reliable diagnostic medium to detect different faults existing in machines, which is vital in providing a new direction for future studies into condition monitoring.

Another feature of this report is to check the variability in healthy motors due to: test repeatability, difference between nominally identical motors, and differences between the phases of the same motor. This has been achieved by conducting extensive series of laboratory tests to examine fault frequency amplitudes versus fault severity, load, and other factors such as test repeatability and machine phases.

The information about the variations in the amplitudes of the fault frequency components is used to check the accuracy and reliability of the experimental set-up, which is necessary for the practical application of the results to reliably detect the different faults in the machines reliably.

Finally, this study also considers the detection of eccentricity faults using fault frequency amplitudes as a function of average eccentricity, instead of as a function of load under different levels of loading. This has not been reported in previous studies.

Declaration

This work contains no material which has been accepted for the award of any other degree or diploma in any university or other tertiary institution and, to the best of my knowledge and belief, contains no material previously published or written by another person, except where due reference has been made in the text.

I give consent to this copy of my thesis, when deposited in University Library, being made available for photocopy and loan subject to the provisions of the Copyright Act 1968

Signed:_____ Date:_____

Acknowledgment

The research work and the experimental work related to this project were carried out at the Power Engineering Laboratory at the School of Electrical and Electronics Engineering, University of Adelaide, Adelaide, South Australia.

Associate Professor Nesimi Ertugrul has acted as a supervisor and I gratefully acknowledge his valuable advice, guidance, and encouragement during the study and also for his positive attitude to my work. I also highly acknowledged the valuable advice from Dr. W. L. Soong during my study.

I am thankful to all technical staff of Power Engineering Laboratory for providing the experimental needs and technical assistance throughout the study. My thanks are also due to all academic and administration staff members for creating a best environment for study.

Special thanks to my wife " Farhat Sultana" for her positive attitude and taking care of children's during study. I deeply appreciate my father Dr. Zaki Ahmad for his encouragement, economical support and looking after my family.

Intesar Ahmed

Contents

List of Figures

List of Tables

Symbols and Abbreviations

$\mathbf{f_1}$	fundamental frequency
$\mathbf{f_2}$	slip frequency
$\mathbf{f_r}$	rotor frequency
$\mathbf{N_s}$	synchronous speed
$\mathbf{N_r}$	rotor speed
T	total sampling time
$\Delta\mathbf{t}$	sampling time
$\Delta\mathbf{f}$	sampling frequency
$\mathbf{L_R}$	total points of record length
s	slip of motor
V	voltage
I	current
p	number of pair of poles
$\mathbf{P_i}$	total active power in three-phase system
PF	power factor
$\boldsymbol{P_{ins}}$	instantaneous power
k	number of integers
$\mathbf{f_{BRB}}$	broker rotor bar frequencies
$\mathbf{f_p}$	supply frequency from power signal
Ir	rated current of motor
Vr	rated voltage of motor
fecc	eccentricity fault frequency
R	number of rotor bars
CM	condition monitoring
BRB	broken rotor bar
FT	Fourier transform
STFT	short time Fourier transform
DE	driving end
NDE	non-driving end
DEH	driving end horizontal
DEV	driving end vertical

Chapter 1

Introduction

1.1 Background

Induction motors are commonly used in industry throughout the world. They account for 95% of all prime movers in industrialized nations, and consume 40 to 50% of all generated electric energy [1]. They are used in applications such as the mining industry, chemical processing plants, nuclear power plants, petroleum industry, paper mills and cooling water systems. Other general applications of induction motors are: air-conditioners, fans, pumps, compressors, crushers, machine tools, lifts, robotics and tractions etc.

Induction motors are inherently reliable and need minimum maintenance. However, like other motors, induction motors eventually deteriorate and fail [2]. Failure of the motors can cause unexpected downtime and loss of production, which is not acceptable in critical industrial applications.

Therefore, the detection of incipient failures and the scheduled replacement of the damaged components prior to failure would eliminate the consequences of unexpected equipment failures [3]. The capability to do this has long been desired by industry to prevent unscheduled downtimes for electrical drive systems and to reduce maintenance costs.

It is generally known that 50% of operating costs in most processing and manufacturing operations are related to maintenance. Therefore, this is one of the major concerns of

industries, and researchers are always in search of new methods, which reduce the maintenance costs and/or decrease the chances of unexpected failures that can result in lost production.

The following three common methods of maintenance are used in industry

1) **Planned Replacement:** Replace machines regularly, simple but most expensive, especially in the case of medium and high power machines.

2) **Planned Maintenance:** Regular overhaul and check machines. This system is commonly used and it is cheaper when compared to the replacement method.

3) **Condition Based Maintenance:** Uses sensor measurements to determine the machine's condition. This can be used to either increase the intervals between maintenance, or to allow continuous monitoring of machines and thus scheduling maintenance only when needed.

Condition monitoring techniques can be classified into two major groups: off-line and on-line tests.

Off-Line Tests: These tests are comprehensive but require shutting down the motor and disconnecting it from the AC main supply.

On-Line Tests: On-line condition monitoring and fault diagnostics of induction motors uses sensors mounted on the machine to detect faults, while the machine is operating. This method produce less disruption, but the results can be more difficult to interpret than off-line tests. This study only considers on-line testing of the motors while they are operating, which is also referred to as on-line condition monitoring.

For the last two decade, a significant amount of research work in the field of condition monitoring and diagnostic techniques for induction motors has been done. A number of methods and techniques have been introduced and successfully used to detect different faults related to machines [4,5,6]. However, the reliability and accuracy of on-line condition monitoring techniques heavily depends upon a good understanding of the electrical and mechanical characteristics of the machines in the healthy state and under faulty state.

For the last few years the use of new analysis techniques with the help of advanced computerized data acquisition and processing systems has provided new directions in the

field of condition monitoring of induction motors [2]. The applications of condition monitoring into induction motors and development of new condition monitoring (CM) techniques have become one of the leading research topics for electrical and energy industries.

Condition monitoring increases the lifetime of electrical machines and minimizes the risk of catastrophic failure. The rapid development in computer and transducer technologies together with signal processing techniques has made it possible to implement the condition monitoring systems more effectively [7,8]. This can make condition monitoring more reliable and can reduce the maintenance cost of induction motors. Furthermore, on-line condition monitoring can provide information about the state of the machine during the maintenance period. This can reduce the chances of catastrophic failure of machines.

As explained later in this study, the information from a baseline study of healthy as well as faulty motors will be used to investigate single and multiple faults using different sensor signals: current, flux, vibration and voltage.

Therefore, it was envisaged to start the thesis by providing basic knowledge about the construction and principles of induction motors. Then the concept of fault frequencies are explained, which is followed by the description of different sensors types and signal processing techniques. A brief overview of different stages of the condition monitoring process is also covered and a literature survey is provided.

1.2 Induction Motors

The development of electric motor has given the most efficient and effective benefits in modern day life. The electric motor is a simple device in principle, which converts electric energy into mechanical energy. Over the years, electric motors have changed substantially in design. However, the basic principles of such machines have remained the same, which works based on the interaction between magnetic flux and current carrying conductors [9].

1.2.1 Basic Construction

An induction motor has two basic electrical parts: a "stator" and a "rotor" as shown in Figure 1.1. The stator consists of a cylindrical laminated and slotted core with windings, placed in a frame of rolled or cast steel or aluminium. The frame provides mechanical protection and carries the terminal box and the end covers and bearings. The three phase stator winding consist of coils of insulated copper wire to produce 2, 4, 6 etc. magnetic poles. The rotor is the rotating electrical component and consists of a laminated and slotted core tightly pressed on the shaft and carrying a set of windings. The rotor is located inside the stator and is separated from it by a small airgap. There is no electrical connection between the stator and rotor windings.

NOTE: This figure is included on page 4 of the print copy of the thesis held in the University of Adelaide Library.

Figure 1.1: View of an induction motor showing its constituent parts [10].

There are two types of rotors used in induction motors namely:

Squirrel-Cage Motor: This type of induction motor is most commonly used. In large motors the rotor winding consists of copper bars, which are inserted into slots in the rotor laminations [11]. The ends of the copper bars are welded to copper end rings, so that all the bars are short circuited as shown in Figure 1.2 (left). In small motors, however the bars and end-rings are diecast in aluminium to form an integral block.

Wound-Rotor Motor: The wound rotor has a three-phase rotor winding, which is similar to the stator winding and is usually connected in a Wye configuration. The rotor winding terminals are connected to three slip rings, which rotate with the rotor as shown

in Figure 1.2 (right). The slip rings and brushes allow external resistors to be connected in series with the rotor winding. The external resistors are mainly used during start-up to improve the starting performance. Under normal running conditions the windings are short-circuited externally.

NOTE: This figure is included on page 5 in the print copy of the thesis held in the University of Adelaide Library.

Figure 1.2: Sketch of the bars and end-rings used in a squirrel-cage rotor (left) and a photograph of a wound rotor (right) [12].

1.2.2 Induction Motor Principles

In induction motor, the currents in the three-phase stator winding are equal in magnitude and 120° phase shifted in time. Each phase winding, produces a sinusoidal time varying magnetic field along the magnetic axis of the phase winding. The magnetic axes of the three phase windings are spatially separated by 120° as shown in Figure 1.3 [13].

NOTE: This figure is included on page 5 in the print copy of the thesis held in the University of Adelaide Library.

Figure 1.3: Cross-sectional view of an induction motor including, three phase supply currents and rotating magnetic field [13].

The combination of the spatial and temporal phase shifts between the magnetic fields produced by each phase produces a net magnetic field, which rotates at constant speed

and has constant amplitude. The speed of this rotating magnetic field is called the synchronous speed.

In an induction motor the rotor speed is lower than synchronous speed. Voltages are induced in the three-phase rotor winding whose magnitude and frequency are proportional to the difference between the rotor and synchronous speed. This induced rotor voltages produce rotor winding currents [9].

In induction motors, the interaction of the rotating magnetic rotating field and the induced rotor current generates torque. This torque is roughly proportional to the difference between the rotor speed and synchronous speed. The motor is designed to deliver rated output power (rated torque) at rated speed. At synchronous speed the output torque is zero as the induced voltages and hence induced currents are zero.

To a first approximation, the torque versus speed characteristic can be modeled as a straight line between synchronous speed and rated speed. Hence the output torque is proportional to the slip speed or slip.

Figure 1.4 shows an example of the torque-speed curve of a 3-phase induction motor. The starting torque is typically 1.5 times of the machine's rated torque and the maximum torque is typically 2.5 times the rated torque of the machine. Pull-In torque is the minimum torque developed by the motor while it is accelerating from rest to the maximum torque.

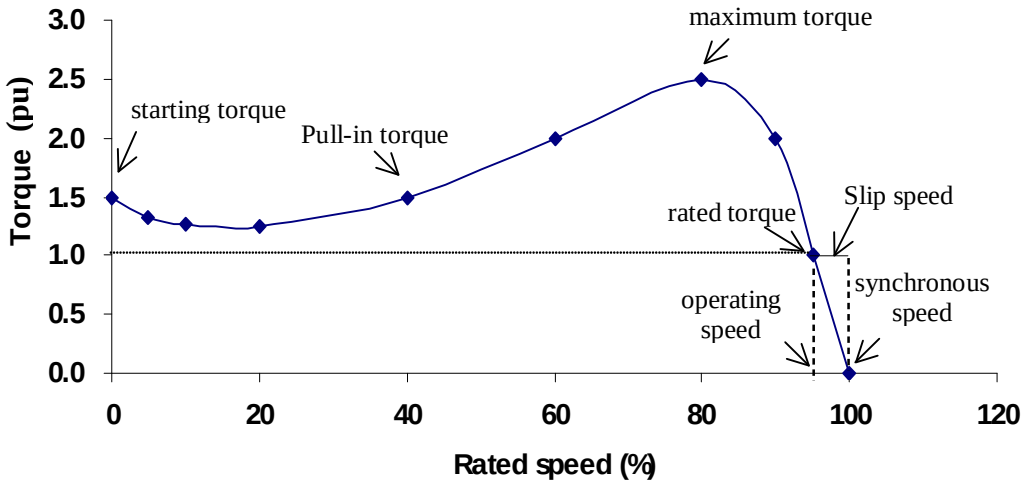

Figure 1.4: A typical torque-speed characteristic curve of a three-phase induction motor.

1.2.3 Key Terms and Formulas

It is important to review the some key terms and mathematical formulas related to the induction machines. Because all the mathematical relationship of characteristics fault frequency components, which is used to detect the different faults are extracted from the basic formulas of machines.

1) **Synchronous speed [N_s]**

Synchronous speed (N_s) is the absolute upper limit of motor speed and determined by the supply frequency (f_1) and the number of poles (p) in the stator [9]:

$$N_s = 120f_1/ p \quad \text{rpm} \tag{1.2.1}$$

2) **Slip Speed**

The difference between the speed of the rotating magnetic field commonly known as synchronous speed, N_s and the actual rotor speed, N_r is known as slip speed [9].

$$\text{Slip speed} = (N_s - N_r) \quad \text{rpm} \tag{1.2.2}$$

3) **Slip [s]**

The difference between the synchronous speed (Ns) and the rotor speed (N_r), expressed as a percentage of synchronous speed is called slip. As explained previously, slip is necessary to produce torque, and is dependent on load. Slip can be determined from the following formula [9].

$$s = (N_s - N_r) / N_s \tag{1.2.3}$$

4) **Slip Frequency [f_2]**

It is the frequency of the rotor e.m.f. and currents and is thus related to an electrical phenomenon and can be determined with the following formula [13].

$$f_2 = (N_s - N_r) / p \quad \text{Hz} \tag{1.2.4}$$

5) **Shaft Output Torque [T_m]**

Torque is the force that produces rotation. It causes an object to rotate. Torque consists of force acting on distance. The torque developed by the motor at any speed is given by

$$T_m = P_m/ \omega_r \quad \text{N.m} \tag{1.2.5}$$

where, P_m = actual mechanical power available to drive the load (watt);

N_r = rotor speed (rpm) and
$\omega_r = 2 \pi N_r /60$

1.3 Survey of Induction Motor Faults

As stated before, AC induction motors are ideal for most industrial and commercial applications because of their simple construction and low number of parts, which reduce maintenance cost. Induction motors are frequently used for both constant-speed and adjustable speed-drive (ASD) applications.

Induction machines are generally symmetrical. Faults in the machine normally affect its symmetry and can produce the following symptoms: unbalanced airgap voltages and line currents, increased torque pulsation, decreased shaft torque, increased losses and reduced efficiency and increased space harmonics [3].

Table 1.1: Summary of motor faults, causes and sensor signals used for fault detection

Motor Faults	Causes	Detection Methods
Bearing Faults (40-50%) Damaged races Damaged balls	Bearing currents Contamination Improper installation and lubrication End of life	Vibration Stator current spectrum
Stator Faults (30-40%) Insulation failure related Shorted turns faults	High resistivity connections Over-heating of stator core or winding Over-voltages Loose laminations Contamination of insulation Mechanical stresses	Axial flux Stator current Negative sequence currents
Rotor Bar/End-Ring (5-10%) Breakage of rotor bar End-ring	Thermal stresses Mechanical stresses Corrosion Dynamic torques Frequent starts	Stator current Axial flux Instantaneous power Vibration Torque and speed
Eccentricity (10-15%) Static eccentricity Dynamic eccentricity	Bent rotor Bearing wear Misalignment Dynamic torques	Stator current Vibration Axial flux

The most common faults in AC machines are shown in Table. 1.1, [14,15,16]. These faults are briefly discussed on the basis of their importance regarding condition monitoring of induction motors. In addition, some hidden faults [13] i.e. voltage imbalance, hot spot within the winding, hot spot within the core, soft-foot, misalignment are also discussed briefly in this section.

1.3.1 Bearing Faults

Bearings are the most critical mechanical elements in electric motors. Rolling element bearings consist of two rings (Figure 1.5), an inner and outer, between which a set of balls or rollers rotates in raceways. Under normal operating conditions of balanced load and good alignment, fatigue failure normally starts with small fissures or cracks, located on the inner and outer surfaces of the raceway and rolling elements, which gradually propagate to the surface generating detectable vibrations and increasing noise levels.

Figure 1.5: A photograph of a rolling element bearing.

It has been reported that up to 40-50 % of faults are bearing related. Bearing faults can also manifest them as rotor asymmetry and produce eccentricity related symptoms. Vibration testing is very popular because of the direct linkage with the problem, though it requires experience to accurately interpret the results [3].

1.3.2 Stator Faults

Figure 1.6 shows the star-connected stator windings of a three-phase induction motor and potential states stator faults. As indicated in Table 1.1 up to 40% of induction motor faults are related to the stator winding. Stator winding faults are normally caused by

insulation failure between two adjacent turns in a coil, which causes large currents to flow. The resulting large fault currents can produce overheating and cause imbalance in the magnetic field of the machine.

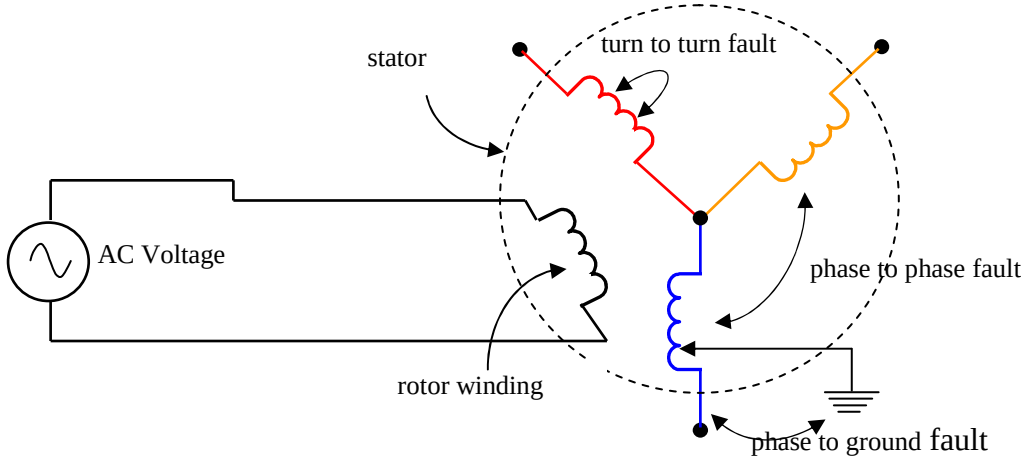

Figure 1.6: Stator winding faults: turn-to-turn, phase to phase and phase to ground.

Turn-to-Turn Faults: In these faults, part of the winding is shorted out. This generates very high fault currents in the shorted part of winding which produces high temperatures and imbalances in the three phase supply currents.

Phase-to-Phase / Phase-to-Ground Faults: These faults produce unbalanced airgap voltages, line currents and increased torque pulsations. The large fault currents will rapidly trip out the circuit breaker.

It was reported in reference [3] that stator faults generally start as undetected turn-to-turn faults, which grow and culminate into a major winding fault. Therefore, timely detection of stator faults at an early stage is very important in condition monitoring to avoid catastrophic failures in motors.

1.3.3 Broken Bars/End Ring Faults

Broken rotor bars or broken end-rings can be cause by frequent direct on-line starting (as the motor cage winding may not be designed to withstand high mechanical and electrical stresses), by pulsating mechanical loads and by imperfections in the manufacturing process of the rotor cage [17,18,19]. Broken rotor bars may not cause immediate failure of an induction machine. However, if pieces of the broken bars break loose and hit stator

end winding this can cause serious damages. Figure 1.7 shows the photograph of a test rotor in which rotor bars have been deliberately broken by cutting a slot in the end-rings.

Figure 1.7: Photograph of a rotor with broken bars

1.3.4 Eccentricity Faults

Airgap eccentricity means the airgap is not a uniform radial length between the rotor surface and the stator bore. Figure 1.8 left, shows the uniform airgap of a healthy motor. If the level of airgap eccentricity is not kept within specified limits then the resulting large radial forces can greatly increase bearing wear. These faults then increase losses and reduce efficiency and cause excessive heating in the machine.

There are two forms of airgap eccentricity in the machines as illustrated in Figure 1.8.

Static Eccentricity: With static eccentricity the angular position of the point of minimum radial airgap length is fixed in space and does not change with time as shown in Figure 1.8 (middle). It can be caused by oval stator cores or by the incorrect positioning of the stator or rotor and it is only space dependent. In rotating electrical machines there is always an inherent level of static eccentricity due to manufacturing tolerance caused by the compound assembly of parts that each have their own tolerances.

Dynamic Eccentricity: In dynamic eccentricity related faults the angular position of the point of minimum radial airgap changes with time. Dynamic eccentricity is both space

and time dependent as shown in Figure 1.8 (right). It can be caused by a non-concentric rotor outer diameter, thermal bowing of the rotor, or bearing wear and movement.

In real motor system, if the level of airgap eccentricity is not kept within the specified limits, then this can greatly increase bearing wear. This also increases the noise levels.

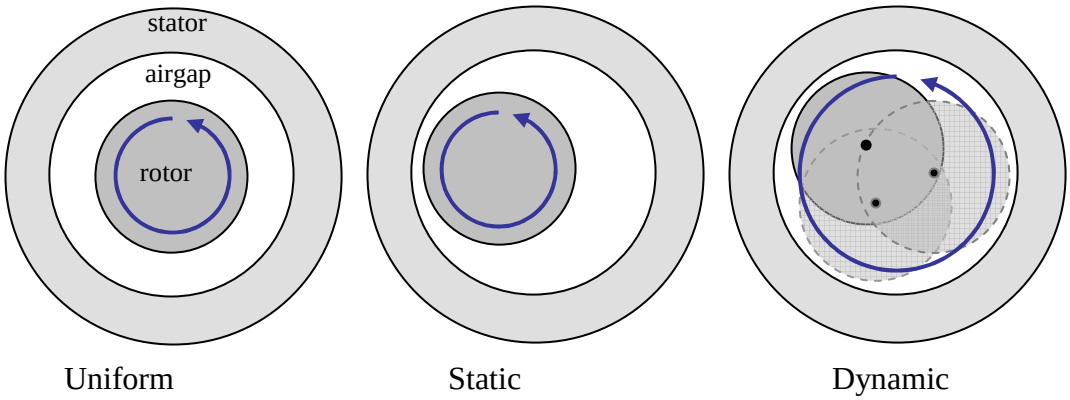

Figure 1.8: Visual illustration of eccentricity faults, from left to right: no eccentricity, static eccentricity and dynamic eccentricity.

1.3.5 Hidden Faults

The hidden faults do not cause an immediate loss of operation of induction motors. However, in long-term these faults reduce the life of motors by about 40% of expected life. Misalignment (angular, offset or combination) fault produces excessive vibration and this can cause an extra stress on the bearing and as a result reduces the life of bearing. Soft-foot fault means, the base on which the motor is mounted is not flat or mounting screws are bolted unevenly, which causes distraction in the airgap and produces current imbalance. Imbalance of the voltage produces the opposite sequence of magnetic field and this will increase the losses and reduce the efficiency of the induction motors [13]. These hidden faults not only affect the performance of the induction motors, but also fail to obtain an accurate and reliable results related to the major faults (broken rotor bars, eccentricity and shorted turns) using different diagnostic medium in condition monitoring.

However, in this study broken rotor bar, shorted turn, eccentricity and misalignment faults are taken into account under varying load conditions because these frequently occur in machines.

1.4 Sensor Types for Non-Invasive Measurements

Different non-invasive on-line sensor types can be used to detect the above mentioned motor faults. The locations of these sensor types are illustrated in Figure 1.9. Brief explanations and features of these non-invasive sensor types [2,3,20] are given below.

1) **Vibration Sensor**

Vibration measurement is the oldest form of condition monitoring and measurements are normally taken at each end of the machine, near the bearings, in the horizontal and vertical axis positions as shown in Figure 1.9. Faults such as mechanical imbalance, bearing faults, eccentricity and misalignment can be detected using vibration measurements [13].

2) **Stator Current Sensor**

The current sensors usually used for condition monitoring consist of electronic circuits that measure the magnetic field produced by the machine current. The measured current signals contain specific frequency components which can be used to detect different faults in the machine, i.e. broken rotor bars, unbalanced rotor, shorted turns in the stator windings and mechanical and magnetic asymmetries.

3) **Stator Voltage Sensor**

Since the stator voltage contains frequencies due to mechanical and magnetic asymmetries and varying load, it can used with the current to calculate instantaneous power, instantaneous torque and negative sequence components. The voltage sensors along with current sensors are used to calculate instantaneous power and negative sequence impedance in order to detect faults in induction machines.

4) **Axial Leakage Flux Sensor**

The leakage flux of an induction motor is a small part of the total flux of machine flowing along the rotor and closing itself through the effect of air. This leakage flux can be measured by using a circular coil that is placed on non-driving end of the motor, which is concentric with the shaft as shown in Figure 1.9. The output voltage produced by such an axial search coil is proportional to the rate of change of the axial leakage flux, and it contains many of similar fault frequencies to the stator current signal. The axial

leakage flux sensor is a good source to estimate the speed as it contains a strong component at the slip frequency.

NOTE: This figure is included on page 14 of the print copy of the thesis held in the University of Adelaide Library.

Figure 1.9: Typical sensors positions used in condition monitoring of machines [13].

1.5 Literature Review of Fault Detection Techniques

Condition monitoring (CM) of induction motors is important as the cost of plant downtime in many applications may far exceed the repair or maintenance cost of the machines concerned. The main target in condition monitoring is the diagnosis of a fault before it becomes catastrophic damage. The early detection of a fault allows for downtime and maintenance of machines to be planned.

Over the years, the researchers working on condition monitoring of induction motors have developed a number of different fault detection methods. The two classes of methods for detecting whether a fault exists or not based on fault features can be classified in two categories; model-based and knowledge-based methods. In addition, various signal-processing techniques for analysing the sensor signals to determine fault features of different faults of induction motors has also been considered.

Model-Based Condition Monitoring: In the model-based approach, the effect of certain faults on the amplitudes of characteristic fault frequencies can be predicted by using different modelling approaches. For example many authors such as in [21,22] looked at Finite-Element based methods to detect the broken rotor bars fault using the stator current. In the research done in [23,24] a Transient-Model technique using a single stator current signal to detect rotor and stator faults in induction motor is described. Another useful model-based technique is thermal monitoring, in which rotor resistance identification is used to detect rotor faults [25].

In addition, time stepping coupled Finite-Element State-Space model based method is reported to be useful for adjustable/variable drives [26,27]. The Parameter estimation method presented by reference [28] in which an algorithm is used to calculate the model parameters based on measurements of current and voltage. The changes in these parameters measurements indicate the severity of faults. This method provides useful results in case when more than few broken rotor bars are under full-load condition.

The use of the above mentioned model-based methods provide comprehensive fault detection information of dynamic systems. However, in modelled-based methods the reliability and accuracy of the results rely on the use of detailed electromagnetic machine design information, which is normally not available. In addition, it is also difficult to use the results from one motor obtained by using model-based methods to set the fault threshold level for other ratings of motor.

Knowledge-Based Condition monitoring: In the Knowledge-based methods, several knowledge-based techniques such as neural networks, fuzzy logic, expert systems, artificial intelligence systems etc. have been used to detect different faults in induction machines.

In references [29,30] the researchers have shown that the neural network technique can be used to identify faults in electrical motors even under overload and under-voltage conditions. Neural networks are modelled on the neural connections in the human brain [3]. However, an extensive set of training data needs to be available for accurate and reliable results when using neural network approaches.

Fuzzy logic was also found to be another useful technique used to determine the state of induction motors to detect faults. In this technique, decisions are based on classification

of signals into a series of bands instead of simply as healthy or faulty based on a single threshold [31,32].

Another technique known as expert systems described in [33,34] depends upon the knowledge of a human expert by defining a series of a rules from which conclusions can be drawn. As can be seen, it may not be possible to generalize these rules for other motors of different ratings.

Identification of different faults related to induction motors was also attempted by using Support Vector Classification (SVC) techniques on the stator current spectrum to separate healthy and faulty motor spectra based on the statistical theory presented in [35]. This method is not found to be useful to detect eccentricity related faults because the features in the stator current are not very sensitive to eccentricity faults.

It can be concluded from the research that the knowledge-based methods require deep knowledge of process structure, functions and qualitative models under various faulty and healthy conditions of machines.

Signal-Processing Techniques: In recent years huge amount of work has been done using signal-processing techniques to detect different faults of induction motors. There are many techniques that have worked successfully to analyse the sampled data to generate specific features or parameters, which are sensitive to the presence or absence of specific faults of induction motor.

Many authors [2,18,36] have studied the common machine parameters that are used for the detection of different failure modes in condition monitoring which include stator current, stator voltage, vibration, axial flux, speed and negative sequence impedance that are used for the detection of different faults, i.e. broken rotor bars, eccentricity, bearing and shorted turns, misalignment and soft-foot faults of induction motors.

A large amount of work has been done to detect the broken rotor bars (BRB) fault using single sensor (stator current) under full-load condition [1,37]. This is based on the theory, that the BRB causes a pulsation at twice the slip frequency in the stator current and is used as a mean of detecting BRB in an induction motors.

As explained by many authors [1,2,3] frequency analysis, using the Fourier transform (FT) is the most common signal-based techniques used for condition monitoring. Other signal-processing techniques such as Higher-Order Statistics, Park's Vector Approach,

Wavelet Analysis, Negative Sequence Current [36,38] and many others techniques has been reported in the literature to detect bearing, rotor and eccentricity faults using current, flux and vibration sensors. However, all these techniques have certain advantages and drawbacks as reported in [2,3].

For example, the Wavelet technique can be applied to non-stationary signals in which the disturbances are varying in only a short time is an appropriate technique for transient analysis. However, in this study the analysis is based on detecting the machine faults in the steady-state condition and hence the Wavelet technique is not a suitable candidate for this analysis.

Research has proven that the negative sequence current is able to detect shorted turns in the stator winding. Although, such method indicates imbalance, but the presence of this imbalance does not always imply system failure [36]. Many authors such as [39,40,41,42] proposed that the Park's Vector technique as a useful technique to detect the shorted turns and air-gap eccentricity faults.

Some other methods such as Partial discharge detection have been used for detecting stator insulation faults in high voltage motors [43]. However, partial discharge also occurs in healthy motors. Furthermore, temperature monitoring provides a useful indication of machine overheating, which can be used to monitor the bearings and stator windings. This however, provides less helpful information to detect faults in early stages. The airgap, torque and magnetic field monitoring has also been reported by various researchers regarding the condition monitoring of induction motors [44].

Only few authors, as reported in [45,46,47] have proposed the instantaneous power as a medium to detect only broken rotor bars fault under full-load condition on the basis of theoretical analysis, computer simulation and experimental results. These studies showed good results of using the instantaneous power as a diagnostic medium when referred to the traditional method of using stator current to detect the broken rotor bars fault.

It has been concluded from the literature survey that the use of Fourier Transform (FT) for frequency spectrum analysis is well established to detect majority of the faults related to induction motors. However, the accuracy and reliability to detect the faults depend upon the signal processing techniques applied to the motor under test to generate features, which are sensitive to the presence or absence of specific faults. In addition, it depends upon the selection

of fault detection methods such as model-based or knowledge-based to examine the fault parameters acquired from signal processing techniques to decide whether the fault exists or not.

1.6 Shortcomings of Condition Monitoring Research

The reliability of signal-processing techniques depends upon a good understanding of the electric and mechanical characteristics of the machine in healthy and faulted state under different loading conditions. The following shortcomings were identified on the basis of information discussed in the literature review.

- Most of the signal-processing techniques used to detect different faults such as broken rotor bars, eccentricity, shorted turns and bearing faults normally use information from one sensor type (current, axial flux leakage or vibration sensors) as mentioned in [1,4,5]. However, it is often not possible to detect and differentiate between a wide range of faults types with a single sensor type, because many faults have similar symptoms e.g. a number of mechanical faults can produce fault amplitudes at a frequency corresponding to twice the rotor speed. It is thus proposed to combine information from different sensor types to improve fault detection.
- There has been only limited research on the effect of load variations on the amplitudes of fault frequency components under healthy and faulty conditions. The majority of the studies only consider the full-load case, with limited research considering partial load cases. References include [2,3,18] looked at broken rotor bar faults under varying load conditions.
- To detect faults and estimate fault severity in the machines using characteristic fault frequencies, it is important to examine the variability in their amplitudes to other effects apart from load and fault severity. This area has had limited research in the literature on condition monitoring.
- A lesser amount of work has been focused on the detection of multiple faults, i.e. the combination of broken rotor bars and eccentricity faults under varying loading condition.

- The majority of studies only considered the stator current as a diagnostic medium to detect the different faults in induction motors. However, only few researchers [46,47] proposed the instantaneous power signal as a diagnostic medium to detect the broken rotor bars fault under full-load condition. The use of instantaneous power to detect the other major faults in the machines (eccentricity, shorted turn and misalignment) and multiple faults (combination of different faults) under varying loading condition was not reported in previous research.

1.7 Aim of Thesis

The aim of this study is to investigate different factors, to overcome the shortcomings related to the detection of different faults i.e. broken rotor bar, eccentricity, shorted turn and misalignment in the machines using the fault frequency components from the current, flux and instantaneous power signals under different levels of loading.

This study develops data acquisition software, which is used for data collection, and then develops a custom-written programmed to analyse the raw sensor data, which produces the frequency spectrum of current, flux and instantaneous power spectra and automatically locate the appropriate peaks in the spectra of different signals simultaneously. These are based on the experimental set-up developed for this research using hardware and software tools to provide the necessary technology for accurate and reliable effective fault detection and prediction of incipient failures in induction motors.

Other aims include the development of a comprehensive experimental database of non-invasive sensor measurements using current, voltage, axial leakage flux, vibration and speed sensors of induction motors with known single or multiple faults of varying severity under a range of load conditions.

Another aim of this research is the practical demonstration of modified fault frequency components ($f_p \pm 4f_2$) and ($f_p \pm 2f_r$) of instantaneous power signal. These could be used to detect single faults i.e. broken rotor bars and eccentricity and multiple faults (combination of broken rotor bars and eccentricity faults) as an alternative of traditional fault frequency components $(1 \pm 2s)\, f_1$ and ($f_1 \pm f_r$) components of stator current.

Furthermore, a detailed analysis of the effect of single and multiple faults on each sensor output is made. Ranges of load conditions are also examined, because the load variations

can cause a significant change in the amplitude of the fault signals. This research also investigates the detection of eccentricity fault using fault frequency amplitudes, as a function of average eccentricity instead of % of rated load, under different loading conditions.

1.8 Significance of Thesis

For electrical machine users, minimizing unexpected failures and unnecessary servicing is the primary goals. This involves minimizing maintenance costs by increasing the allowable intervals between inspections or only servicing machines when necessary.

Previously, using correlations amongst the different types of sensors to detect both single and multiple faults (combination of broken rotor bars and eccentricity, shorted turns and broken rotor bars, eccentricity and shorted turns, misalignment and broken rotor bars and eccentricity with misalignment) have not been studied.

This study proposes using multiple sensors i.e. current, voltage, axial flux, vibration and speed simultaneously to detect both single and multiple faults on the basis of experimental test results on laboratory test machines. A custom-built program developed for this study provides the results of current, flux and instantaneous power spectrums simultaneously. This will help in the detection of faults more accurately by comparing the spectra results of different measured signals.

It is foreseen that this research project results in improving the accuracy and reliability of fault detection and diagnosis techniques, especially in detecting single and multiple faults while they are in an early stage at different loading conditions by using current, axial flux, voltage and vibration sensors simultaneously. As mentioned before, normally a single sensor type is used to detect a single fault. This work can form the basis of more sophisticated fault classification techniques for multiple fault detection.

The use of instantaneous power as a diagnostic medium to detect the single and multiple faults will give the significantly improvement in the field of condition monitoring of induction machines.

1.9 Thesis Layout

This thesis consists of nine chapters:

In Chapter 1, a brief introduction about the background of condition monitoring is given and problems related to monitoring were identified. In Section 1.2 the basic construction and operating principles of induction motors are discussed. Section 1.3 presents detail of common motor faults and their causes. Sensor types for non-invasive measurements to detect the different faults in motors are discussed in Section 1.4.

A literature survey is presented in Section 1.5. In Section 1.6 the shortcomings of existing condition monitoring research are reviewed. The aim of the thesis and its contribution to the field of study is briefly explained in Section 1.7 and the significance of the thesis is presented in Section 1.8.

Chapter 2 starts with a summary of different signal processing techniques for feature extractions used to detect induction motor faults in Section 2.2. Features of sampled signals and frequency measurements and motor loading are described in Sections 2.3 and 2.4. Explanation of frequency spectrum from current, flux and instantaneous power are presented in Section 2.5.

Chapter 3 explains the details of the experimental condition monitoring system developed in this research. This chapter describes the characteristics of the sampled data and provides detail of the data acquisition system that is used to collect the data. LabVIEW based software used for data logging, and MATLAB based software for spectrum analyses are also presented in this chapter.

Chapter 4 examines the experimental test results of a set of healthy and faulty motors with partial, two and four broken rotor bars over a wide range of loading conditions to investigate the variations of the amplitudes of the fault frequency components as a function of motor load. In addition, investigation of the variations in the amplitudes of sideband components of healthy motors due to others effects apart from severity and load are also described.

Chapter 5 investigates the detection of Eccentricity faults. All loading conditions are presented in detail. A comparison with healthy motors is also presented. The use of

average eccentricity to detect the eccentricity fault is also described in detail. Methods to detect the fault frequency peaks are also presented with examples.

Chapter 6 investigates the detection of shorted turn faults using the fault frequency components from current, flux and instantaneous power signals. To detect the shorted turn faults using single signal (combination of flux and instantaneous power signals) are also presented in Section 6.2.

In Chapter 7, the use of the misalignment faults to detect single and multiple faults is examined. In addition, comparison of results obtained from current, flux and instantaneous power spectrums are also shown in the different sections of this chapter.

In Chapter 8, detection of multiple faults using non-invasive multiple type sensors are used to investigate different faults in the presence of other faults. In addition, comparison of results obtained from current, flux and instantaneous power spectrums are also shown in this chapter.

In Chapter 9, a summary of the overall research study is presented in detail. Some suggestions for future work are also provided. Finally, the Appendices present further details of some results including MATLAB analysis files related to the experiments.

Chapter 2

Analytical Methods used for Condition Monitoring

2.1 Introduction

It is important to obtain a comprehensive database of non-invasive sensor measurements of induction motors through laboratory testing on a large set of identical motors in the healthy state, as well as with single and multiple faults. Condition-monitoring tests are normally carried out on the sites of the machines. This test data is used for experimental purposes, such as to improve the accuracy of detection of faults in the machines at early stages. Due to limitations of access in certain applications and the physical location of the induction machines, it may not be possible to obtain sufficient meaningful data, which is required to make preventive decisions. Therefore, it is planned to overcome the problems using well-structured laboratory tests. However, the primary limitation of laboratory testing is the size of the induction motors selected for laboratory tests, which depends upon the available facilities.

This chapter describes the sensors i.e. vibration, axial flux, three-phase voltage and three-phase current, and the signal processing technique, which are used to collect detailed information about the variations of the magnitudes of signal components at fault frequencies with the degree of severity of a fault. The aim is to improve the accuracy and reliability of fault detection techniques, especially in detecting faults at early stages.

As is well known, the induction machine is highly symmetrical. Therefore, the presence of any kind of fault in it modifies its symmetry and produces well-understood characteristic fault frequencies in the measured sensor signals [2]. The magnitudes of the characteristic fault frequencies can be used for fault detection. However, it is observed that even healthy machines have observable fault frequencies. In the following subsections a variety of signal processing techniques including Wavelet Transform (WT), Short Time Fourier Transform (STFT), Negative Sequence Impedance and Park's Vector Approach will be briefly described along with frequency spectrum analysis using the Fourier Transform (FT), which is used in this study.

2.2 Signal Processing Techniques for Feature Extraction

In a condition monitoring system, the signals are in time-amplitude form and need to be processed (transformed) into the frequency domain. Such a transformation is needed to generate information that may provide more accurate and reliable data about the motors' condition. The principal of signal processing steps related to condition monitoring are shown in Figure 2.1.

Figure 2.1: The steps for transforming a time domain signal into the frequency domain, which is used in condition monitoring system [13].

As indicated earlier, the presence of any prevalent fault changes the symmetry of induction machines. Moreover, a given fault affects each sensor type differently. In the

case of asymmetry (which is due to fault) the interaction of flux between rotor and stator is changed, which can affect the stator currents, voltages, magnetic flux as well as the machine vibration. Therefore, measurements of these variations in signals taken from different sensors types can be used for condition monitoring.

For accurate and reliable frequency-domain measurements, a low pass filter is required as shown in the figure (block C). The next step is to sample the sensor signals using A/D converters. As shown in Figure 2.1, a digital signal processing technique, such as the FFT can be employed. The ratings and specifications of the sensors, the low-pass filter and the A/D converter that is used in this study, will be given in Chapter 3.

Different signal processing techniques can be used to analyze the sampled sensor data. These techniques can generate features that are sensitive to the presence or absence of specific faults. The signal processing technique is chosen based on the fault-related signal characteristics, and also the conditions under which the measurement was performed, for example steady state or transient.

This study concentrates in detecting single and multiple faults in induction motors under steady-state conditions. The different signal processing techniques that have been used in condition monitoring of induction motors are discussed below.

2.2.1 Frequency Spectral Analysis

In on-line condition monitoring, frequency analysis based on the Fourier transform (FT) is a common signal processing method used to detect bearing, stator, and rotor and eccentricity faults in induction motors. This is because different electrical and mechanical faults produce fault frequency signal components whose frequencies can be easily determined from motor parameters such as the number of poles and the slip.

Sensor signals such as vibration, current, voltage and flux contain these fault signals and hence provide information regarding different faults in the machine [2]. Frequency analysis can also be applied to the instantaneous power that can be calculated from the measured voltage and current signals (as will be discussed in Chapter 6 of this thesis).

In frequency analysis, the amplitude at each discrete frequency can be obtained as compared to the overall amplitude monitoring approach of time domain analysis. A fault that causes a small change in amplitude of a certain frequency component can therefore

be detected more easily in comparison with time-domain analysis. A logarithmic scale for the amplitude axis is normally chosen to improve the dynamic range of the representation. Using this process, faults that generate specific characteristic fault frequencies, can be detected early, diagnosed accurately, and the fault severity can be monitored over the time as the condition deteriorates.

As is known the FT is applied to a time domain signal to convert it into a frequency domain representation. As shown in Figure 2.1, the time domain signal is sampled and digitized into discrete values. Therefore, the discrete time form of the Fourier Transform (DFT) is used which produces, the frequency domain components in discrete values. The Fast Fourier Transform (FFT) is an optimized version of the DFT that performs the similar calculations in shorter time, which is calculated as [11]:

$$X(k) = \frac{1}{N}\sum_{n=0}^{N-1} x(n) \cdot e^{-j\frac{2\pi kn}{N}} \qquad (2.2.1)$$

where,

$X(k)$ is the FT of the signal x(n), k is the frequency index, n is the time index, and N is the total length of the signal.

The use of the FT for frequency analysis implies two important relationships. The first one refers to the highest frequency that can be analyzed to the sampling frequency and the second relationship links the frequency resolution to the total acquisition time, which is related to the sampling frequency and the block size of the FT. The Fourier transform performs well when estimating periodic signals in steady state. In some cases, the results of the estimation can be slightly improved with windowing.

2.2.2 Selection of Window Size in FFT Technique

Limiting the time duration of the interval over which the signal is observed is known as "*windowing*" and this process is used for the measurement of non-stationary signals, which may be divided into short segments of a quasi-stationary nature. Windowing consists of multiplying the time domain signal by another time domain waveform, known as a window, whose amplitude tapers gradually and smoothly toward zero at edges [13]. The result is a windowed signal with no (or very small) discontinuities, and

thus reduces spectral leakage, which occurs when a frequency component of a signal does not fit exactly into one of the computed frequencies in the spectrum. The window should be applied to the signal after the A/D converter has digitized it.

In general, window functions are used to reduce the side lobes in the spectrum of the FFT analysis. Hence, the peaks are easier to identify in spectrums. There are many different types of windows. The typical trade-off between windows is between amplitude accuracy and frequency accuracy. These common types of windows are Hamming, Hanning and Rectangular windows [13]. The Hanning window provides good frequency accuracy and can produce amplitude errors up to 1.4 dB, as compared to Hamming windows with 1.8 dB and the Rectangular window with 3.9 dB amplitude errors.

Figure 2.2 shows the frequency spectrum of a measured signal obtained from the data acquisition system with sampling frequency f_s = 400 Hz and time T =100 seconds. Note that, the calculation of the FFT corresponds to the FFT of the total length of the signal (100 seconds) of which only a zoomed fraction is shown in Figure 2.2.

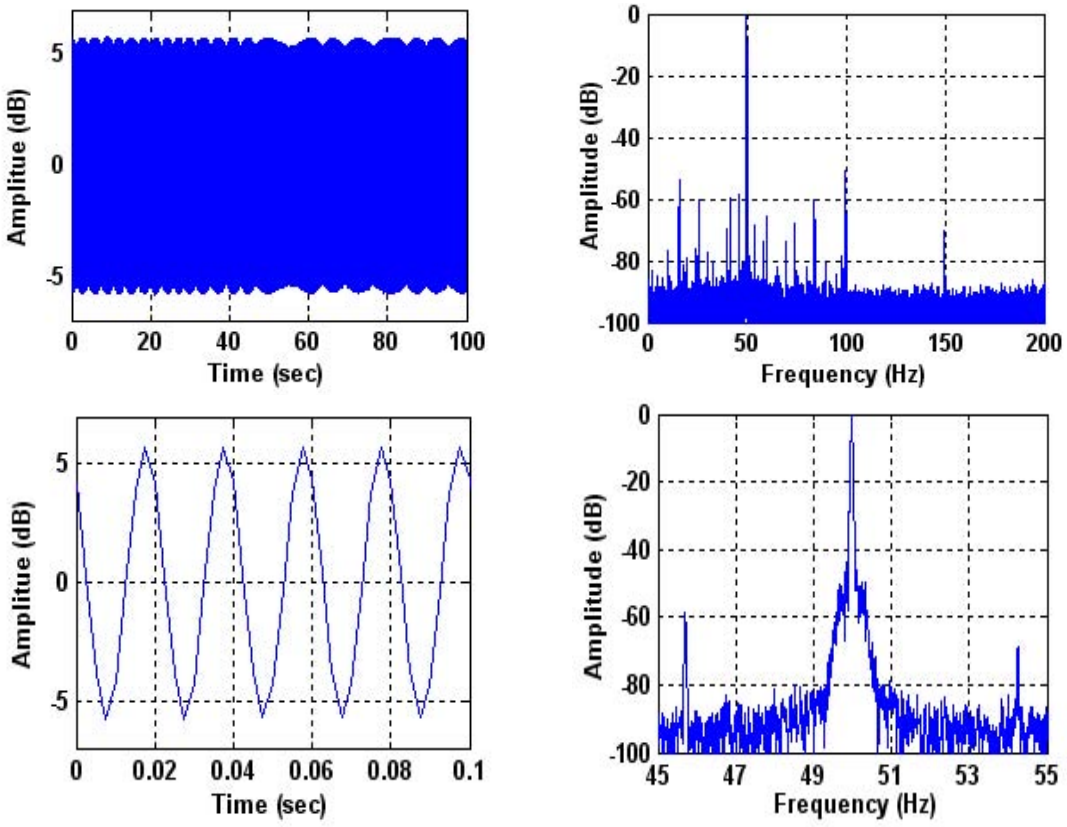

Figure 2.2: Left column (top and bottom) illustrates the full (100s) and zoomed (0.1s) version of the measured stator current waveform as a function of time. Right column (top and bottom) represents the full (200 Hz) and zoomed (45 to 55 Hz) versions of the FFT results of the measured signals.

2.2.3 Short-Time Fourier Transform (STFT)

The Short-Time Fourier Transform (STFT) is a modified form of the Fourier Transform. In this transform, the subject signal is divided into small segments, which are assumed to be stationary. Using a window function of a chosen width, which is shifted and multiplied with the signal to produce the short stationary signals does this.

Finally the Fourier transform is then applied to each of these segments to obtain the Short-Time Fourier transform of the signal, which shows the changes in the frequency spectrum of the signal with time. This process is defined by [38].

$$STFT(\omega,t) = \int_{-\infty}^{+\infty} i(t) \cdot w(t-\tau) \cdot e^{-j\omega t} \cdot dt \qquad (2.2.2)$$

where,

$STFT(\omega, t)$ is the Short-time Fourier transform of the current signal $i(t)$,

$\omega = 2\pi f$, where f is the frequency of the signal,

$w(t-\tau)$ is a window function,

t, is time, and

τ, is the delay parameter.

The STFT is used to transform the original measured signal into a time-frequency spectrum to capture the time variation of the frequency components. Then in the condition monitoring application the resulting spectrum is analysed to distinguish fault conditions from the normal operating conditions of the motor.

As an example, for condition monitoring analysis, the STFT can be used for detection of broken bars and bearing faults in motors using the stator current waveform.

Figure 2.3 shows the application of the STFT to transform a motor current signal into a time-frequency spectrum. Although this technique incorporates the time information, it suffers from the trade-off between the time and frequency resolutions due to the window size that must be selected *a priori*.

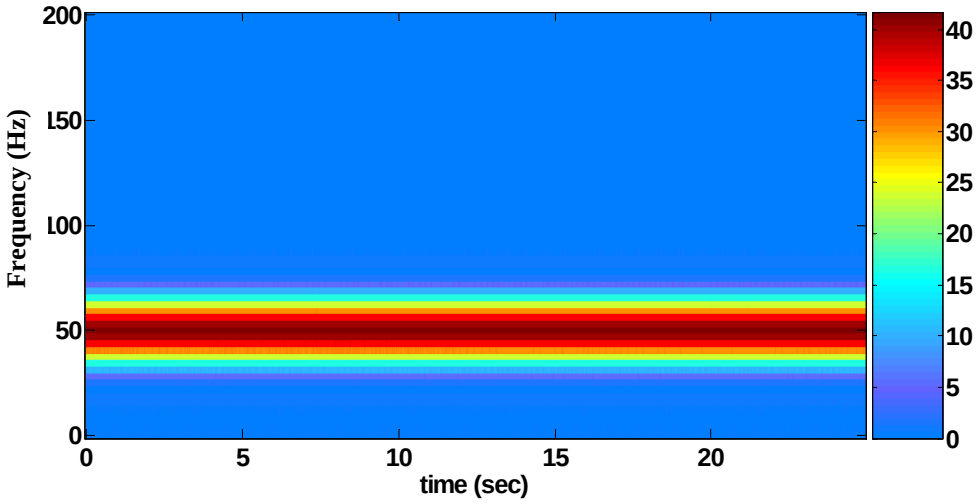

Figure 2.3: Application of Short-Time Fourier Transform on the measured current signal shown in Fig 2.2.

2.2.4 Wavelet Analysis

The Wavelet technique can be applied to non-stationary signals in which the disturbances are varying in only a short time [49]. The analysis process in the Wavelet Technique consists of convolving the studied signal with small window functions called wavelets. The length of these wavelets is varied depending on the frequency content in the signals. Therefore, this technique allows the study of different frequency signals at different time resolutions. A long window size is used for low frequency contents and a shorter window is used for high frequency content. The Wavelet Technique can also be used for localized analysis in the time-frequency or time-scale domain.

The general Wavelet Transform of a signal is defined by:

$$WT(a,\tau) = \frac{1}{\sqrt{a}} \int_{-\infty}^{+\infty} i(t) \cdot \psi_{a,\tau}^{*}\left(\frac{t-\tau}{a}\right) \cdot dt \qquad (2.2.3)$$

where:

WT is the Wavelet Transform of the current signal, *i(t)*

$\psi_{a,\tau}$ is the Wavelet function (basis function)

a and τ are the scaling and the translation respectively, and the asterisk in the equation denotes the complex conjugate of the function.

The application of the Wavelet transform to the measured current signal in Figure 2.2 is shown in Figure 2.4. The main disadvantage of this technique is its redundancy where a large number of scales are used for the calculation.

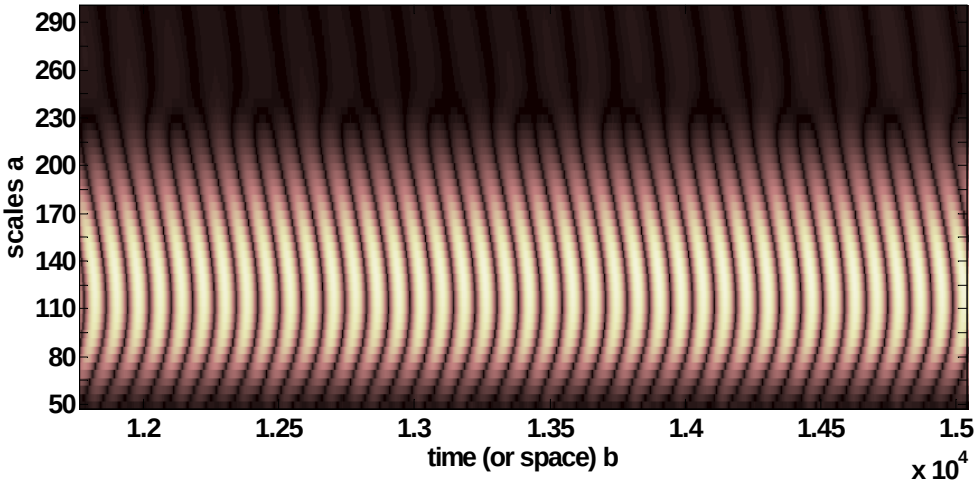

Figure 2.4: Application of the Wavelet Transform on a measured current signal shown in Fig 2.2.

2.2.5 Park's Vector Approach

In condition monitoring, the Park's Vector Approach can be used for detection of shorted turns in stator windings and the level of air-gap eccentricity [41]. These faults result in stator current imbalance, which can be detected using the locus of the instantaneous spatial vector sum of the three-phase stator currents. The locus pattern can be analyzed graphically or else the frequency spectrum of the spatial magnitude can be examined.

The following equations are used to determine the Park's Vector currents (I_d, I_q) as a function of the three-phase currents (i_a, i_b, i_c). The ideal representation of Park's Vector is a circular locus centered at the origin of the I_d and I_q coordinate.

$$\boldsymbol{I_d} = [\sqrt{2}/\sqrt{3}]\, i_a - [1/\sqrt{6}]\, i_b - [1/\sqrt{6}]\, i_c \qquad (2.2.4)$$

$$\boldsymbol{I_q} = [1/\sqrt{2}]\, i_b - [1/\sqrt{2}]\, i_c \qquad (2.2.5)$$

In the case of an ideal healthy motor, the three phase currents lead to a Park's Vector with the following components:

$$\boldsymbol{I_d} = \sqrt{6}/2\; i_M . \mathrm{Sin}\,(\omega t) \qquad (2.2.6)$$

$$\boldsymbol{I_q} = \sqrt{6}/2\; i_M . \mathrm{Sin}\,(\omega t - \pi/2) \qquad (2.2.7)$$

Where, 'i_M' is the maximum value of the supply phase current and 'ω' is the supply frequency. Under faulted conditions, I_d and I_q change and the shape of the pattern of the faulty motor is different from the healthy motor as shown in Figure 2.5 (right).

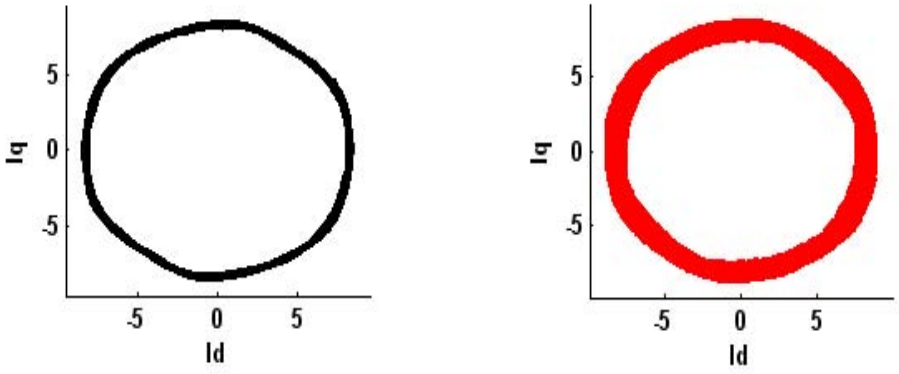

Figure 2.5: Park's Vector representing a healthy motor (left) and faulty motor (right).

2.2.6 Negative Sequence Impedance

An alternative to the Park's Vector approach for detecting stator phase imbalances is the concept of Negative Sequence impedance. This is based on the theory of symmetrical components in which, unbalanced three-phase voltages or currents can be separated into positive and negative sequence components [36]. The ratio of the negative sequence supply voltage to the negative sequence motor current is known as the negative sequence impedance and this is sensitive to the presence of unbalanced faults. Negative Sequence impedance Z_R can be calculated by:

$$Z_R = V_R / I_R \tag{2.2.8}$$

where, 'V_R' and 'I_R' are the negative sequence components of the machine voltages and currents, and

$$V_R = 1/3\ (V_A + a^2 V_B + a V_C) \tag{2.2.9}$$

$$I_R = 1/3\ (I_A + a^2 I_B + a I_C) \tag{2.2.10}$$

Where, a = 1<120° and V_A, V_B, V_C and I_A, I_B, I_C are the phasor voltages and currents

If a fault exists in an induction machine, the negative sequence impedance reduces, because of these effects 'Z_R' is changed. This can be used to detect the shorted turn's faults.

2.3 Features of Sampled Signals

An analog signal is continuous in both time and amplitude. In order to process such signals in computers, it is necessary to convert the signals into "digital" form, which is discrete in both time and amplitude using a process called sampling.

Sampling involves measuring the signal's values at certain intervals in time. The inverse of time between two consecutive samples is referred to as the sampling frequency, and each measurement is referred to as a sample. The Nyquist frequency is equal to half the sampling frequency. To avoid the aliasing of the sampled signals, the Nyquist frequency must be greater than the signal.

For example, Figure 2.6, shows a 100 sec record of current waveform taken with a 400 Hz sampling frequency. A zoomed version of the waveform is also shown in the figure.

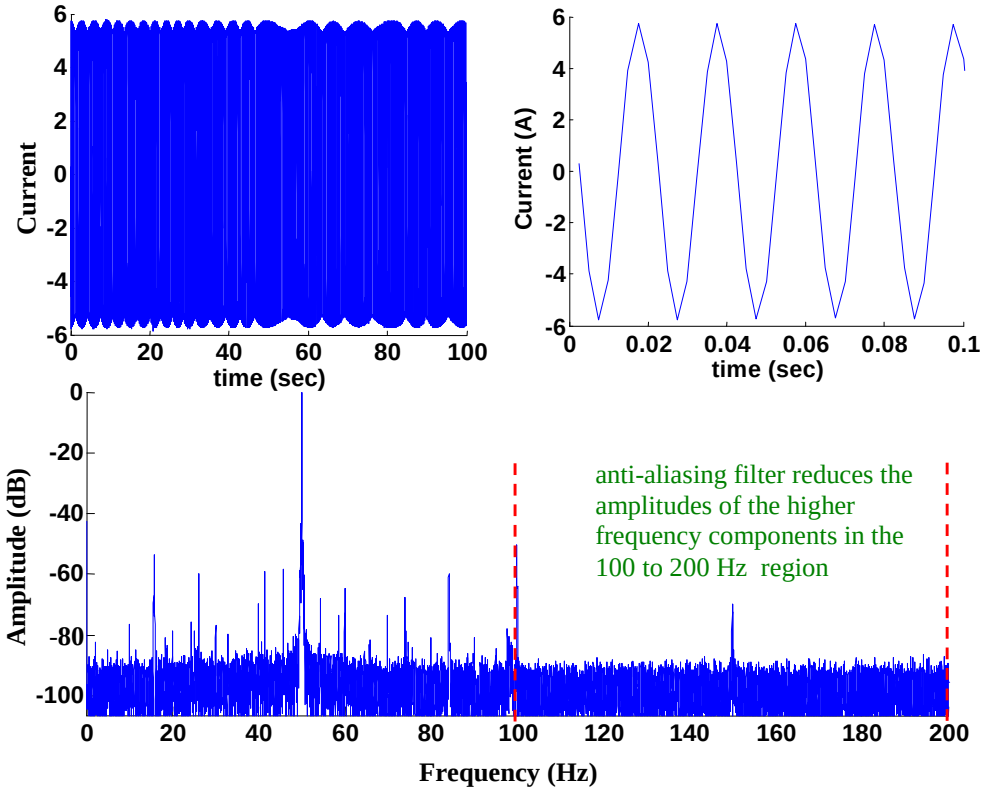

Figure 2.6: Waveform of current versus time with a 400 Hz sampling frequency of 0.1 second (top left) and its zoomed version (top right). The spectrum of the current waveform is shown (bottom) for (0 to 200 Hz).

The 100 sec time record gives a vary high frequency resolution of 0.01 Hz and the 400 Hz sampling frequency implies a Nyquist frequency of 200 Hz. A low-pass filter with a cut-off frequency of 100 Hz was used to avoid aliasing. Due to the low-pass filter, there are only few peaks present in the frequency spectrum between 100 Hz and 200 Hz as shown in Figure 2.6 (bottom) dashed lines.

Similarly, the current waveform for an 8 kHz sampling frequency with a 5 sec sampling time, having a frequency resolution of (0.2 Hz) is shown in Figure 2.7. The complete 5 seconds record on left and a zoomed version of 0.1 sec is shown in Figure 2.7 (top).

In this case the Nyquist frequency is 4 kHz and a 2 kHz anti-aliasing filter was used. The effect of the low-pass filter is evident as there are only few peaks of significant amplitude present in the region between 2 kHz and 4 kHz as shown in Figure 2.7 (bottom) with red dotted lines.

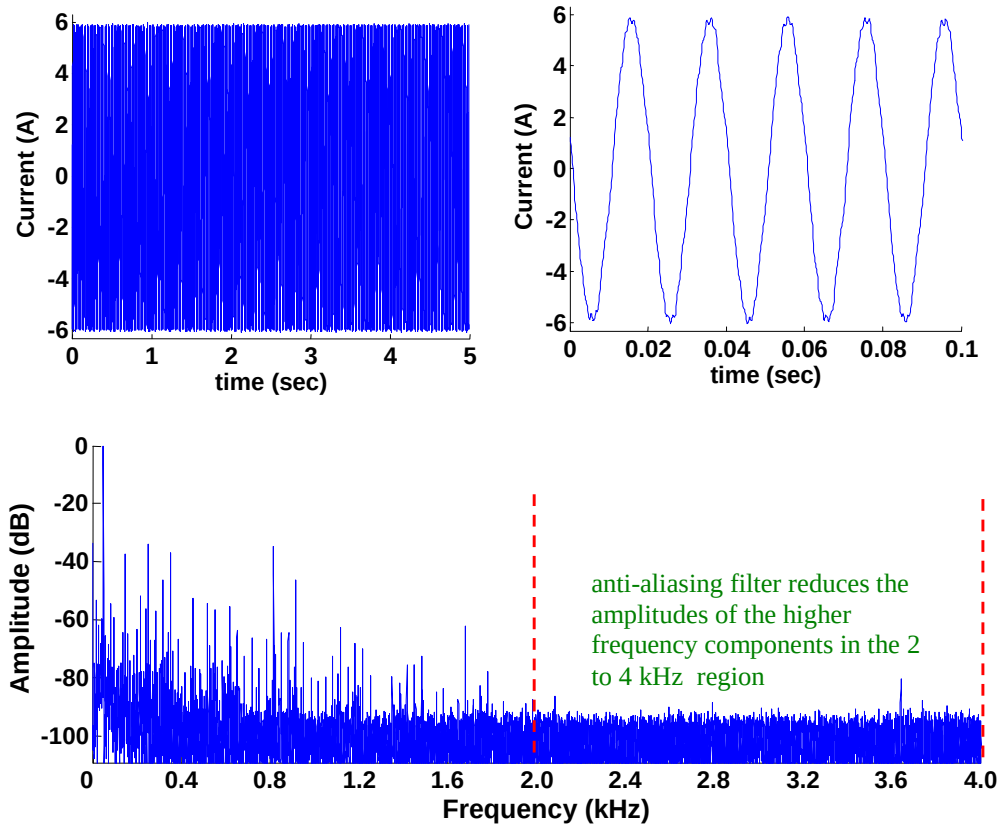

Figure 2.7: Waveform of current versus time with a 8 KHz sampling frequency (top left) and its zoomed version of 0.1 second (top right). The spectrum of the current waveform is shown (bottom) for (0 to 4 kHz).

2.4 Frequency Measurement and Motor Load

Fault frequencies are related to the supply frequency and slip. Therefore, an accurate value of the fundamental and slip frequency is paramount to determine these fault frequencies.

The voltage frequency spectrum is used to determine an accurate value of the fundamental frequency of the mains supply. In addition, the flux spectrum is used to determine the slip frequency sf_1 and hence estimate the amount of load on the motor.

2.4.1 Supply Frequency [f_1]

The supply frequency is determined by converting the time domain voltage signal into the frequency domain by passing it through a Hanning window and then applying the FFT technique. In the frequency domain, the fundamental frequency is the dominant peak in the spectrum. The supply frequency can also be determined by using the FFT of the current or flux spectrum. Figure 2.8 shows the supply frequency f_1 in the current spectrum.

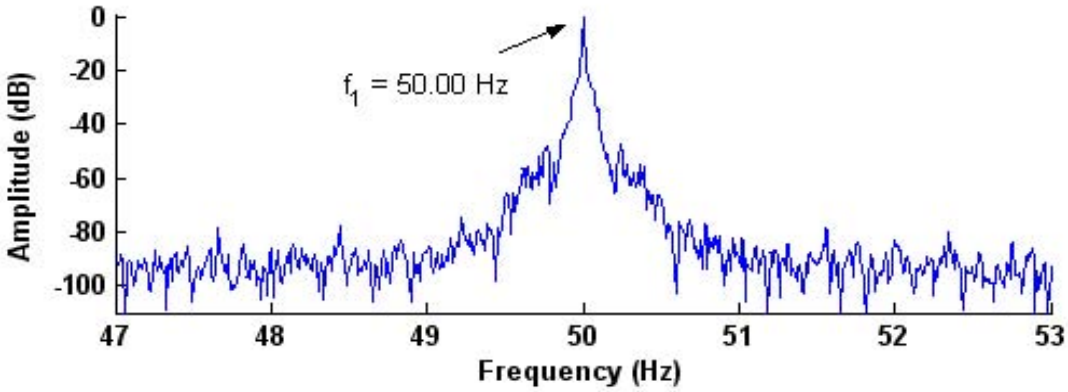

Figure 2.8: Spectrum of motor current phase “A” showing the supply frequency.

2.4.2 Slip Frequency [f_2]

As illustrated in Figure 1.4 of chapter 1, to a first approximation the rotor speed falls linearly with increasing load on the motor. Therefore, the slip frequency sf_1 increases as the load increases and the amplitude of the slip component also varies for different loading conditions. The slip frequency flux component sf_1 caused by the rotor currents in the rotor end-windings, has the largest peak in the low frequency region in the flux

spectrum. This is illustrated in Figure 2.9. The current spectrum from (0-5 Hz) clearly indicates the value of slip frequency, which in this case is $f_2 = sf_1 = 2.75$ Hz.

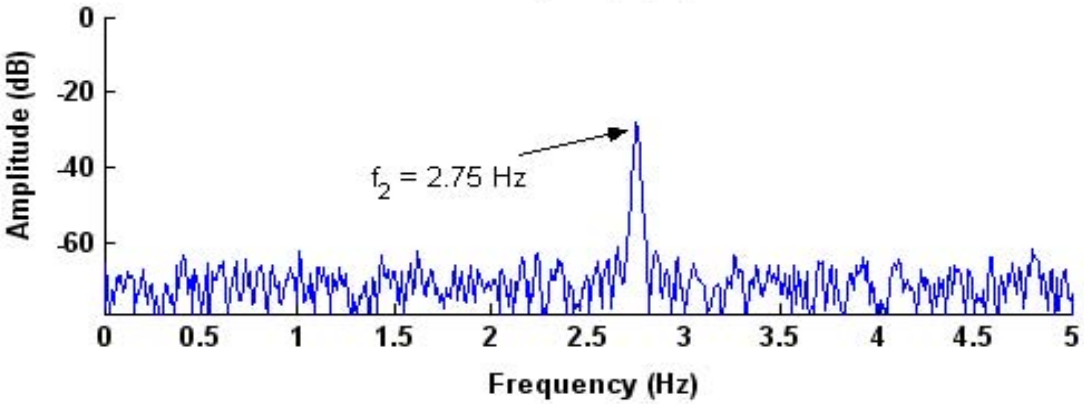

Figure 2.9: Frequency spectrum of flux signal showing the slip frequency components.

The effect of different loading conditions on the amplitude of the slip frequency component in a healthy induction motor is shown in Figure 2.10. The figure illustrates the frequency spectrum of the flux signal around the slip frequency range.

As can be seen in the figure, under no-load conditions, the slip frequency cannot be identified clearly, because at no-load the value of slip frequency is very small (0.26 Hz). Therefore, there is a need to improve the identification of the slip frequency at no-load operating condition of the induction motors. It can be seen from the figure that the amplitude of the slip frequency components increases significantly with increasing load.

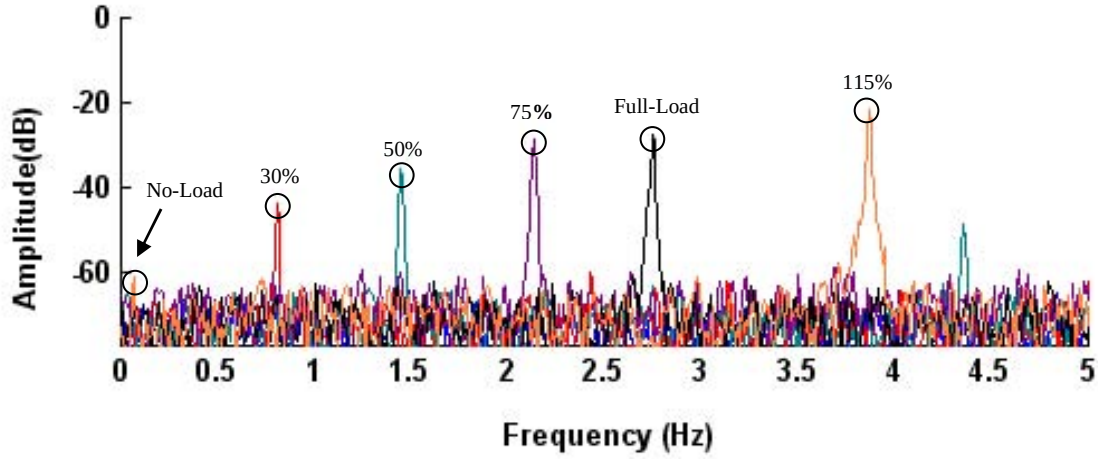

Figure 2.10: Measured slip frequency components and their respective amplitudes in the flux spectrum under different loading conditions. This figure is obtained using multiple plots on the same axis.

2.4.3 Methods to Identify Motor Load

Percentage of rated load is a term used to describe the actual load torque on the motor compared to its rated output torque [49]. It is known that the loading condition of the machines affects the amplitudes of the sideband components in the FFT analysis. Therefore, it is important to know the loading condition of the machine accurately. Different methods have been utilized in the practice for measuring this. In this section three methods i.e. input power, measured line current and slip/speed are described for determining the percentage of rated load.

Using Input Power

When electrical input power measurements are available, they can be used to estimate the percentage of loading of the motor. Equation 2.5.1 is used to calculate the rated three-phase input power to the motor [45].

$$P_{ir} = P_{or} / \eta_r \qquad (2.5.1)$$

where:

P_{ir} = rated input power (kW)
P_{or} = rated output power
η_r = efficiency

Percentage of loading is estimated by taking the ratio of the measured input power P_{ir} under load to the power required when the motor operates at rated load. This relationship is shown in equation 2.5.2.

$$\% \text{ Load} = (P_i/P_{ir}) \times 100\% \qquad (2.5.2)$$

Using Measured Line Current

The input current of an induction machine consists of two components: the magnetizing current, which to a first approximation is constant and independent of load, and the torque producing current, which is proportional to load. The input current is the vector sum of the magnetizing and torque producing currents, which have a 90° phase-shift.

At low loads, the magnetizing current component dominates, and there is little change in the input current with load. At high loads, the torque producing current component dominates, and the input current is roughly proportional to load as shown in Figure 2.11.

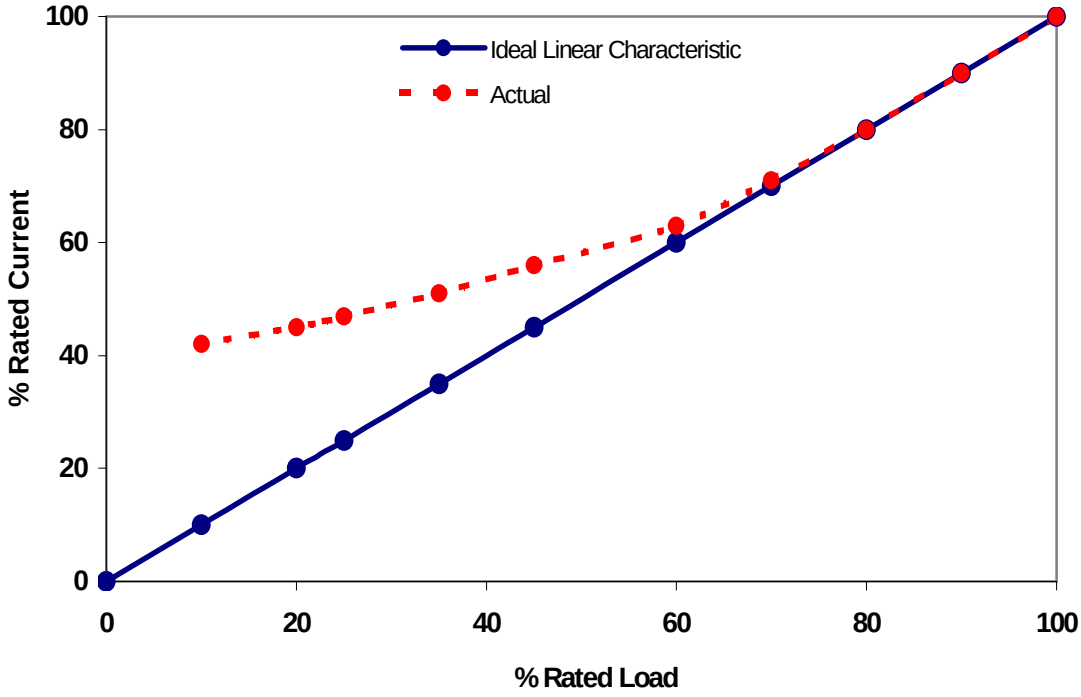

Figure 2.11: Typical relationship between % rated current and % of rated load of the induction motor.

Using Speed/ Slip Method

As illustrated in Figure 2.12 the slip frequency is proportional to the rated load on the motor. There are two means for measuring slip frequency:

1) By using a speed sensor to measure the actual motor speed directly and so calculate the slip frequency.

2) By determining the slip frequency using the flux signal (Figure 2.9).

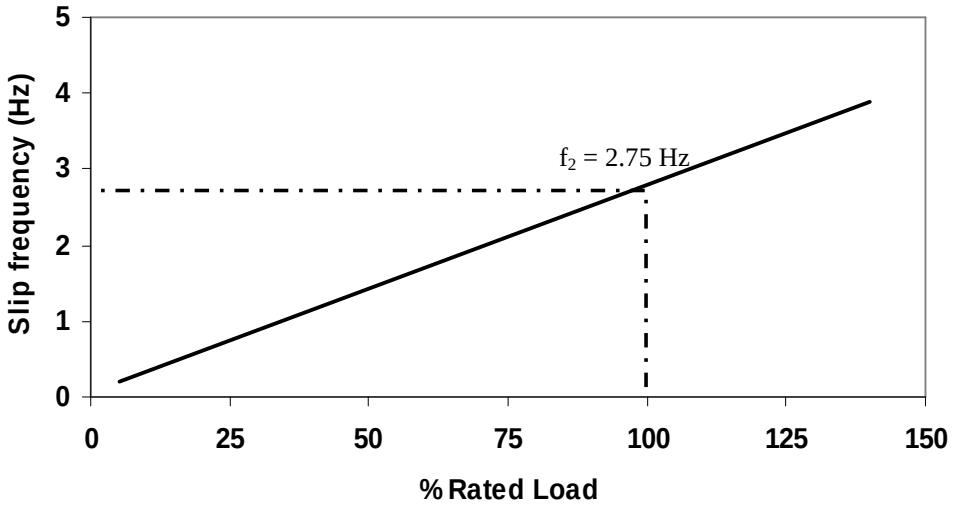

Figure 2.12: Slip frequency f_2 versus % of rated load for a healthy motor.

2.5 Identification of Fault Frequencies From Current/Flux Spectra

The detection of faults in induction motor depends upon the identification of fault frequencies and the accurate detection of their amplitudes in the sensor signals. Therefore, a brief explanation will be given about the identification of fault frequency components from current, flux and instantaneous power spectra.

2.5.1 Broken Bar Fault Frequency Components from Current/Flux Spectra

It is known that the presence of broken rotor bar in machine results in the increase in the amplitude of sideband components around the supply frequency component in the spectrum whose fault frequencies are given by the following equation [46].

$$f_{BRB} = (1 \pm 2s) f_1 \tag{2.5.1}$$

where,

f_{BRB} is the broken bar fault frequency components,
f_1 is the supply frequency in the power signal and
s is slip.

As can be seen in the equations above, the supply frequency affects the detection of the sidebands and so potential changes in supply frequency should also be considered during measurements. An example of the identification of broken rotor bar sideband components in the current spectrum is shown in Figure 2.13.

In the figure, only the frequency region relevant to the fault frequencies is shown. The FT current spectrum is normalized to the amplitude of the supply frequency component.

For the sample figure, the fault frequency components can be estimated as:

Supply frequency: $f_1 = 50.00$ Hz (Figure 2.8)

Slip frequency: $f_2 = 2.75$ Hz (Figure 2.9)

Slip: $s = f_2/f_1 = 2.75/ 50.00 = 0.055$

Lower sideband: $f_{BRB} = (1-2s)f_1 = 44.50$ Hz

Upper sideband: $f_{BRB} = (1+2s)f_1 = 55.50$ Hz

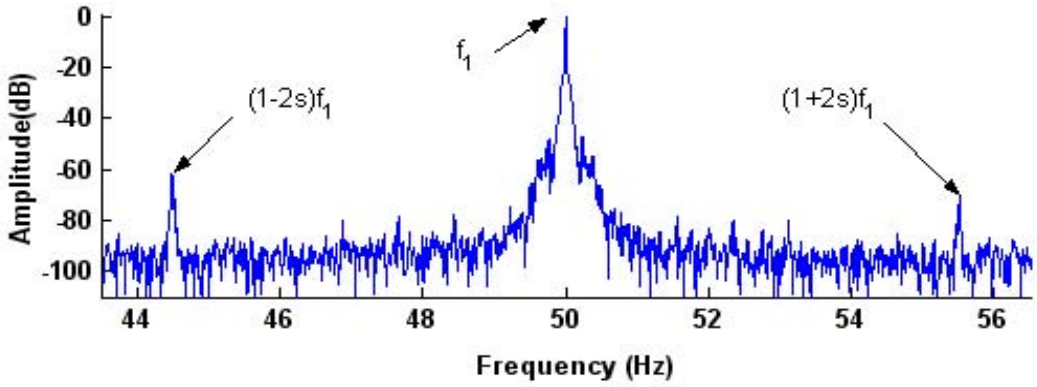

Figure 2.13: A sample current spectrum illustrating the broken bar sideband components (full-load).

For the sample figure above, the fault frequency components can be estimated as

Supply frequency: $f_1 = 50.00$ Hz (Figure 2.8)

Slip frequency: $f_2 = 2.75$ Hz (Figure 2.9)

Slip: $s = f_2/f_1 = 2.75/ 50.00 = 0.055$

Lower sideband: $f_{BRB} = (1-2s)f_1 = 44.50$ Hz

Upper sideband: $f_{BRB} = (1+2s)f_1 = 55.50$ Hz

It is well known that another method to calculate the slip is to use a speed sensor directly attached to the motor shaft. The slip can then be estimated by using equation 1.2.3. It should be noted that the use of current or flux sensors or a speed sensor to calculate the fault frequency sidebands might affect the accuracy of the results.

2.5.2 Eccentricity Fault Frequency Components from Current/Flux Spectra

The standard equations for the fault frequency components to detect the eccentricity fault from the current and flux spectra of eccentricity due to rotor slotting are [46]:

$$f_{ecc} = f_1 [(R/p)(1-s) \pm k)] \quad (2.5.2)$$

$$f_{ecc} = f_1 \pm f_r \quad (2.5.3)$$

where,

k=1, 3, 5 …

f_r = rotational speed frequency,

R is the number of rotor slots, and

p is the number of pairs of poles.

It is noticed from practical measurements that the rotor frequency is found to be strong in the vibration spectrum. Therefore, the rotor frequency is measured directly from vibration spectrum as shown in Figure 2.14, which is in this case is 23.58 Hz.

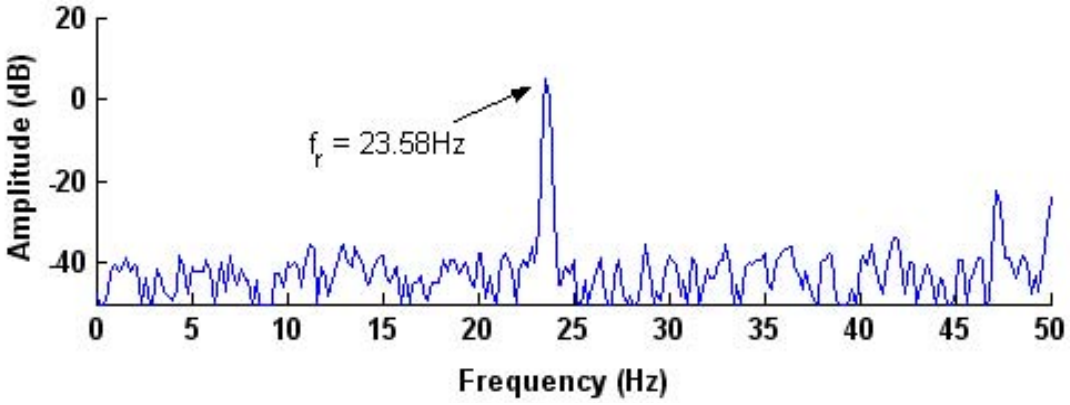

Figure 2.14: Vibration spectrum illustrating the rotor frequency f_r at full-load

The rotor frequency is the main parameter to calculate the eccentricity fault frequencies ($f_1 \pm f_r$). The calculated sideband frequencies are:

$f_r = (1-s)f_1/p = (1-f_2/f_1)f_1/p = 23.58$ Hz

$(f_1-f_r) = 50-23.6 = 26.42$ Hz

$(f_1+f_r) = 50+23.58 = 73.58$ Hz.

The measured sideband frequencies ($f_1 \pm f_r$) from the flux spectrum are 26.38 Hz and 73.63 Hz respectively as shown Figure 2.15. It can be observed that the calculated values are very similar to the measured values. The difference in the calculated and measured values of the positive and negative sideband fault frequencies was 0.04 Hz and 0.05 Hz respectively.

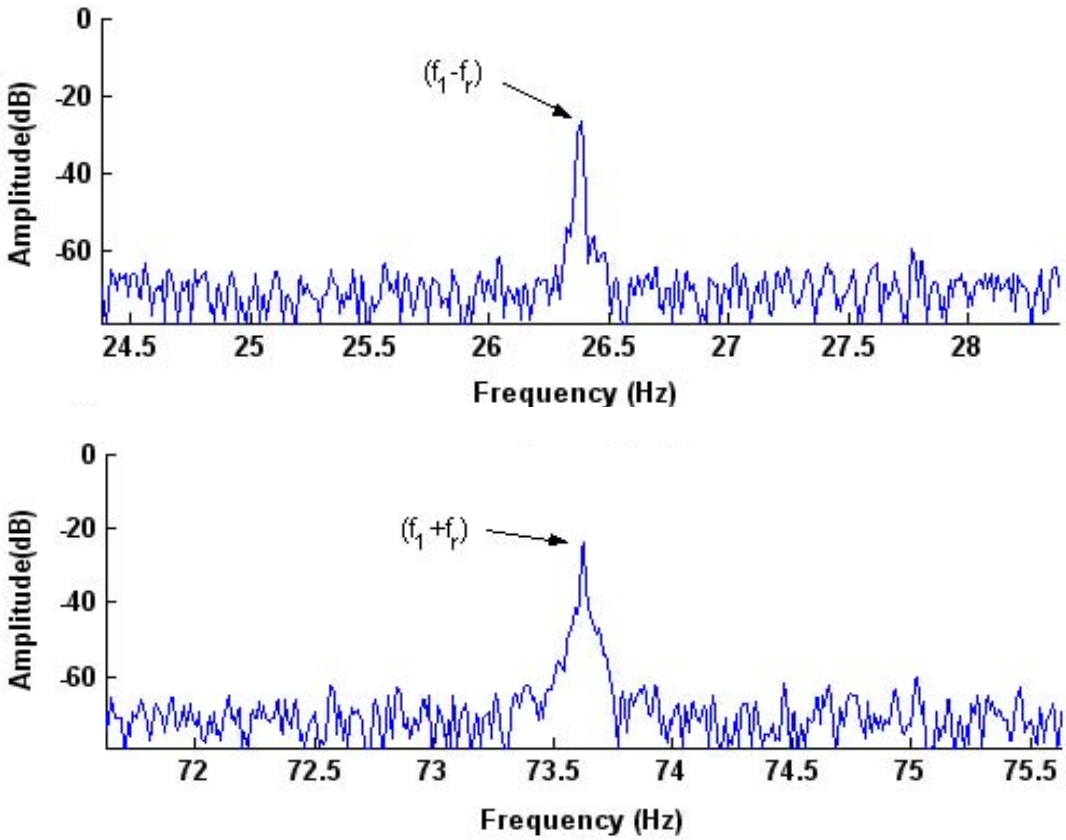

Figure 2.15: Flux spectrum illustrated the negative sideband component (top) and positive sideband component (bottom) at full-load

2.5.3 Shorted Turn Fault Frequency Components from Current/Flux Spectra

It is well understood that shorted turns fault in induction motors produce characteristic fault frequencies that can be observed using spectrum analysis of one or more sensor quantities mentioned above (i.e. current voltage, flux, and vibration). The shorted turn sideband can be observed at frequencies of [34]:

$$f_{ST} = f_1 [(n/p) (1-s) \pm k)] \quad (2.5.4)$$

The current and flux spectra can be used to identify the shorted turn fault frequency components. Figure 2.16 demonstrate the location of the negative and positive sidebands for n=1 and k = 3 in the flux spectrum. The calculated values for n=1 and k = 3 and p =2 current and flux fault frequencies are as follows:

$$f_{ST} = f_1 [(n/p) (1-s) - k)] = 126.4 \text{ Hz}$$
$$f_{ST} = f_1 [(n/p) (1-s) + k)] = 173.6 \text{ Hz}$$

Although both current and flux spectra are useful to detect shorted turn faults, the flux spectrum is preferred due to the higher amplitude of the sidebands components and lower noise level when compared to the current spectra.

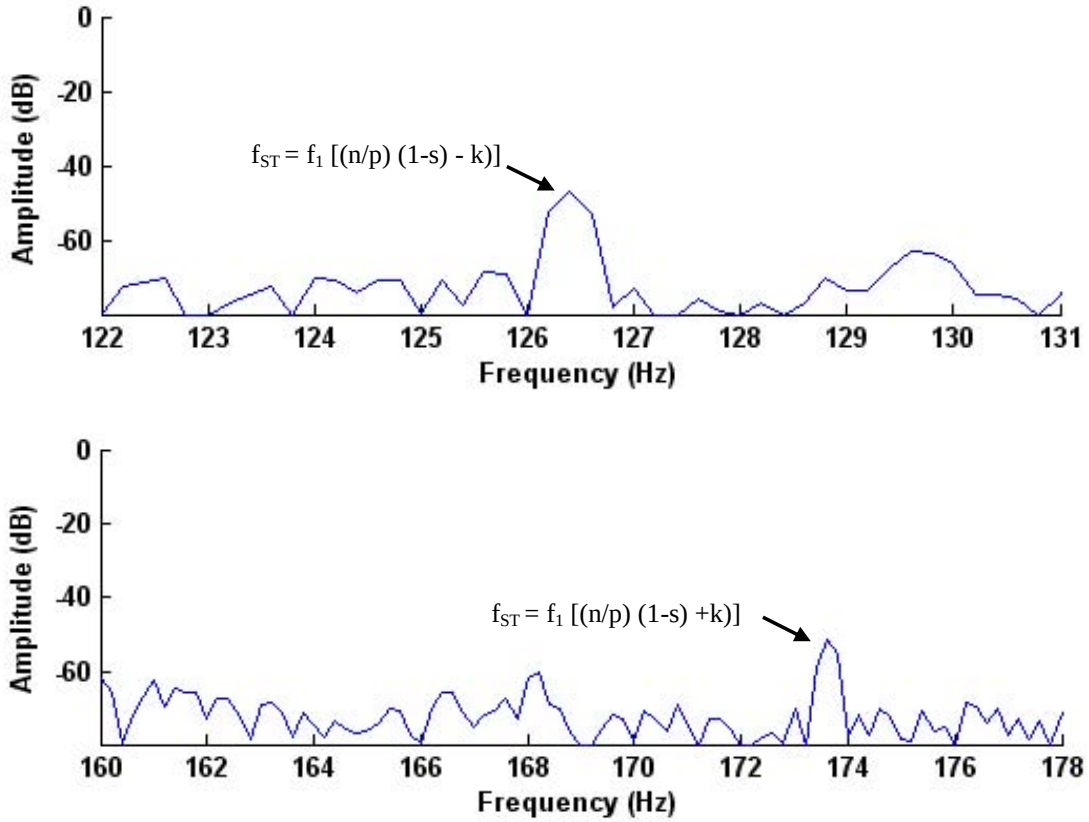

Figure 2.16: Flux spectrum illustrated the negative sideband (top) and positive sideband (bottom) at full-load.

2.5.4 Fault Frequencies Components From Instantaneous Power Spectra

Stator current and axial flux act as excellent sensors for detecting faults in the motor. Although the use of instantaneous power instead of stator current as a parameter for the detection of faults in a three-phase induction motor in generalized form has been reported in references [48,49]. They only considered the broken bars that were faulty at full- load condition. This study emphasizes the advantage of using instantaneous power (product of voltage and current) based on a real-time signal. The instantaneous power "P_{ins} (t)", which is derived from the instantaneous voltage and current signal, is calculated as follows [50, 51]:

$$P_{ins}(t) = V_P(t) \times I_p(t) \quad (2.5.5)$$

Here, "V_p" is the input phase voltage and "I_p" is the input phase current to the motor.

Modified fault frequency components to detect the broken rotor bar and eccentricity faults in the machines (reflecting the motor's condition) are shown in equations 2.5.6 and 2.5.7. These equations arrived at from the traditional current signature sideband equation, which is based on the observation of the sideband components in induction motors.

$$(f_p \pm 4f_2) \quad (2.5.6)$$

$$(f_p \pm 2f_r) \quad (2.5.7)$$

Here, f_2 is the slip frequency and f_p is the supply frequency of the power signal where, $f_p = 2f_1$ and f_1 is the supply frequency of current or voltage signal.

One set of real data consisting of current, voltage and instantaneous power spectrum at 30% load of healthy motor is shown in Figures 2.17.

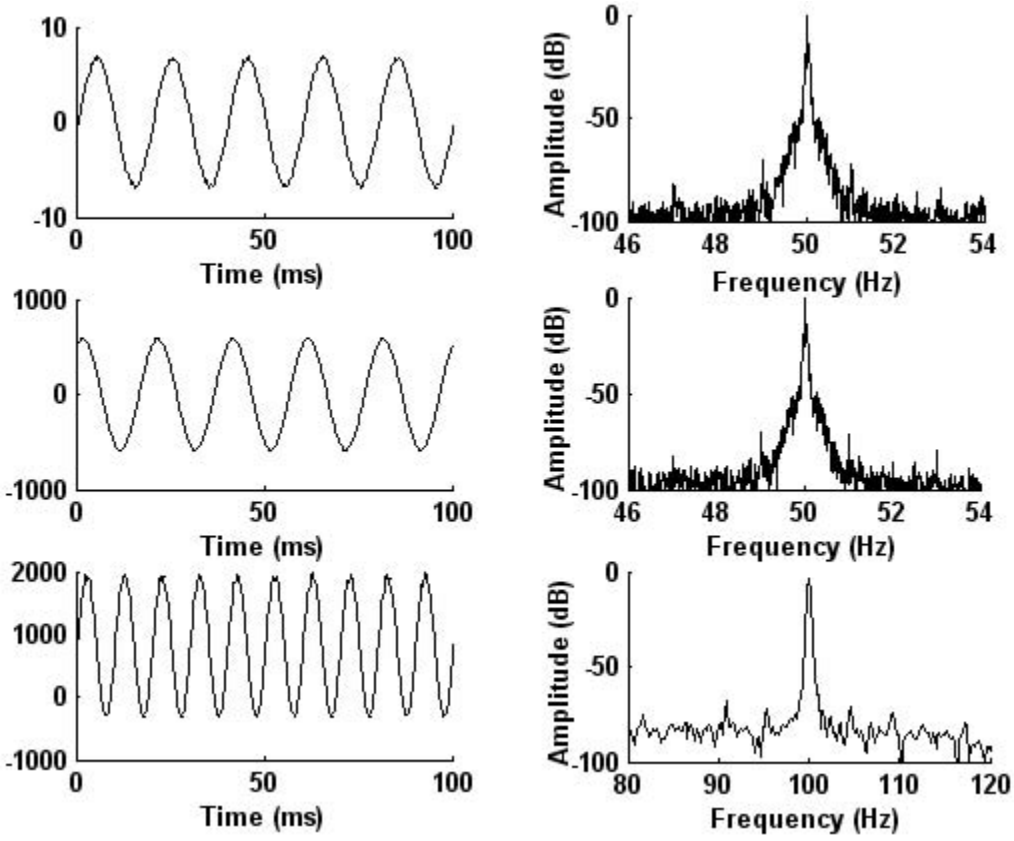

Figure 2.17: Left column (top, middle and bottom) illustrates the real measured waveforms of current, voltage and instantaneous power signals as a function of time. Right column represents the FFT results of measured signals.

2.6 Summary

The focus of this chapter was on a number of important factors related to the different analysis methods used to identify the characteristic fault frequencies in the frequency spectrum. The variations in the amplitudes of fault frequency components is used in this study to identify different faults in induction motors e.g. broken rotor bars, eccentricity and shorted turns etc. Detail of different signal processing techniques such as Frequency Spectrum Analysis, STFT, Wavelet Analysis, Park's Vector Approach and Negative Sequence Currents are presented.

The reason for selecting the Fourier Transform (FT) to detect the different faults in induction motors over the other signal processing techniques is because different electrical and mechanical faults produce fault frequency signal components whose frequencies can be easily determined from motor parameters such as the number of poles and the slip under steady-state conditions.

Different types of windows i.e. Hanning (used in this study), Hamming and Rectangular, are used to reduce the side lobes in the spectrum are also described.

Details of the sampling process for converting a signal from continuous time to discrete time and an explanation of the two sampling frequencies used are discussed.

An accurate value of supply and slip frequency is paramount to locate the fault frequencies in the frequency spectrum. The voltage/current frequency spectra are used to determine an accurate value of the fundamental frequency of the main supply.

The flux spectrum is used to determine the slip frequency f_2 that is also related to the amount of load on the motor. In addition, the importance of motor loading and methods for determining this using the line current, speed/slip and input power is discussed.

The detection of faults in induction motors depends upon the identification of fault frequencies and the accurate measurements of their amplitude. Therefore, a brief explanation how to identify the fault frequencies using the FFT of the measured sensor (current, voltage, vibration axial flux leakage) signals is provided.

Chapter 3

Experimental Set-up and its Features

3.1 Introduction

Faults in induction motors produce characteristic fault frequencies that can be observed using spectrum analysis of one or more sensor quantities, as mentioned in the previous chapter. For example, broken rotor bar sideband magnitudes can be observed at frequencies of $(1\pm2s)f_1$, shorted turn faults can be monitored at frequencies of $f_1[(n/p)(1-s)\pm k]$ and rotor eccentricity can be inspected at frequencies of $f_1\pm f_r$. In these expressions, f_1 represents the supply frequency, f_r is the rotor frequency ($f_r=N_r/60$), R refers to the number of rotor bars, s represents the slip, p refers to the number of pole pairs, and n and k are integers [2]. It can thus determined an accurate value for the fundamental and slip frequencies.

The ultimate goal of machine condition monitoring is to obtain accurate and reliable information about the condition of induction motors to make timely decisions. In order to do this, requires a good understanding of the effect of fault severity and loading condition on the amplitudes of the characteristic fault frequency components. This is studied using an extensive series of laboratory tests.

This chapter gives an overview of the experimental condition monitoring system hardware and software modules used in the study. In addition, detail of MATLAB programme, which is developed in order to identify the characteristic fault frequencies, is also described.

3.2 Condition Monitoring System

On-line condition monitoring means to assess the actual condition of a machine using measurements taken whilst the machine is operating. A general block diagram of a condition monitoring system is shown in Figure 3.1. In this stage it is aimed to briefly describe all the related terms used in condition monitoring during this study.

NOTE: This figure is included on page 46 of the print copy of the thesis held in the University of Adelaide Library.

Figure 3.1: Condition monitoring system for baseline analysis [18].

In this study, an extensive series of tests on a set of identical motors with a range of faults and under a variety of load conditions as mentioned in Block (A) in Figure 3.1 is performed. These faults affect the symmetry of the machine and as a result produce characteristic fault frequencies in the different types of sensors, shown in block (B).

In block (C), the data acquisition system is used to record the sensor signals in digital form. These signals can be analysed by different digital signal processing techniques to extract features, which are sensitive to the presence of faults. Some of the common techniques, which were discussed in Chapter 2, are shown in block (D).

In next step, the characteristic fault frequencies of different faults are detected from the processed signals. In this study, a customized MATLAB program is developed to detect these fault frequencies efficiently as shown in block (E).

Finally, in block (F), the fault frequency characteristics that relate to different fault conditions are analysed in the different sensor signals, (voltage, current, flux, and instantaneous power). This helps to better understand the relationship between fault type and severity versus the amplitudes of the characteristic fault frequencies.

3.3 Experimental Test Set-up

3.3.1 Test Motors

The experimental work in this study was conducted using the test rig and data acquisition system as shown in Figure 3.2. The tests were conducted on a set of 4 new identical three-phase induction motors (T-DF100LA, manufactured by Brook Crompton), which were loaded by a dynamometer consisting of a 5 kW separately excited DC machine. The detailed technical specifications of the induction motors under test are shown in Table 3.1.

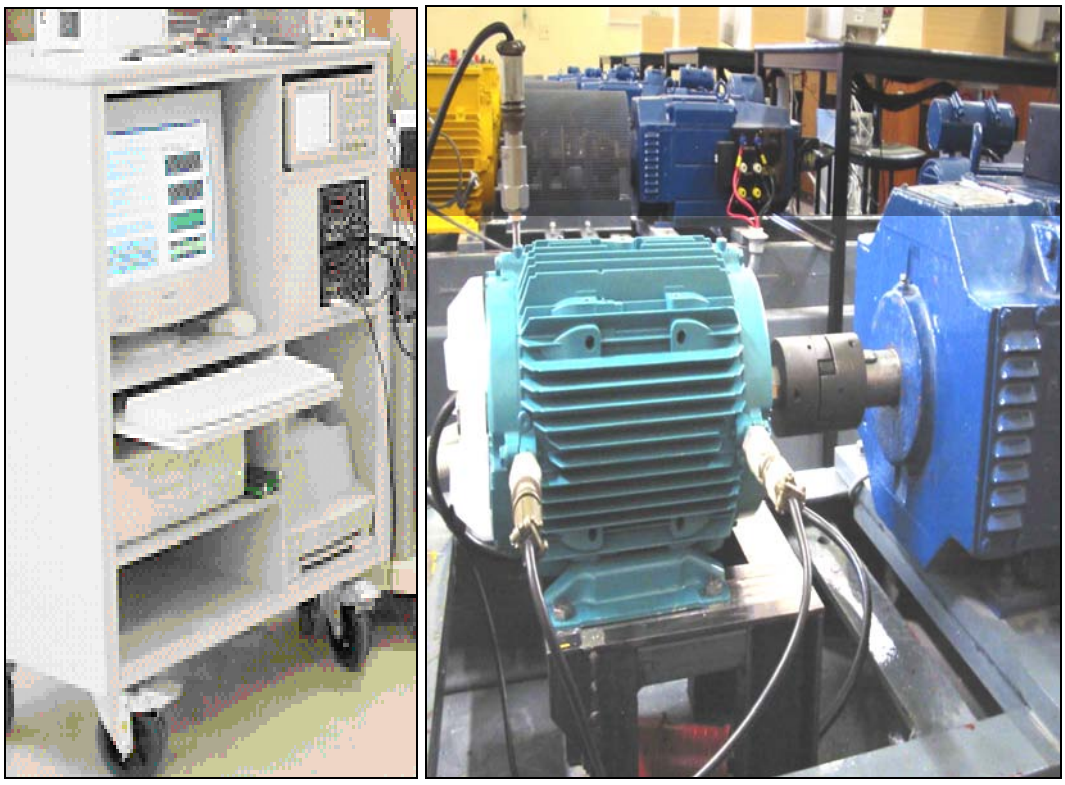

Figure 3.2: Data-acquisition hardware (left) and motor/load test set-up (right).

Table 3.1: Technical information for the induction motors used in the testing

Performance Data	Value
Rated voltage (V)	415
Rated frequency (Hz)	50
Rated current (A)	4.8
Power (kW)	2.2
Number of Poles	4
Rated speed (rpm)	1415
Rated torque (Nm)	14.8
Number of rotor slots	32
Power factor at full-load	0.81

The induction motor under test was mechanically coupled to a separately excited DC machine, which was loaded using a variable-resistance bank. The wiring diagram of the AC and DC systems is shown in Figure 3.3. The specifications of the DC machine used as a load in the testing are shown in Table 3.2.

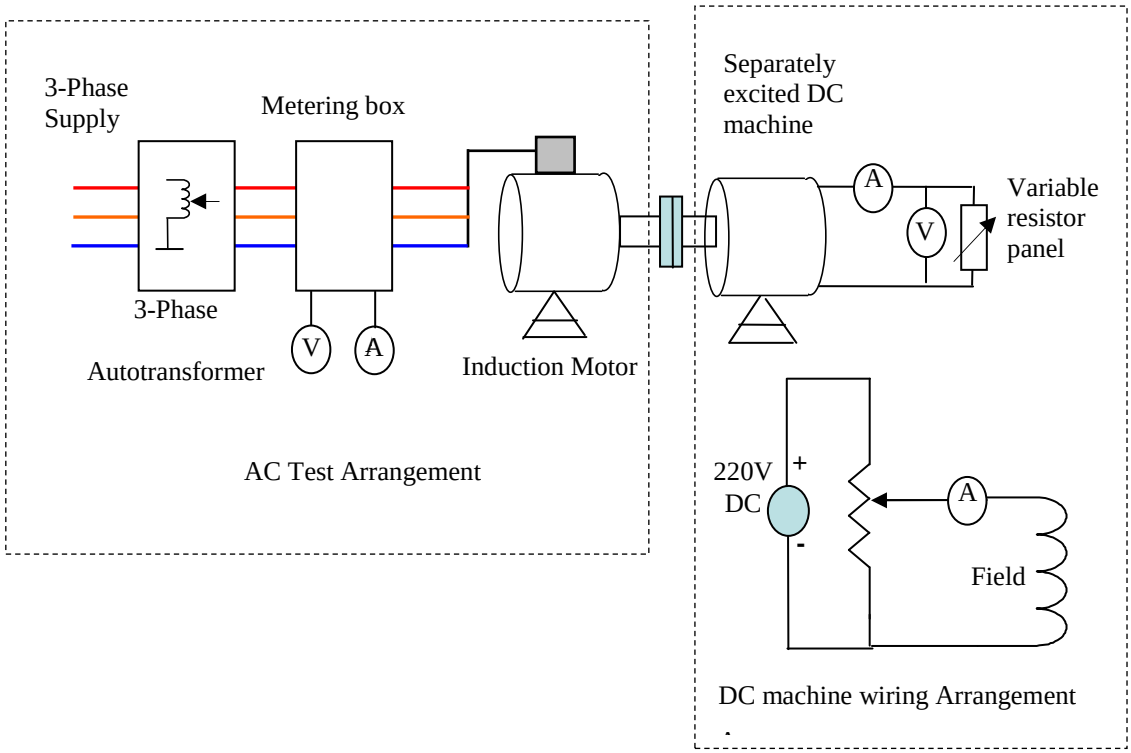

Figure 3.3: Diagram of AC and DC test arrangement.

Table 3.2: Technical information about the DC machine used in the testing

Performance Data	Value
Rated shaft power (kW)	5.5
Rated speed (rpm)	1500
Rated armature voltage (V)	220
Rated armature current (A)	28
Rated field current (A)	0.65

3.3.2 Critical Issues and Features of the Test Arrangement

There are number of factors which can affect the accuracy of the measurements. Some of these factors are the rigidity of the foundation of the test motor and the accuracy of the shaft alignment. The motors must have a firm and rigid foundation to eliminate soft foot problems and to reduce vibration.

There are number of cost benefits of precision alignment. It can help to reduce operating costs by reducing energy costs. Precision alignment also results in increased maintenance savings through reduced parts consumption and reduced overtime.

Typically, a precision alignment of machines can reduce the energy costs from 3 to 10%. A recent study showed that even small amounts of misalignment could significantly reduce bearing life. The definition of “Correct” alignment is based on the acceptable range of alignment values that is given for the specified motor speed provided by the manufacturer of the laser alignment tool.

Figure 3.4: Laser Alignment Device used for precision alignment.

Figure 3.5: Torque Wrench used in experimental set-up.

To eliminate alignment faults, the motors were installed on the test rig using a precision laser alignment tool (purchased for this study) shown in Figure 3.4 and a torque wrench (Norbar set at the recommended value of 35 Nm for ideal mounting) as shown in Figure 3.5. These two tools were used to ensure the accuracy and the repeatability of the mounting as well as to introduce the misalignment faults in machines.

Table 3.3 shows a set of results that compares the acceptable limits and the values obtained for a motor under test. The table demonstrates the measured values are equal or below the acceptable limits in the vertical and horizontal directions and so the motor is considered properly aligned.

Table 3.3: Alignment limits and the actual measured values obtained for a test motor

Alignment	Acceptable limit (mm)	Measured value (mm)
Vertical offset	0.09	0.09
Vertical gap	0.07	0.05
Horizontal offset	0.02	0.02
Horizontal gap	0.07	0.07

3.3.3 Sensors Arrangements and Measuring Tools

During the tests, the two current sensors for line currents, two voltage sensors for line voltages, one axial leakage flux senor, two vibration sensors: drive-end horizontal (DEH) and drive-end vertical (DEV), and one speed sensor that is directly connected to the shaft of motor, were used.

The position of the sensors in the test arrangement is shown in Figure 3.6. The axial leakage flux measurement was taken with a circular search coil of comparable diameter to the motor, which is mounted concentrically with the shaft on the rear of motor. For reliability and consistency of the flux measurements, a fixed position for the flux coil is defined.

The vibration sensors were screw-mounted to the motor housing to achieve the highest measurement bandwidth. Measurements of the input stator currents and voltages were taken using a custom-built measurement box that was located between the auto-transformer and the test motor. The speed sensor was directly attached to the motor shaft to obtain the running speed of motor as shown in Figure 3.6.

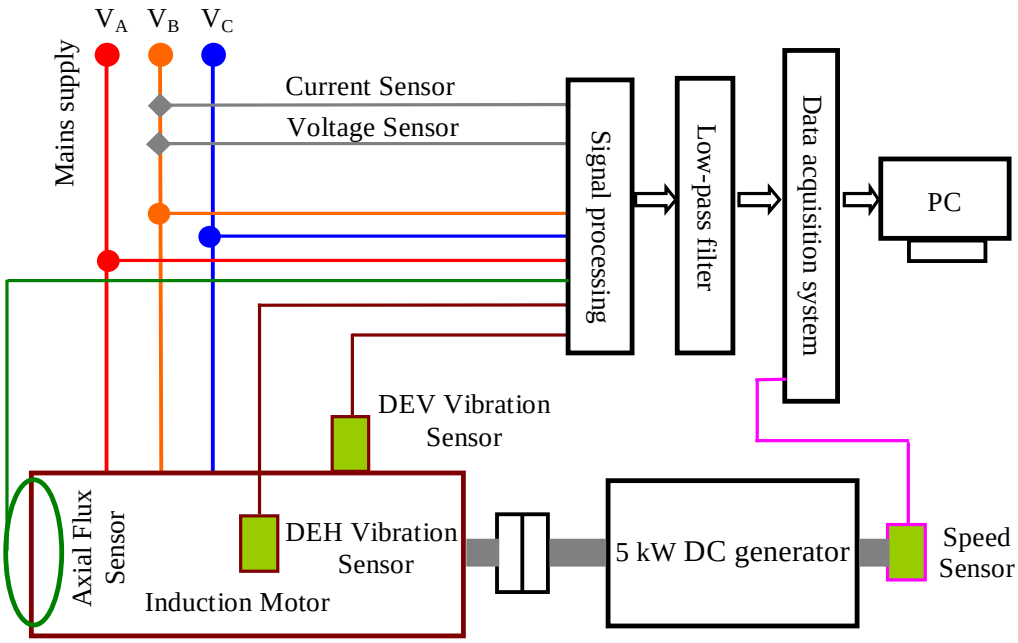

Figure 3.6: The block diagram of the test set-up including the positions of the sensors.

The analog signals from the sensors are passed through low-pass filters to remove any high frequency components that may cause aliasing. This is performed by an 8 channel, 8^{th} order Butterworth analog low-ass filter unit with selectable cut-off frequencies of 100 Hz for the 400 Hz sampling frequency and 2 kHz for the 8 kHz sampling frequency.

This unit also has individually adjustable channel gains of x1, x10 and x100 to allow amplification of low-level sensor signals [5]. Table 3.4 illustrates the specifications of the sensors used for measurements in this study.

Table 3.4: Sensor specifications

Signal	Device	Function	Band width	Input Range	Output Gain
Voltage	Differential Amplifier	Allows safe measurements of high voltages.	30 kHz	± 600 V	100 V = 1V
Current	Hall-effect sensor	Detects magnetic field produced by current.	50 kHz	± 10 A	10 A = 1 V
Flux	100 turn search coil	Measures axial leakage flux produced by currents flowing in the stator and rotor end windings.	10 kHz	± 1V	-
Vibration	Piezoelectric accelerometer	Acceleration measurements.	20 kHz	± 2 g	1 g = 1 V
Speed	Tacho-meter	Measures shaft speed directly	-	-	-

3.3.4 Sampling Information

During the measurements the sensors were sampled simultaneously and two different sampling rates used in this study are as follows:

- Low-frequency measurement with a 400 Hz sampling frequency that gives a Nyquist frequency of 200 Hz, and 100 s sampling time, which allows very high-resolution frequency analysis (40,000 data points, 0.01 Hz resolution).
- High-frequency measurement at 8,000 Hz sampling frequency with a sampling time of 5 seconds (40,000 data points, 0.2 Hz resolution).

The parameters of the two sampling rates, achieved frequency resolution, frequency range, setting of anti-aliasing filter and hence useable frequency ranges of each sampling rate used for experiments are illustrated in Table 3.5.

Table 3.5: Summary of sensor signal sampling information

	Low Frequency Sampling	**High Frequency Sampling**
Sampling Frequency	400 Hz	8 kHz
Total Sampling Time (T)	100 sec	5 sec
Frequency Resolution $\Delta f = (1 / T)$	0.01 Hz	0.2 Hz
Total number of points in record $L_R = fs / \Delta f$	40,000	40,000
Nyquist Frequency	200 Hz	4 kHz
Cut-off frequency	100 Hz	2 kHz

3.3.5 Testing Procedure

It is necessary to follow a consistent testing procedure to obtain reliable results. The procedure used for carrying out experiments on the test arrangement is as follows:

- Set the auto-transformer output = 0 Volts.
- Set the DC = 0 Volts and turn-off load bank
- Turn the AC “ON” and DC power “ON” using the main switches.
- Set the field current = 0.2 Ampere
- Increase the autotransformer voltage slowly up to rated voltage (415V).
- Adjust the variable load resistance and field current and keep the DC machine armature voltage < 220V and current <10A. The warm-up time for the machine is twenty minutes before taking any measurements.
- The LabVIEW programme was used to capture the sensor signals with sampling frequency of 400 Hz for low frequency data and 8 kHz for high frequency data.

For each test start from no-load and gradually increase the load. After collecting the data at different loads, turn-off the machine completely and a settling time is provided before the machine start again for another load test. This is necessary because the Fourier transform is useful for stationary signals.

3.4 Data-Acquisition System

The data acquisition system used in this study consists of two sections: the hardware and the software. The hardware used consists of: two four-channel plug-in cards from National Instruments (NI-PCI-6110, 12-bit, 5MS/sec, simultaneous sampling), anti-aliasing filter (as described previously), and eight sensors (two voltage sensors, two current sensors, two vibration sensors, flux sensor, and a speed sensor).

The data-acquisition software used for data collection was written using LabVIEW. The principal aim of this software is to collect the data, display it and save it for further analysis. The graphical user interface of the software is shown in Figures 3.7 and 3.8.

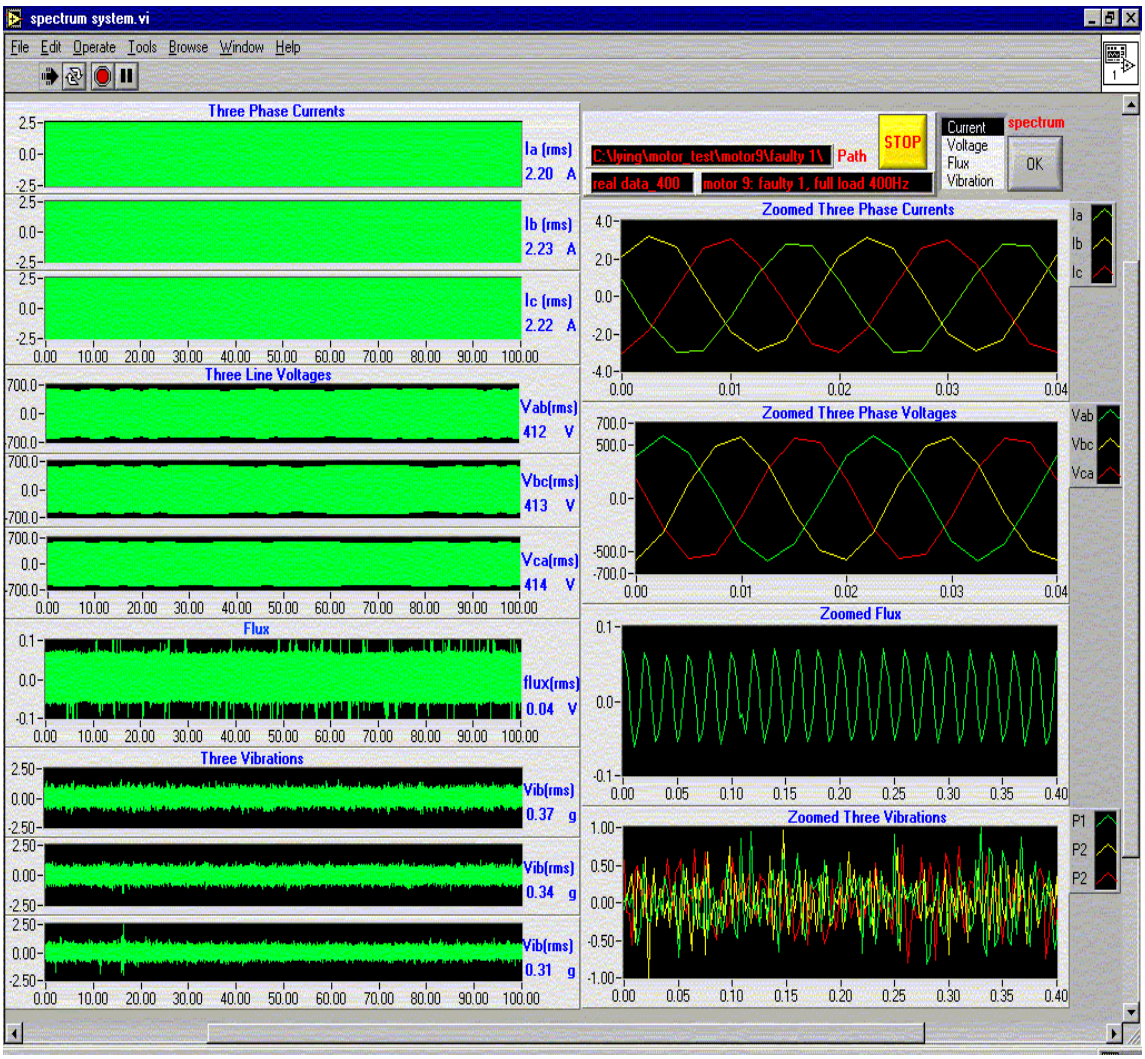

Figure 3.7: Front panel of the LabVIEW program showed sampled signals

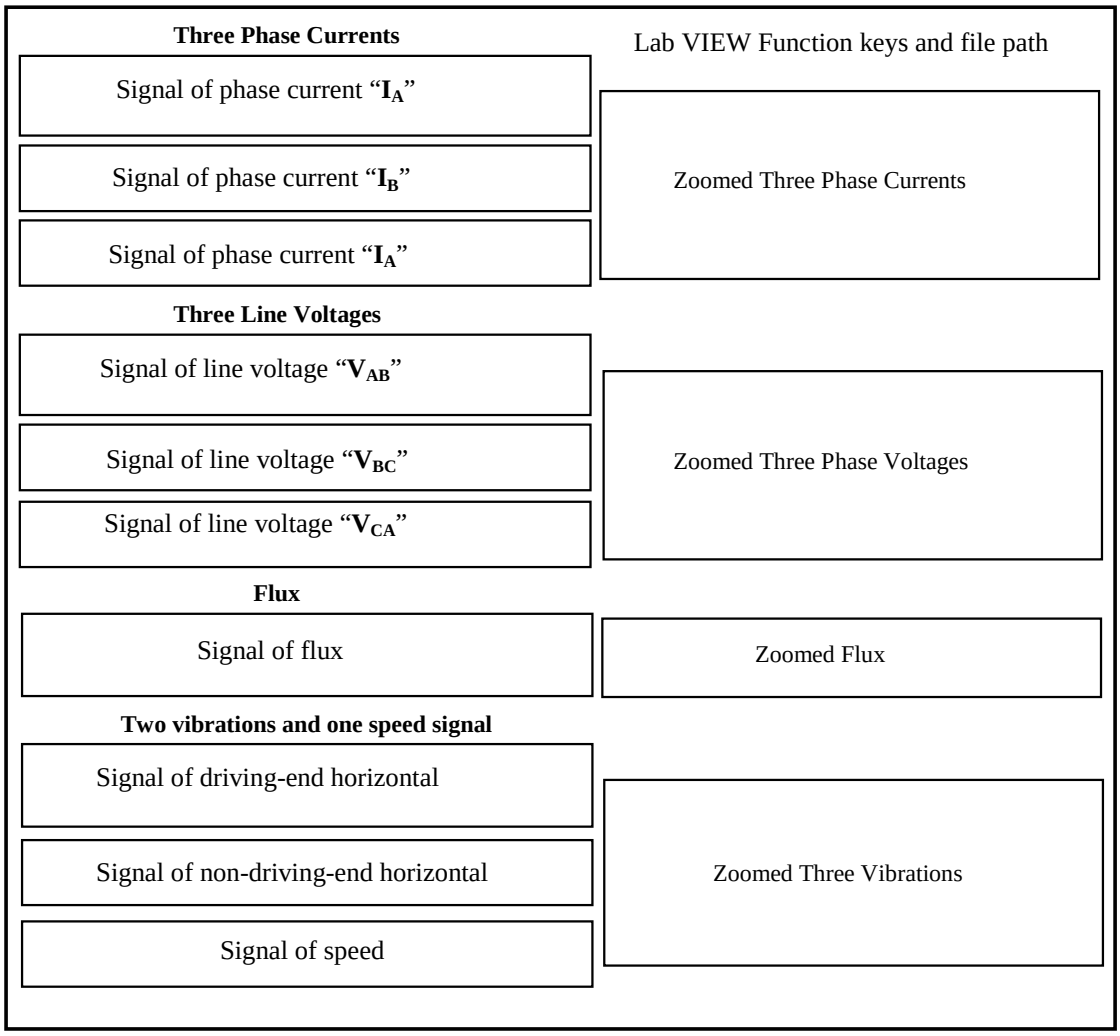

Figure 3.8: Brief user guide of the LabVIEW program showed in figure 3.7.

3.5 Fault Analysis Software

Spectrum analysis is used to identify the specific fault frequencies of the machine, which are used as indices to diagnose its faulty/healthy condition. In this study, a custom written program developed in MATLAB is used to identify the fault frequencies from the current, flux and instantaneous power spectra.

The program reads the data files saved using the data logging software described in the previous section, and then applies a Hanning window on the specified data i.e. current, flux or voltage. It then performs the Fourier transform (FT) on the data. The spectrum is normalized with respect to the highest peak (normally the fundamental) before converting to decibel (dB) and being plotted for future analysis. Figure 3.9 show a flow

chart of the program used for analysing the data. The program starts by reading the raw data saved during the experiments in a digital form. Analysis of the data is performed, by calculating the Fourier transform of the voltage, the current, the flux, the vibration, and the instantaneous power signals.

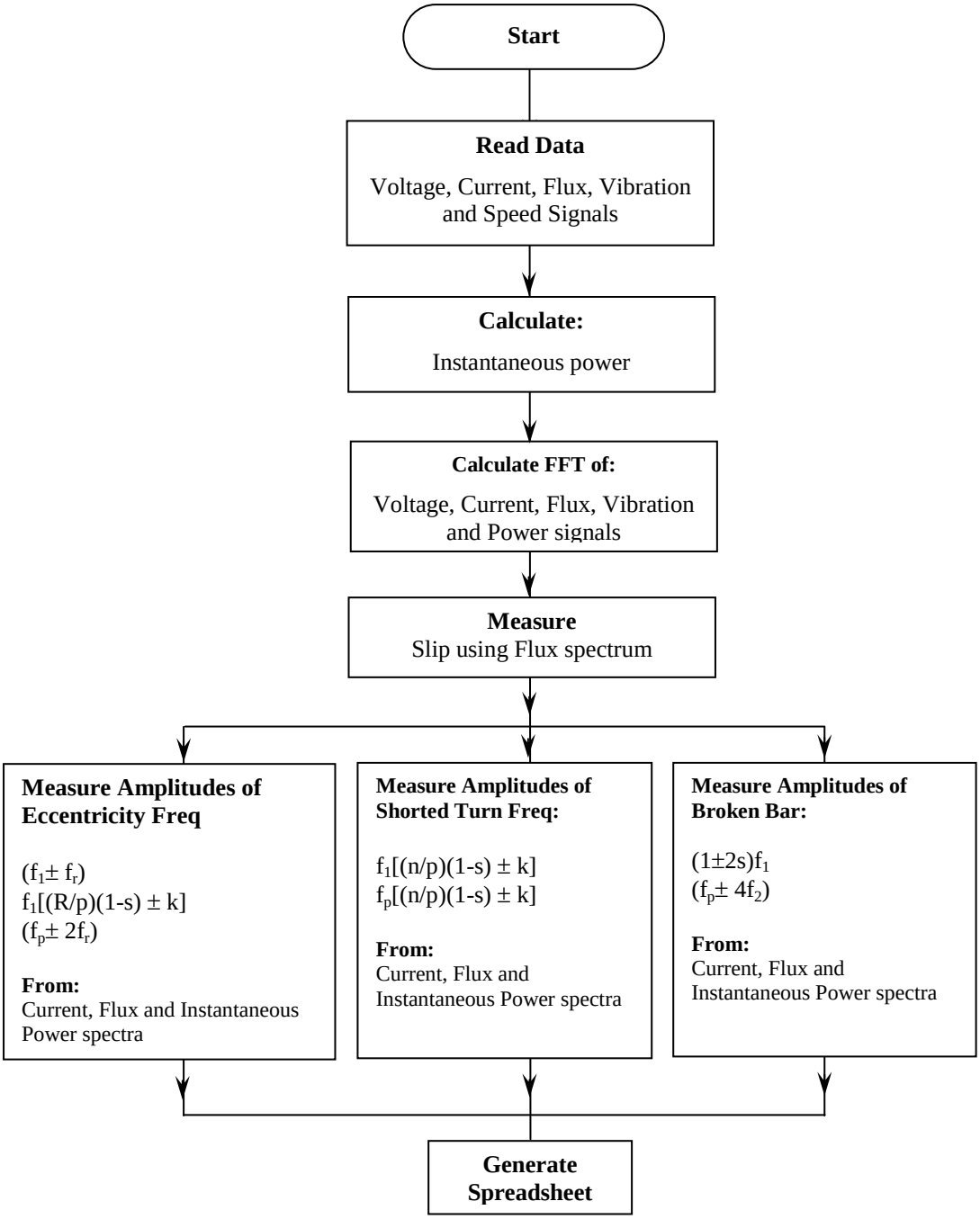

Figure 3.9: Flow chart of MATLAB program developed for spectrum analysis

Since the slip value plays a crucial role in determining the fault frequencies of induction motors, an additional speed signal is acquired to obtain the instantaneous speed

information of the motor. The speed information from speed sensor is used to make sure that the measured slip frequency from the flux spectrum is accurate. Once the slip frequency is calculated, the amplitude of the fault frequency components of the motor is measured by using the spectra of the sensor signals.

A sample spreadsheet file based on the two sampling frequencies of (400 and 8,000 Hz), is shown in Appendix. This gives details of the characteristic fault frequencies of the induction motor under test, which are obtained from the current (phase a and phase b), voltage (phase a and phase b), flux, and speed and vibration sensors. Data from different sensors gives the measured and calculated values of supply frequency, slip frequency, speed, percentage of rated load, current (rms) and voltage (rms). In addition this data will also provide certain fault frequencies that helps to detect the existence of different faults i.e. (broken rotor bars, shorted turns, and eccentricity).

Figures 3.10 and 3.11 show a set of sample test results for broken rotor bar and shorted turn fault frequencies using the software developed. These results were obtained from current and flux spectra of a healthy motor at full-load. For broken rotor bar sampling frequency is 400 Hz whereas for the shorted turn sampling frequency is 8 kHz.

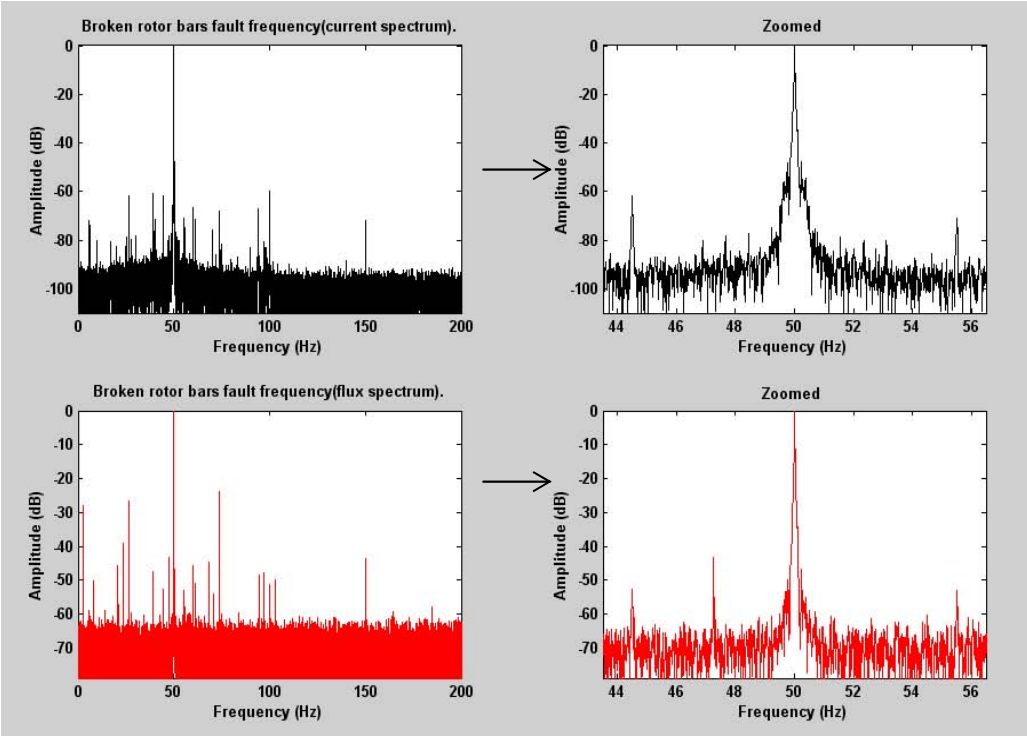

Figure 3.10: Broken rotor bar fault frequencies and their respective amplitudes of a healthy motor from current spectrum (top row) and flux spectrum (bottom row) spectra at full-load.

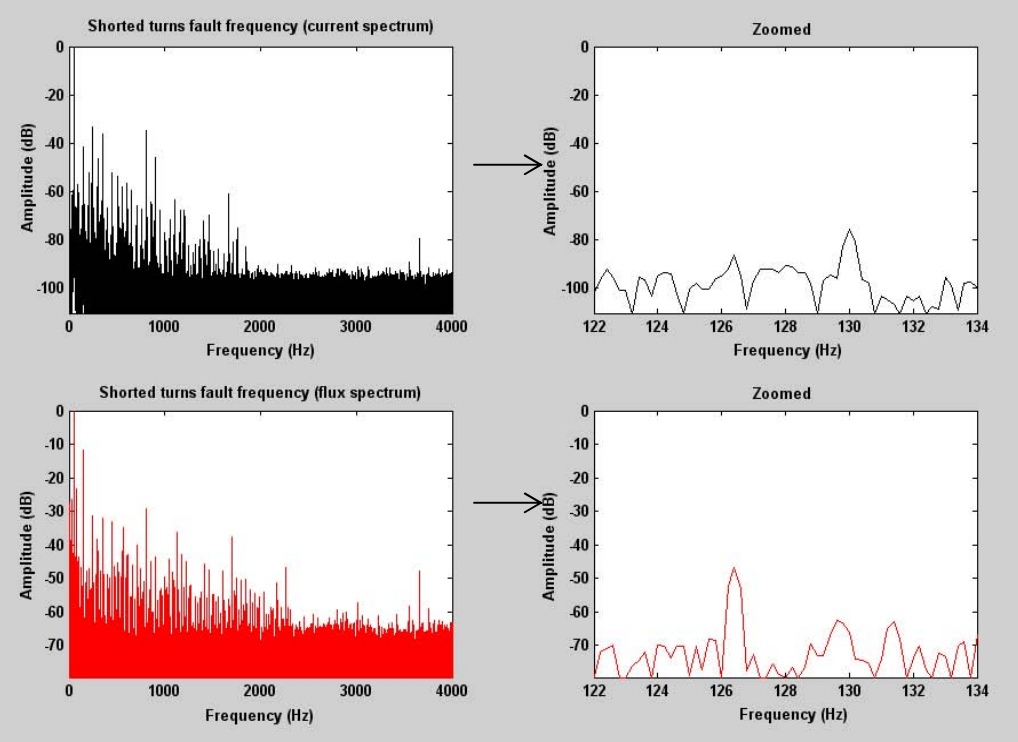

Figure 3.11: Shorted turn fault frequencies and their respective amplitudes of a healthy motor from current spectrum (top row) and flux spectrum (bottom row) spectra at full-load.

3.6 Summary

This chapter described the test set-up, measurement system, and MATLAB program used for this study. The features of the test arrangement are presented. A precision laser alignment tool and a torque wrench were used for accuracy and reliability of the system set-up.

The sensors were sampled at two different sampling rates, a 400 Hz sampling frequency for high-resolution frequency analysis (0.01 Hz resolution), and a high-frequency measurement at 8,000 Hz sampling frequency for signal frequencies up to 2 kHz.

The detail of data-acquisition software used for data collection written using LabVIEW is presented. The fault analysis software developed in MATLAB is used to identify the fault frequencies of induction motor from the current, flux and instantaneous power spectra. This set-up and measurement process is used for obtaining the experimental results shown in later chapters. Figure 3.7 shows the front panel window of the data logging software and Figure 3.8 shows brief descriptions of each part of the panel. It

should be mentioned that because only eight channels are available from the data acquisition-system, the data logging software calculates the third line voltage and current from the captured voltage and current signals.

Chapter 4

Broken Rotor Bar Faults

4.1 Introduction

The basis of any reliable condition monitoring system hinges on understanding the electric, magnetic and mechanical behaviour of a machine in both the healthy and faulty state [34]. An induction machine is highly symmetrical and the presence of any kind of fault modifies its symmetry and produces changes in the measured sensor signals, or more precisely, in the magnitudes of certain "fault" frequencies [4].

As described in Chapter 2, faults in induction motors produce characteristic fault frequencies that can be observed using spectrum analysis of one or more sensor quantities such as current, voltage, vibration and axial leakage flux. The current and voltage can be used to compute the instantaneous power. A summary of these fault frequencies is provided in Table 4.1. This indicates that the fault frequencies in the current and flux are the same but they are different for the instantaneous power.

Table 4.1: Summary of fault frequencies associated with different types of faults.

	Current and Flux	**Instantaneous Power**
1. Broken Bars	$(1 \pm 2s)f_1$	$(f_p \pm 4f_2)$
2. Eccentricity	$(f_1 \pm f_r)$, $f_1[(n/p)(1-s) \pm k)]$	$(f_p \pm 2f_r)$
3. Shorted Turns	$f_1 [(n/p) (1-s) \pm k]$	$f_p [(n/p) (1-s) \pm k]$
4. Misalignment	$(1 \pm 2s)f_1$, $(f_1 \pm f_r)$	$(f_p \pm 4f_2)$, $(f_p \pm 2f_r)$

However, fault frequency components also exist in healthy machines as described in Chapter 2, which makes it difficult to determine whether the measured characteristic fault frequency component amplitudes correspond to a fault or not. The major task in machine condition monitoring is to detect the faults accurately and so provide useful information about the condition of the motor under test.

Therefore, it is important to know what magnitude of the characteristic fault frequency components indicate the severity of different faults in motors. The aim of this chapter is to describe experimental results from healthy and faulty motors examining broken rotor bar faults of differing severities. Tests are done at different values of loading and the current, flux and instantaneous power spectra are analysed. The variations of the test results from healthy machines are also examined from test to test, between phases and between nominally healthy machines.

4.2 Broken Rotor Bar Faults

The rotor bars of an induction motor run axially through the rotor and are joined to the end-rings at both ends. These bars may partially or completely break due to mechanical and electrical stresses, or manufacturing defects.

Broken bars in the rotor create an electrical rotor asymmetry, which produces a stator current component with a frequency of $(1-2s)f_1$. This current component interacts with the fundamental stator current to produce a torque component with a frequency of $2sf_1$. This torque component produces a speed variation at the same frequency.

The interaction of the speed variation and the fundamental stator current produces another frequency component at $(1+2s)f_1$ [34]. Thus broken rotor bars produce $(1\pm2s)f_1$ fault frequency components in the stator current. These fault frequency components can also be found in the axial leakage flux.

It may be difficult to detect partially broken rotor bar faults as the change in the bar resistance due to partially broken rotor bars is small and hence the change in the rotor current distribution is small.

4.2.1 Rotor Bar Fault Detection using Current Spectra

4.2.1.1 Comparison of Healthy and Faulty Current Spectra

Figure 4.1 compares the frequency spectra of the stator current for a healthy 2.2 kW induction motor and a faulty 2.2 kW motor with two broken rotor bars (BRB), at three levels of loading. The frequency spectra are normalised relative to the amplitude of the fundamental component. The circles in the figures indicate the broken rotor bar sideband fault frequencies. The noise level is about −90 dB.

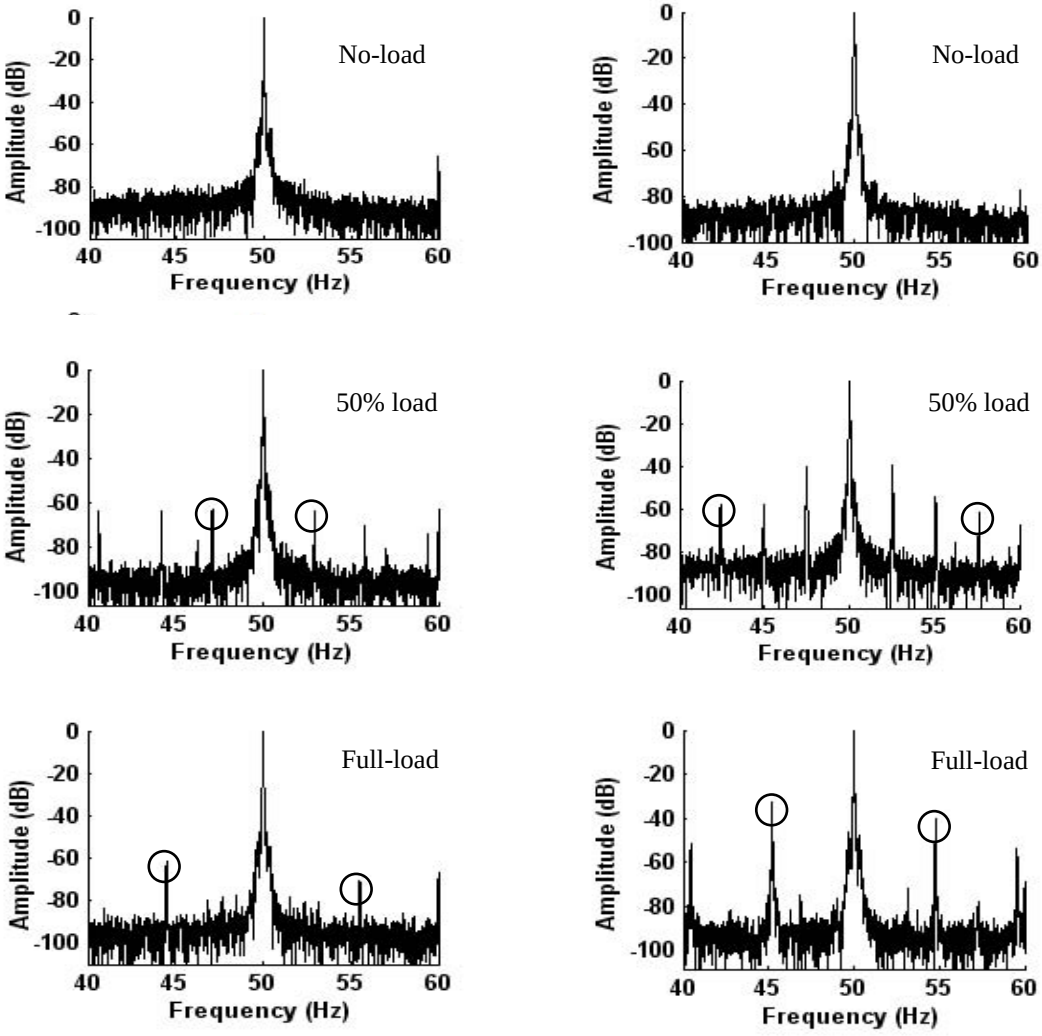

Figure 4.1: Comparison of the current spectrum from a healthy machine (left) and a faulty machine with 2 BRB (right), at no-load, 50% load and full-load. The circles indicate the broken bar sideband components.

At no-load the sidebands are not clearly visible. This is due to the low slip frequency, which means the broken rotor bar sidebands $(1\pm2s)f_1$ are very close to the supply

frequency f_1. By increasing the load the slip frequency is increased and the sideband components are easier to identify. Note that to a first approximation the load and slip frequency are linearly related.

In general, the negative sidebands are either higher or equal in magnitude to the positive sidebands. This is because the negative sidebands are inherently caused by the rotor asymmetry due to broken bars while the positive sidebands are created as a second-order effect.

Figure 4.1 show that there is a substantial increase of over 28 dB in the amplitudes of both the negative and positive sidebands with a two BRB fault at full-load compared to a healthy machine. However, changes in the amplitudes of sidebands are less than 5 dB under the 50% loading condition, which is small. The sidebands are not detectable at no-load. Thus it is clear that the detection of broken bar faults in the stator current is sensitive to the loading condition and works best at higher loads.

4.2.1.2 Broken Bar Fault Frequencies from Current Spectrum

A custom-written programme was used to analyse the raw sensor data, produce the frequency spectrum and automatically locate the appropriate peaks. A sample of the test results output is shown in the Appendix.

Figure 4.2 shows the amplitudes of the positive and negative sidebands in the current spectrum as a function of load for a healthy 2.2 kW machine, and faulty 2.2 kW machines with a partially broken rotor bar, and two and four broken rotor bars.

The figure shows that for two or four broken bars, for loads above about 70% of rated load there is a 30 dB or larger difference in the sideband amplitudes between faulty and healthy machines. At 30% and 50% of rated load the difference is much smaller at about 5 to 10 dB. The sidebands for the four broken bar case are about 5 to 10 dB higher than for the two broken bar case. The negative sidebands are generally higher in amplitude than the positive sidebands except at light loads (30%).

The amplitudes of the sidebands of the healthy machine are relatively constant (with 10 dB) with load, while machines with two or four broken bars show significant increases in the broken bar amplitudes between 50% and 70% of full-load.

The results for the partial broken bar case are not consistent. At higher loads (70% or greater), the sidebands are between 0 and 5 dB higher than the healthy machine. At 50% load the positive sideband dips 10 dB lower compared to the healthy machine, and at 30% load both the positive and negative sidebands are about 10 dB higher than even the four broken bar case.

It is thus difficult to detect partial broken bars using the current spectrum, and also difficult to make broken bar fault severity estimates below 70% of rated load.

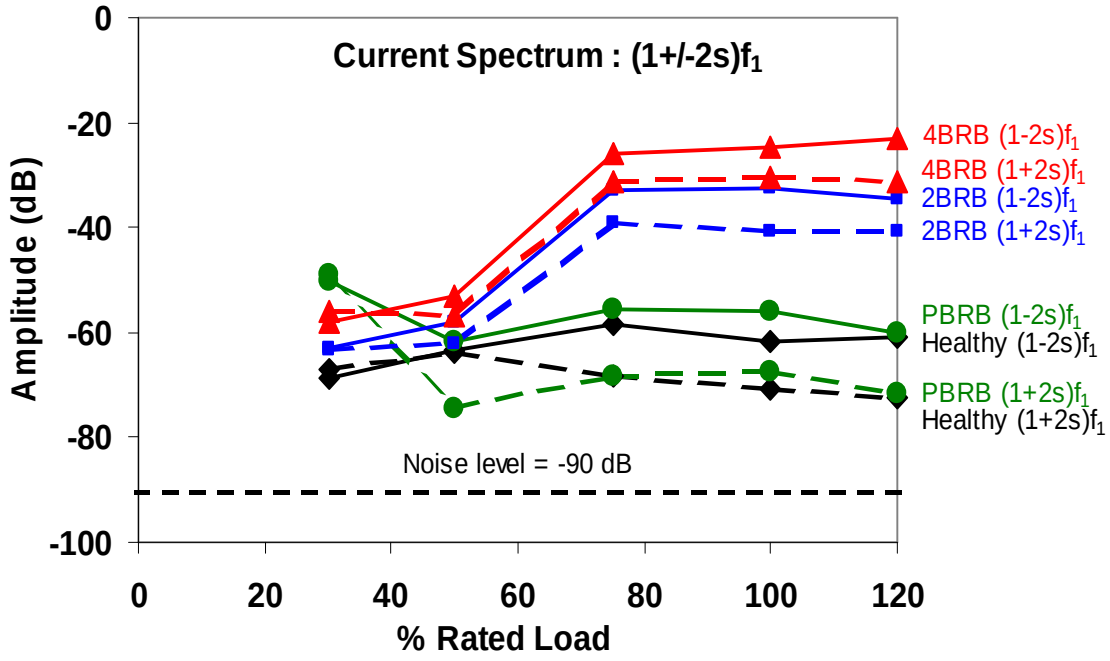

Figure 4.2: Comparison of variation in sidebands amplitudes versus % of rated load of a healthy motor with faulty motors (partial, two and four broken rotor bars) from current spectrum.

4.2.1.3 Current Spectrum Variations for Healthy Machines

When considering the use of any fault frequency component to detect faults and estimate fault severity, it is important to examine the variability in its amplitude to other effects apart from fault severity and load.

This area has often been neglected in the literature on condition monitoring but is very important in the practical application of the results.

In this section we will examine the variability of the healthy motor results to:

- repeatability tests on the same motor (Figure 4.3)

- differences between motors: two nominal identical new motors were tested, (Figure 4.4)
- differences between two of the phases of the same motor (Figure 4.5)

Figure 4.3 shows the test results from a set of three tests on the same healthy motor. Each test was conducted after the motor had been removed from the test arrangement and then replaced, to investigate the consistency of the test set-up as well as the testing procedures. The maximum variation in the sideband amplitudes at any load level was less than about 4 dB, which is relatively small.

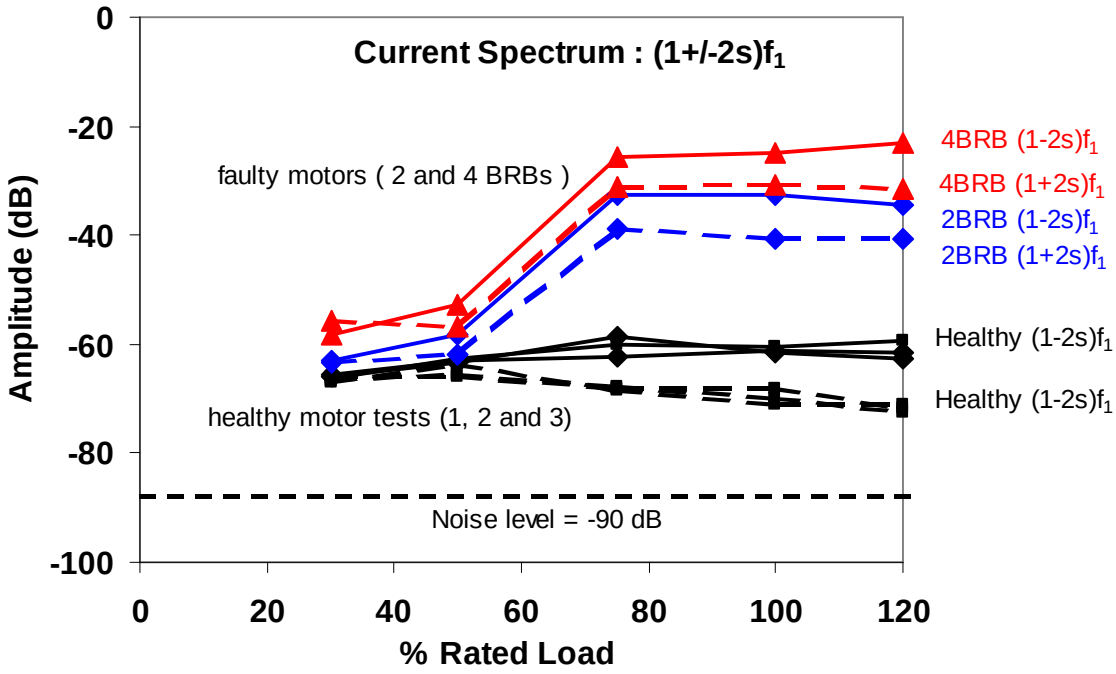

Figure 4.3: Variations in BRB sideband amplitudes for three tests on the same healthy motor. The faulty motor results are shown for reference.

Figure 4.4 shows a comparison between the current sideband amplitudes versus load for two nominally identical healthy motors. It has been concluded from the figure that there is only a small variation between the sideband amplitudes at the same level of loading, up to a maximum of ~ 4 dB.

The variation of the sideband amplitudes between phases A and B of a healthy motor and a faulty motor with 4 BRB are shown in Figure 4.5. The variation at any load level is small (<3 dB) for the healthy case, but there is a larger variation from 5 to 10 dB for the 4 BRB case.

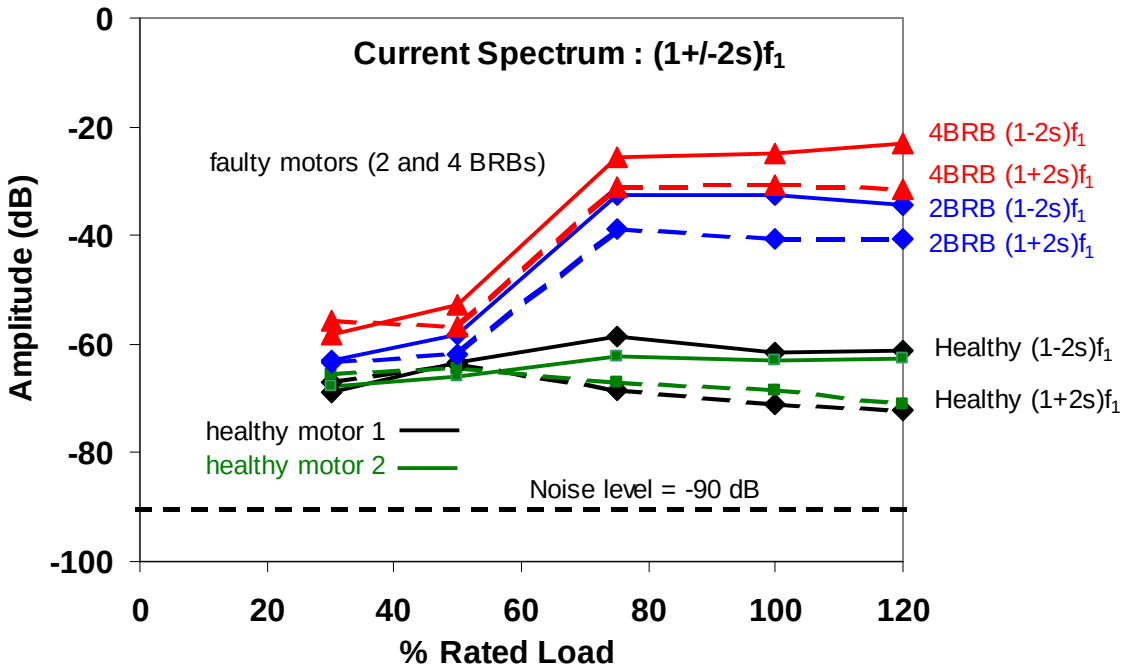

Figure 4.4: Variations in BRB sideband amplitudes for tests on two nominally identical healthy motors. The faulty motor results are shown for reference.

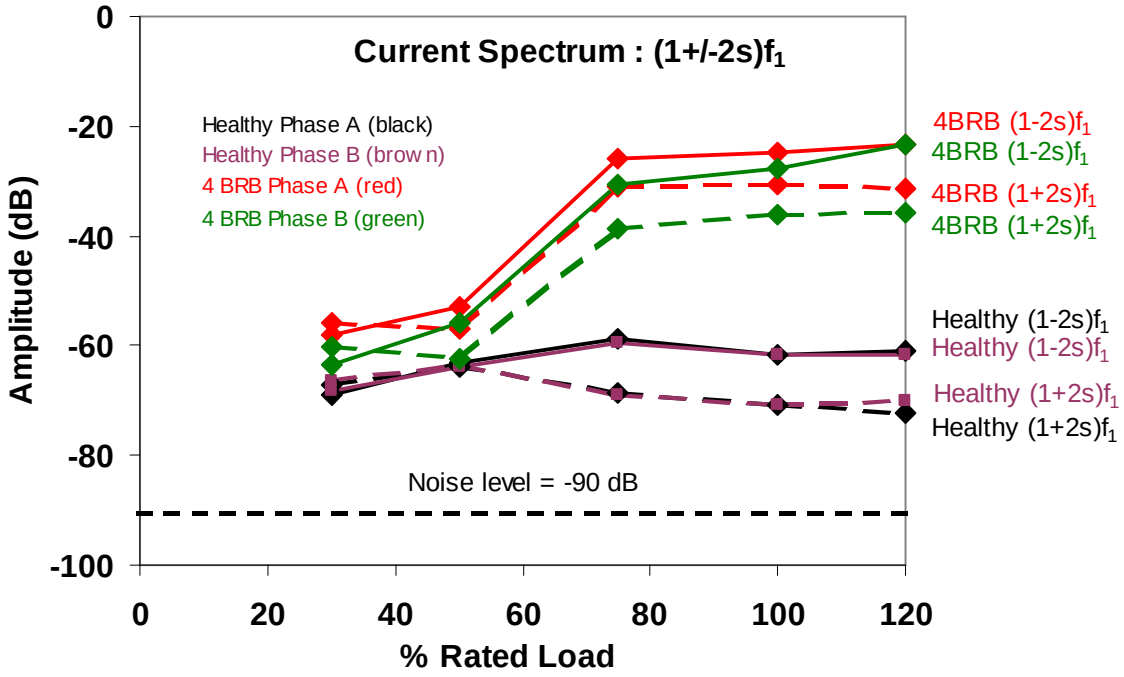

Figure 4.5: Variations in BRB sideband amplitudes of healthy motor 1 and the 4 BRB motor between phases A and B.

In summary, the above results have shown that for the 2.2 kW test machine, faults of two broken bars or more can be readily distinguished from healthy machines for load levels

of 70% and higher. There is some overlap between the results for two and four broken bars and it may be difficult to reliably distinguished between these two fault conditions.

4.2.2 Rotor Bar Fault Detection using Flux Spectrum

4.2.2.1 Comparison of Healthy and Faulty Flux Spectra

The fault frequency sideband components (1±2s) f_1 around the supply frequency f_1 in the flux spectrum were used to detect the broken rotor bar fault.

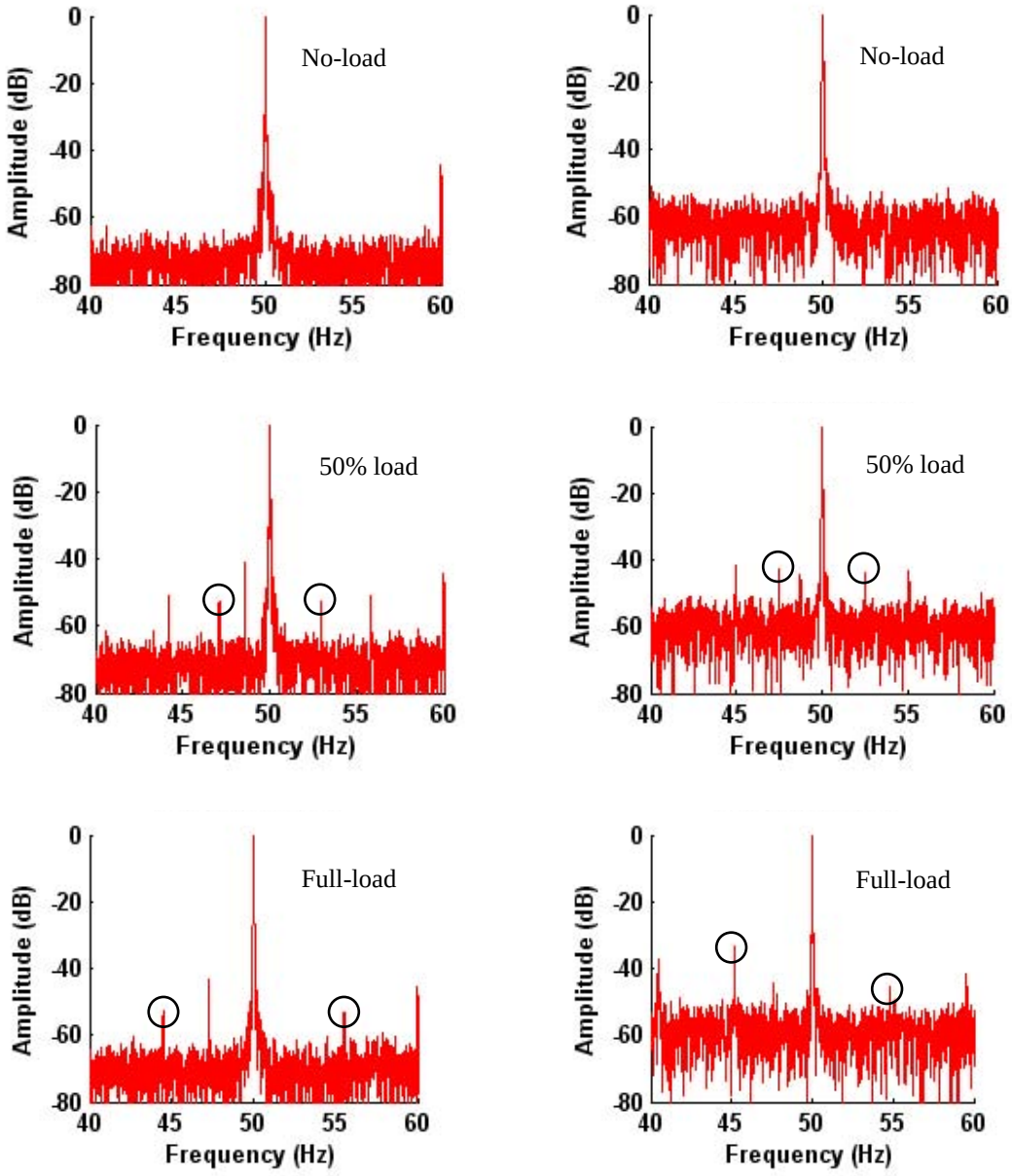

Figure 4.6: Flux spectrum from a healthy machine (left) and a faulty machine with 2 BRB (right), at no-load, 50% and full-load. The circles indicate the sidebands.

The healthy and faulty flux spectra in Figure 4.6 show similar trends to the current spectra. The fault frequencies are not visible at no-load but are clearly visible at higher loads. The noise level is about –90 dB in the current spectra.

The change in the broken rotor bar sideband amplitudes between the healthy and faulty motor is small (<2 dB) at 50% load. However at full-load, a noticeable increase in the amplitudes of both the negative (20 dB) and positive (8 dB) sideband components were observed.

4.2.2.2 Broken Bar Fault Frequencies from Flux Spectrum

Figure 4.7 illustrates the amplitude of the fault frequency sideband components of the flux spectra around the supply frequency range, when the machine is operating at different level of loads for various broken bar fault severities.

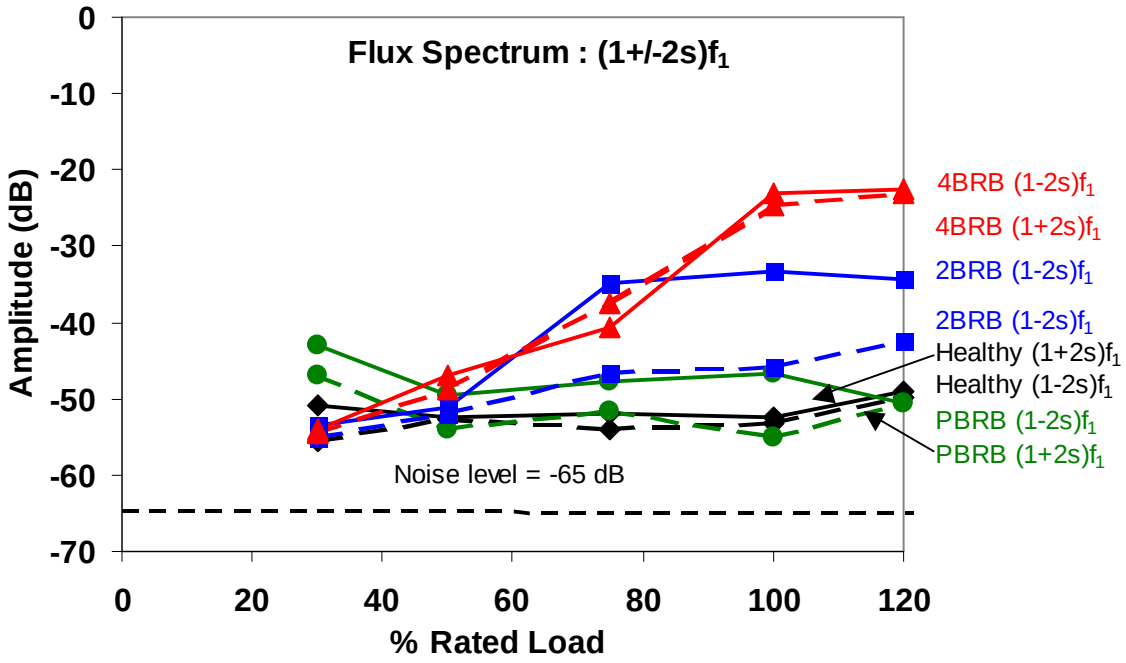

Figure 4.7: Comparison of variations in sideband amplitudes versus % of rated load of healthy motor with faulty motors (partial, two and four broken rotor bars) from flux spectrum.

As was found with the current spectra results, broken bar faults can be detected only at higher loads (70% and above). At 50% load the change in the fault frequency components is less than 2 dB.

For loads above 70% of rated load the differences in the sideband amplitudes were found to be about 20 dB for the negative sideband and 8 dB for the positive sideband. This variation is less than the variation at the same level of loading in the current spectra.

The results in Figure 4.7 show that the negative sidebands (solid lines) generally indicate larger change from the healthy machine for a given fault severity and loading condition, while the positive sidebands (dashed lines) show a smaller changes but the change is perhaps easier to correlate to fault severity at high load level.

The amplitudes of the sideband components for the 4 BRB fault at high load show a significant increase of about 13 dB respectively, when compared with the motor having two broken rotor bars. It can be concluded from the figure that the use of the flux signal also provides useful information to detect BRB faults.

It may be possible to detect the partial BRB faults using the negative sideband as this shows a significant increase over the healthy motor results except at 120% load condition. More investigation of this condition is required.

4.2.2.3 Flux Spectrum Variations for Healthy machines

Figure 4.8 represents the test results of three consecutive tests on the same healthy motor. Each test was conducted after the motor had been removed and then replaced, to investigate the consistency of the test set-up as well as the testing procedures.

The maximum variation in the sideband amplitudes was found to be 4 dB at any load level, which is small and hence the test procedure has good repeatability.

A comparison of the variation in the amplitudes of the sideband components versus % of rated load for two similar rating (2.2 kW) of motors is shown in Figure 4.9. The variations at the any level of loading were found to be less than 4 dB, which is not significant.

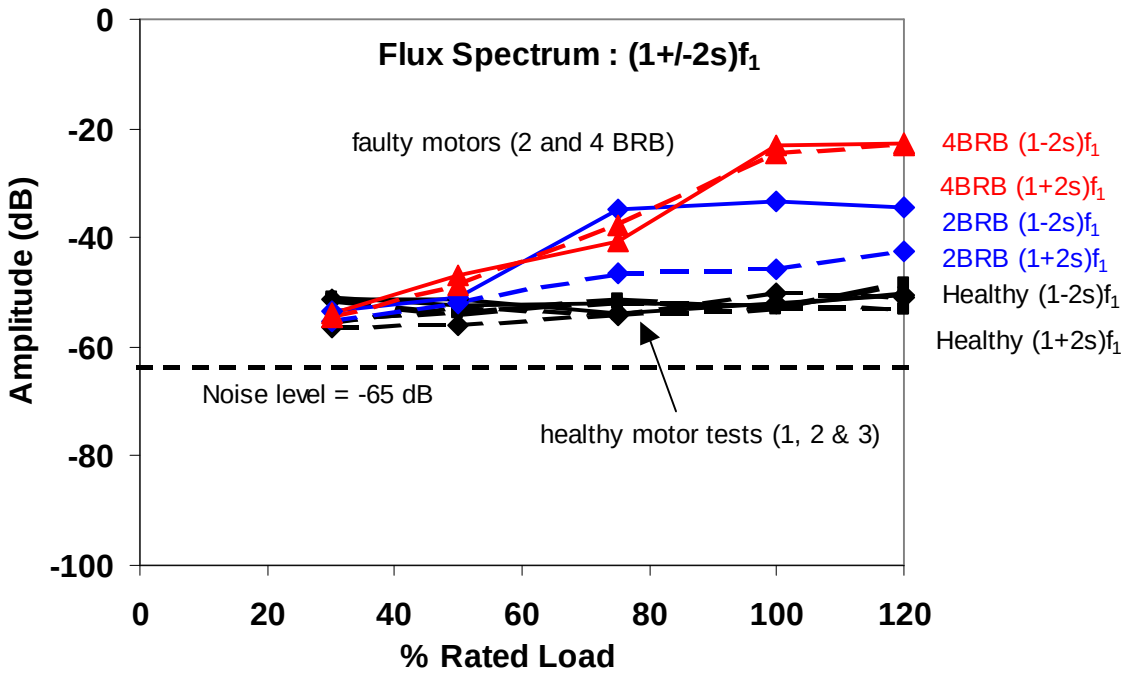

Figure 4.8: Variations in BRB sideband amplitudes for three tests on the same healthy motor from flux spectrum. The faulty motor results are shown for reference.

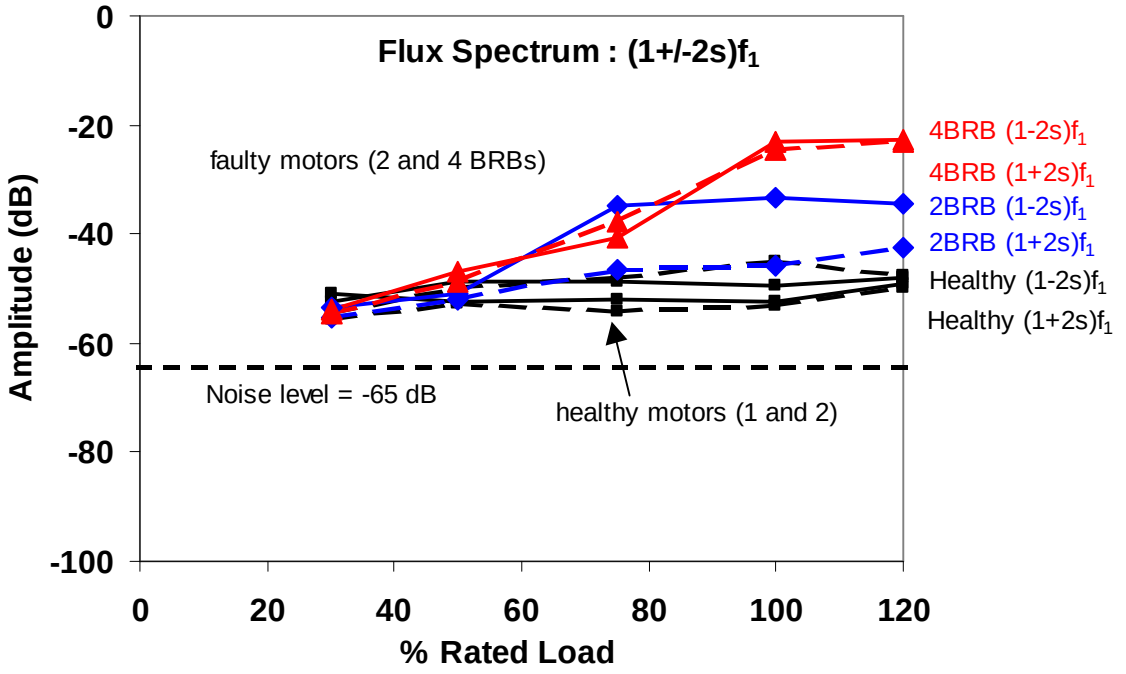

Figure 4.9: Variations in BRB sideband amplitudes for tests on two nominal identical healthy motors from flux spectrum. The faulty motor results are shown for reference.

4.2.3 Rotor Bar Fault Detection using Instantaneous Power

4.2.3.1 Comparison of Healthy and Faulty Instantaneous Power Spectra

The comparison of the frequency spectra of the instantaneous power for a healthy motor and a motor with two BRB is shown in Figure 4.10. The severity of the broken rotor bars is indicated by the magnitudes of the fault frequency sideband components.

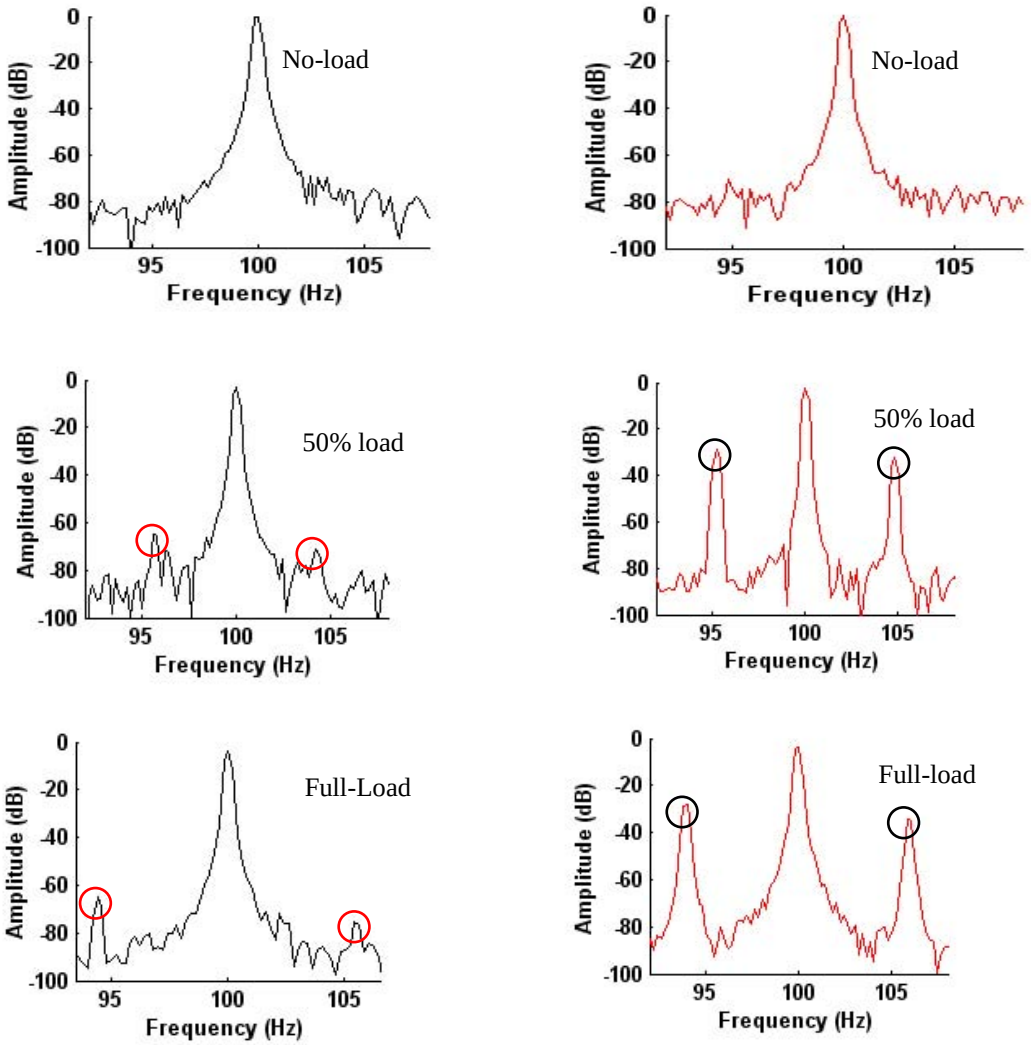

Figure 4.10: Instantaneous power spectra from a healthy machine (left) and a faulty machine with 2BRB (right), at no-load, 50% and at full-load. The circles indicate the sidebands

As was seen with the current and flux spectra, the negative and positive sideband components of the healthy and faulty motor were not visible at no-load. The noise level relative to the amplitude of the 100 Hz fundamental component is about –80 dB.

As the load on the motor is increased, the slip frequency also increases which makes the sideband components more visible in the spectra. At full-load it was found that the fault motor sideband amplitudes were more than 35 dB larger than that of the healthy motor, which is very promising.

4.2.3.2 Broken Bar Fault Frequencies from Instantaneous Power Spectra

The frequency spectrum of the instantaneous power is used to identify the broken rotor bar faults in the machine. The broken rotor bar fault frequencies under different load tests were investigated both in the healthy motor and with motors with varying degrees of broken rotor bar faults as shown in Figure 4.11.

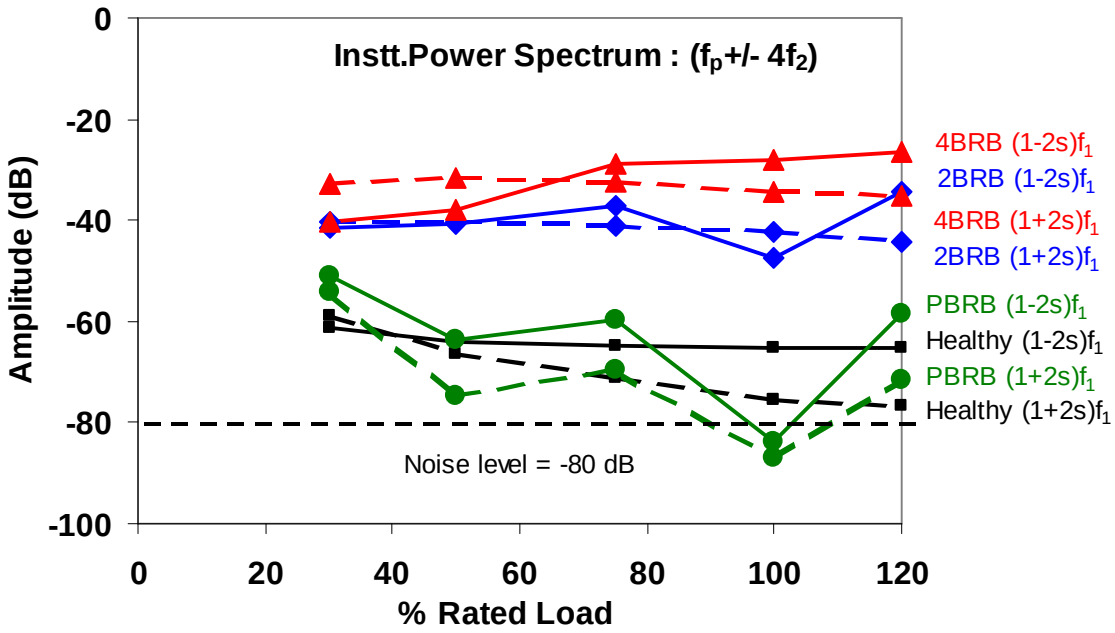

Figure 4.11: Comparison of variations in sideband amplitudes versus % of rated load of healthy motor with faulty motors (partial, two and four broken rotor bars) from instantaneous power spectrum.

The results in the above figure show a much clearer separation than previously observed with the current and flux signals between healthy and fault machines. Apart from the partial results, the healthy and faulty results for the instantaneous power signal show generally less variation with load than the results for the current and flux spectra.

This makes it easier to detect faults, as there is a more consistent difference between the healthy and faulty cases. In particular it is possible to detect two and four BRB faults

even at 30% compared to 70% load for the current and flux spectra. With two BRB the difference between the healthy and faulty results is about 20 to 25 dB while with four BRB it can approach 40 dB at higher load levels.

The partial BRB results varied inconsistently with load tests and substantially overlap the amplitudes of the healthy motor. Therefore, it is difficult to detect the partial broken rotor bar accurately using instantaneous power as a diagnostic medium.

These significant variations between healthy and faulty motors both at light and high loads show the usefulness of the instantaneous power signal as medium to detect BRB faults over the current and flux spectra.

4.2.3.3 Instantaneous Power Spectrum Variations for Healthy Machines

As with the current and flux signals, we will now explore the variability of the instantaneous power in its amplitude to other effects apart from fault severity and load. Figure 4.12 shows the variation in the sideband amplitudes as a function of load based on three tests on the same healthy motor. The variation was found to be less than 4 dB.

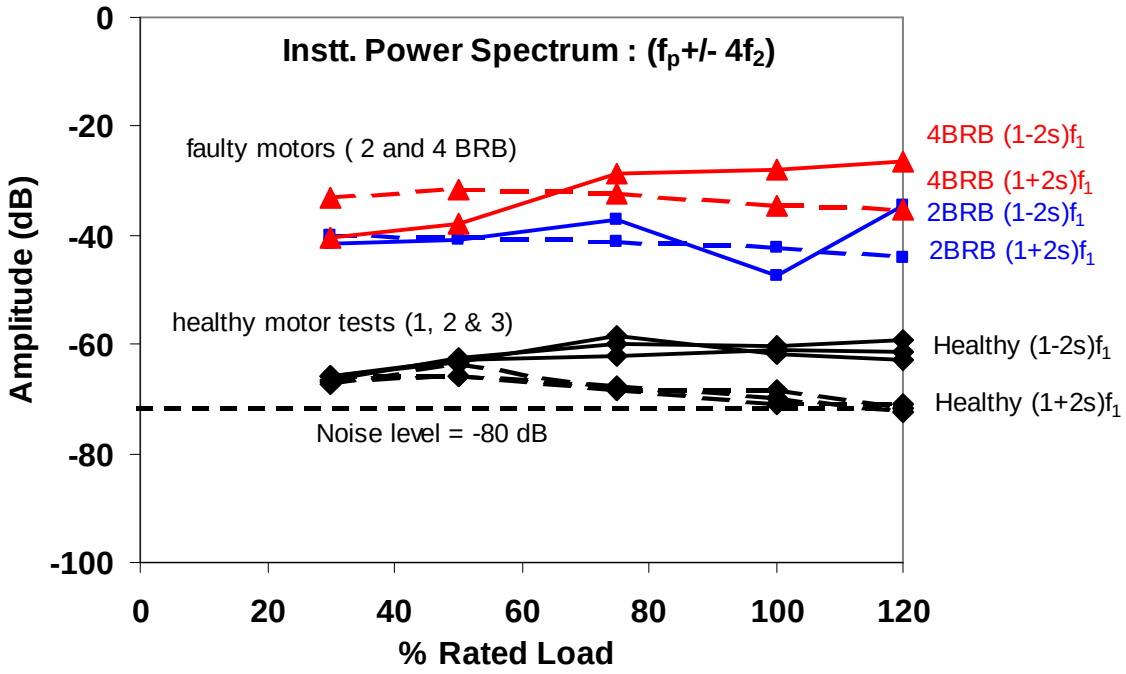

Figure 4.12: Variations in BRB sideband amplitudes for three tests on the same healthy motor. The faulty motor results are shown for reference.

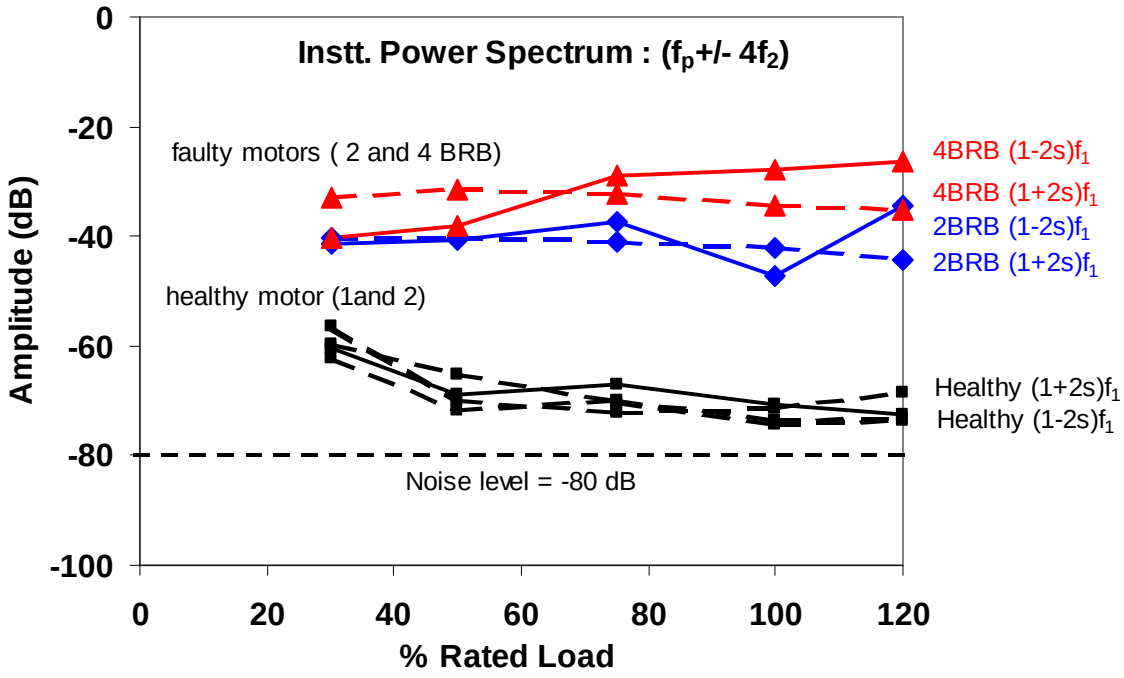

Figure 4.13: Variations in BRB sideband amplitudes for tests on two identical healthy motors. The faulty motor results are shown for reference.

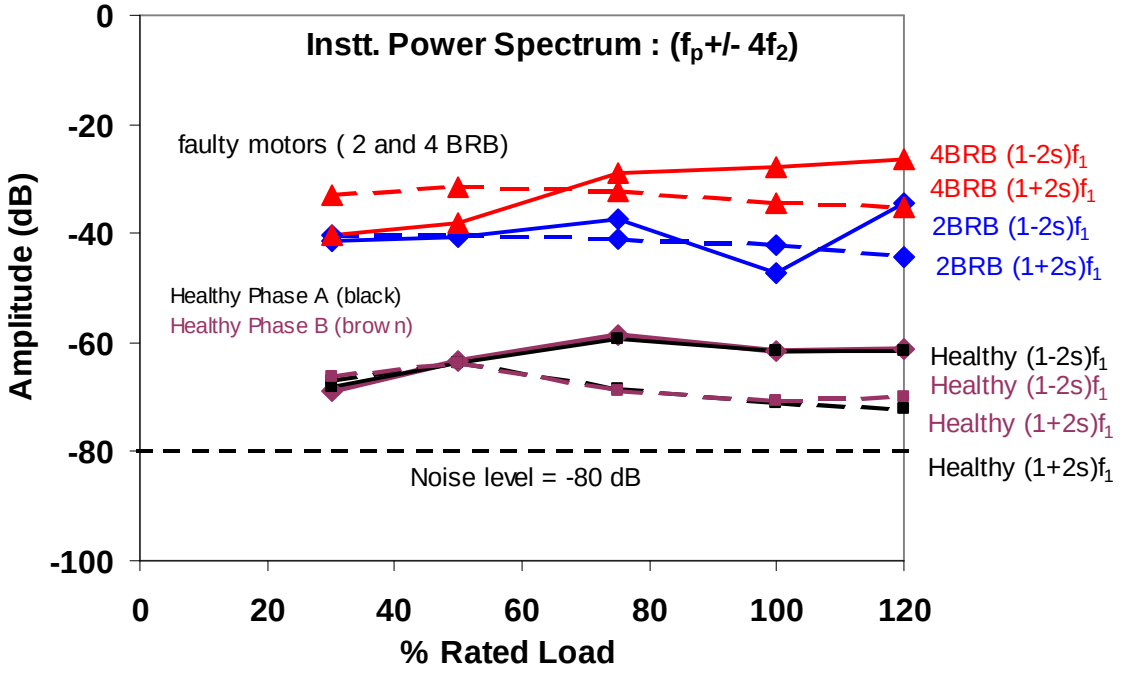

Figure 4.14: Variations in BRB sideband amplitudes of healthy motor 1 between phases A and B. The faulty motor results are shown for reference.

Figure 4.13 shows a comparison between the instantaneous power sideband amplitudes versus % of rated load for two nominally identical healthy motors. A small variation of 4 dB at any level of loading was found, which is small. The variation between the sideband amplitudes between phases A and B of the same healthy motor is shown in Figure 4.14. The variation at any load value is less than 3 dB.

The investigation of the variations in the amplitudes of sideband components of healthy motors due to other effects apart from severity and load, as shown in the Figures 4.12, 4.13 and 4.14 has been confirmed the repeatability of the tests results and as well as the reliability of experimental set-up.

4.2.4 Analysis of Broken Rotor Bar Fault Frequencies from Current, Flux and Instantaneous Power spectra

We investigated the use of the flux, current and instantaneous power signals to detect broken rotor bar faults. The result from the flux spectrum showed it is not suitable to detect the broken rotor bar faults. The current spectrum showed reliable results at higher levels of load (>50%). The instantaneous power spectra showed the best result over the full range of loads tested (from 30% to 120% loading).

Detecting broken rotor bar at light load from current is difficult because of the small currents in the rotor bars and the low slip frequency. In addition, the results for the partial broken rotor bar case are not consistent. It is thus difficult to detect partial broken rotor bar using current, flux or instantaneous power spectra

In summary, the use of instantaneous power signal showed the best features to reliably detect and estimate the severity of broken rotor bar faults over a wide range of loading.

For each of the above signals, tests were also performed to check its variability in healthy motors due to: test repeatability, differences between nominally identical motors, and differences between the phases of the same motor. The results confirm the test repeatability and reliability of the experimental set-up and testing procedures.

The comparison of features of fault frequency components from current, flux and instantaneous power spectra to detect the broken rotor bar faults at different level of load tests is shown in Table 4.2.

Table 4.2: Comparison of healthy and faulty motors results to detect the broken rotor bar faults using current, flux and instantaneous power spectra.

Sensor Signal	**Fault**	**Minimum load when the variations between the healthy and faulty motor is >20 dB**	**Amplitude difference between the negative sideband of healthy and faulty motor in (dB)**	**Amplitude difference between the positive sideband of healthy and faulty motor in (dB)**	**Comments**
Current	PBRB	Not found	Not found	Not found	Not applicable.
	2BRB	75%	26	30	Suitable to detect BRB faults only at high loads and the machines have one or more broken rotor bars.
	4BRB	75%	33	38	
Flux	PBRB	Not found	Not found	Not found	Not applicable.
	2BRB	100% load	Not found	Not found	Not applicable.
	4BRB	100%	30	28	Suitable but not preferable because it cannot be able to detect faults when the number of broken rotor bars is than 4.
Instt. Power	PBRB	Not found	Not found	Not found	Not applicable
	2BRB	30%	21	20	Suitable and preferable to detect BRB faults over a wide range of loads when the machines have one or more broken rotor bars.
	4BRB	30%	22	26	

Chapter 5

Static Eccentricity Faults

5.1 Static Eccentricity Faults

Eccentricity is defined as unbalanced airgap between the rotor and stator of an induction motor. It may be caused by incorrect position of the stator or rotor. In static airgap eccentricity, the angular position of the minimal radial airgap length is fixed in space. As indicated previously in Section 1.3.4, this may be due to ovality of the stator core or incorrect positioning of the rotor or stator.

Figure 5.1 shows some modification made for the induction motor under test conditions. This motor served as the basis of analysing the fault frequency sideband components under static eccentricity faults.

In this set-up the position of the minimal radial air-gap length was fixed in space. Incorrect positioning of the rotor or stator for any reason may cause static air-gap eccentricity to emerge.

Therefore to create a state of airgap eccentricity, two rotational knobs one at driving-end of the motor and another one at non-driving-end of the motor were used.

By rotating these knobs in an upward or downward direction the position of minimal airgap length in space is altered to create an airgap eccentricity. The total air-gap between the rotor and stator of a machine is 0.8 mm (0.4 mm on both sides).

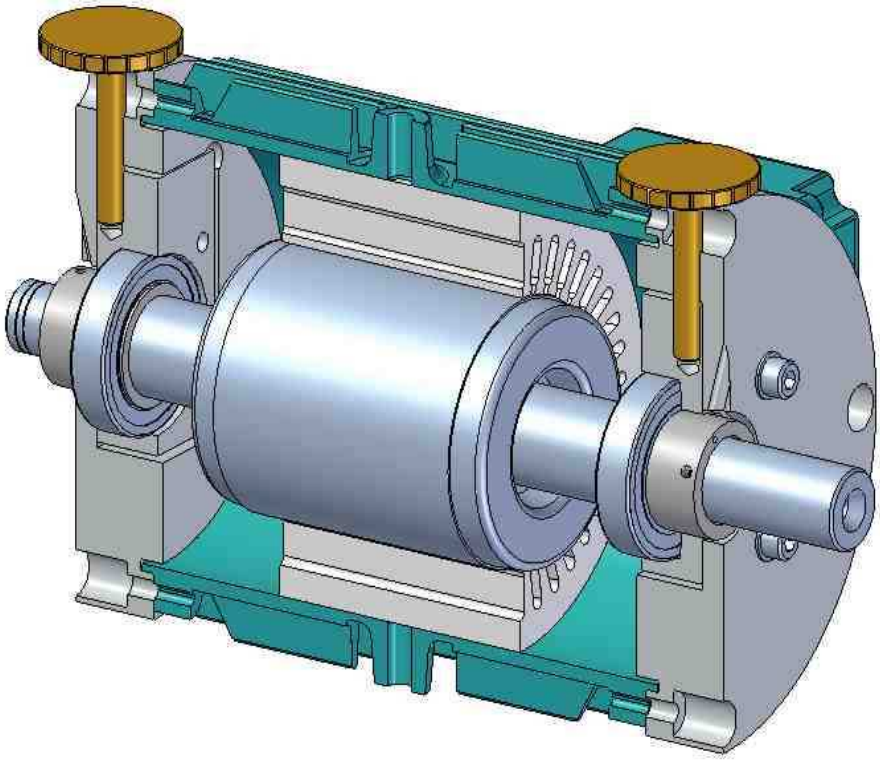

Figure 5.1: Test motor with two rotational knobs that are used to create unequal air-gap between stator and rotor.

Different combinations are used to analyse the eccentricity fault frequencies from current, flux and instantaneous power spectra under different load tests and compare the results to a healthy motor.

The different levels of eccentricity to be considered are as follows:

- Non-driving and driving-end is at 0.1mm and non-driving-end and non-driving-end is at 0.3 mm respectively.
- Non-driving-end is fix at 0.1mm (downward) and driving-end is at 0.2mm and 0.3mm upward (direction).
- Non driving-end is fix at 0.3mm (downward) and driving-end is at 0.2mm and 0.3mm (upward) direction.

To detect eccentricity faults using the frequency spectrum of current, flux and instantaneous power signal, combinations of the airgap at both driving-end (DE) and at non-driving- end (NDE) under different loading conditions will be used (Table 5.1).

Table 5.1: Different combinations of airgap eccentricity developed in the machine to study the severity of eccentricity faults under different loading conditions.

Airgap	**Driving-End (mm)**				
Non-Driving-End (mm)		**+0**	**+0.1**	**+0.2**	**+0.3**
	0	X	X	X	X
	-0.1	X	X	X	X
	-0.2	X	X	X	X
	-0.3	X	X	X	X

5.2 Detection of Eccentricity Fault Frequencies

As discussed earlier, variations in the fault frequencies were used to locate different faults in induction machines. Few authors [1,2,3] suggested eccentricity faults produce fault frequency components at $(f_1 \pm f_r)$ and at $f_1[(R/p)(1-s) \pm k]$ in the current, flux and instantaneous power spectra. These components are centred on the rotor slot passing frequency Rf_r (R is the number of rotor bars) and integers k for different values ±1, ±3, and ±5. However, accurate detection of eccentricity faults heavily depends on the accurate measurement of slip frequency sf_1 and rotor frequency f_r. Therefore, it is important to understand how to locate the correct eccentricity fault frequency peaks in the frequency spectrum of current, flux and instantaneous power signals.

At this stage it is thus important to understand the different steps involved in locating eccentricity faults in the frequency spectrum using fault frequencies from different signals. To explain these steps, a healthy motor (2.2 kW) under full-load test is used to identify the correct fault frequency peaks in the current spectrum with the help of slip frequency sf_1 measured from flux spectra and slot passing frequency, which is measured from vibration spectra. It should be noted that a similar method is used to detect the faults using flux and instantaneous power spectra.

- Measured supply frequency f_1 from current spectra as described in section 2.3 of Chapter 2, which is in this case is 50.03 Hz.
- Measured slip frequency $sf_1=f_2$ from flux spectra as described in section 2.4 of Chapter 2, which is in this case is 2.29 Hz.
- Measured rotor frequency f_r from vibration spectra as shown in Figure 5.2, which is 23.87 Hz.

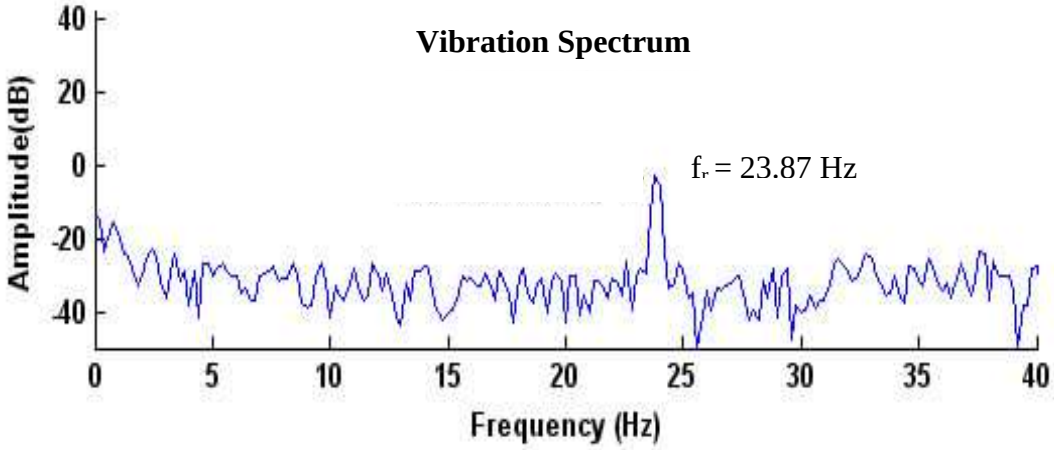

Figure 5.2: Frequency spectrum of vibration signal showing the rotor frequency.

- Measured slot passing frequency using vibration spectrum, which is Rf_r=763.84 Hz as shown in Figure 5.3 (top).
- Measured fault frequencies related peaks and their respective sideband amplitudes for different values of k in the current spectra are shown in Figure 5.3 (bottom), dashed lines represent the fault frequencies peaks.

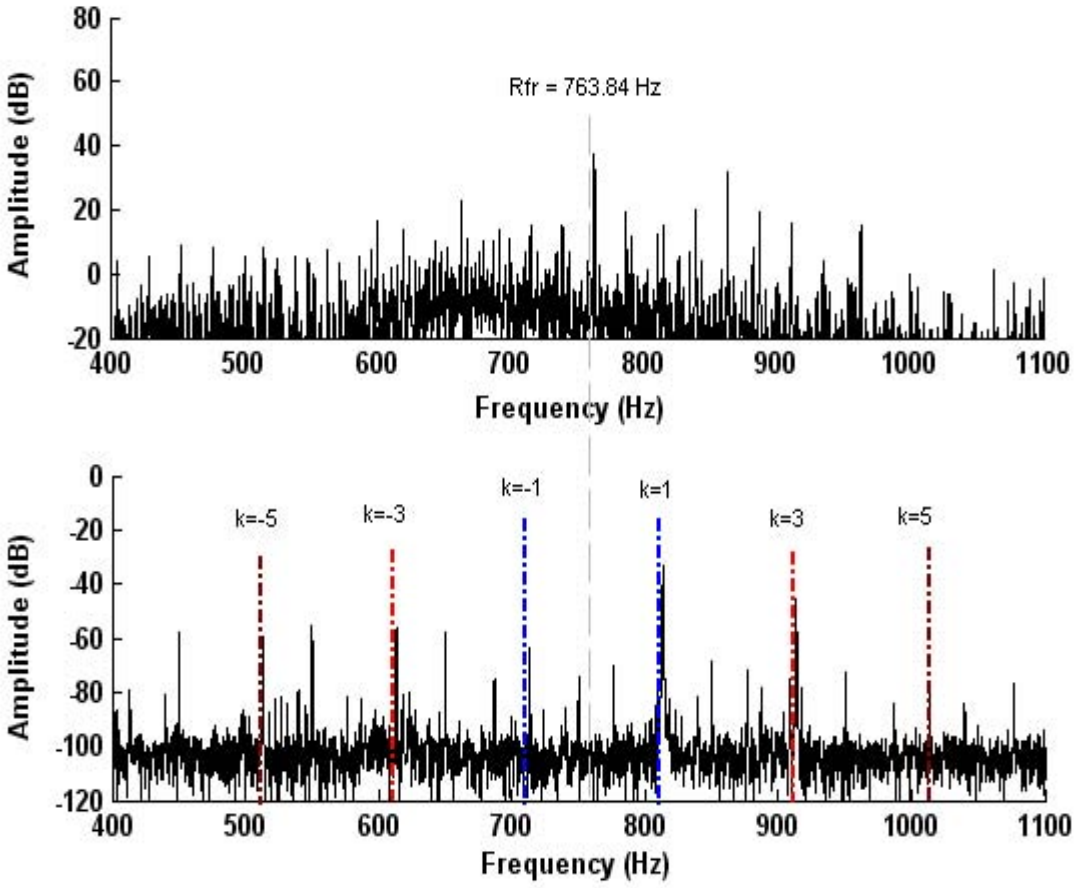

Figure 5.3: Frequency spectrum of vibration signal (top) showing slot passing frequency and current spectrum (bottom) showing eccentricity fault frequency peaks.

To confirm the accuracy and reliability of fault frequency components detecting the eccentricity faults using current, flux and instantaneous power signals, these measured values of rotor and slot passing frequencies from current, flux and instantaneous power spectra should be same or very close to the calculated values of the rotor and slot passing frequencies.

It is important to calculate the rotor and slot passing frequencies of the same healthy motor. Checking the utilisation of fault frequency peaks may lead to eccentricity faults being detected in the frequency spectrum of current, flux and instantaneous power signals. Calculation steps are as follows:

- To calculate the rotor frequency from $f_r = (f_1 - sf_1)/p$, the slip frequency sf_1 is calculated from equation 1.2.4, which is 23. 87 Hz.
- Than calculate the slot passing frequency by using the relationship Rf_r that is equal to 763.84 Hz (when the number of rotor bars R = 32).

It has been concluded from the results, that there is almost no difference between the measured and calculated values of rotor and slot passing frequencies, which confirm the accuracy and reliability of characteristics fault frequency components to detect the eccentricity faults using current, flux and instantaneous power spectra.

The following section, we will consider the current, flux and instantaneous power signals to detect the eccentricity faults as shown in Table 5.1 under different levels of loading.

5.2.1 Eccentricity Fault Detection using ($f_1 \pm f_r$) from Current Spectra

5.2.1.1 Comparison of Healthy and Faulty Current Spectra

The comparison of eccentricity sideband components ($f_1 \pm f_r$) for healthy and faulty motor with airgap of (-0.1mm at NDE and +0.3mm at DE) at 30% load and at full-load is shown in Figure 5.4. The circles indicate the eccentricity sideband components. The noise level is about –90 dB.

It can be concluded from Figure 5.4, that, variation in the amplitudes of sideband components of a faulty motor at 30% load is more when compared to the faulty motor at full-load. In addition, amplitudes of the fault frequencies decreased as the load on the

motor increase. The high amplitudes of fault frequency peaks can be helpful in assessing the motor's condition.

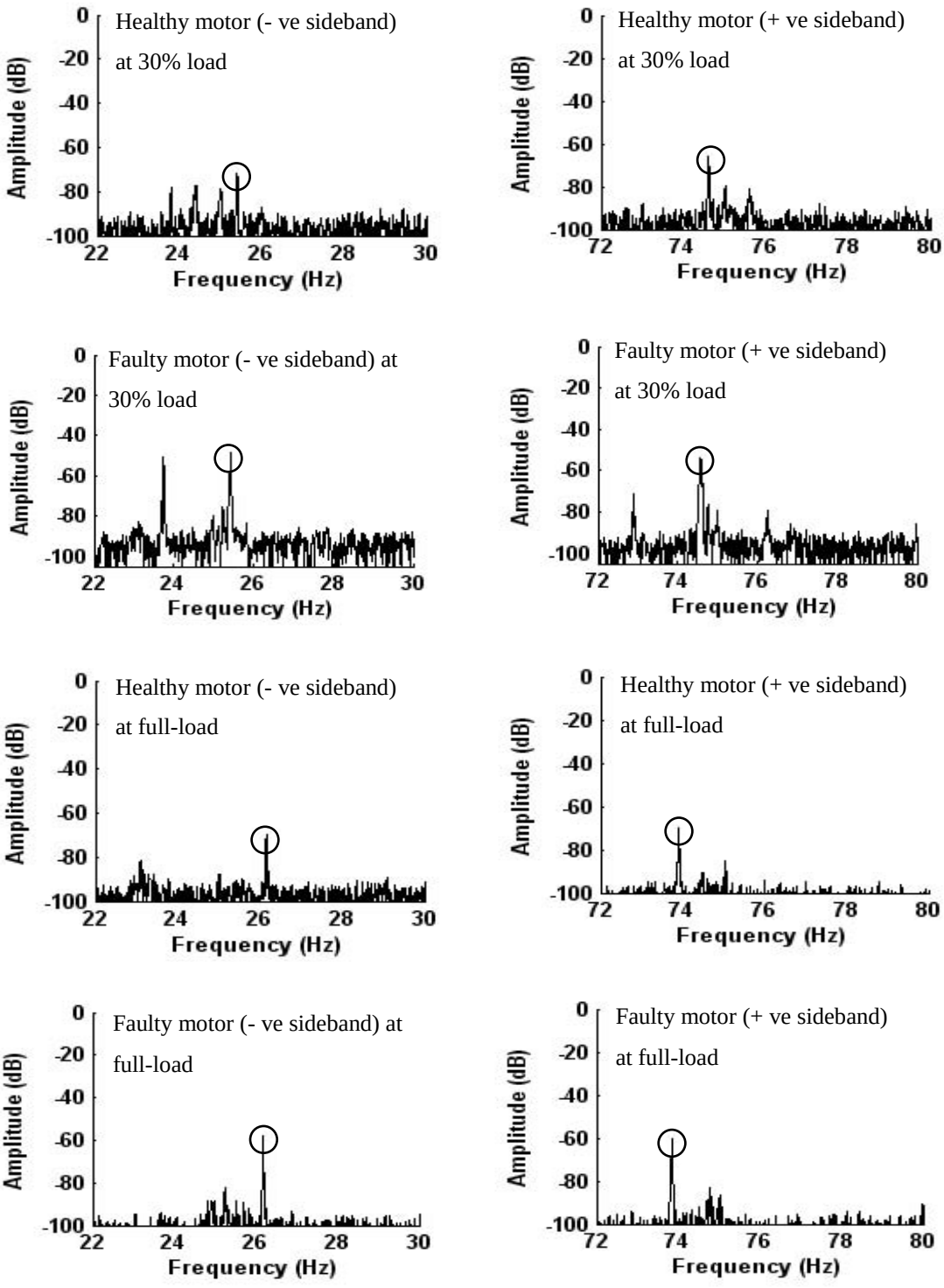

Figure 5.4: Current spectrum from a healthy motor (row 1 and 3) and a faulty motor (row 2 and 4) at 30% and full-load respectively.

5.2.1.2 Eccentricity Fault Frequencies from Current Spectra

The variations in the amplitudes of eccentricity fault frequency components ($f_1 \pm f_r$) between the healthy motor (zero eccentricity) and faulty motors with eccentricity (>0.05 mm) were found to be more than (20 dB), which is significant and clearly visible at light load as shown in Figure 5.5. The results indicate the consistent increase in the fault frequency components with the increase in eccentricity levels, making it easier to differentiate between healthy and faulty motors using current spectrum.

Figure 5.6 also shows that the variations in the sideband amplitudes between the healthy and faulty motors at full-load are consistent when the airgap is (>0.05 mm). However, a slight declined in the variations of sideband amplitudes was found between the healthy and faulty motors under full-load test conditions when compared to the variations for the same motors running at 30% load.

The above results present that the eccentricity fault frequency components are suitable to detect eccentricity faults at any level of eccentricity under any level of loading conditions (specifically at light loads).

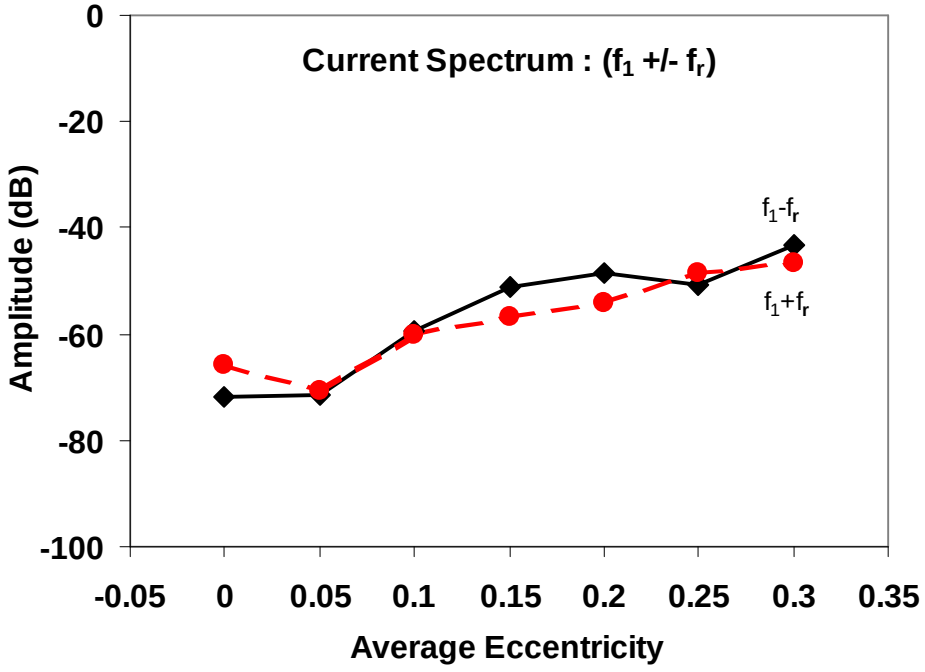

Figure 5.5: Comparison of variations in the sideband amplitudes versus average eccentricity at 30% load (top) and at full-load (bottom) between the healthy and faulty motors from current spectrum

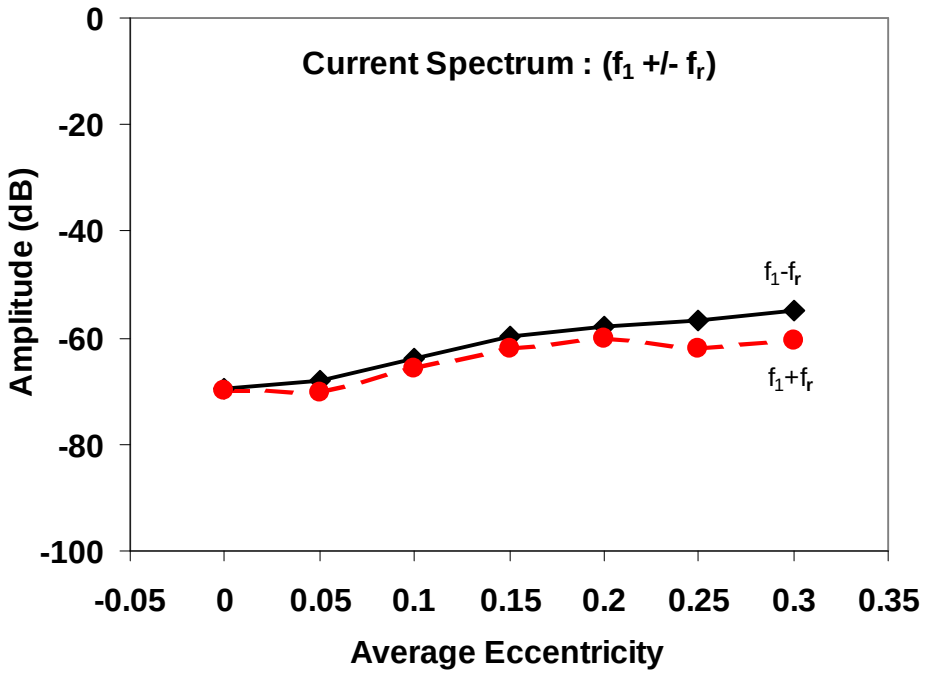

Figure 5.6: Comparison of variations in the sideband amplitudes versus average eccentricity at 30% load (top) and at full-load (bottom) between the healthy and faulty motors from current spectrum

Since the current spectrum is suitable for finding the eccentricity faults, it is important to check how the current signal in its amplitude varies from the other effects apart from fault severity and load. For this reason we consider the same three cases as outlined in Section 4.2.1.3.

5.2.1.3 Current Spectrum Variations for healthy Machines

Figure 5.7 represents the results of two consecutive tests on the same motor. The maximum variations in the amplitudes of fault frequency components were found to be 4 dB at any load level, which is not significant.

The comparison between the sideband amplitudes for two nominal identical healthy motors can provide small variations, which is less than 4 dB as shown in Figure 5.8.

Similarly, the variations in the sideband amplitudes between phases A and B of a healthy and a faulty motor at any load level were found to be less than 2 dB as shown in Figure 5.9, which is almost negligible. The figures demonstrate the repeatability of the test results and reliability of experimental set-up used to detect the eccentricity faults with fault frequency components ($f_1 \pm f_r$) in the current spectrum.

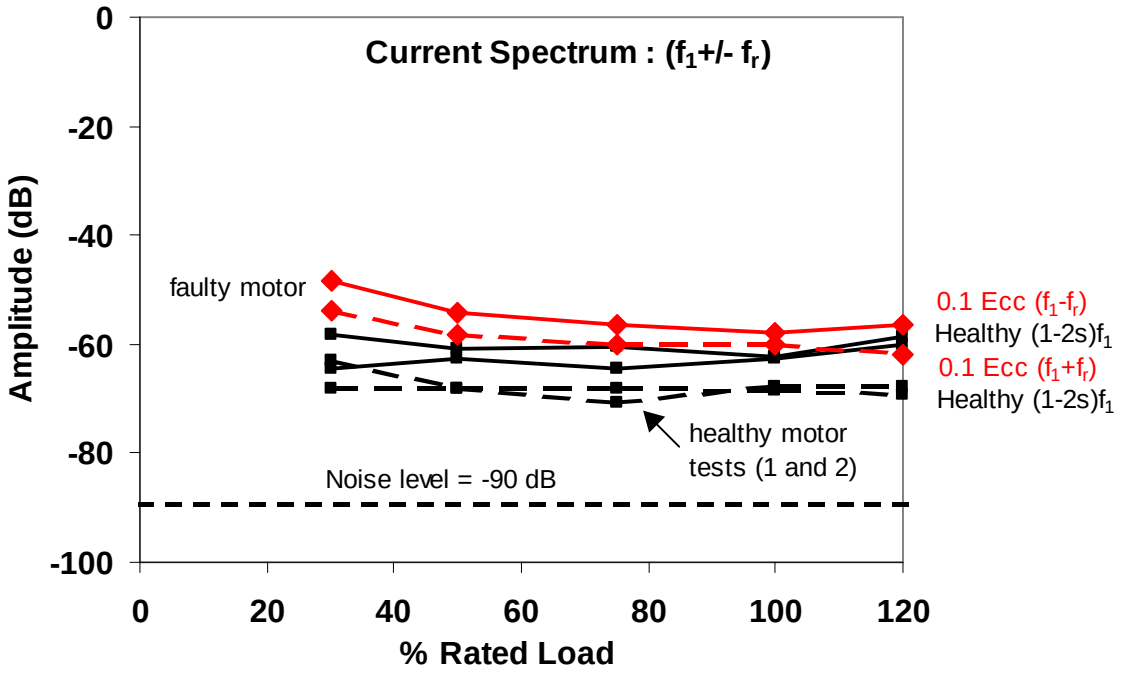

Figure 5.7: Comparison of variations in current sideband amplitudes for two tests on the same healthy motor. The result for the faulty motor is shown for reference.

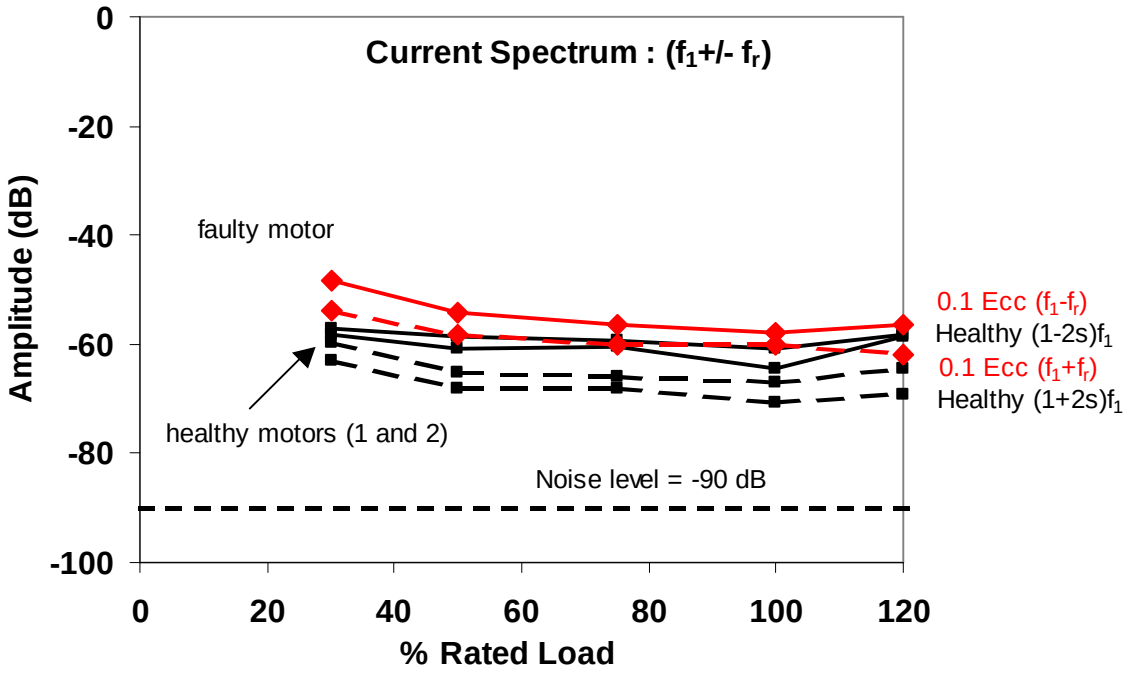

Figure 5.8: Variations in current sideband amplitudes for tests on two nominally identical healthy motors. The result for the faulty motor is shown for reference.

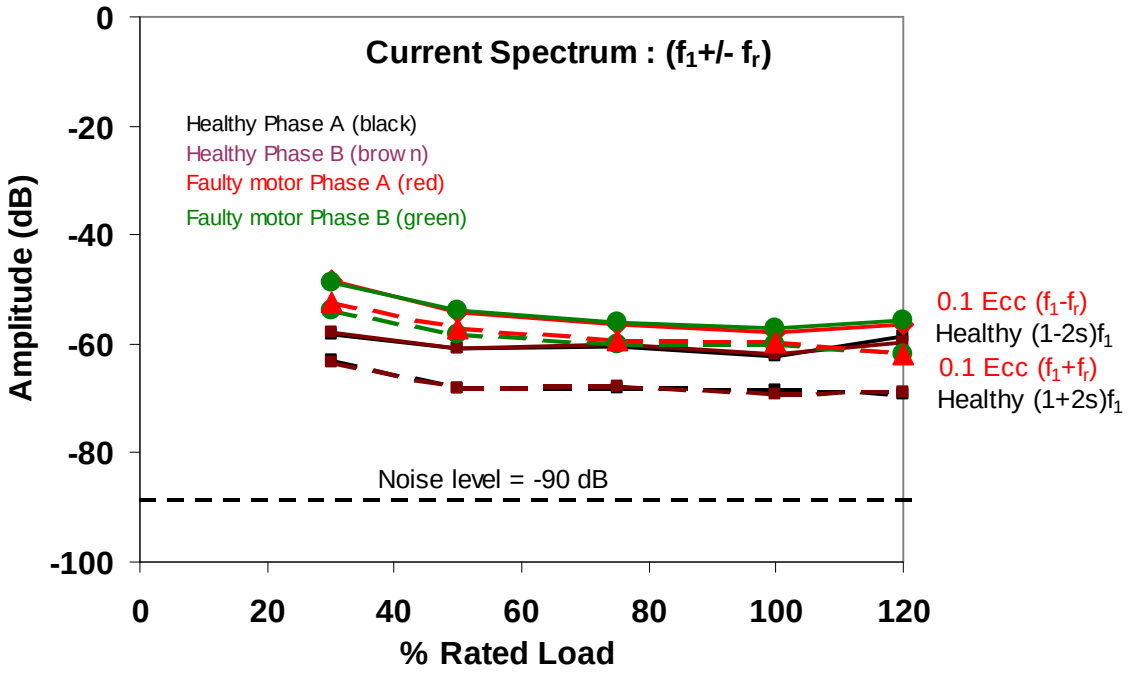

Figure 5.9: Variations in current sideband amplitudes of healthy motor 1 and the faulty motor (NDE at -0.1mm and DE at +0.3mm between phases A and B.

5.2.2 Eccentricity Fault Detection using Flux Spectrum

5.2.2.1 Comparison of Healthy and Faulty Flux Spectra

It has been observed in Figure 5.10, that variations in the amplitudes of the eccentricity fault frequency components of a faulty motor at 30% load and at full-load are higher than the current spectrum at the same level of loading. The noise level is (–70 dB), which is high (Figures 5.10).

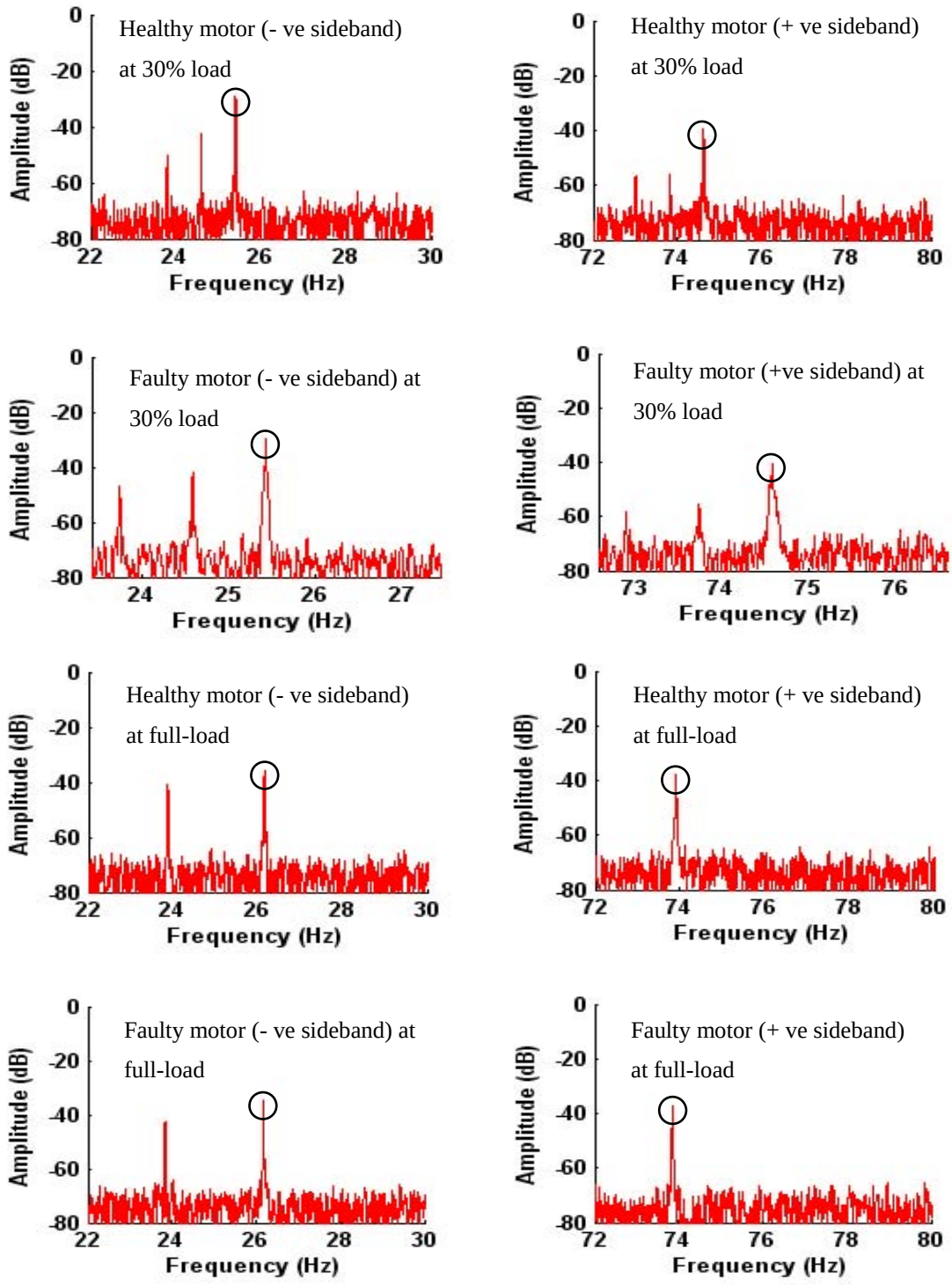

Figure 5.10: Flux spectrum from healthy motor (row 1 and 3) and a faulty motor with airgap of –0.1 mm at NDE and +0.3 at DE (row 2 and 4) at 30% load and at full-load. The circle indicates the sideband components.

5.2.2.2 Eccentricity Fault Frequencies from Flux Spectra

Eccentricity fault frequency components ($f_1 \pm f_r$) from the flux spectrum for 30% and at full-load are shown in Figure 5.11.

It shows that variations in the sideband components of the faulty motors were not affected at 30% load compared to the top illustration in the Figure 5.11. However, at full-load slight increase in the fault frequency components at the different levels of average eccentricity were found when reference was made to the faulty motor at 30% load as shown in Figure 5.11 (bottom).

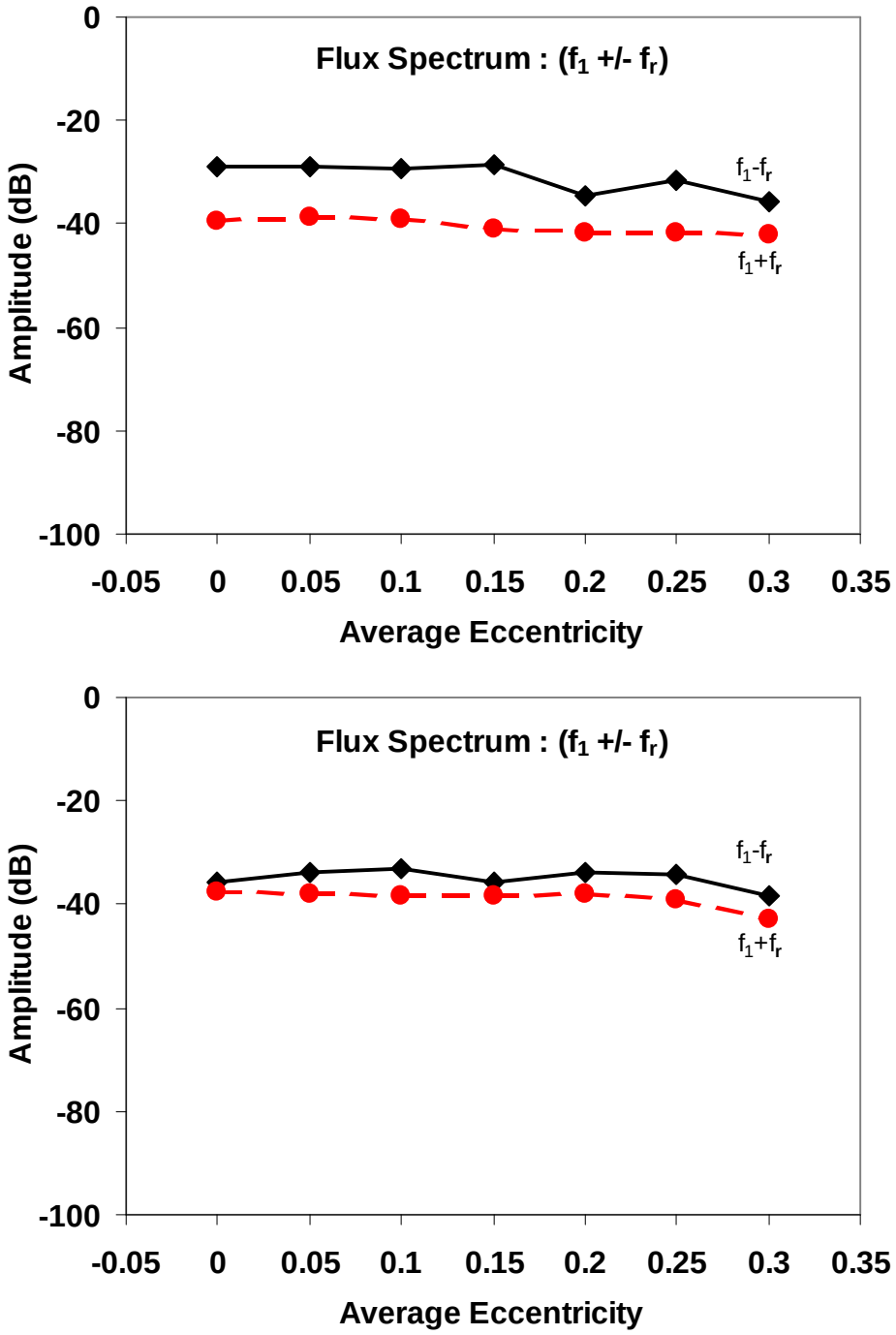

Figure 5.11: Comparison of variations in the sideband amplitudes versus average eccentricity at 30% load (top) and at full-load (bottom) between the healthy and faulty motors from flux spectrum

It is evident from test results that the eccentricity fault frequency components are more detectable in the current spectrum. Furthermore, the results obtained from the flux spectrum clearly indicate that the variations in the sideband amplitudes are not significant at both light and heavy loads. Therefore, it is not a suitable medium to detect eccentricity faults using fault frequency components ($f_1 \pm f_r$).

5.2.3 Eccentricity Fault Detection using Instantaneous Power

5.2.3.1 Comparison of Healthy and Faulty Instantaneous Power Spectra

It can be seen from that the magnitude of the fault frequency obtained from the Figures 5.12 and 5.13 that the changes in the amplitudes of positive sideband component of faulty motor at 30% load is slightly higher and clearly visible in the spectrum, when compared to the healthy motor.

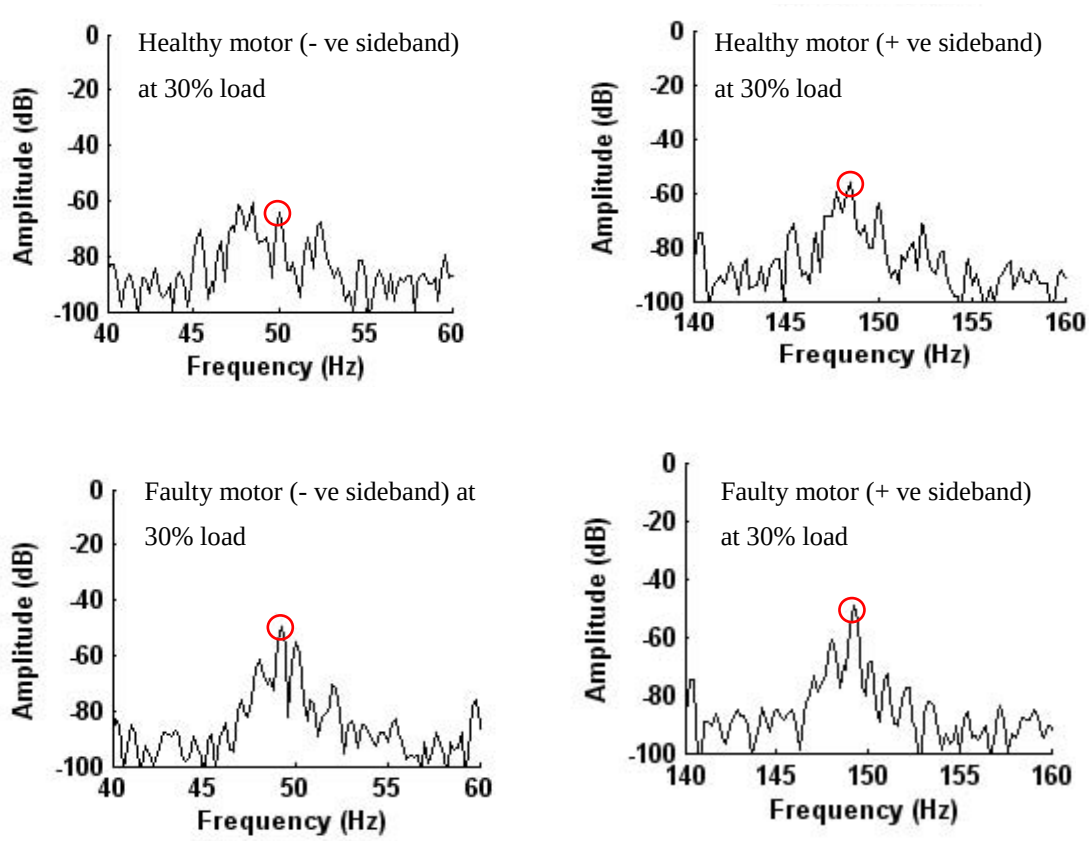

Figure 5.12: Instantaneous power spectrum from healthy motor (row 1 and 3) and faulty motor (row 2 and 4) at 30% and at full-load.

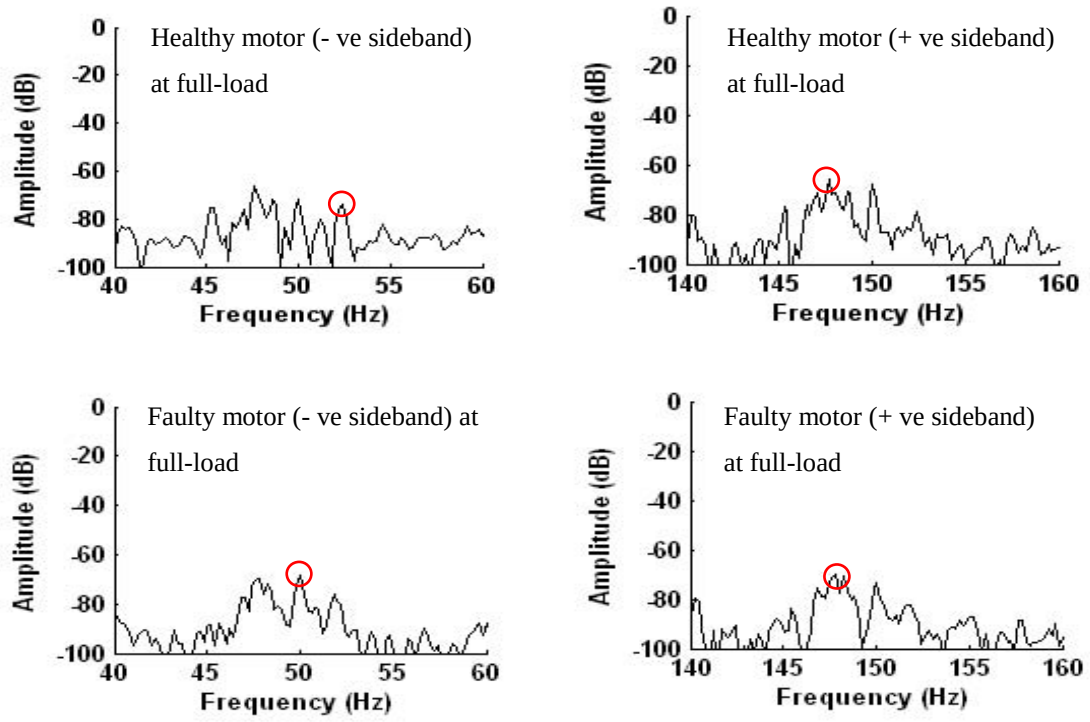

Figure 5.13: Instantaneous power spectrum from healthy motor (row 1 and 3) and faulty motor (row 2 and 4) at 30% and at full-load.

5.2.3.2 Eccentricity Fault Frequencies from Instantaneous Power Spectra

Amplitude of fault frequency components ($f_p \pm 2f_r$) versus average eccentricity is shown in Figure 5.14 (top) at 30% load and Figure 5.14 (bottom) at full-load. Variations in the amplitudes of components of faulty motors at different level of eccentricity were found to be significant. The results showed that the maximum variations in the negative sideband component occurred when the levels of airgap eccentricity are 0.05, 0.2 and 0.25 mm. For the positive sideband component the maximum variations were found when the levels of airgap eccentricity were 0.2 and 0.3 mm.

However, the result presented in Figure 5.14, indicate that any variation in the sideband components was only significant when the degree of eccentricity was 0.25 mm at full-load. It can be concluded from the results, that instantaneous power is suitable for detecting the eccentricity fault at light loads. Since the instantaneous power provides good results to detect the eccentricity faults. It can therefore be assumed that it is necessary to check its variability in healthy motors as indicated in the three case studies as mentioned in Section 4.2.1.3.

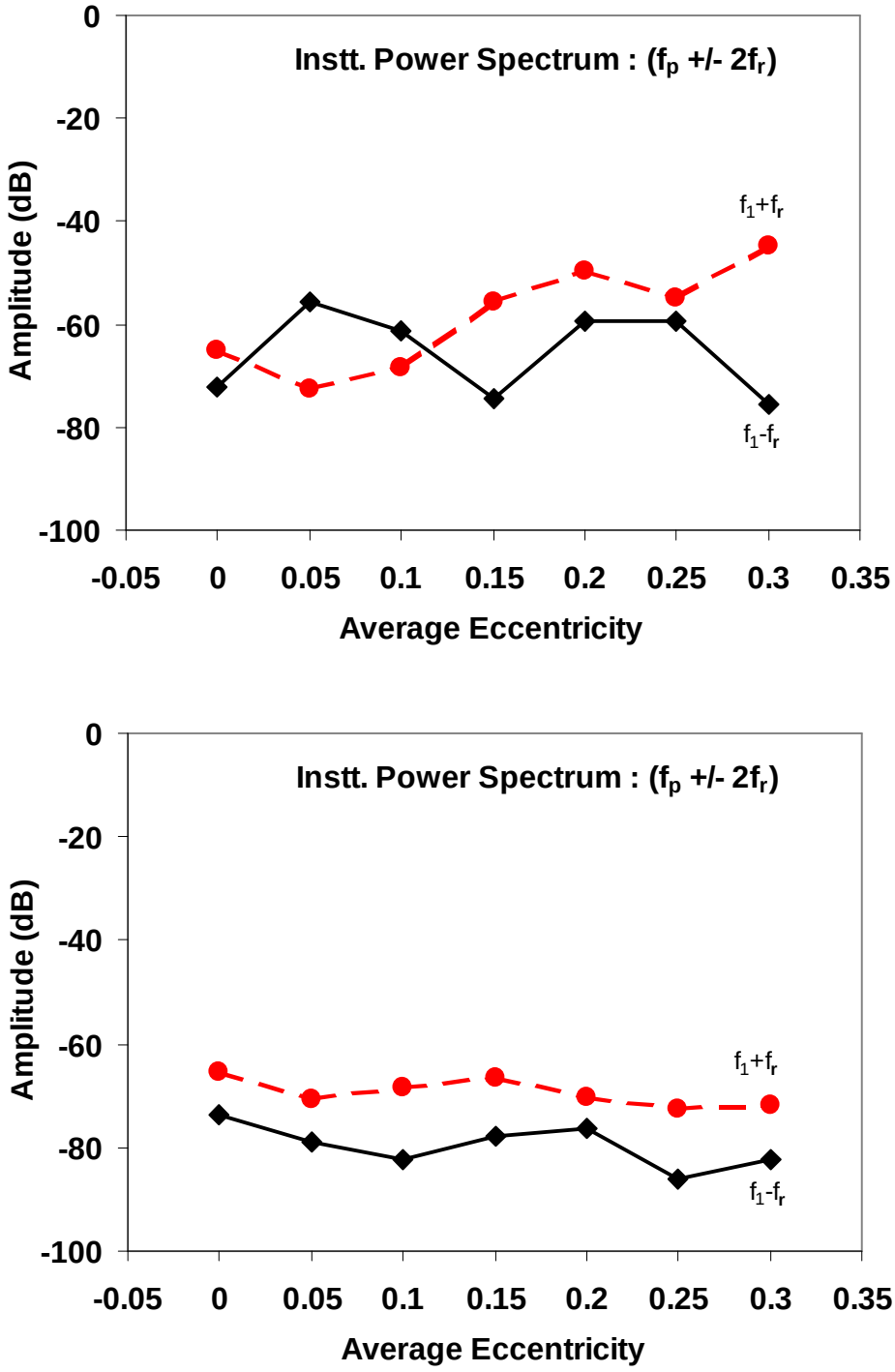

Figure 5.14: Comparison of variations in the sideband amplitudes versus average eccentricity at 30% load (top) and at full-load (bottom) between the healthy and faulty motors from instantaneous power spectrum

5.2.3.3 Instantaneous Power Spectrum Variations for Healthy Machines

Figure 5.15 shows the test results from a set of three tests on the same healthy motor, tests that investigated the consistency of the test set-up and the testing procedures. The maximum variations in the sideband amplitudes at any load level were about 8 dB.

From Figure 5.16 it can be concluded that there is a small variation of 5 dB between the sideband amplitudes of two healthy motors, which is not significant.

Figure 5.17 shows depicts variation in the sideband amplitudes between phases A and B of a healthy and a faulty motor is (< 8 dB).

In summary, in all three cases, results showed the accuracy and reliability of test results obtained from instantaneous power spectra using the experimental set-up developed for this study.

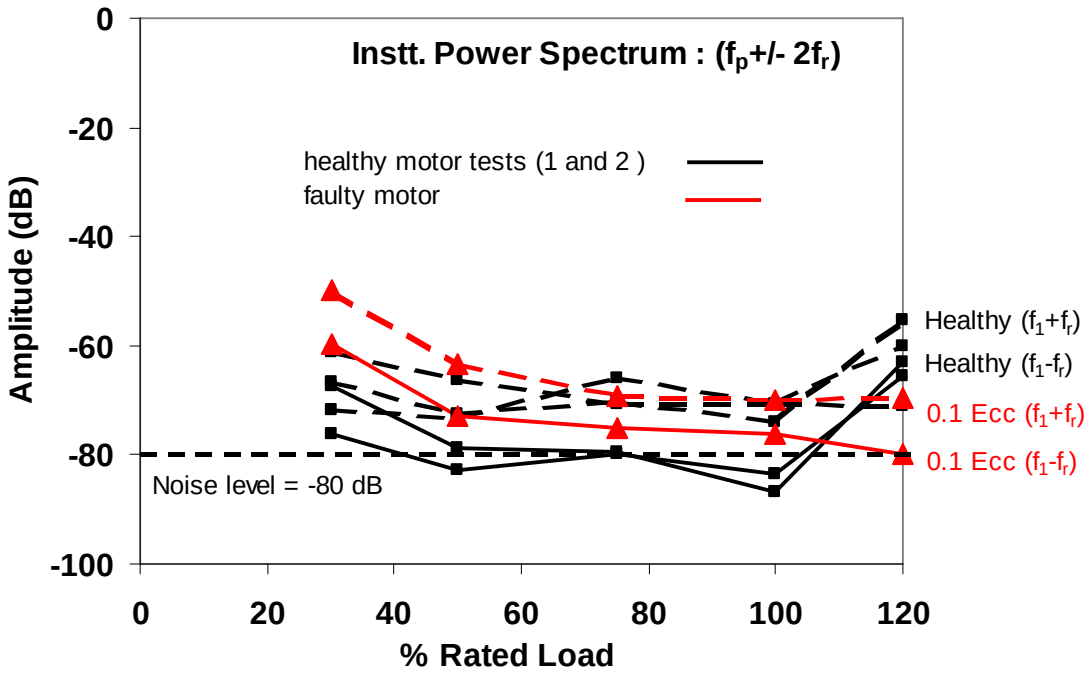

Figure 5.15: Variations in instantaneous power sideband amplitudes for two tests on the same healthy motor. The faulty motor results are shown for reference.

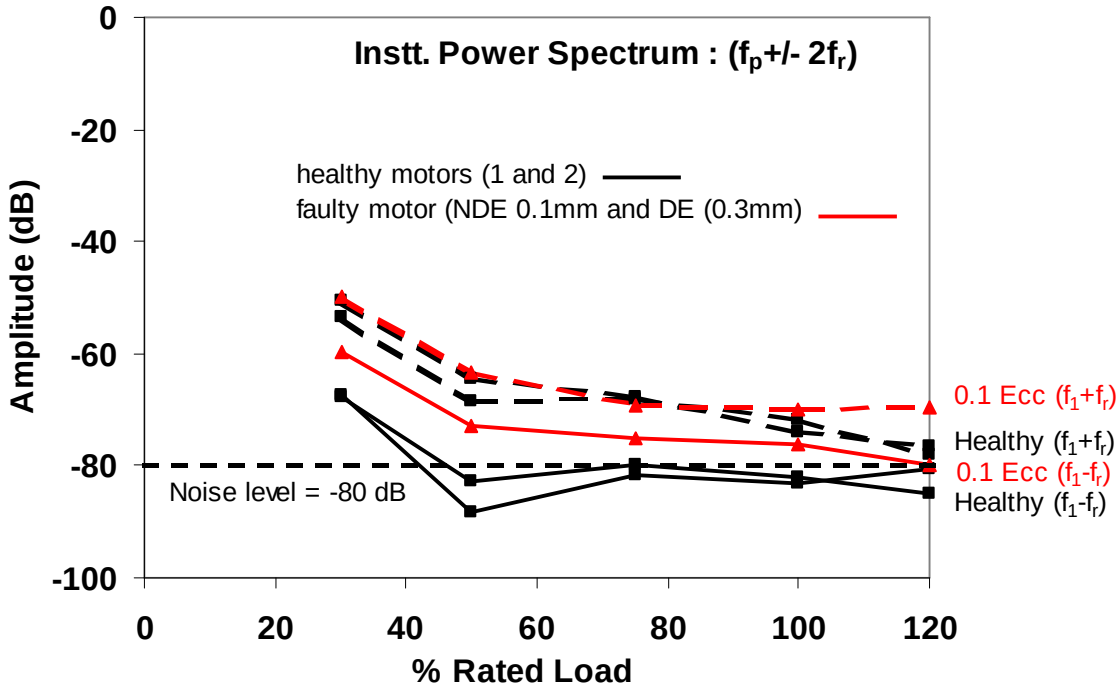

Figure 5.16: Variations in instantaneous power sideband amplitudes for tests on two nominally identical healthy motors. The faulty motor results are shown for reference.

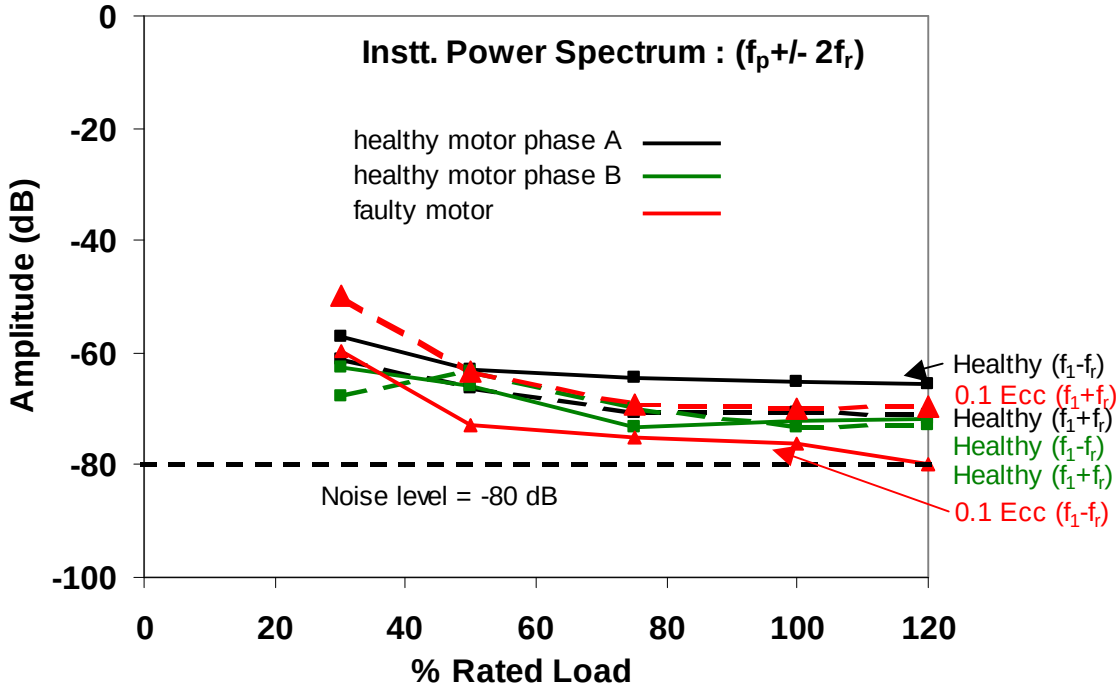

Figure 5.17: Variations in instantaneous power sideband amplitudes of healthy motor 1 and the 4 BRB motor between phases A and B.

In summary, the above results have shown that the current signal can detect eccentricity faults using fault frequency components ($f_1 \pm f_r$) with any degree of airgap under any level of loading. However, instantaneous power can also pick up eccentricity faults at light loads.

The results showed that the flux signal is not suitable for finding eccentricity faults when using variations in the amplitudes as function of average eccentricity.

5.3 Detection of Faults using Eccentricity Components $f_1[(R\backslash p)(1-s)\pm k]$

This section examines the use of fault frequency components $f_1[(R\backslash p)(1-s)\pm k]$ in the current, flux and instantaneous power signals to detect the eccentricity faults at different levels of eccentricity (refer to Table 5.1, for varying load conditions).

For this purpose, selected values of k i.e. ±1, ±3and ±5 are used to check either the variations in the amplitudes of fault frequency components will be useful in differentiating between healthy and faulty motors.

5.3.1 Eccentricity Fault Detection from Current Spectra

5.3.1.1 Comparison of Healthy and Faulty Spectra

The comparison of eccentricity sideband components for k=±3 of healthy and faulty motor with the airgap of (-0.1mm at NDE and +0.3 mm at DE) is shown in Figure 5.18.

It can be observed here that the fault frequency components for k=±3 under full-load test are visible in the current spectrum. The change in the sideband components between the healthy and faulty motor were found to be more than 28 dB, which is significant.

The noise level is about -90 dB.

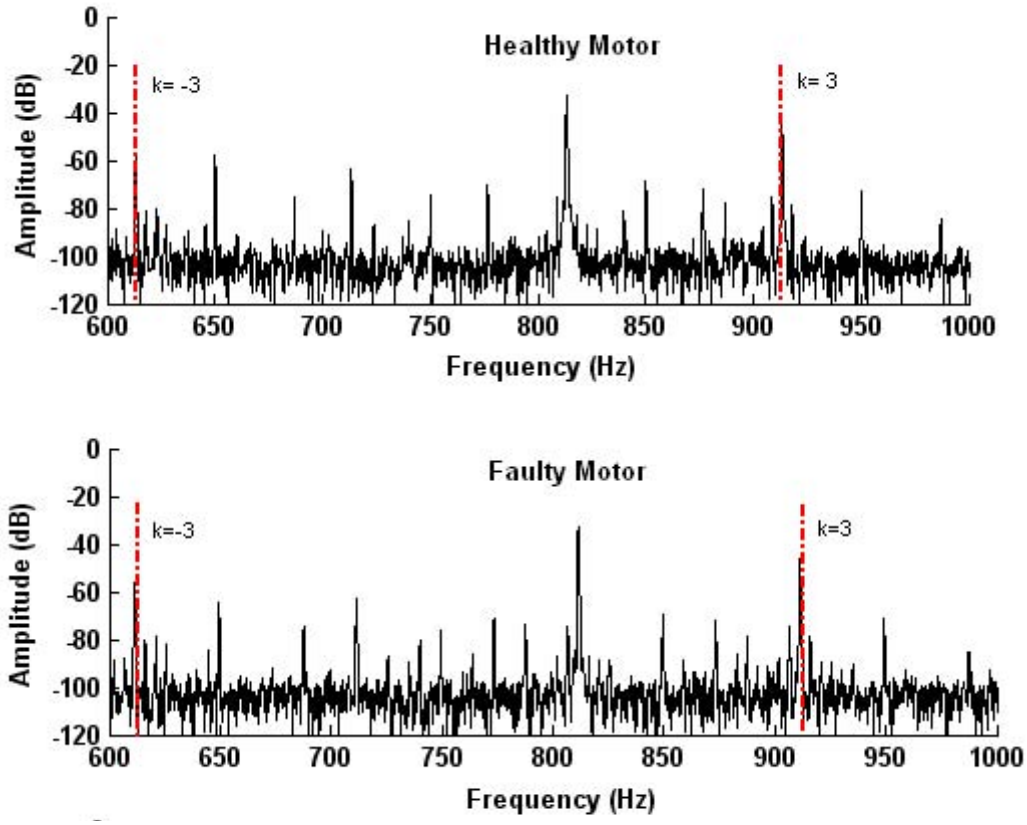

Figure 5.18: Current spectrum from a healthy machine (top row) and a faulty machine (bottom row) at full-load for k=±3.

5.3.1.2 Eccentricity Fault Frequencies from Current Spectra

Figure 5.19 summarises the amplitudes of the eccentricity fault frequency components as a function of load at different values of k for a healthy motor and faulty motor at 30% (top) and at full-load (bottom).

The results demonstrate that the maximum variation in the sideband amplitudes of a faulty motor was (5 dB) at k= ±5 under 30% load test, although this change is small when compared to the healthy motor. At full-load, similar changes were found even with the increase in load as shown in Figure 5.16 (bottom). The eccentricity fault frequency components $f_1[(R\backslash p)(1-s)\pm k]$ showed a small variation in the amplitude, which found eccentricity faults both at light and heavy loads for the certain values of k.

It is concluded from the results showed in the Figure 5.19 that it is hard to differentiate between a healthy and faulty motor on the basis of small variation in the amplitude of the eccentricity fault frequency components to detect the eccentricity fault at any level of loading for different values of k.

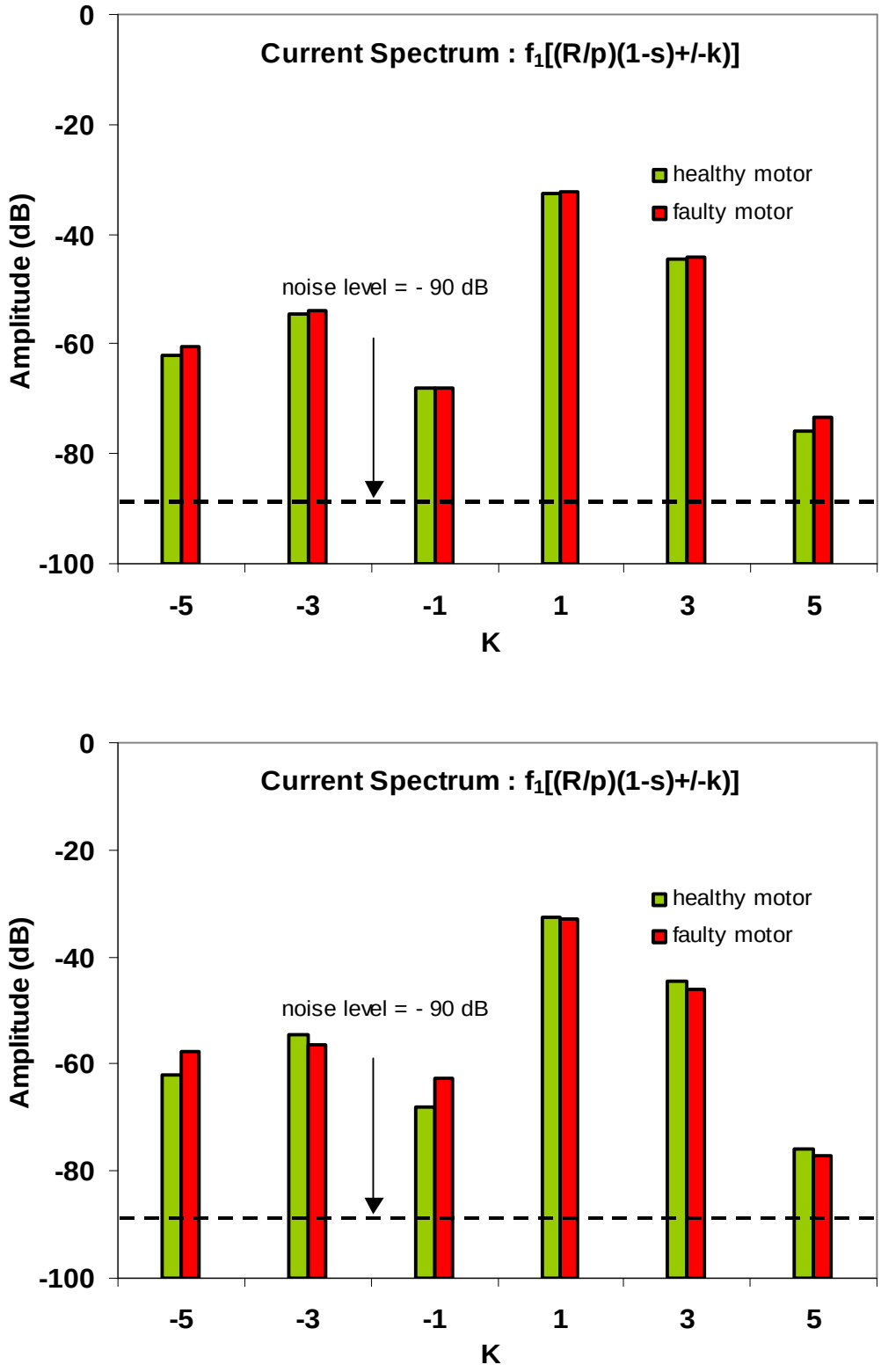

Figure 5.19: Comparison of variations in the sideband amplitude of a healthy motor with faulty motor with airgap at NDE is -0.3mm and DE is +0.3mm at 30% load (top) and at full-load (below) from current spectrum.

5.3.2 Eccentricity Fault Detection using $f_1[(R/p)(1-s)\pm k]$ from Flux Spectra

5.3.2.1 Comparison of Healthy and Faulty Flux Spectra

Comparison of eccentricity sideband components for k=±3 of healthy and faulty motor with the airgap of (0.3mm at NDE and +0.3mm at DE) at full- load is shown in Figure 5.20. It can be concluded that the fault frequency components are clearly visible in the spectrum of both the healthy and faulty motor, although the change in the sideband amplitudes is small. The noise level is about –65 dB.

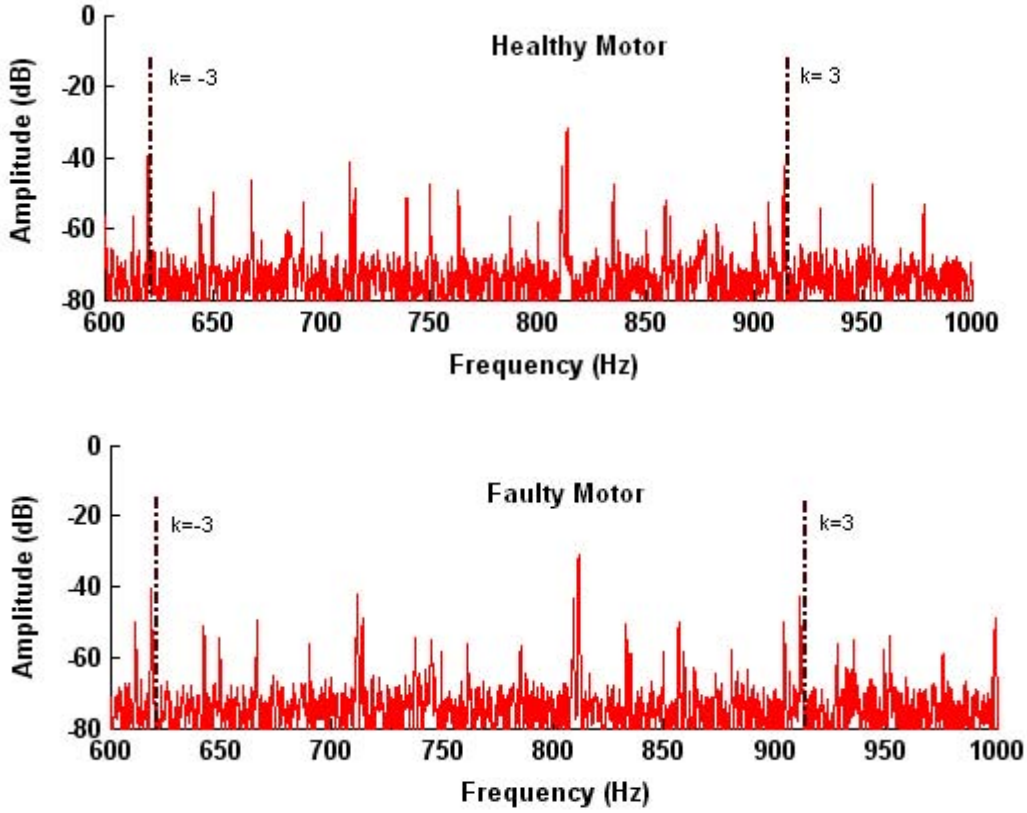

Figure 5.20: Comparison of the flux spectrum from a healthy machine (top row) and a faulty machine (bottom row) for k=±3, at full-load.

5.3.2.2 Eccentricity Fault Frequencies from Flux Spectra

Figure 5.21 records the results of the variation of the amplitude of the measured fault frequency components $f_1[(R\backslash p)(1-s)\pm k]$ under 30% and full-load for different values of k at eccentricity level of 0.3 mm at driving-end . It can be concluded from the results, that variation in the sideband amplitudes of the faulty motor at 30% load test was found to be

very small (<4 dB) for the different values of k in comparison to the healthy motor. However, similar variation in the magnitude of the fault frequency components was found under full-load test. It is hard to distinguish between the healthy and faulty motor in the flux spectra by using the variation in the sideband amplitude of the fault frequency components under different loading conditions.

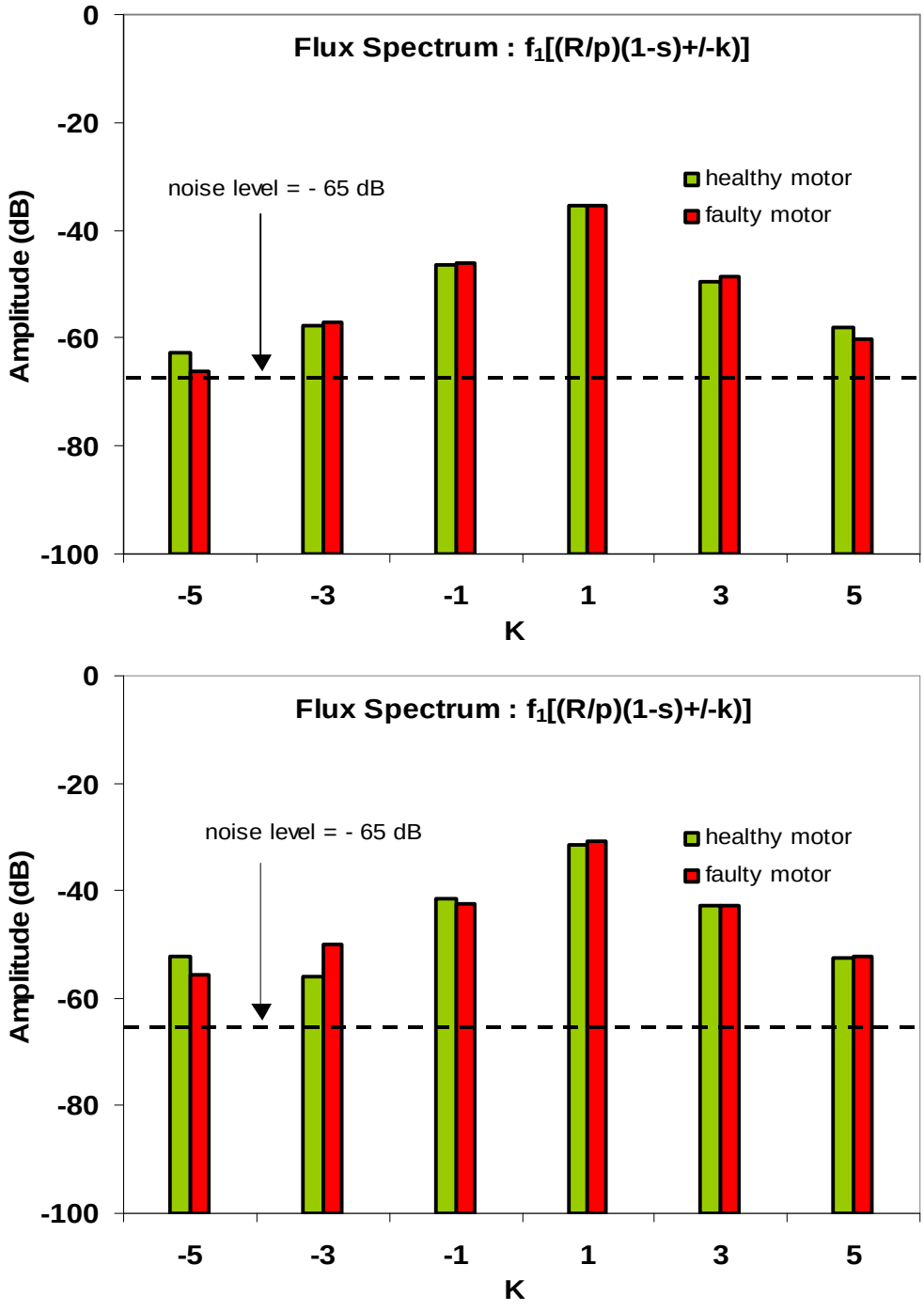

Figure 5.21: Comparison of variation in the sideband amplitudes of the healthy and faulty motor at eccentricity level of (–0.3mm at NDE and +0.3mm at DE) under 30% load (top) and at full-load (bottom).

5.3.3 Eccentricity Fault Detection using $f_p[(R/p)(1-s)\pm k]$ from Instantaneous Power Spectrum

5.3.3.1 Comparison of Healthy and Faulty Instantaneous Power Spectra

Figure 5.22 compares the frequency spectrum of the instantaneous power for a healthy and a faulty motor at full-load for k=±3 at full-load. It has been observed that the amplitudes of the characteristics fault frequency of the faulty and healthy motor are clearly visible in the spectrum. However, the variations in the sideband amplitudes between the healthy and faulty motor is (<3 dB) is not significant. The noise level is about –99 dB.

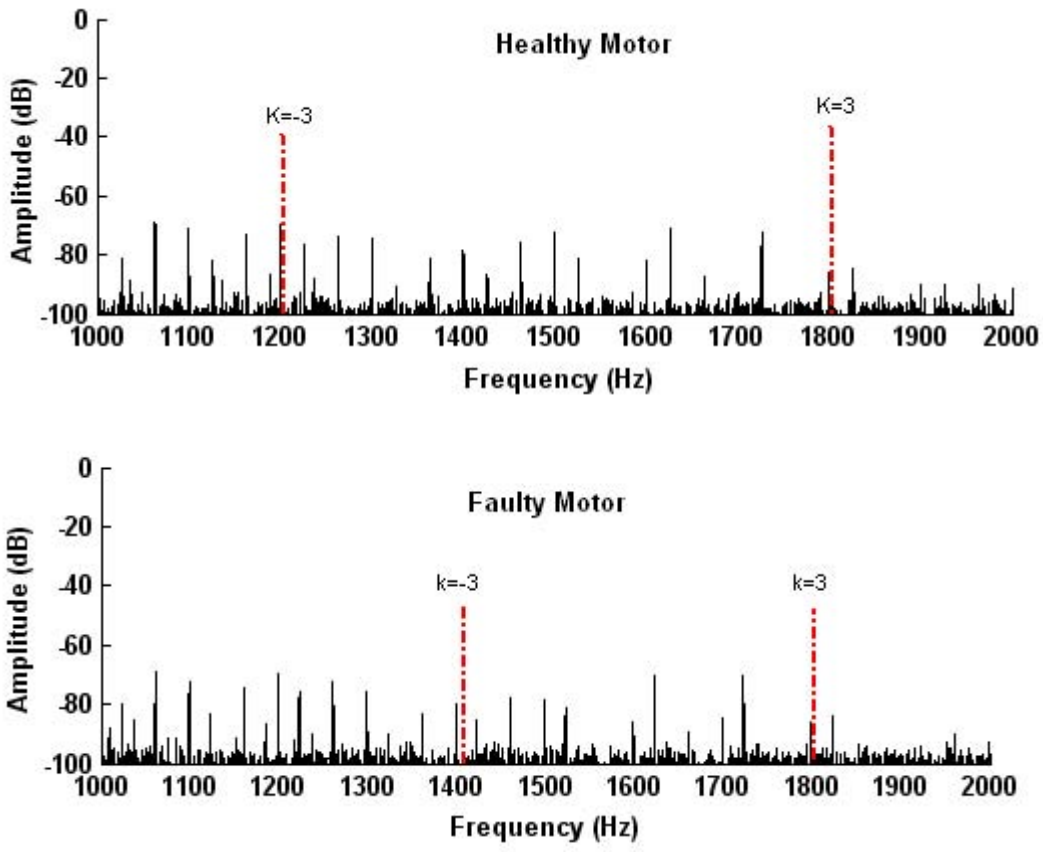

Figure 5.22: Comparison of the instantaneous power spectrum from a healthy machine (top row) and a faulty machine (bottom row) for k=±3, at full-load.

5.3.3.2 Eccentricity Fault Frequencies from Instantaneous Power Spectra

Measured fault frequency sideband components ($f_p \pm 2f_r$) for at k=±1, ±3 and ±5 under 30% and at full-load tests are shown in Figure 5.23. It can be concluded from the results, those variations in the amplitude of the fault frequency components between the healthy

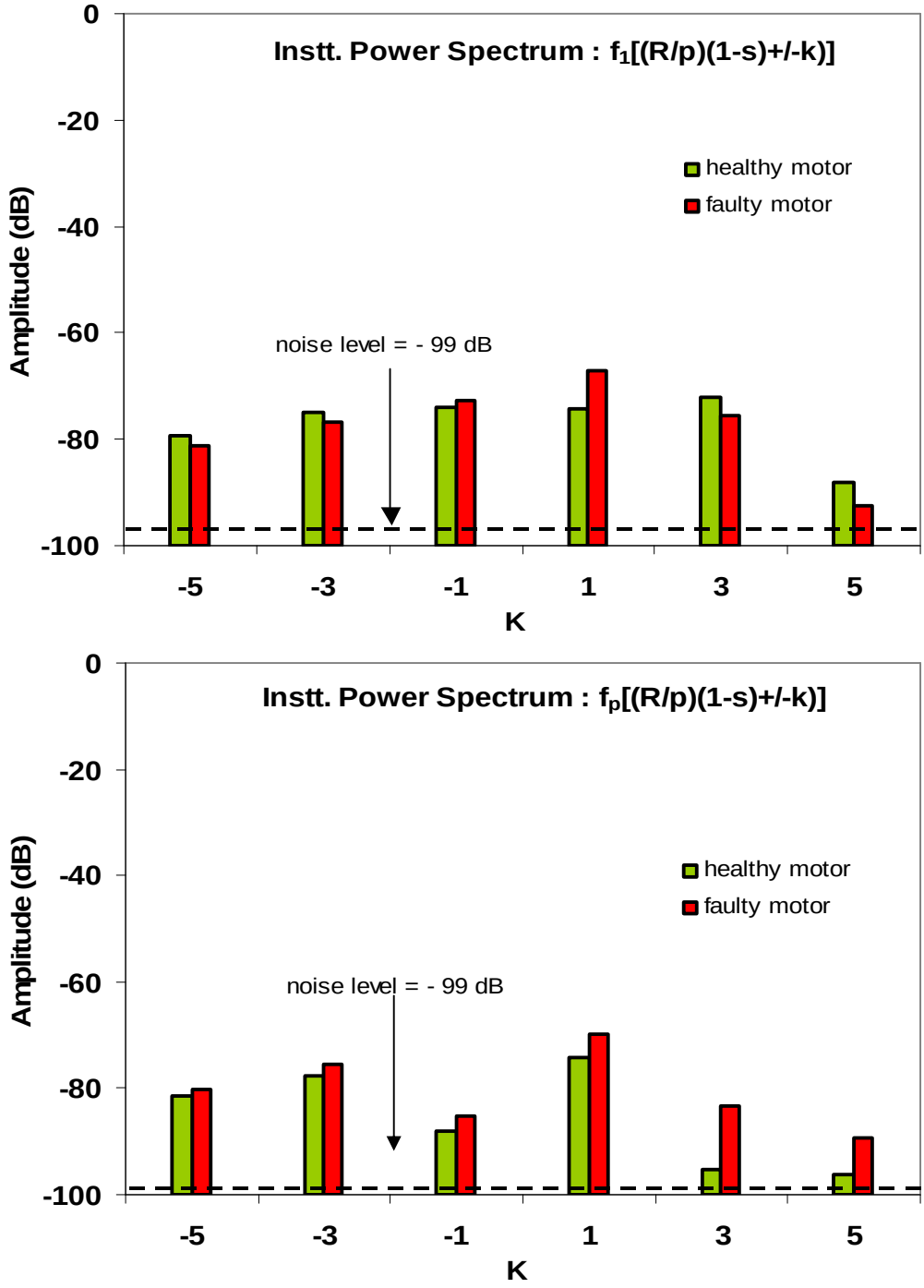

Figure 5.23: Variations in eccentricity sideband amplitudes for two tests on the same healthy motor. The result of faulty motor is shown for reference.

and faulty motor for different values of k both at light and high load were found to be better than current and flux spectra. Instantaneous power signal has the capacity to detect the eccentricity faults for different values of k at any level of loading. Since the eccentricity fault frequency components showed useful features to detect the eccentricity fault using instantaneous power spectra, it is therefore important to check variability in its amplitudes of healthy motors due to: repeatability tests on the same motor, differences between motors and differences between two of the phases of the same in its amplitude. These are the result of other effects apart from fault severity and load.

5.3.3.3 Instantaneous Power Spectrum Variations for Healthy Machines

Test results from a set of three tests on the same healthy motor showed a slight variation (< 3dB) in the sideband amplitudes of the healthy motor for different values of k at full-load shown in Figure 5.24.

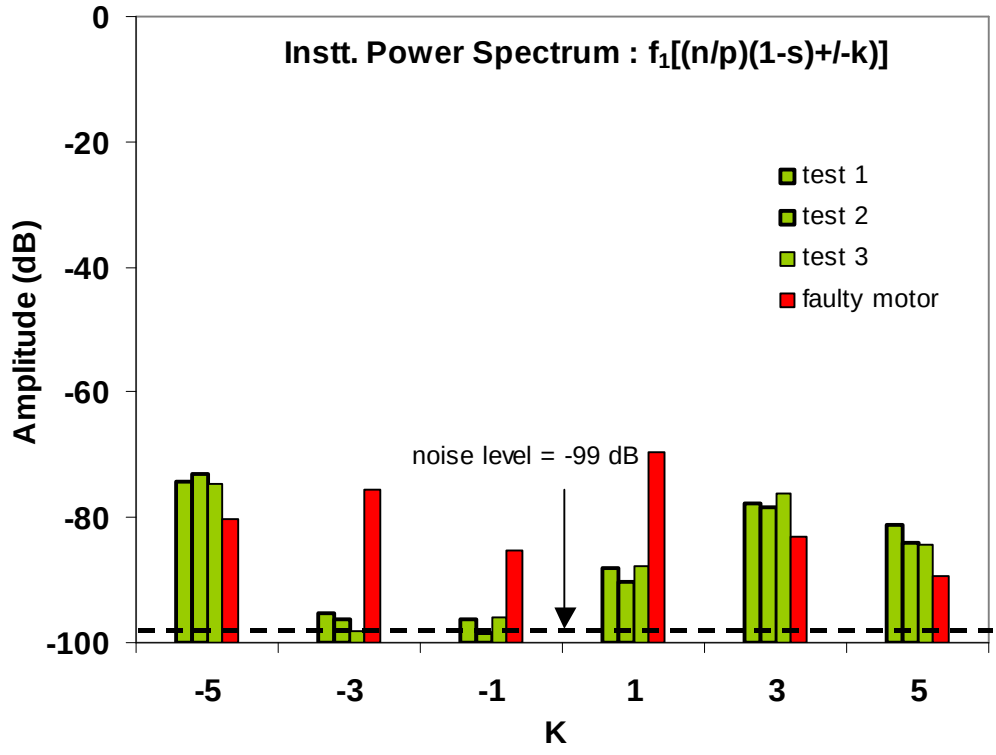

Figure 5.24: Variations in eccentricity sideband amplitudes for two tests on the same healthy motor. The result of faulty motor is shown for reference.

Figure 5.25 shows a comparison between the current sideband amplitudes versus load for two nominally identical healthy motors. Small variation of less than 3 dB was found between the sideband amplitudes of two healthy motors at full-load for different values of k, which is not significant

Figure 5.26 indicates the variations in the sideband amplitudes between phases A and B of a healthy motor at full-load for k=±1and k=±3 is less than 3 dB, which is also very small.

In summary, variability in its amplitude to other effects apart from fault severity and load of the healthy motor test results is small, which shows that the test results are the accurate and reliable.

The results obtained using fault frequency components in the instantaneous power spectra consistently showed that instantaneous power signal is suitable for detecting eccentricity faults in induction machines (specifically for small rating).

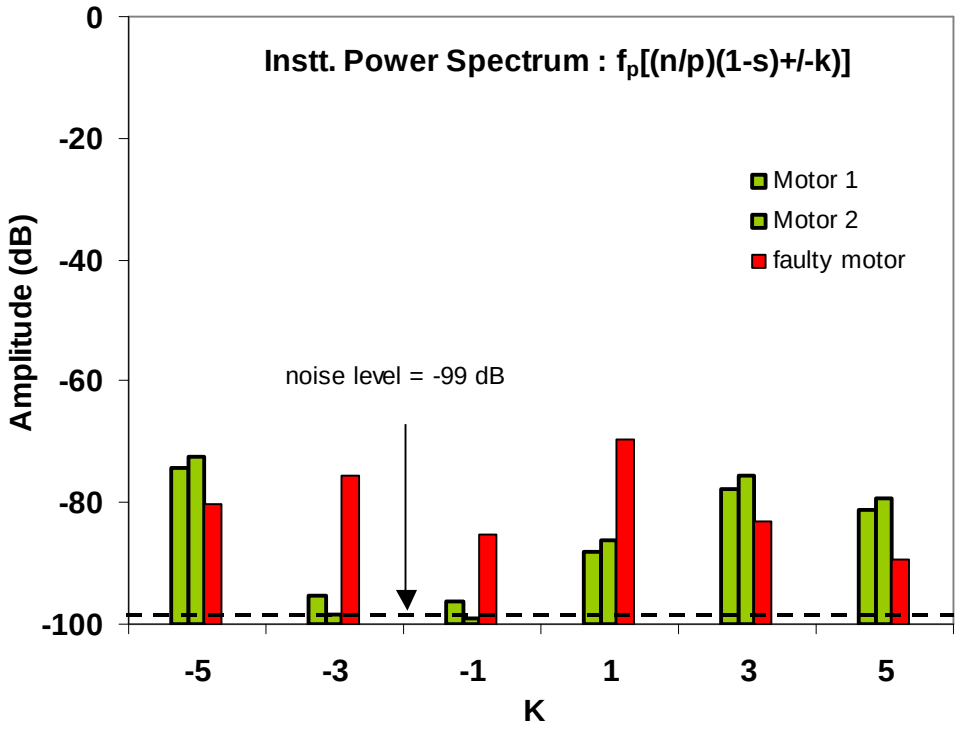

Figure 5.25: Variations in eccentricity sideband amplitudes for tests on two identical healthy motors. The faulty motor results are shown for reference.

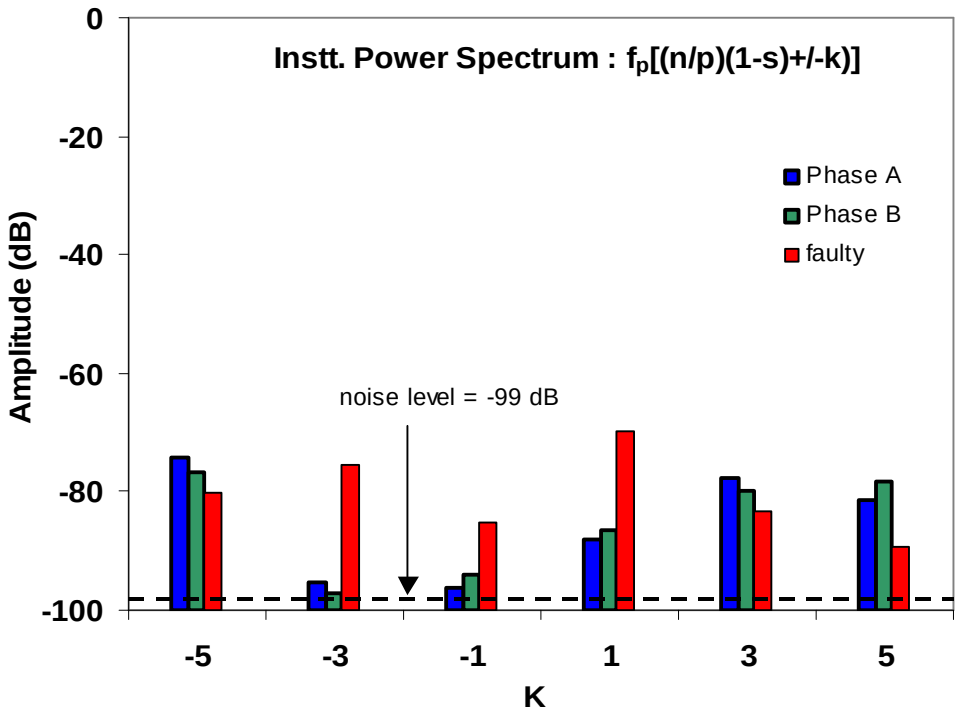

Figure 5.26: Variations in eccentricity sideband amplitudes of healthy motor between phases A and B. The faulty motor results are shown for reference.

5.4 Summary

In this chapter we investigated the current, flux and instantaneous power signal as a medium for detecting eccentricity faults by using different equations of the eccentricity fault frequency components.

The results of eccentricity fault frequency components ($f_1 \pm f_r$) as a function of average eccentricity to detect under different levels of loading from the current, flux and instantaneous power spectra are shown in Table 5.1.

The variations in the sideband amplitudes ($f_1 \pm f_r$) between the healthy and faulty motors showed good features over the full range of load tested to detect the eccentricity fault in the current spectra. However, flux signal alone is not suitable for detecting eccentricity faults for the same.

The results from instantaneous power indicate that the variations between the healthy and faulty motors are significant when the level of average eccentricity is 0.2 mm and the minimum rated load is 30%. Therefore, instantaneous power is useful but less effective due to random changes in the sideband amplitudes.

Table 5.2: Comparison of healthy and faulty motors for detecting eccentricity faults using components ($f_1 \pm f_r$) under different levels of loading. The average eccentricity level is considered from 0 to 0.3 mm at the non-driving-end.

Signal	**Minimum average eccentricity level when the difference between the healthy & faulty motor amplitude is ≥ 12 dB**	**Minimum % Rated Load when the amplitude is ≥ 12 dB**	**Δ = Av.Ampl. Difference between the healthy & faulty motor (dB)**		**Comments**
			(-) Amplitude	**(+) Amplitude**	
Current	0.2 mm	30%	24	12	Suitable and preferable to detect eccentricity faults under any load conditions (specifically at light loads).
Flux	Not found	Not found	Not found	Not found	No significant variations were found that helps to detect the eccentricity faults reliably and accurately.
Instt. Power	0.2 mm	30%	13	16	Suitable and Useful but less effective because of random variations in the sideband amplitudes

The results from current, flux and instantaneous power signals for detecting the eccentricity faults using characteristic fault frequency components $f_1 \pm f_r$ as a function of load at full-load are shown in Table 5.2.

Current and flux signals showed very small variations between the healthy and faulty motors for the different values of k under any level of loading, whereas, instantaneous power could extract some useful information for the value of integer k =-3 and when the minimum load on the motor was about 30% of rated load. However, detection of eccentricity faults using characteristic fault frequency components $f_1[(R\backslash p)(1-s) \pm k]$ as a function of load for different values of k under any range of loading is not suitable as shown in Table 5.3.

Table 5.3: Comparison of healthy and faulty motors to detect the eccentricity faults using components $f_1[(R\backslash p)(1-s)\pm k]$ under different levels of loading. Eccentricity level is +0.3 mm at non-driving-end.

Signal	**Value of integer k when the difference between the healthy & faulty motor amplitude is ≥ 12 dB**	**Minimum % Rated Load when the amplitude is ≥ 12 dB**	**Average amplitude difference between the healthy & faulty motor (dB)**	**Comments**
Current	Not found	Not found	Not found	Not suitable because of small variations in the amplitudes of faulty motor.
Flux	Not found	Not found	Not found	Not applicable.
Instt. Power	-3	30% load	13	Suitable and useful to detect eccentricity faults only at light loads.

Finally, the results showed that detection of eccentricity faults using fault frequency components ($f_1 \pm f_r$) as a function of average eccentricity in the current signal are found to be superior. This is because firstly, for these components the values of rotor frequency is directly measured from vibration spectra and secondly supply frequency is measured from current/voltage spectra, which are more accurate and reliable.

Chapter 6

Shorted Turns Fault

6.1 Introduction

It has been reported that 30-40% of machines failures are due to shorted turn faults [18,34]. It is well understood that the impact of shorted turns in stator winding at early stages on the induction machines is small. Shorted turn faults result from insulation failure in a part of the winding. This insulation failure can be caused by thermal damage due to excessive currents, insulation breakdown as the result of voltage spikes/transients, or mechanical damage. It is also depends on the location of the insulation failure and voltage difference between the two parts of the winding, which are shorted. Shorted turn faults can produce either large fault currents, which will rapidly trip the circuit breaker or else produce little external symptoms as shown in Figure 6.1.

Figure 6.1: View of stator winding showing effect of shorted turns in early stages.

In the latter case, however, the localised heating caused by the fault will gradually result in further insulation damage until the motor fails. It is useful to be able to detect such faults at an early stage so that a pre-planned shut down can be arranged for the motor to be replaced by a healthy motor.

6.2 Shorted Turns Fault

This chapter explores non-invasive multiple sensors types for the detection of shorted turns fault using fault frequency components from current, flux, instantaneous power and single signal (combination of flux and instantaneous power signals) over a wide range of loads. To achieve this task, stator winding of the machine rewound with taps to introduce shorted turns fault is shown in Figure 6.2. An extensive series of laboratory tests was conducted to examine fault frequency amplitudes for the healthy motor and faulty motors with different shorted turns (as shown in Table 6.1). Equations 2.5.6, 2.5.7 and 2.5.8 (as described in Chapter 2) were used to detect the frequency sideband components.

Figure 6.2: View of shorted turns in stator winding of faulty motor with.

Table 6.1: Number of turns short-circuiting to investigate the severity of shorted turns fault versus % of rated loads.

% of Rated Load	**Number of shorted turns**				
	0	5	10	15	20
30	✓	✓	✓	✓	✓
50	✓	✓	✓	✓	✓
75	✓	✓	✓	✓	✓
100	✓	✓	✓	✓	✓
120	✓	✓	✓	✓	✓

6.2.1 Shorted Turn Fault Detection using Current Spectra

6.2.1.1 Healthy and Faulty Current Spectra

Figure 6.3 demonstrates the location of the shorted turn fault frequencies of the healthy motor and faulty motor with 20-shorted turns in the current spectrum. The top figures represent the shorted turn sideband components of the healthy motor and the bottom row shows the shorted turn sideband components of the faulty motor at full-load for n=1 and k=±5 at 30% of rated load. The spectra were taken at a sampling frequency of 8 kHz and have a frequency resolution of 0.2 Hz.

The figure also indicates small variations in the amplitudes of sideband components in the faulty motor as being clearly visible in the spectra. However, variations in the amplitudes at full-load are significant at high load. The noise level is –90 dB.

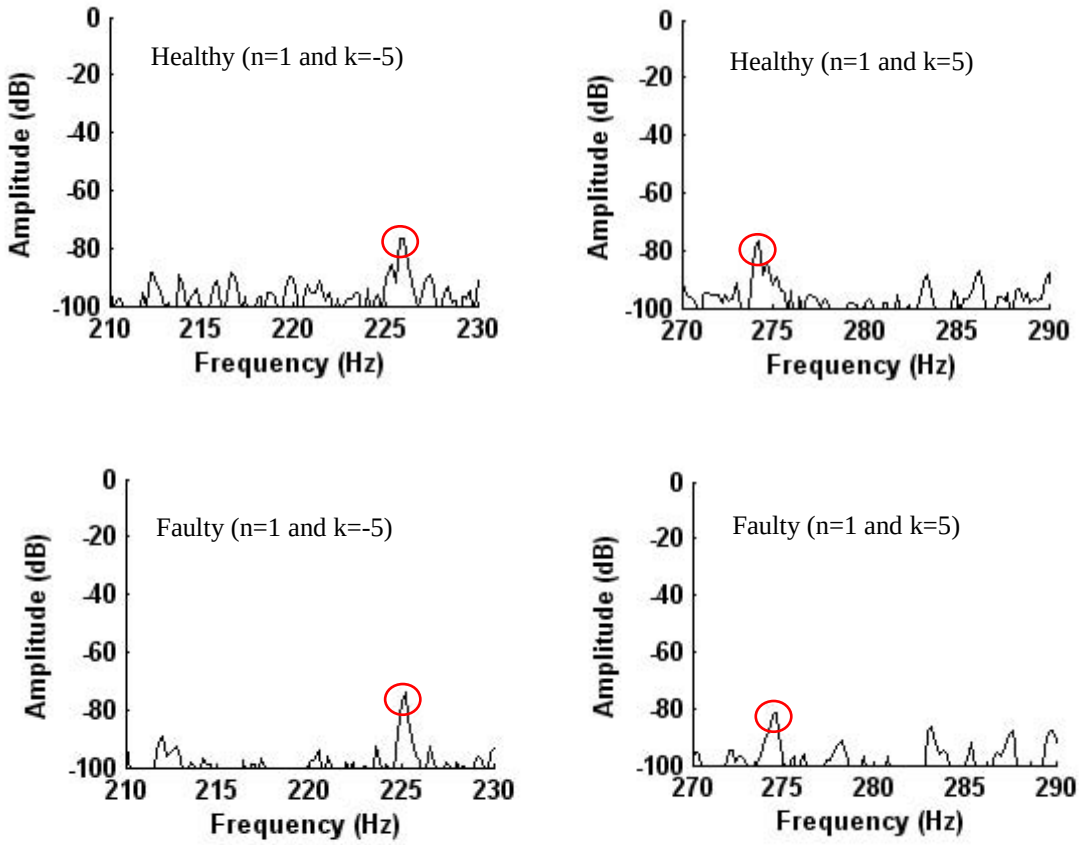

Figure 6.3: Current spectrum from a healthy motor (top row) and a faulty machine with 20 shorted turns at 30% load. The circles indicate the shorted turns fault frequencies at 30% and at full-load.

6.2.1.2 Shorted Turn Fault Frequencies from Current Spectra

Figure 6.4 shows that the variation in the amplitudes of sideband components for the healthy and faulty motors were less than 5 dB, which is quite low and therefore not able to detect shorted turn faults reliably using the current spectra under 30% of rated load.

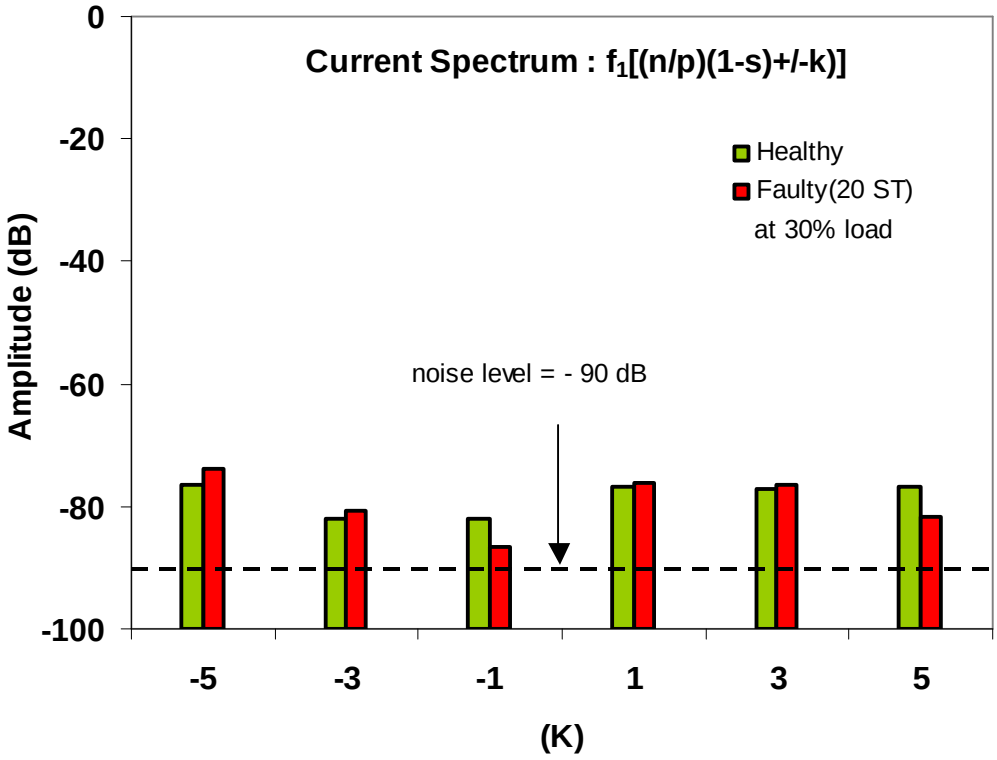

Figure 6.4: Comparison of variation in the sidebands amplitudes of a healthy motor with faulty motor (20 shorted turns) at 30% load from current spectrum.

Figure 6.5 shows the result for the faulty motors are not consistent at higher loads (full-load) because the variation is only 1 to 3 dB higher than the healthy motor, which is not significant.

The use of frequency components to detect the faults and estimate fault severity in the machines relies heavily on variations in the amplitude of sideband components. It is therefore clear that to detect shorted turn faults' using the current spectrum is not suitable under any level of load tests.

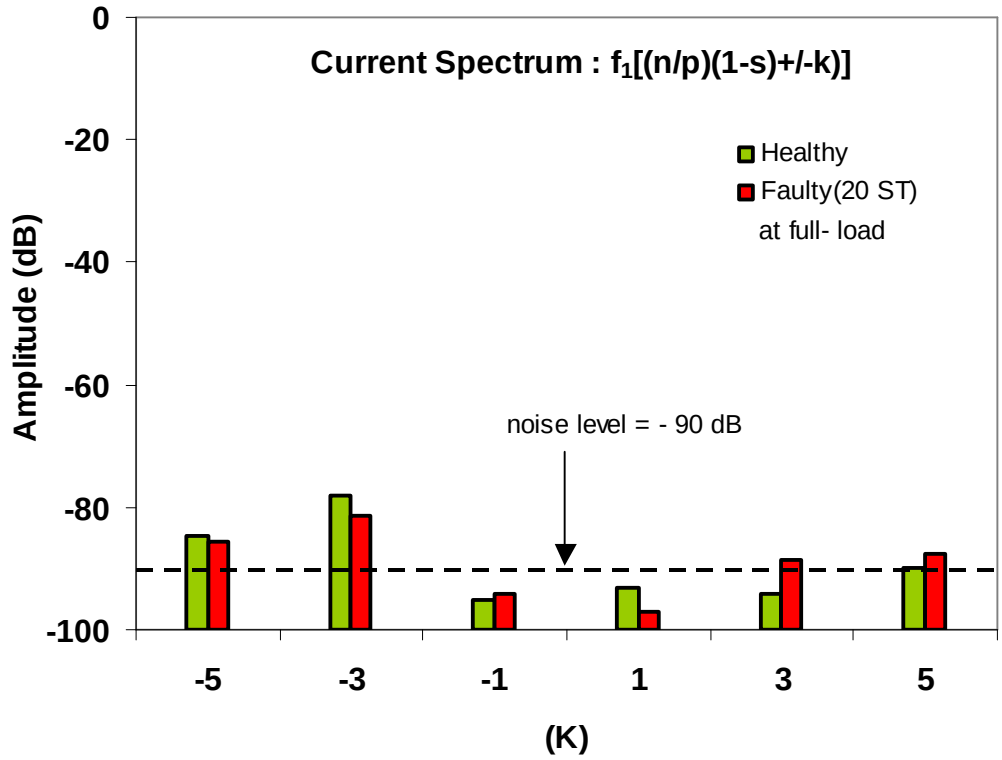

Figure 6.5: Comparison of variation in the sidebands amplitudes of a healthy motor with faulty motor (20 shorted turns) at full-load from current spectrum.

6.2.2 Shorted Turn Fault Frequencies Detection using Flux Spectrum

6.2.2.1 Healthy and Faulty Flux Spectra

Measured fault frequencies and their respective magnitudes for the healthy and faulty motor (20 shorted turns) for n=1 and k= ±1, ±3, ±5 at 30% and at full-load is shown in Figure 6.6.

The spectra showed significant decrease for both negative and positive sideband in the amplitude of fault frequency components regarding the healthy and faulty motors. The amplitude of the sidebands are clearly visible in the flux spectrum for different values of n and k, event in the presence of other peaks and high noise level when compared to the current spectrum. The noise level is about –65 dB.

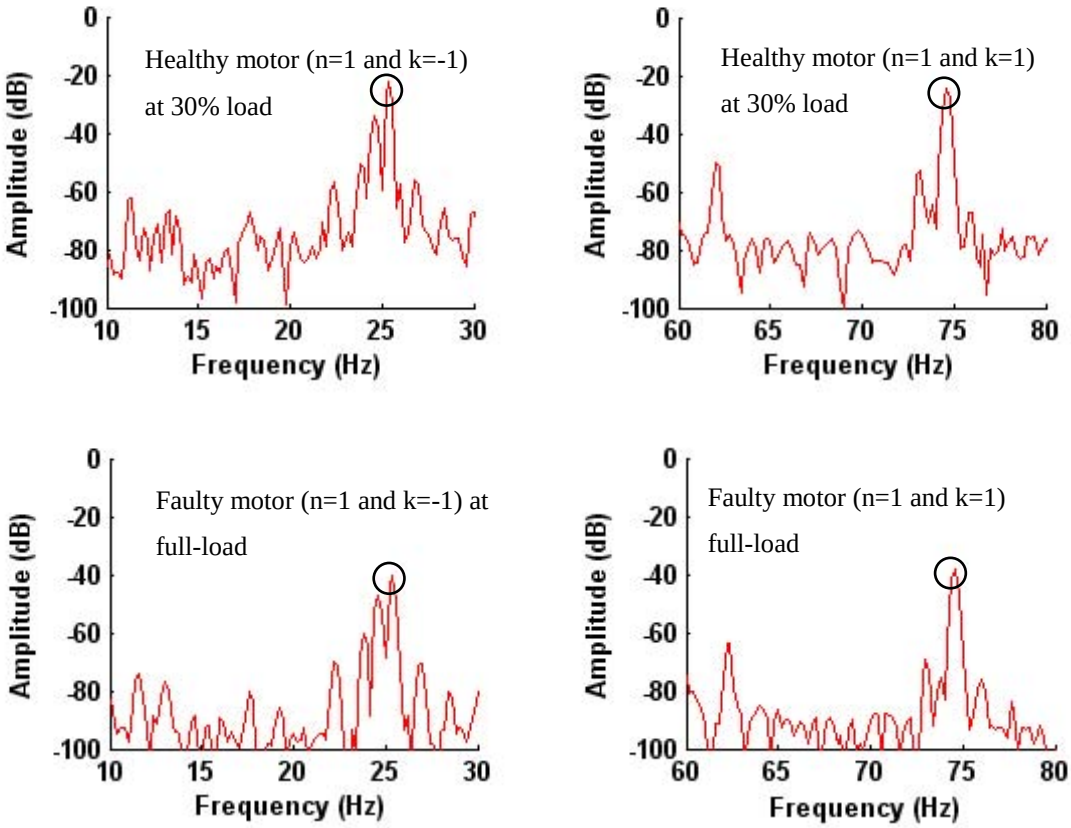

Figure 6.6: Comparison of the flux spectrum from a healthy motor (top row) at 30% load and at full-load (bottom row).

6.2.2.2 Shorted Turn Fault Frequencies from Flux Spectrum

Figure 6.7 (top) highlights variation in the amplitudes of sideband components for n=1 and k= ±1 is more than 14 dB for both the negative and sideband components at 30% load, which is sufficient to distinguish between the healthy and faulty motors in the flux spectra. Under full-load test conditions, variations in the amplitudes of the healthy and faulty motors were found to be less than 4 dB for all values of k except for k=1,which is clearly visible in the spectra as shown in Figure 6.7 (bottom).

The results show that it is useful to detect shorted turn faults at light loads using flux signal. However, the flux signal's features cannot provide useful information to detect shorted turn faults at high loads.

Since the flux signal could detect shorted turn faults at light loads therefore, the next section examines the variability in healthy motors. This is made possible by test repeatability, difference between identical motors, and difference between the phases of

the same motors tests. This will confirm the accuracy and reliability of the test results in finding shorted turn faults using shorted turn fault frequency components.

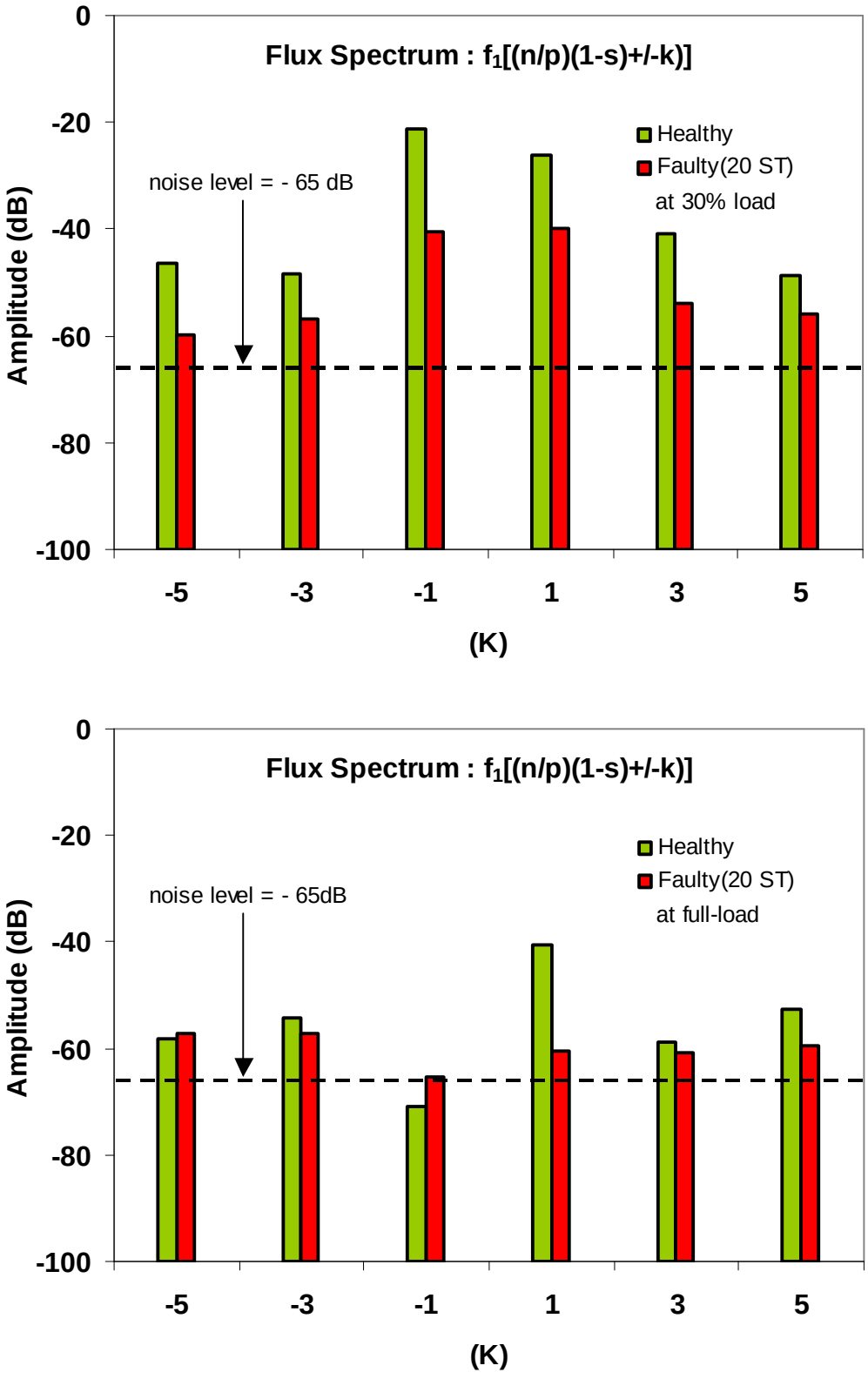

Figure 6.7: Comparison of variation in shorted turn sideband amplitude versus % of rated load of healthy motor at 30% load and at full-load.

6.2.2.3 Flux Spectrum Variations for Healthy Machines

To examine the accuracy and reliability of the test results to detect shorted turn faults using fault frequency components from flux signal, a set of three tests on the same healthy motor was conducted. Each test was repeated after the motor had been removed from the test rig and returned.

Figure 6.8 summaries the test results of three consecutive tests on the same healthy motor at 30% load for the different values of k. The results show the maximum variations in the sideband amplitudes for the healthy motor is less than 4 dB at 30% load, which is not significant and does not affect the accuracy and reliability of the test results obtained by using the shorted turn fault frequency components.

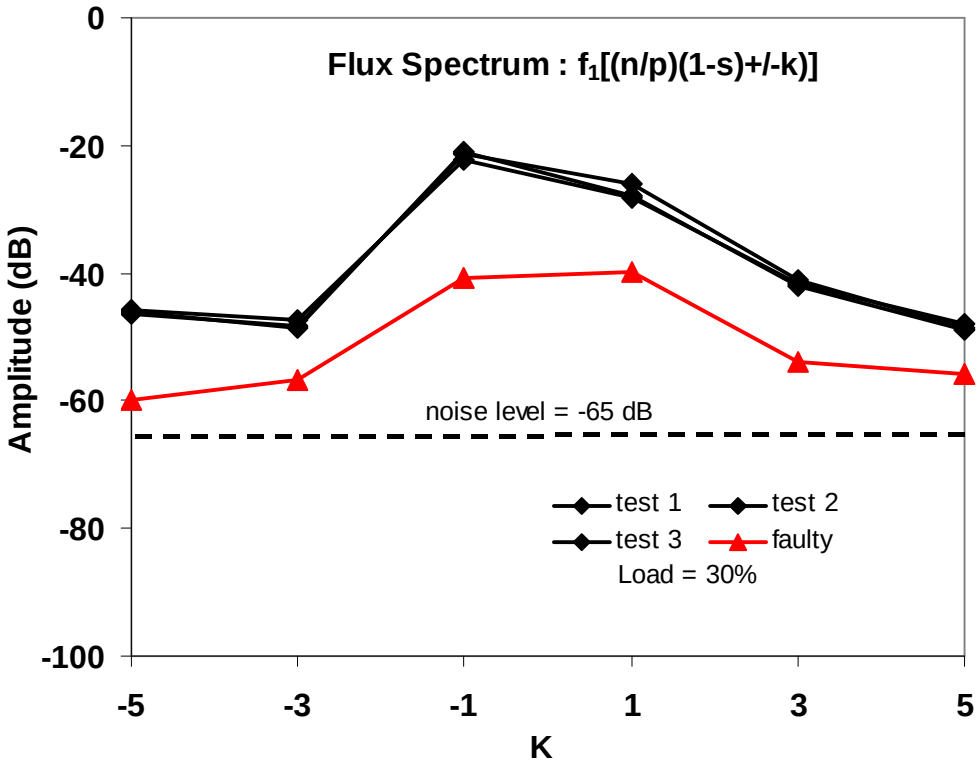

Figure 6.8: Comparison of variations in flux sideband amplitudes for three tests on the same healthy motor. The faulty motor result is shown for reference.

Figure 6.9 shows a comparison of the variation in the amplitudes of the shorted turn sideband components versus % of rated load for two similar rating (2.2 kW) of motors and the variations for any value of k is less than 4 dB, which are not significant. The finding demonstrates the reliability of test results.

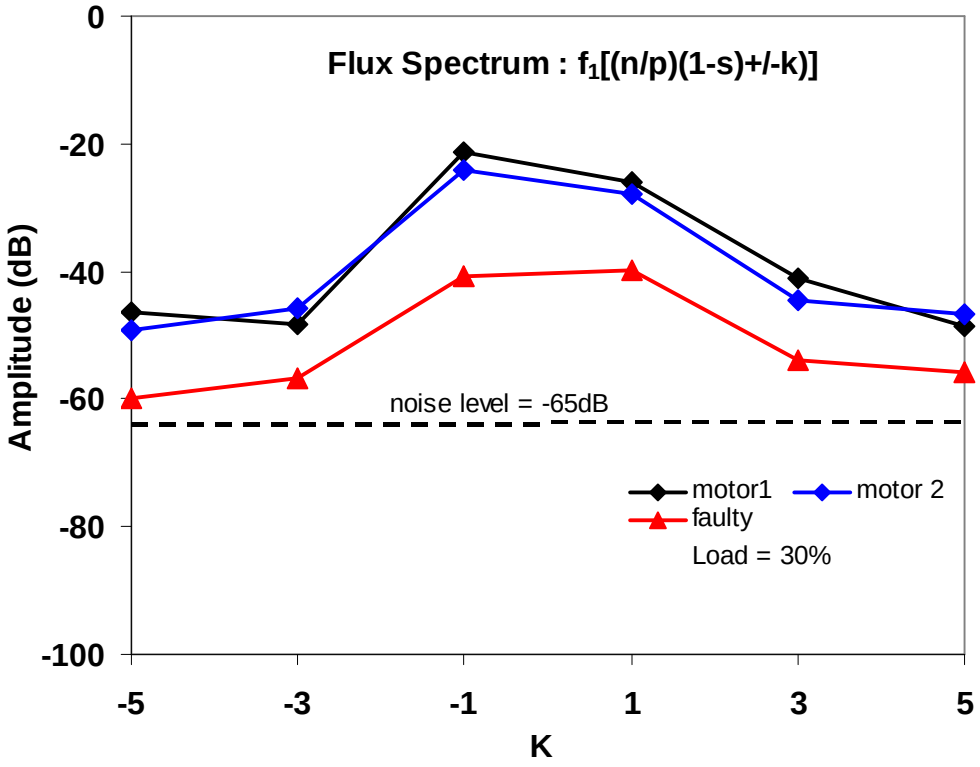

Figure 6.9: Variations in shorted turn sideband amplitudes for tests on two nominal identical healthy motors. The result of faulty motor is shown for reference.

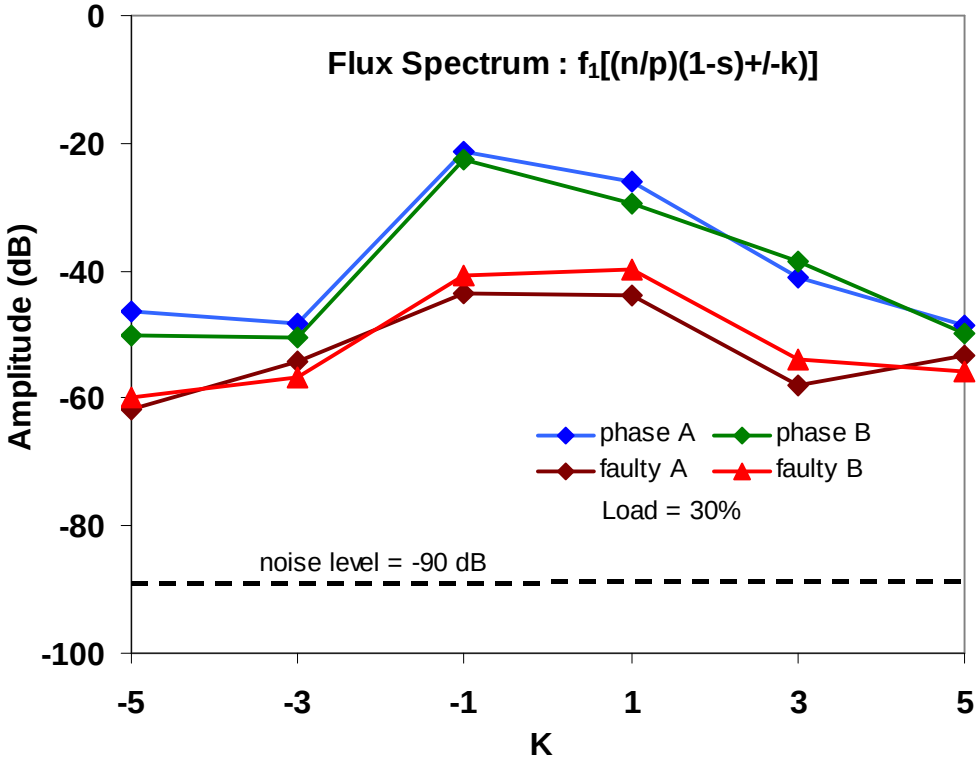

Figure 6.10 Variations in shorted turn sideband amplitudes for tests on two nominal identical healthy motors. Faulty motor result is shown for reference.

Figure 6.10 shows variation in the sideband amplitudes between phases A and B for a healthy motor and faulty motor with 20 shorted turns for different values of k at 30% load. The variations in the amplitudes of fault frequency components for the two phases of the healthy and faulty motors showed slight variations of less than 3 dB for any value of k. In summary all three tests showed that the test results are accurate and reliable.

6.2.3 Shorted Turn Fault Detection using Instantaneous Power Spectrum

6.2.3.1 Healthy and Faulty Instantaneous Power Spectra

The instantaneous power signal's frequency spectra for a healthy and a faulty motor for n=1 and k=±1 at full-load are shown in Figure 6.11, which are used to detect shorted turn faults in the machines. The spectrum showed the significant variations emerged in the amplitude of fault frequency sideband components in the faulty motor and are clearly visible in comparison to the healthy motor.

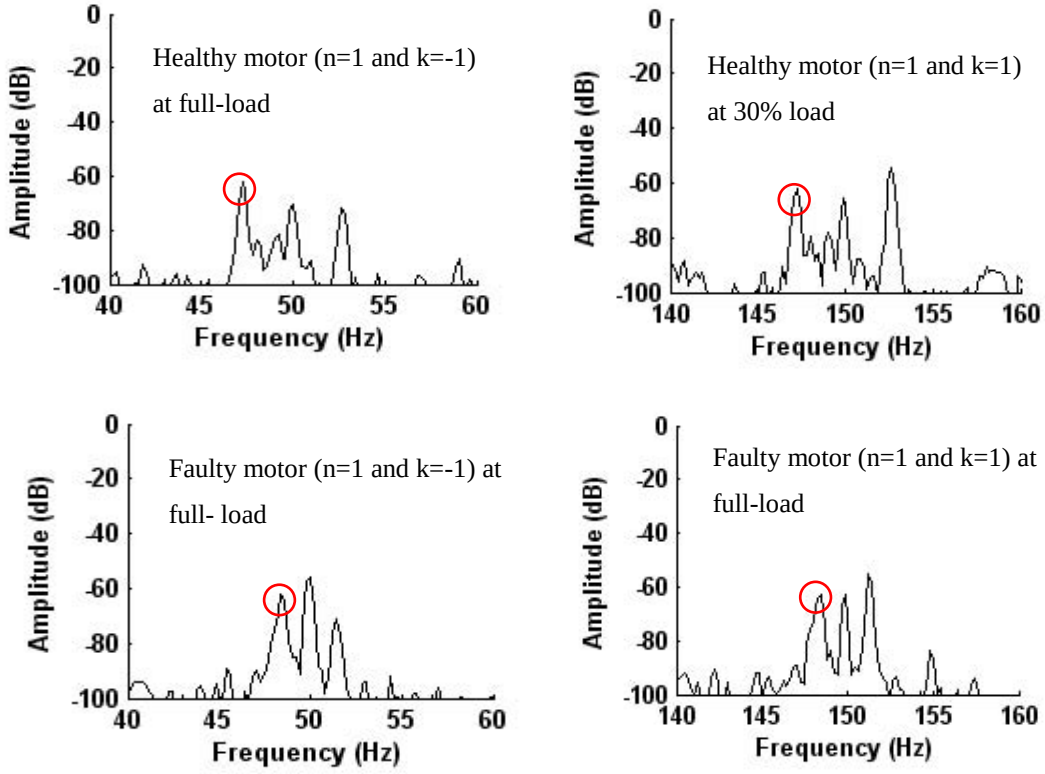

Figure 6.11: Comparison of the instantaneous power spectrum from a healthy motor at 30% load (top row) and at full-load (bottom row).

6.2.3.2 Shorted Turn Fault Frequencies from Instantaneous Power

Figure 6.12 indicates variation in the amplitudes of the healthy and faulty motor with 20 shorted turns at 30% and full-load tests for n=1 and k=±1.

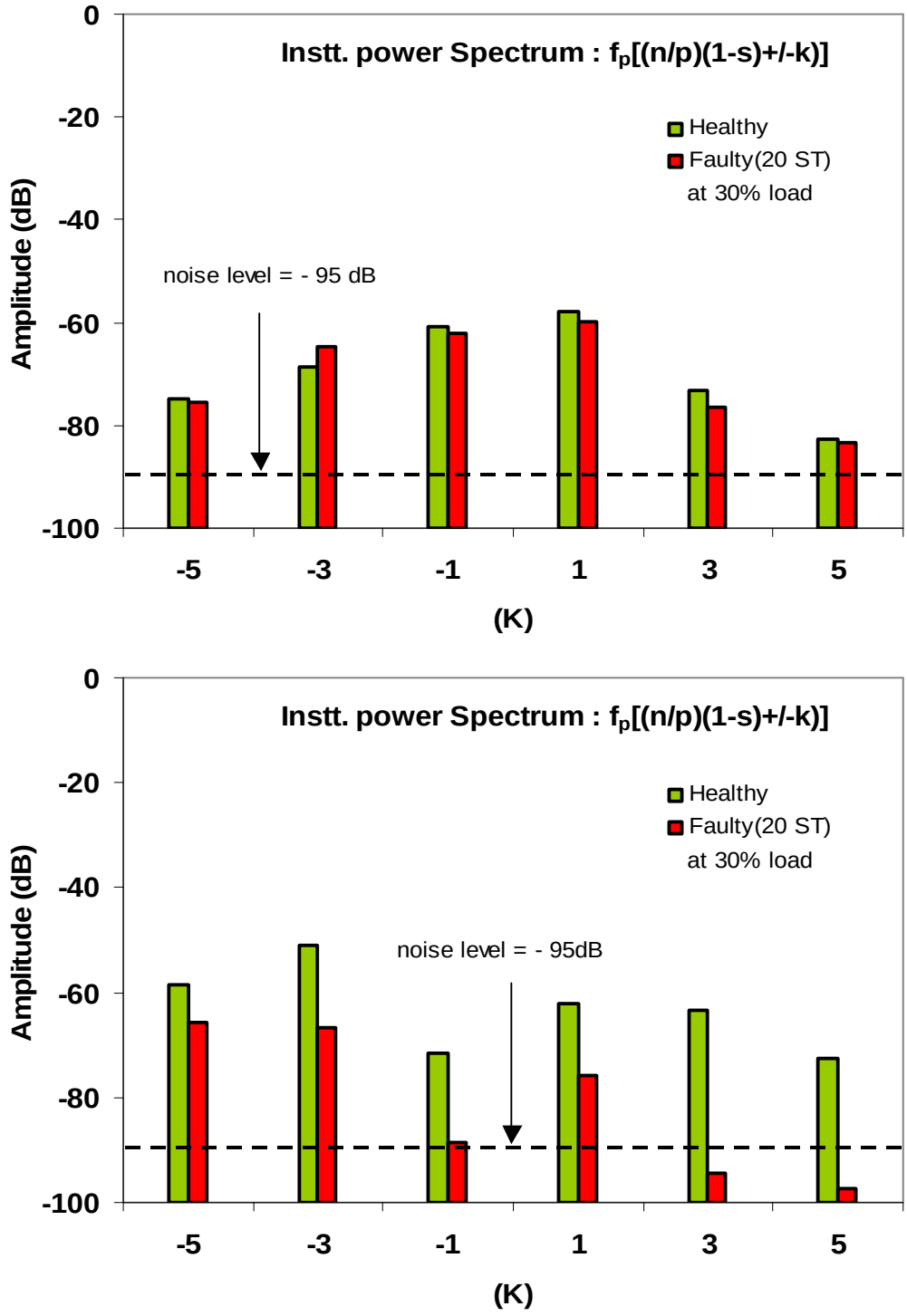

Figure 6.12: Variations in the shorted turn sidebands amplitudes versus % of rated load of healthy motor for different values of k from instantaneous power spectrum.

The result shows a much clearer separation in the amplitude of sideband component at 100% load for n=1 and k=±1. It can be concluded that the instantaneous power signal showed slightly more variation in the amplitude of negative sideband components at 100% load when compared to the result for the current and flux spectra. However, results obtained at 30 % load showed slight variations in the amplitude of fault frequency component for the healthy and faulty motor. Therefore, on the basis of these results, instantaneous power is useful for detecting shorted turn faults at 100% load.

Since the instantaneous power signal can detect shorted turn faults at higher loads, it is important to examine the variability of the instantaneous power signal in order to confirm its reliability of the test results to detect shorted turn fault using instantaneous power signal.

6.2.3.3 Instantaneous Power Variations for Healthy Machines

Figures 6.13, 6.14 and 6.15 depict the healthy motor results regarding: repeatability tests on the same motor; differences between motors; and differences between the motor's phases for confirming the reliability of the test results in detecting shorted turn faults from the instantaneous power signal.

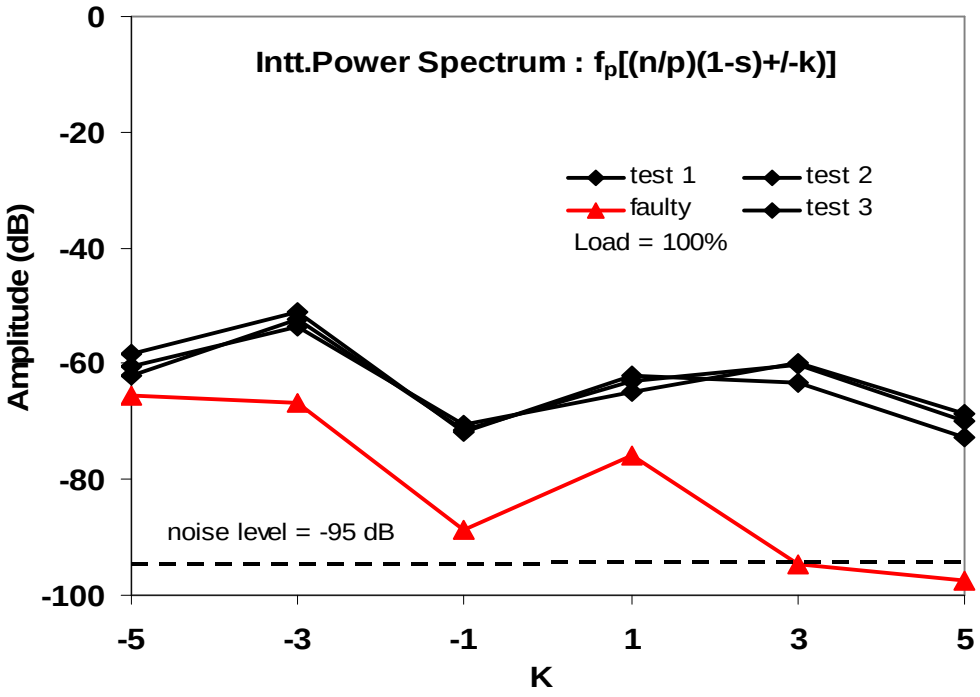

Figure 6.13: Variations in shorted turn sideband amplitudes for three tests on the same healthy motor at full-load.

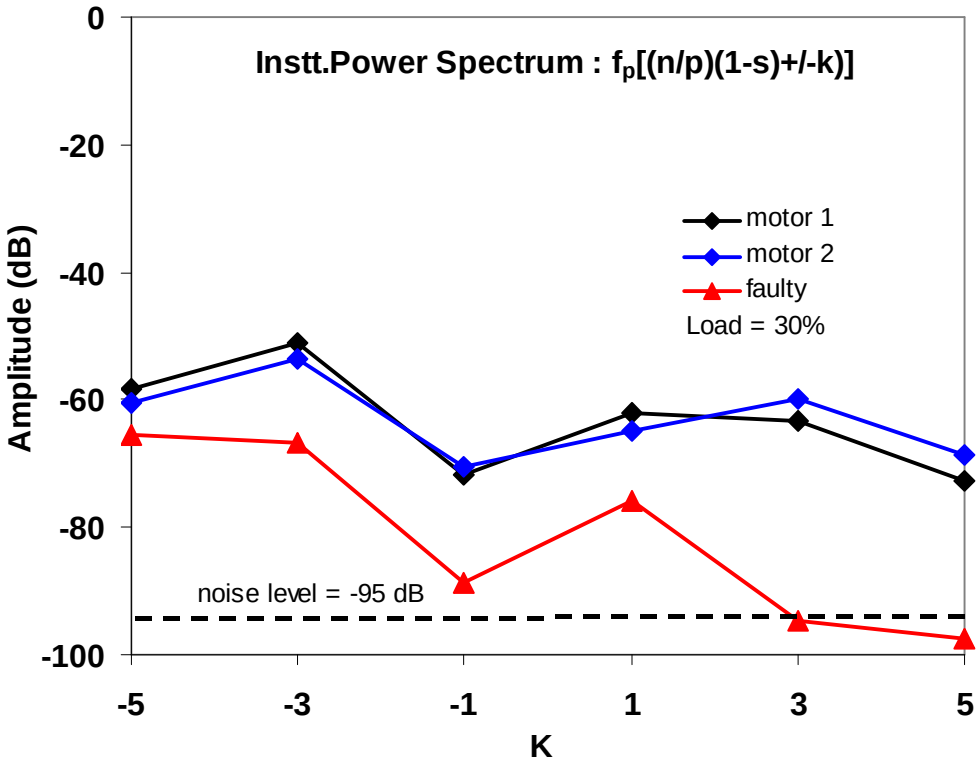

Figure 6.14: Variations in the shorted turn sideband amplitudes for tests on two identical healthy motors at 100% load.

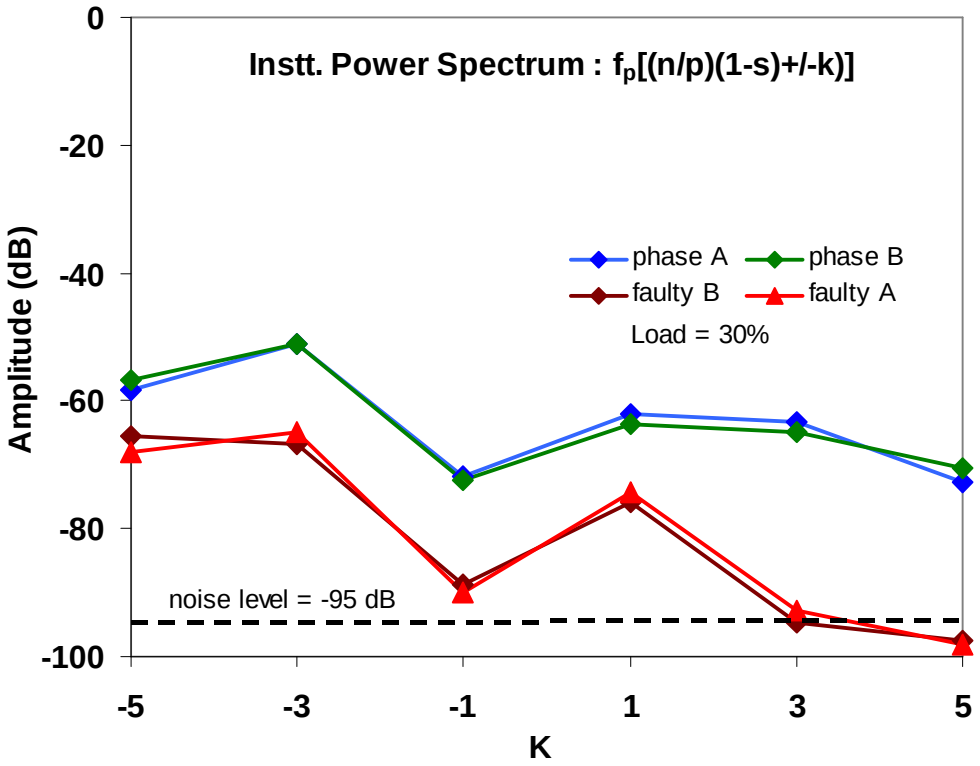

Figure 6.15: Variations in shorted turn sideband amplitudes of the healthy and faulty motor between phases A and B at full-load.

Figure 6.13 summarises the variation in the sideband amplitude versus different values of k at 100% load and set of three tests. The variation was found to be less than 3 dB, which is very small.

Figure 6.14 compares the instantaneous power sideband amplitude versus different values of k at 100% load for the two nominally identical healthy motors and demonstrated a small variation of 4 dB, which is not significant.

Figure 6.15 highlights the variation in the sideband amplitude between phases A and B for a healthy and faulty motor. The variation in the amplitude for both phases is less than 3 dB, which is also very small.

It can be concluded from the three different tests on the healthy motor that there no significant variations were found in the amplitudes of fault frequency components, and this confirms the accuracy and reliability of the test results.

6.2.4 Combination of Flux and Instantaneous Power Spectra

Figure 6.16 shows the measured shorted turn sideband amplitudes for healthy and faulty motor (20 shorted turns) over a wide range of loads from the flux, instantaneous power and single signal.

The results obtained from the flux and current signals indicate that shorted turn causes sideband amplitude to decrease as the load on the motor increases. However, flux signal proved more suitable and in fact preferable on detecting shorted turn faults at light loads, while the instantaneous power is able to detect shorted turn faults at higher loads. It is difficult to set a threshold between the healthy and faulty motors.

To overcome this difficulty, the single signal, which is a combination of both flux and instantaneous power signals, is investigated further. The best feature of the single signal is that the sideband amplitude between the shorted turn fault frequency components are generally higher as shown in Figure 6.16 (bottom row). It is thus easier to set a threshold between the healthy and faulty motors to determine the shorted turn fault severity.

In summary, the single signal is preferable detecting shorted turn faults over a wide range of loads for the different values of k when compared to the flux and instantaneous power signal

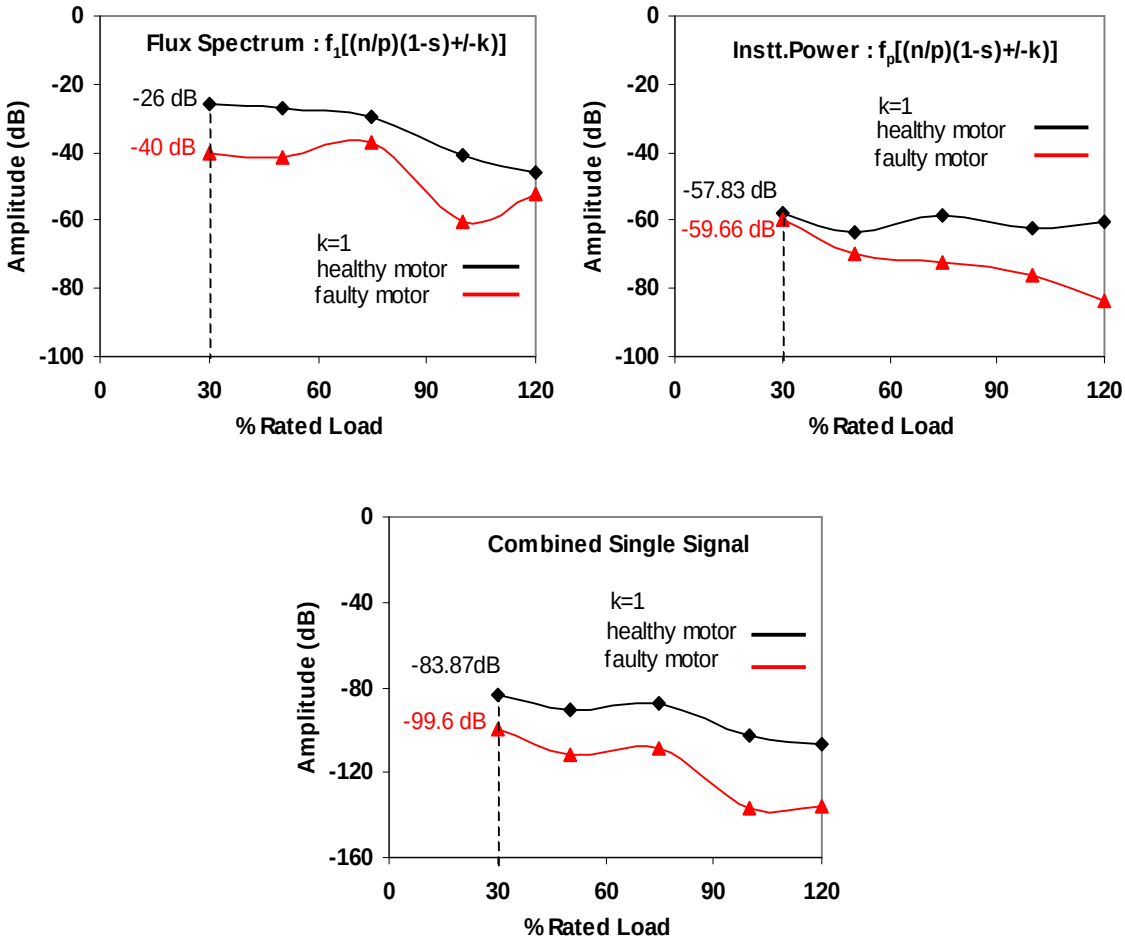

Figure 6.16: Variations in the sideband amplitudes for the healthy and faulty motor (with 20 shorted turns). Top row (left) and top row (right) show the flux and instantaneous power. The Bottom (row) represents a single signal.

6.3 Summary

We investigated the use of current, flux and instantaneous power signals to detect shorted turn faults using standard fault frequencies for the different values of k over a wide range of varying loads. Using fault frequency components to detect the faults and estimate fault severity in the machines relies heavily on variations in the amplitude of sideband components.

The results for the current signal show that it is not suitable for detecting the shorted turn faults under any level of loading. The flux signal indicates that it is useful for finding shorted turn faults at light loads but only for the specific values of k. However, the flux signal is not able to provide useful information to detect shorted turn faults at higher load

because at higher loads the variations in the amplitudes of sideband components between the healthy and faulty motor are small. The summary of results is shown in Table 6.2.

Table 6.2: Comparison of healthy and faulty motors in detecting shorted turn faults using components $f_1[(n\backslash p)(1-s)\pm k]$ under different levels of loading.

Signal	**Value of integer k when the difference between the healthy & faulty motor;s amplitude is ≥ 14 dB**				**Minimum % Rated Load when the amplitude is ≥ 14 dB**	**Variations in the amplitudes between the healthy and faulty motors**	**Comments**
	Number of shorted turns						
	5	**10**	**15**	**20**			
Current	X	X	X	X	Not found	Not found	Not applicable because of small variations in the amplitudes of faulty motors.
Flux	X	X	X	±1	30%	19 dB	Suitable and useful for detecting shorted turn faults for the specific value of k and when the motor has more than 20 number of shorted turns.
Instt. Power	X	X	X	±1	100%	15 dB	Suitable and useful for detecting shorted turn faults at higher loads for the specific value of k and when the motor has motor more than 20 shorted turns.
Combined Single Signal	X	X	±1	±1, ±3	30%	25 dB	Preferable for detecting shorted turn faults for the different values of k and when the motor has over or about 15 shorted turns.

The results for the current signal show that it is not suitable for detecting the shorted turn faults under any level of loading. The flux signal indicates that it is useful for finding shorted turn faults at light loads but only for the specific values of k. However, the flux signal is not able to provide useful information to detect shorted turn faults at higher load because at higher loads the variations in the amplitudes of sideband components between the healthy and faulty motor are small.

Instantaneous power shows that there is enough separation between the healthy and faulty motors in the frequency spectra at full-load for the different values of k. In contrast, results obtained at 30 % load showed small variations in the amplitudes of fault frequency components. Therefore, on the basis of the results obtained, instantaneous power is useful for detecting shorted turn faults only at higher loads.

The use of single signal, which is obtained by combining the flux and instantaneous power signals to detect shorted turns fault, showed much clearer variations between healthy and faulty motors over a wide range of loads. Therefore, it is suggested that to detect shorted turns fault using the combined single signal for different level of loadings is preferred.

Chapter 7

Misalignment Faults

7.1 Introduction

This chapter investigate the misaligned motors by analysing a number of non-invasive sensor quantities such as current, flux and instantaneous power spectra. There are two types of misalignment in machines as shown in Figure 7.1; angular misalignment, that is the amount by which the alignment of driver and driven shafts are skewed; and the second one is known as parallel misalignment, it is the amount by which the alignment of driver and driven shafts are out of parallel alignment. The measurements are performed at different levels of loading to detect the misaligned motors, and takes into consideration the characteristic fault frequencies of broken rotor bar, shorted turn and eccentricity (as described in Chapter 2) from current, flux and instantaneous power spectrums.

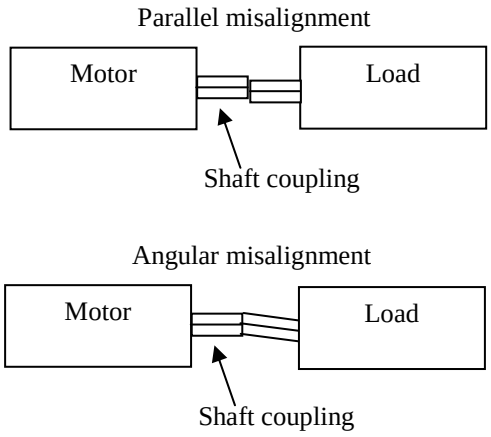

Figure 7.1: schematic diagram of parallel and angular misalignment.

7.2 Detection of Misalignment using Broken Bar Sidebands from different Spectra

7.2.1 Comparison of Healthy and Faulty Spectra of different Signals

Figure 7.2 compares the frequency spectrums of the stator current, axial flux and instantaneous power signals for a healthy motor to the misaligned motor. The circles in each diagram indicate the broken rotor bar sidebands at full-load. The noise levels are about –90 dB, -65 dB and –80 dB respectively.

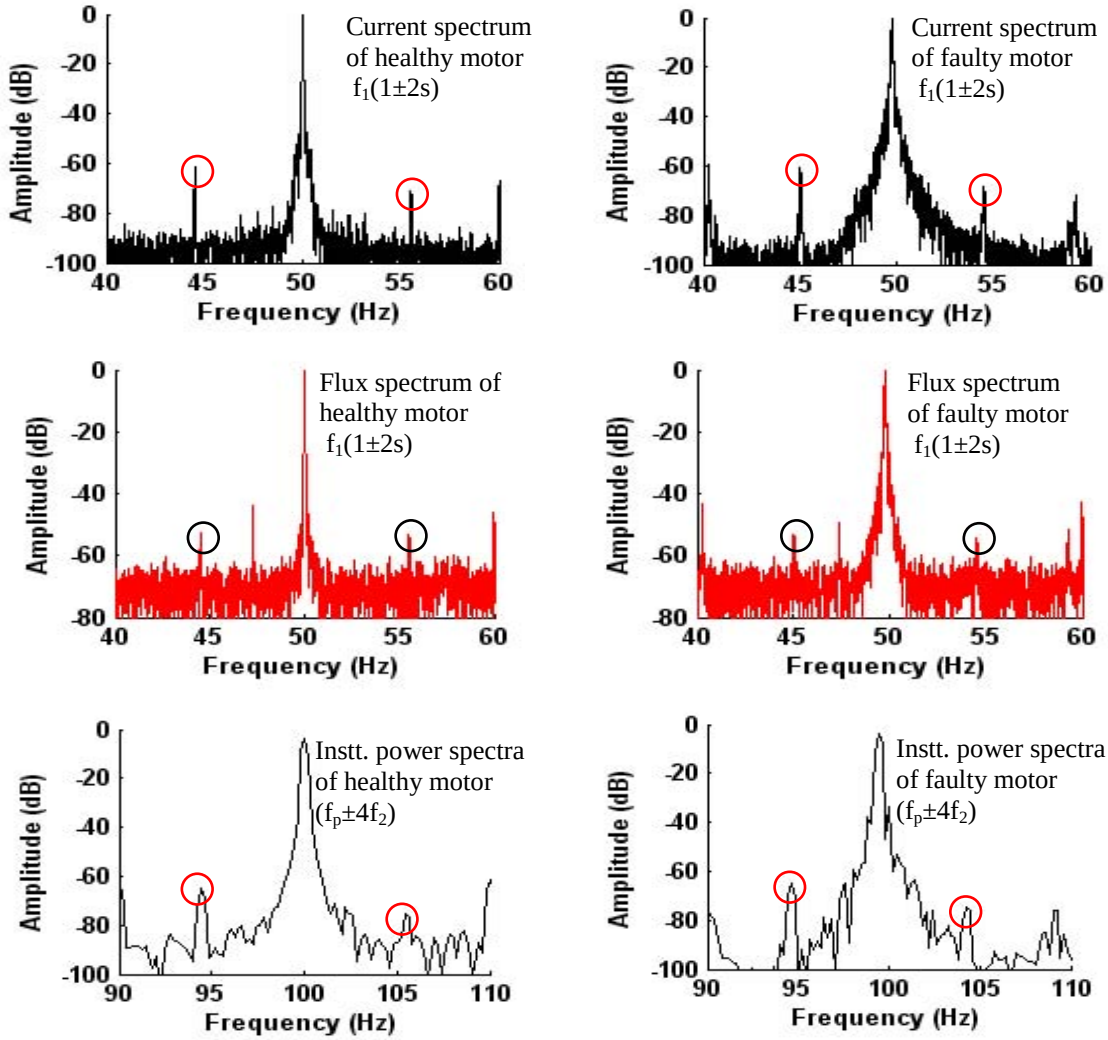

Figure 7.2: Comparison of the current, flux and instantaneous power spectrums from a healthy machine with a misaligned machine showed in (top, middle and bottom row) at full-load.

It can be concluded from Figure 7.2 that variation in the sideband components of BRB fault frequency due to misalignment are clearly visible in the frequency spectrum of healthy and misaligned motor in the current when compared to the sideband components in the flux and instantaneous power spectra. However, variations in the sideband amplitudes between the healthy and faulty motor were found to be less than 4 dB, which is not significant.

7.2.2 Misaligned Broken Bar Fault Frequencies from different Spectrums

Due to misalignment fault, changes in the amplitudes of BRB fault frequencies from current signal at different level of load tests were found to be (< 3 dB) as shown in Figure 7.3 below. This variation is small because the misalignment developed in the machines for the experiment is small.

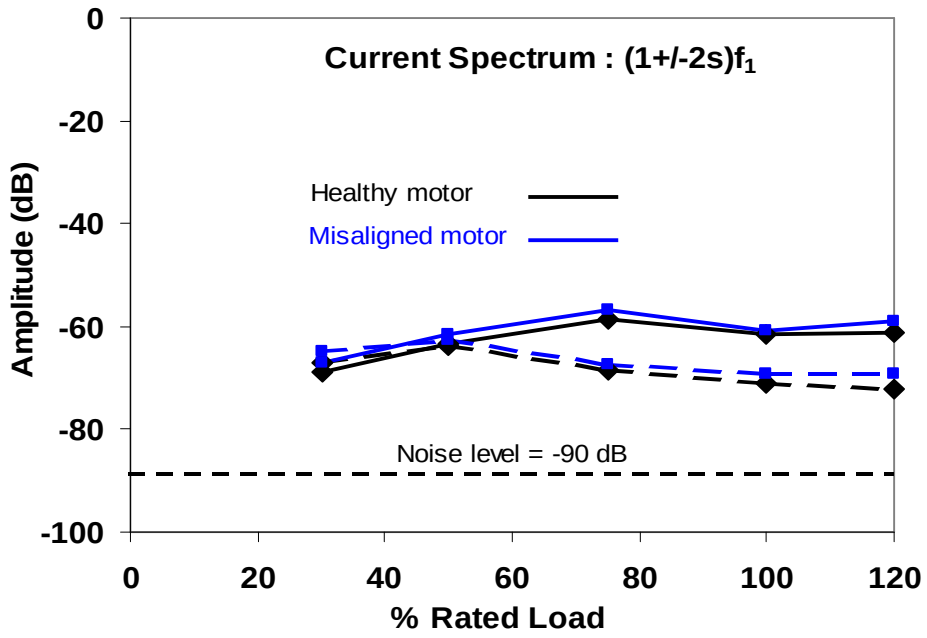

Figure 7.3: Comparison of variation in sideband amplitudes versus % of rated load of a healthy motor with misaligned motor from current spectrum.

The difference in the sideband amplitudes from the flux spectrum was found to be about 3 dB. This variation was not clearly visible due to inconsistent decrease/increase and some overlap in the amplitudes of sideband components between the healthy and misaligned motor under different load tests (Figure 7.4).

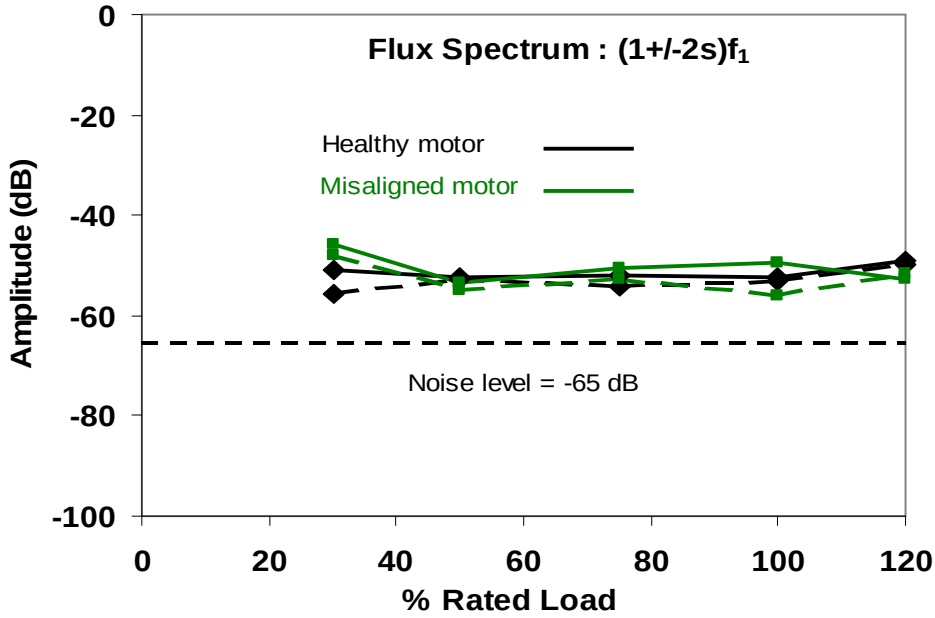

Figure 7.4: Comparison of variation in sideband amplitudes versus % of rated load of a healthy motor with misaligned motor from flux spectrum.

Figure 7.5 shows the change in the amplitudes of BRB fault frequency components due to misalignment in machine were approximately more than 10 dB when compared to the healthy motor. Furthermore, they are clearly visible in the spectrum under different load tests. It has been observed from the above results that instantaneous power is more useful detecting the misalignment fault when compared with current and flux signals.

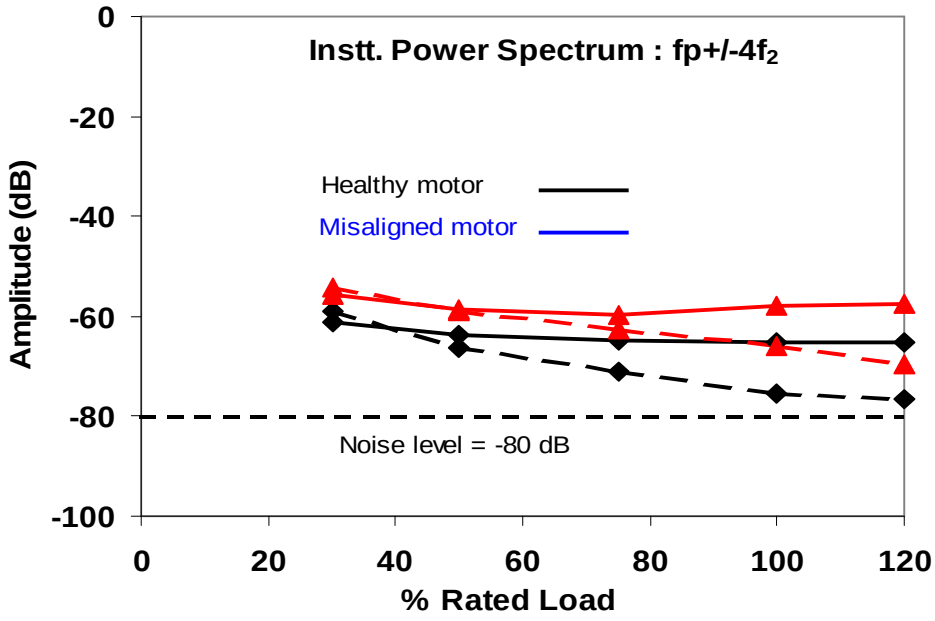

Figure 7.5: Comparison of variation in sideband amplitudes versus % of rated load of a healthy motor with misaligned motor from instantaneous power spectrum.

7.3 Detection of Misalignment using Eccentricity Sidebands from different Spectra

7.3.1 Comparison of Healthy and Faulty Spectra of different Signals

Figures 7.6, 7.7 and 7.8, compare the sideband amplitude of the misaligned machine with a healthy motor using eccentricity fault frequencies from the current, flux and instantaneous power spectrum versus % of rated load of full-load. It can be concluded from Figure 7.6 that changes in the amplitudes of eccentricity sideband components in the current spectra between healthy and faulty motor are clearly visible. The noise level is –90 dB.

Figure 7.7 shows that the amplitudes of eccentricity fault frequencies from the flux spectrum for the healthy and faulty motor are high, when compared to the current spectrum. However, the affect of misalignment is small and hard to differentiate between the healthy and faulty motor. The noise level is –65 dB.

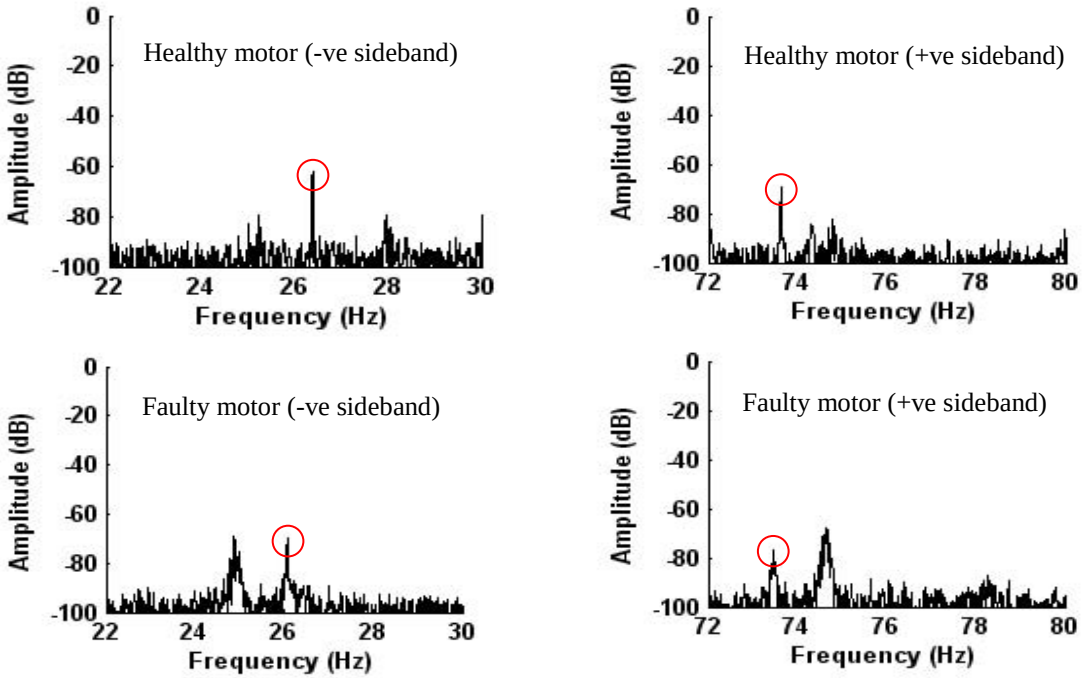

Figure 7.6: Current spectrum from a healthy machine (top row) and a misaligned machine (bottom row) at full-load.

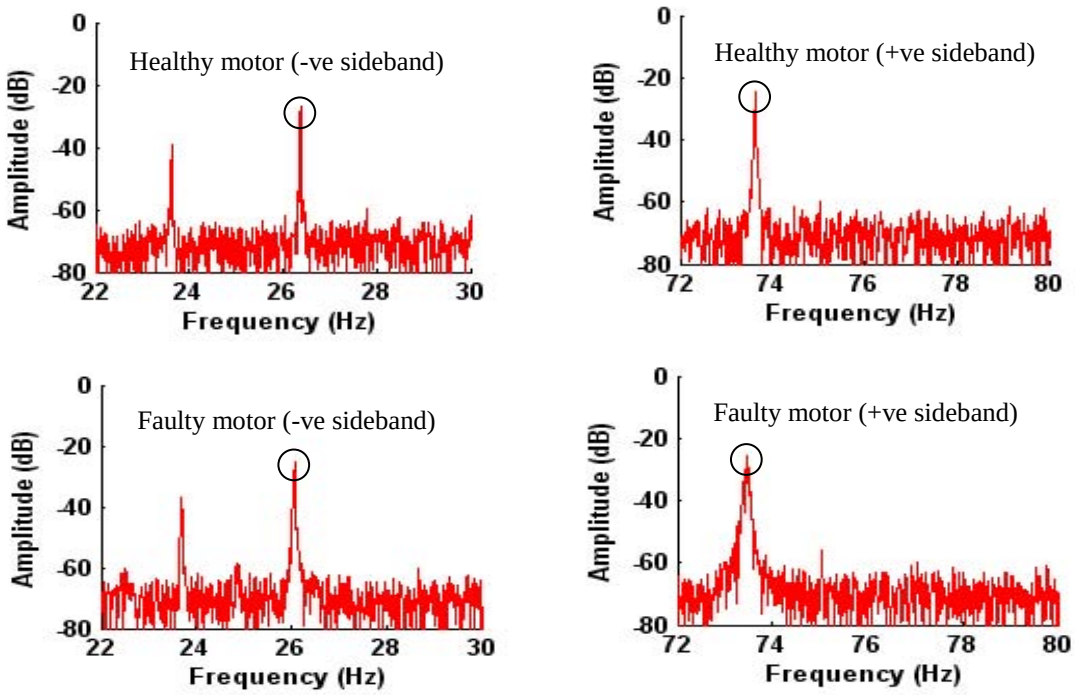

Figure 7.7: Flux spectrum from a healthy machine (top row) and a misaligned machine (bottom row) at full-load.

Figure 7.8 shows that the amplitude of eccentricity fault frequencies from the instantaneous power spectrum between healthy and faulty motor are very small, when compared to the current and flux spectrums. The noise level is –90 dB.

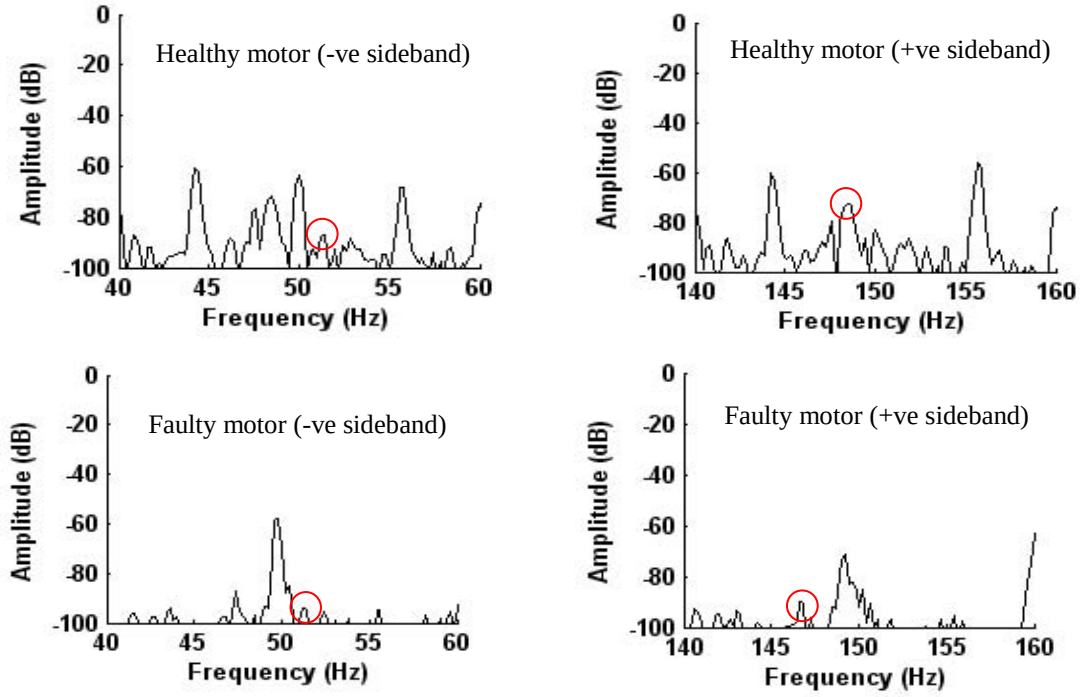

Figure 7.8: Instantaneous power spectrum from a healthy machine (top row) and a misaligned machine (bottom row) at full-load.

7.3.2 Misalignment Eccentricity Fault Frequencies from Current, Flux and Instantaneous Power Spectrum

The maximum variations in the amplitude of sideband components ($f_1 \pm f_r$) between the healthy and misaligned motor from the current spectrum were found to be less than 2 dB, which is small as shown in the Figure 7.9. Furthermore, the variation of the sideband amplitudes between healthy and misaligned motor at any load level are not consistent. Therefore, it is difficult for detecting the misalignment from current signal.

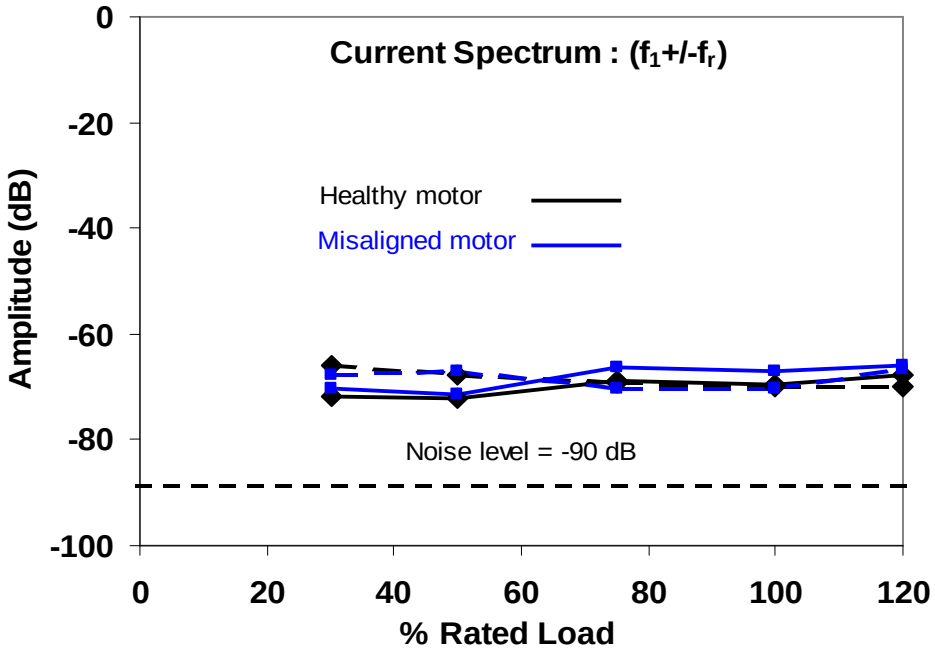

Figure 7.9: Comparison of variations in sideband amplitudes versus % of rated load of healthy motor with misaligned motor from current spectrum.

Figure 7.10 demonstrates a measurable variation of less than 4 dB in the amplitude for the healthy and misaligned motor. It is concluded from Figure 7.10 that due to high amplitudes of fault frequency sideband components, it is preferable to use flux signal instead of stator current. The noise level is about – 65 dB.

The investigation of the instantaneous power to detect the misalignment fault in machines shows small variations of less than 3 dB in the amplitudes of characteristic fault frequencies at any level of loading. It is thus difficult to detect the misalignment fault using instantaneous power signal as shown in Figure 7.11. The noise level is about –85 dB.

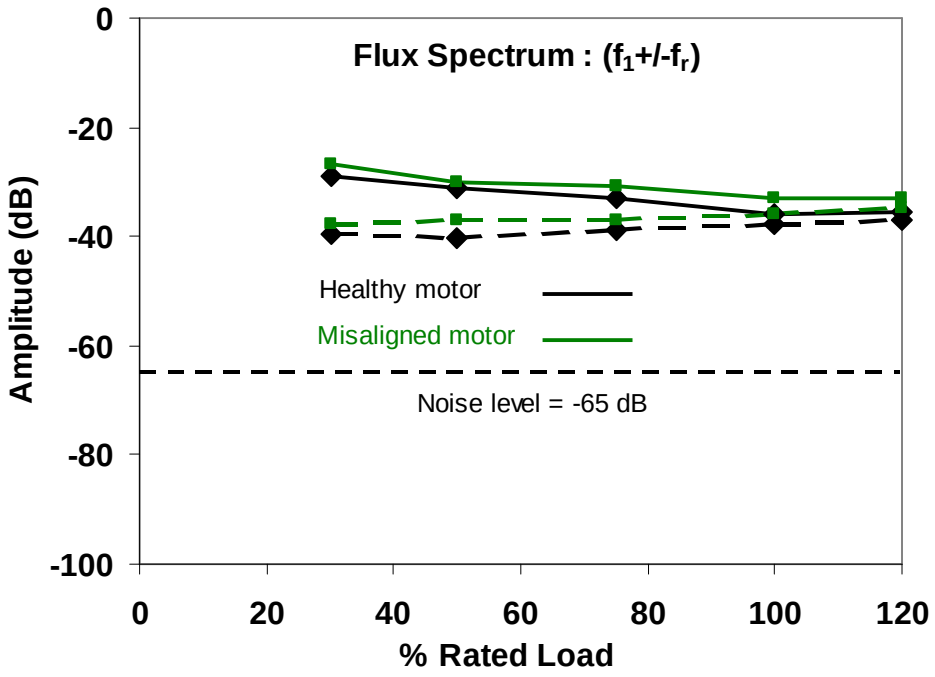

Figure 7.10: Comparison of variations in sideband amplitudes versus % of rated load of healthy motor with misaligned motor from flux spectrum.

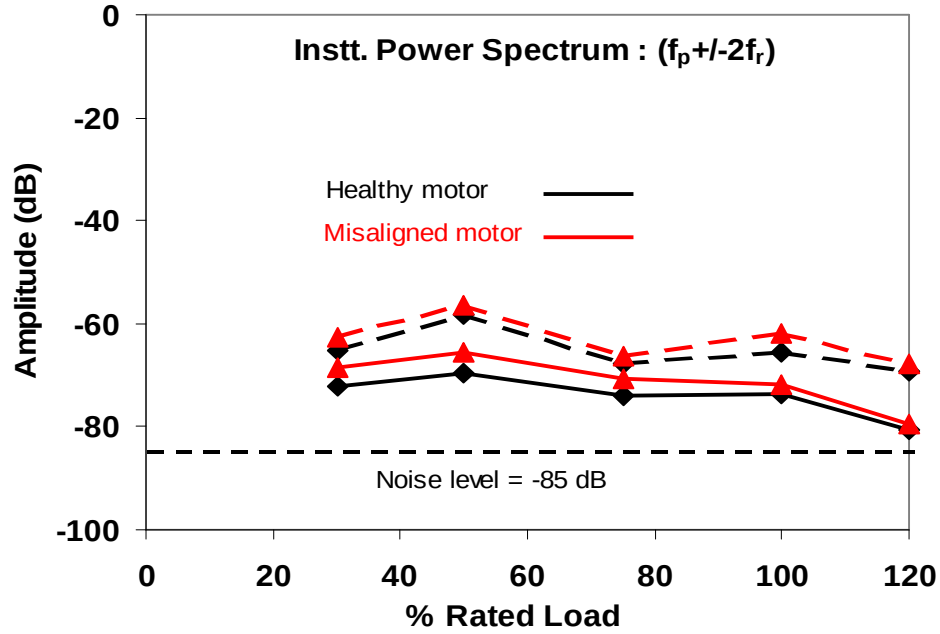

Figure 7.11: Comparison of variations in sideband amplitudes versus % of rated load of healthy motor with misaligned motor from instantaneous power spectrum.

7.4 Detection of Misalignment using Shorted Turn Sidebands from different Spectra

7.4.1 Comparison of Healthy and Faulty Spectra of different Signal

Figures 7.12, 7.13 and 7.14 compares the effect of the misaligned and healthy machine using the shorted turn (ST) sideband components of the stator current, axial flux and instantaneous power signals at full-load for n=1 and k=±3.

It can be concluded from these particular figures that only the flux spectrum clearly shows variations in the amplitude of fault frequency components due to misalignment in motor (Figure 7.13). In current and instantaneous power spectra, fault frequency components are not clearly visible. The noise level is about –90 dB.

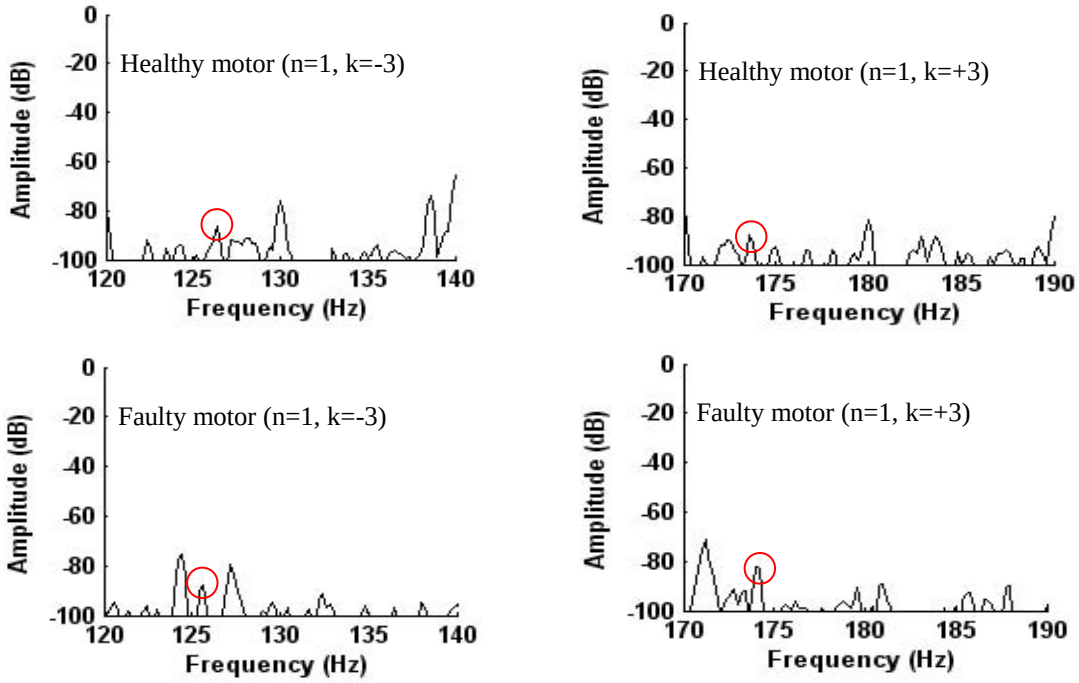

Figure 7.12: Current spectrum from a healthy machine (top row) and a misaligned machine (bottom row) at full-load.

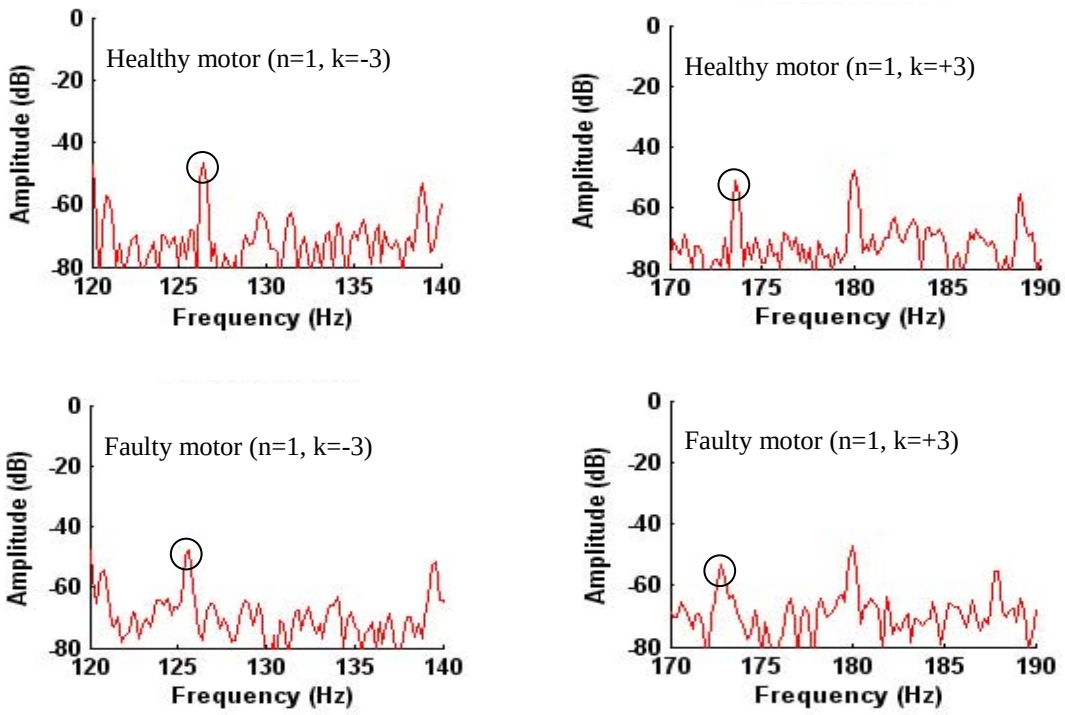

Figure 7.13: Flux spectrum from a healthy machine (top row) and a misaligned machine (bottom row) at full-load.

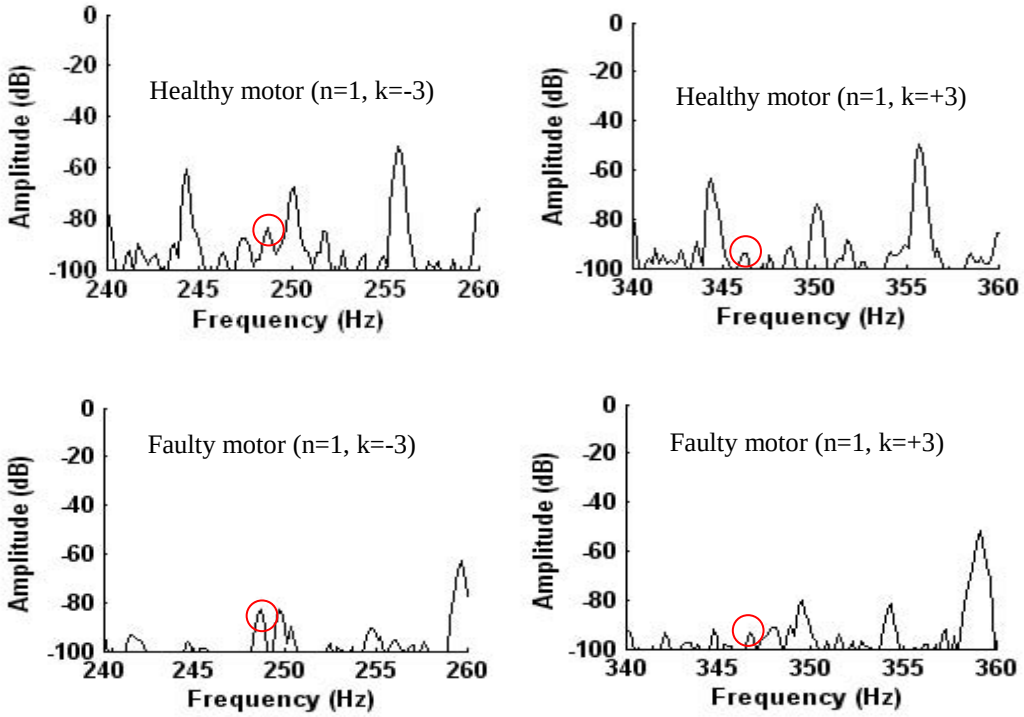

Figure 7.14: Instantaneous power spectrum from a healthy machine (top row) and a misaligned machine (bottom row) at full-load.

7.4.2 Shorted Turn Misalignment Fault Frequencies from Current, Flux and Instantaneous Power Spectra

Figures 7.15, 7.16 and 7.17 illustrates the sideband amplitude for n=1 and k=±1 and ±3 from current, flux and instantaneous power spectrums at full-load.

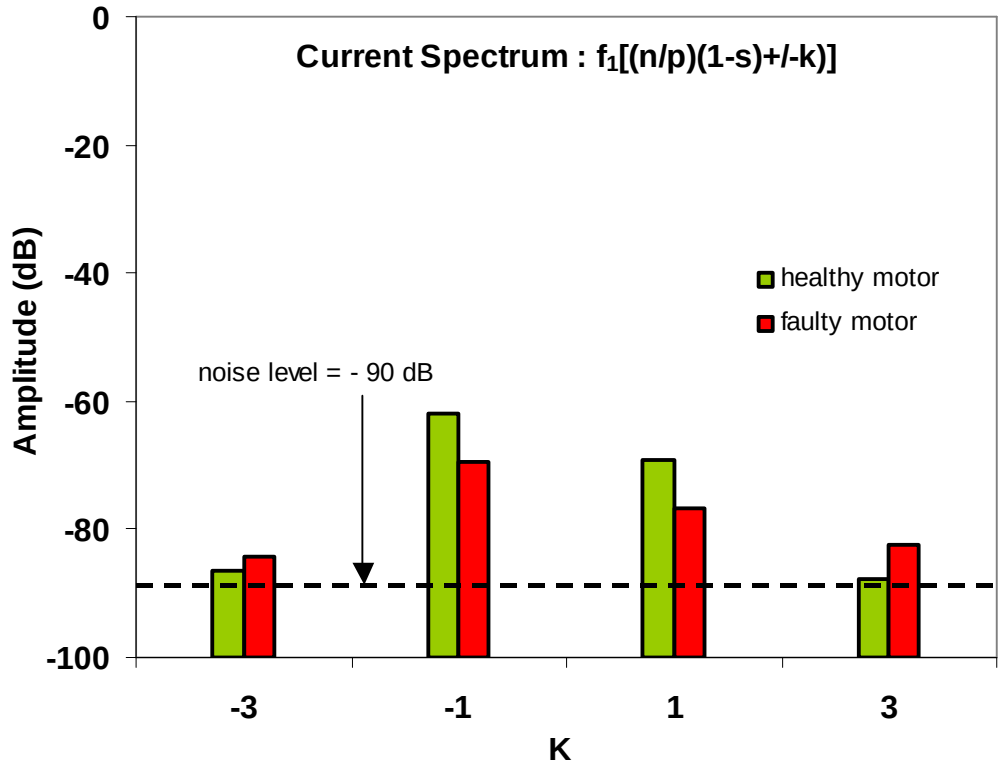

Figure 7.15: Comparison of variations in sideband amplitudes versus % of rated load of healthy motor with misaligned motor from current spectrum.

The variations in the sideband amplitude between the healthy and misaligned motor were found to be less than 4 dB in current, flux and instantaneous power spectrum. Current spectrum shows more variations at k=±1 and 3. In contrast, there is hardly any variation in flux spectrum as indicated in Figure 7.16.

Similarly instantaneous power shows some variations at k=±1 (Figure 7.17). Therefore, the variations in the sideband amplitude developed in current spectrum are useful for estimating the misaligned faults in machine. However, it is more reliable to detect the misalignment in machines using eccentricity fault frequency components because the effect of misalignment is more sensitive to the flux signal.

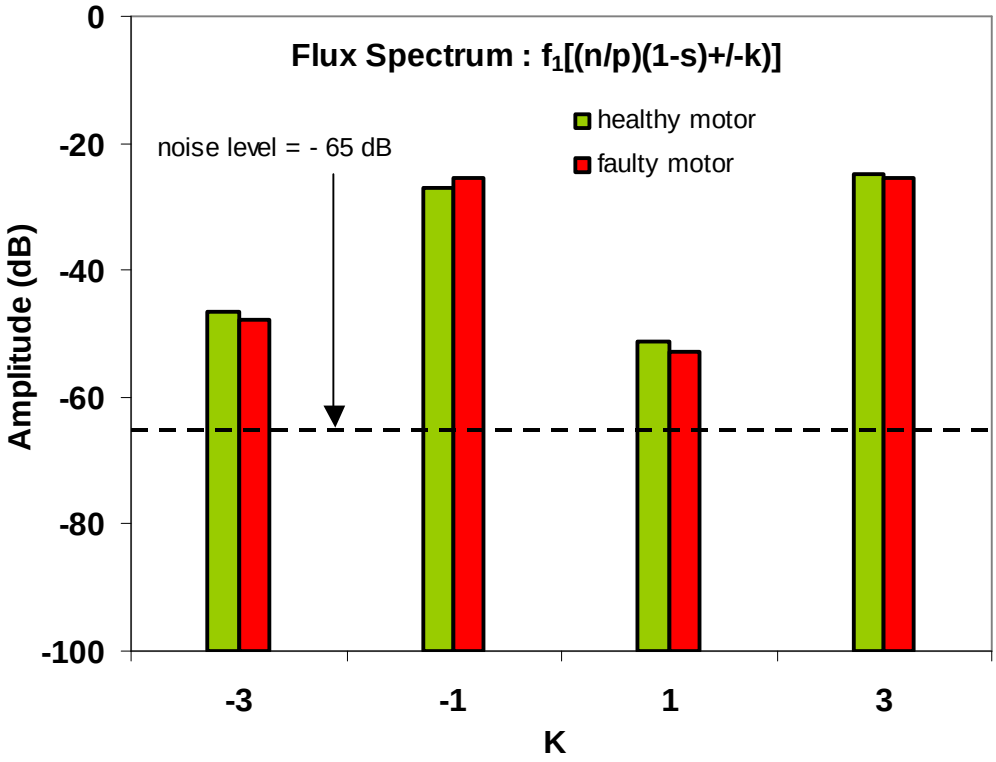

Figure 7.16: Comparison of variations in sideband amplitudes versus % of rated load of healthy motor with misaligned motor from flux spectrum.

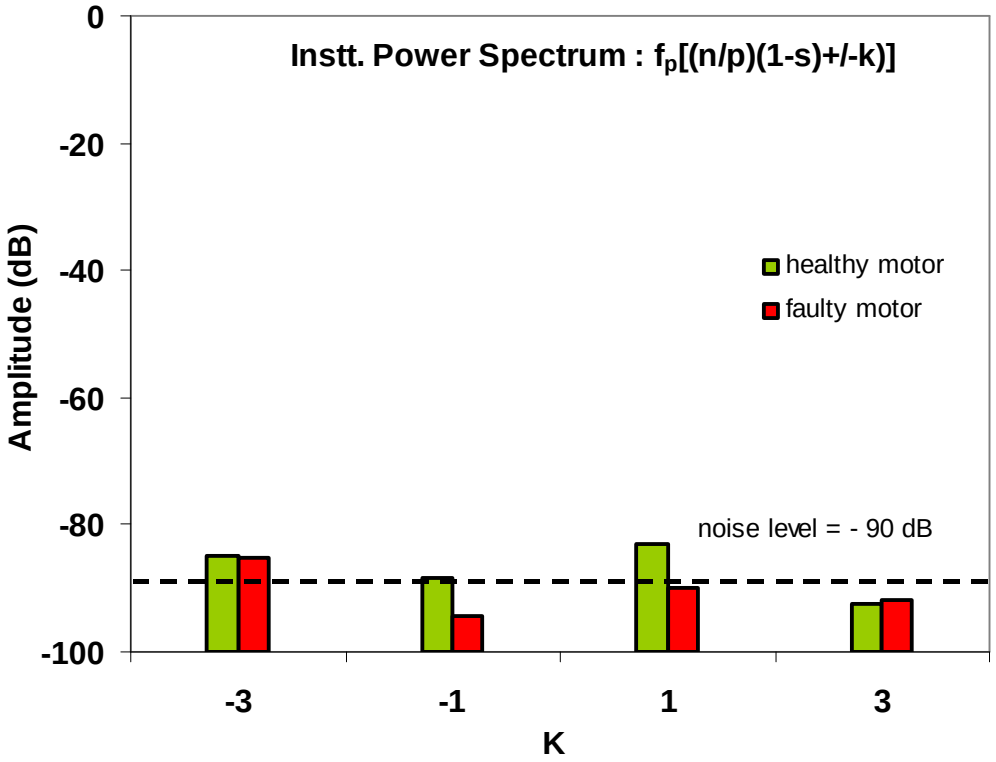

Figure 7.17: Comparison of variations in sideband amplitudes versus % of rated load of healthy motor with misaligned motor from instantaneous power spectrum.

7.5 Summary

The misalignment in the machines can decrease the accuracy and reliability of the test results. The presence of misalignment may cause eccentricity and may result in noise, vibration and increase in temperature. This can be detected, using BRB fault frequencies of $(1\pm2s)f_1$, $(f_1\pm f_r)$ and $(f_p\pm4f_2)$ from current, flux and instantaneous power signals.

However, it may be useful to use eccentricity fault frequency components $(f_1\pm f_r)$ from the flux signal for the purpose of detecting misalignment in the machines such misalignment normally causes the eccentricity faults. In the long-term, misalignment may cause catastrophic failure because of excessive vibration, stress on rotor and bearing and short-circuiting in the stator and rotor windings. Any slight visible variations in the sideband amplitudes of misalignment motor can be useful for aligning the motor. This will increase the accuracy and reliability of the test results, when considering ability to find different faults in machines. For each of the above signals, tests were also performed to check its variability in healthy motors due to test repeatability tests on the same motor, differences between nominally identical motors, and differences between the phases of the same motor.

Chapter 8

Investigation of Multiple Faults

8.1 Introduction

In induction motor monitoring normally single sensor is normally used to detect a single fault. Previously, the correlation between different types of sensors and their ability to diagnose multiple faults has not been studied thoroughly. The most prevalent faults in machines are broken rotor bar, stator or armature, misalignment, eccentricity and bearing related faults (bearing fault can also cause rotor eccentricity) [1,2].

This chapter's main purpose is to investigate fault frequencies in motors with multiple faults to be able to detect and to uncover the most prevalent that may occur in machines. The airgap between the rotor and stator of a healthy motor (2kW) used in this study is 0.4 mm (each side). Therefore, airgap of ±1, ±2 and ±3 mm at the driving and at non-driving-end are considered for the experiment.

The investigation of multiple faults (combination of broken rotor bars and eccentricity faults) at different levels of loading will involve the following:

- two broken rotor bars and eccentricity (0.1mm at driving-end)
- two broken rotor bars and eccentricity (0.3mm at driving-end)

8.2 Detection of Multiple Faults using Broken Bar Fault Frequencies

Combination of broken rotor bars and eccentricity faults may cause severe damage machines. Generally, researchers have examined the detection of faults at full-load level, although in practice the actual load may vary and can be significantly less.

It is important to detect any multiple faults (combination of broken rotor bars and eccentricity of different levels at non-driving and driving-end and driving-end) in the machines using characteristic fault frequencies of broken rotor bars and eccentricity at any load test levels.

As described in Chapter 2, fault frequencies are directly related to the supply and slip frequency. Any change in the fault frequencies due to fault in machines will also affect the slip frequency.

Frequency spectrum of the flux signal in the slip frequency range is shown in Figure 8.1 when the machine with multiple faults operates at different levels of load tests. This figure shows that multiple faults significantly affect the slip frequency when compared to the healthy motor.

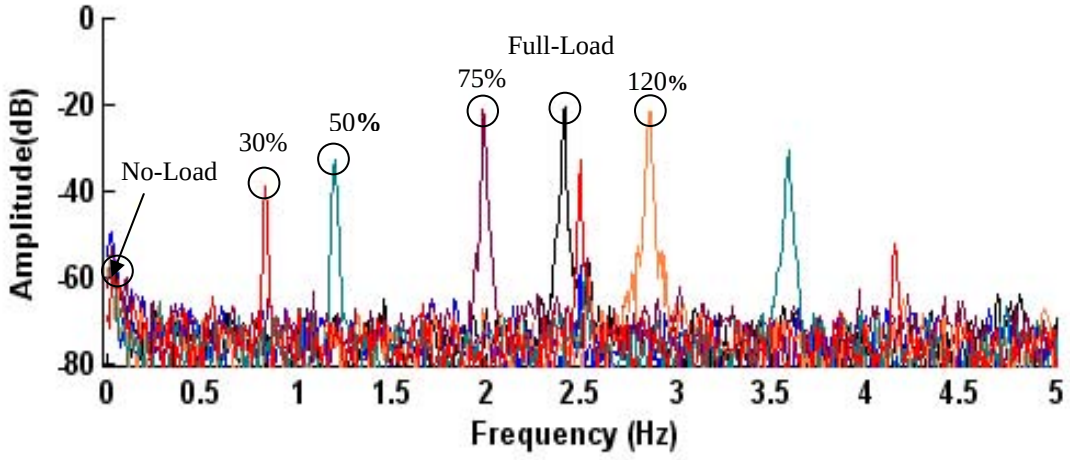

Figure 8.1: Flux spectrum of slip frequency versus sidebands amplitudes under different level of load tests.

8.2.1 Multiple Fault Detection using Current Spectra

8.2.1.1 Comparison of Healthy and Faulty Current Spectra

Figure 8.2 show a comparison of frequency spectra for a healthy machine and one that has multiple faults. At no-load the sideband components are not visible in the current spectra of the faulty machine. This is because of low slip frequency (Figure 5.1). However, at or above 50% of load there is a significant change of (>20 dB) in the amplitudes of faulty motor to a healthy motor. The noise level is about –90 dB.

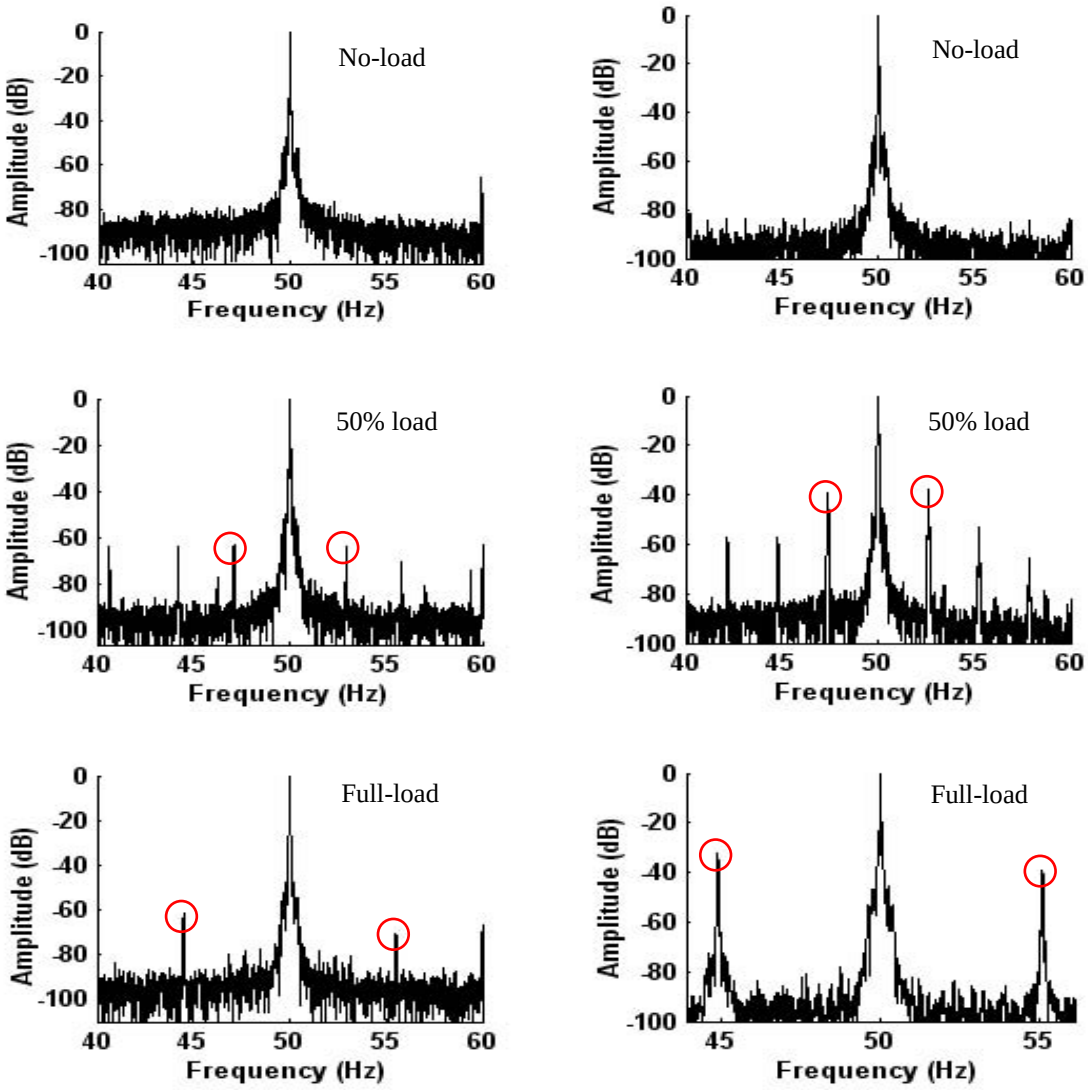

Figure 8.2: Current spectrum from a healthy machine (left) and a faulty machine with two broken rotor bars and eccentricity of +0.3mm at driving-end (right), at no-load, 50% load and full-load. The circles indicate the sidebands.

8.2.1.2 Broken Rotor Bar Fault Frequencies from Current Spectrum

The same custom-written program (as described in Chapter 3) was also used to analyse the raw data, produce the frequency spectrum and automatically locate the appropriate characteristic fault frequency peaks of multiple faults in the machines.

Figure 8.3 shows the broken rotor bars sideband amplitudes of the healthy motor and faulty motors with multiple faults (two broken bars and eccentricity level of +0.3 mm at driving-end).

The result shows that for multiple faults, at any load test levels, variations in the sideband amplitude between healthy and faulty machines were found to be more than 40 dB, which is significant and can be readily distinguished from healthy motors.

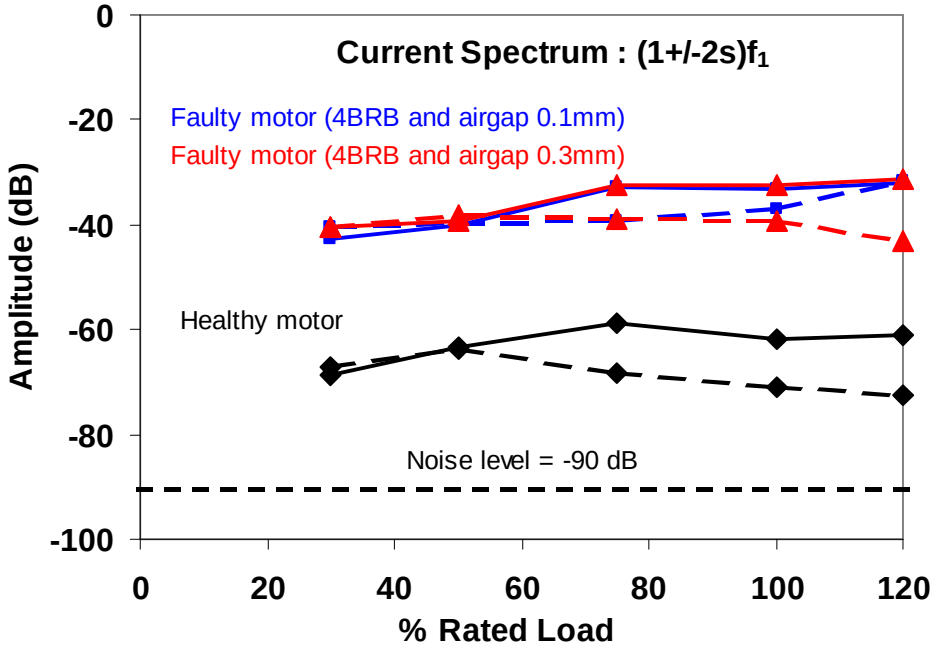

Figure 8.3: Comparison of variation in sidebands amplitudes versus % of rated load of a healthy motor with faulty motors (combination of two broken bars and eccentricity of +0.1mm and +0.3 mm at driving-end) from current spectrum.

8.2.2 Multiple Fault Detection from Flux Spectra

8.2.2.1 Comparison of Healthy and Faulty Flux Spectra

Figure 8.4 shows the amplitude of sideband components for fault frequency from the flux spectra at different levels of load for healthy and machines having multiple faults. The difference in the sideband amplitude of the faulty motor at less than or about 50%

load was found to be (<8 dB) when compared to the healthy motor. However, at full-load the increase in the amplitudes of sideband components was more (>20 dB) when compared to the healthy motor, which is significant. The noise level is about – 65 dB.

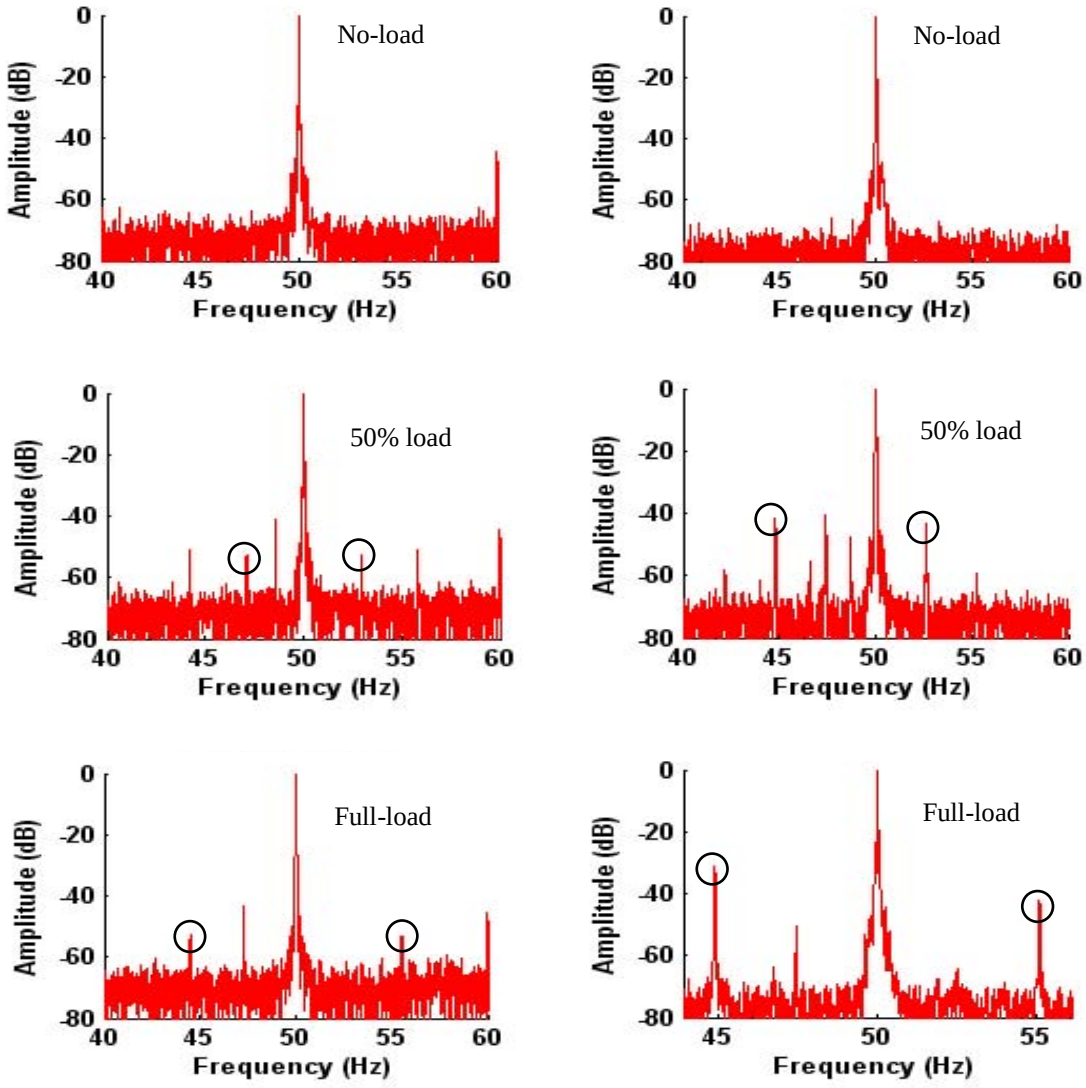

Figure 8.4: Flux spectrum from a healthy machine (left) and a faulty machine with two broken rotor bars and eccentricity of +0.3mm at driving-end (right), at no-load, 50% load and full-load. The circles indicate the sidebands.

8.2.2.2 Broken Rotor Bar fault frequencies from flux spectrum

Figure 8.5 indicates the variations in amplitude for fault frequencies of a healthy motor and unhealthy motors with multiple faults in the flux spectra, when the machine is operating at different load levels.

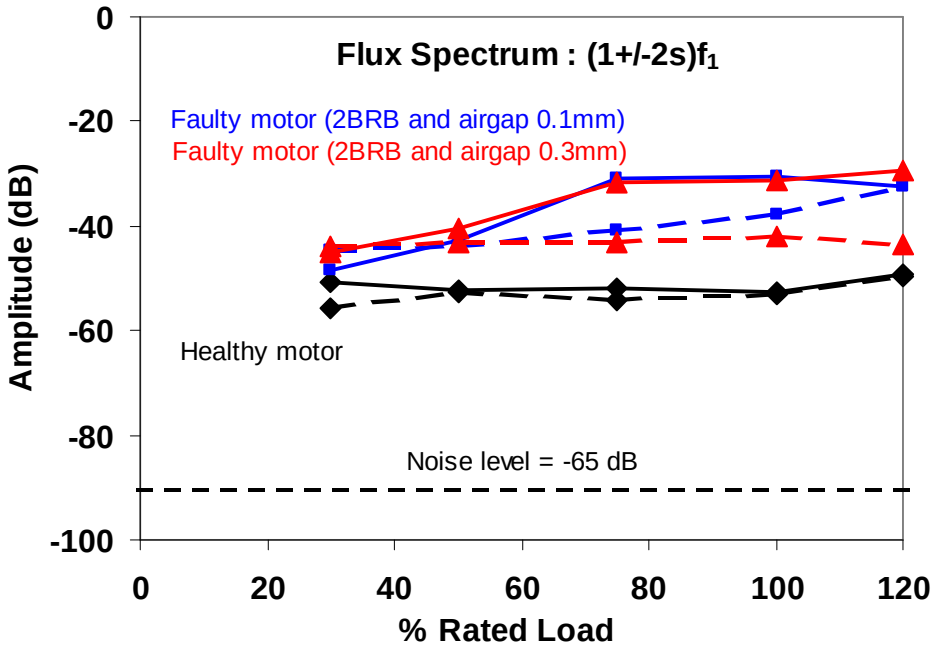

Figure 8.5: Comparison of variation in sidebands amplitudes versus % of rated load of a healthy motor with faulty motors (combination of two broken bars and eccentricity of +0.1mm and +0.3 mm at driving-end) from flux spectrum.

Figure 8.5 show the change in the sideband components is less than 7 dB at 30% load while at 50% load change in the fault frequency components is about 10 dB, which is relatively high. However, significant increase of (> 15 dB) in the amplitudes of sideband components was found at or more than 75% load.

These results lead to the conclusion that using the flux signal can detect multiple faults at high loads. However, this variation is less than the variation at the same level of loading in the current spectra.

8.2.3 Multiple Fault Detection using from Instantaneous Power Spectra

8.2.3.1 Comparison of Healthy and Faulty Instantaneous Power Spectra

The comparison of characteristic fault frequencies from the flux spectrum is shown in Figure 8.6. The differences in the sideband amplitudes between the healthy and faulty motors were found to be more than 20 dB. However, the number of other peaks present

at light load is more when compared to the scenario of heavy loads. The noise level is about –80 dB.

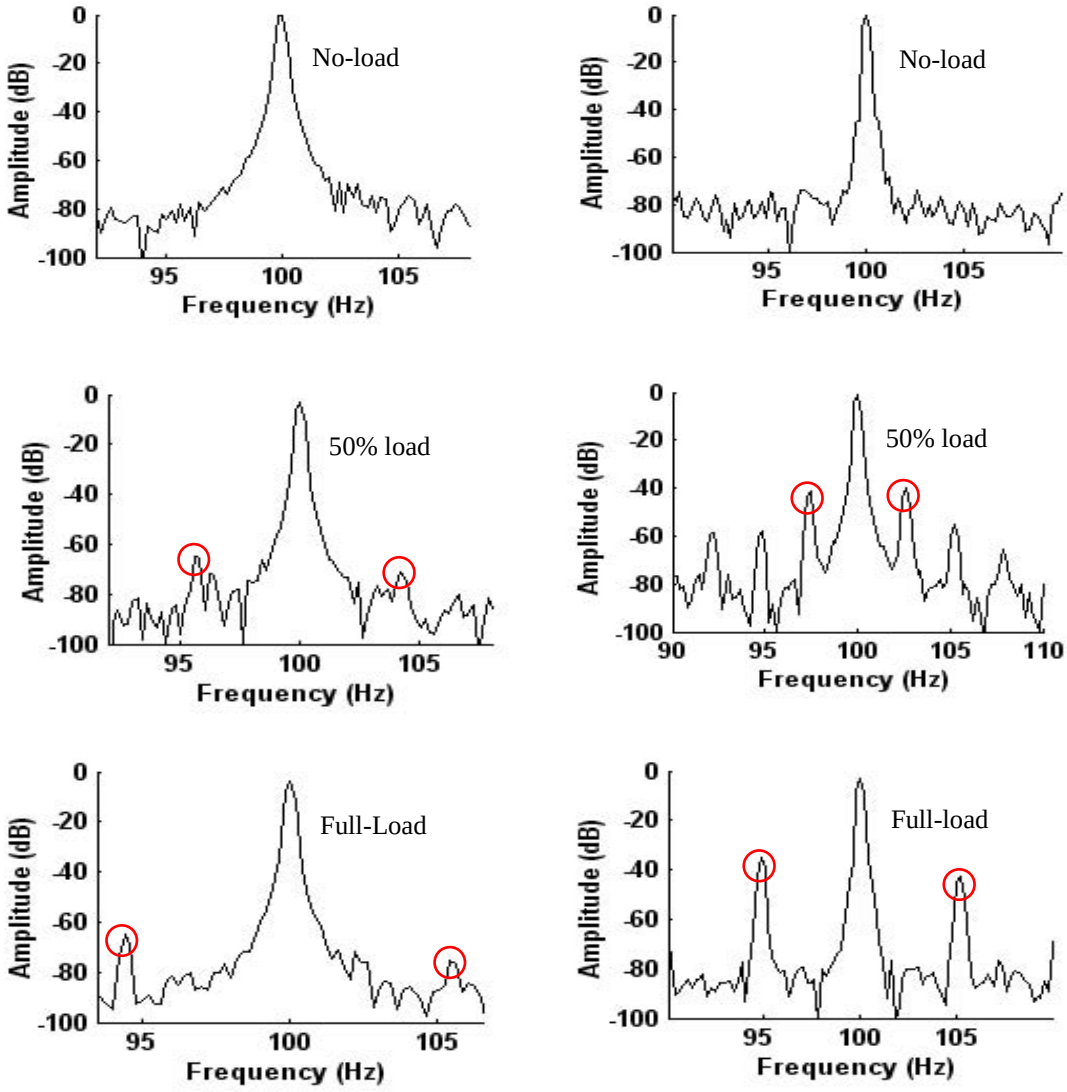

Figure 8.6: Instantaneous power spectrum from a healthy machine (left) and a faulty machine with two broken rotor bars and eccentricity of +0.3mm at driving-end (right), at no-load, 50% load and full-load. The circles indicate the sidebands.

8.2.3.2 Broken Bar Fault Frequencies from Instantaneous Power Spectrum

Frequency spectrum of the instantaneous power is used to identify broken rotor bar faults in the machine. The broken rotor bar fault frequencies under different load tests were investigated both in the healthy motor and motors with multiple faults as shown in Figure 8.7.

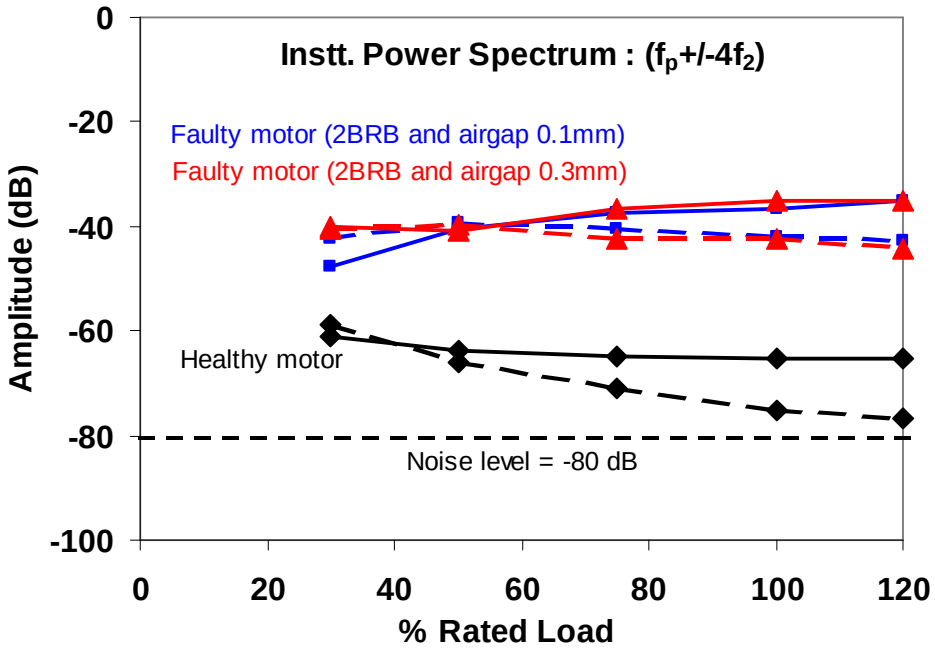

Figure 8.7: Comparison of variation in sidebands of a healthy motor with faulty motors (combination of two broken bars and eccentricity of +0.1mm and +0.3 mm at driving-end) from instantaneous power spectrum.

The result from the instantaneous power spectra shows significant variations of 30 dB or over in the amplitude of broken rotor bars fault frequencies for the healthy motor and faulty motors. These variations occur at any load level and make it easier to detect multiple faults.

In summary, instantaneous power signal can detect multiple faults at any load level confirmed its superiority to the flux signal. However, the current signal does have certain usefulness, when compared to the results obtained from the instantaneous power signal for finding any multiple faults in the machines.

8.3 Analysis of BRB Fault Frequencies

A comprehensive investigation to find the multiple faults using broken rotor bar fault frequencies in the presence of characteristic fault frequency components from the current, flux and instantaneous power signal has been performed. Table 8.1 shows the variations in the amplitudes of broken rotor bar fault frequencies in the presence of eccentricity faults.

The results from the current spectrum showed capacity to detect multiple faults, which consist of broken bars and airgap eccentricity over a wide range of loading. In addition, significant variations in the sideband amplitudes (>27 dB) between healthy and faulty machines, at any level of loads were found and readily differentiated from healthy motors in the current spectra.

Table 8.1: Comparison of healthy and faulty motors to detect the multiple faults in the presence of eccentricity level of 0.3 mm using BRB components $(1\pm2s)f_1$.

Sensor Signal	**Minimum load when the variations between the healthy and faulty motor is >20 dB**	**Negative sideband Amplitude**	**Positive sideband Amplitude**	**Comments**
Current	30%	29	27	Suitable for detecting the multiple only at light loads.
Flux	Not found	Not found	Not found	Not applicable because of small and inconsistent variations in the amplitudes of fault frequency components of faulty motors.
Instt. Power	75%	30	30	Suitable and preferable for detecting multiple faults only at high load.

The flux spectrum showed it is not suitable for finding multiple faults under any level of loading. Instantaneous power also presents equally reliable and preferable results for detecting multiple faults using modified fault frequency components ($f_p\pm4f_2$) at any levels of load. However, variations in the sideband amplitudes are relatively high, when compared to the current spectra. In summary, results from the current and instantaneous power spectra were found to be best when detecting detect multiple faults in the machines under the wide range of loading.

8.4 Detection of Multiple Faults using Eccentricity Fault Frequencies

Detection of multiple faults i.e. the combination of broken rotor bars and eccentricity at different level of loads using broken rotor bar fault frequencies from the current, flux and instantaneous power spectra has been investigated in Section 5.3. The current and instantaneous power signals were found to be better mediums for uncovering multiple

faults in machines. We now examine the usefulness of the results of eccentricity characteristic fault frequencies in detecting multiple faults for different levels of loading conditions.

8.4.1 Multiple Fault Detection using Eccentricity Fault Frequencies from Current Spectra

8.4.1.1 Comparison of Healthy and Faulty Current Spectra

It can be concluded from the Figures 8.8 and 8.9 that variations in the amplitude of sideband components of a faulty motor at 30% and at full-load are clearly visible in the frequency spectrum. However, variations in the sideband amplitude of a faulty motor at 30 % load were found to be (> 20 dB) when compared to the faulty motor at full-load. The noise level is about –90 dB.

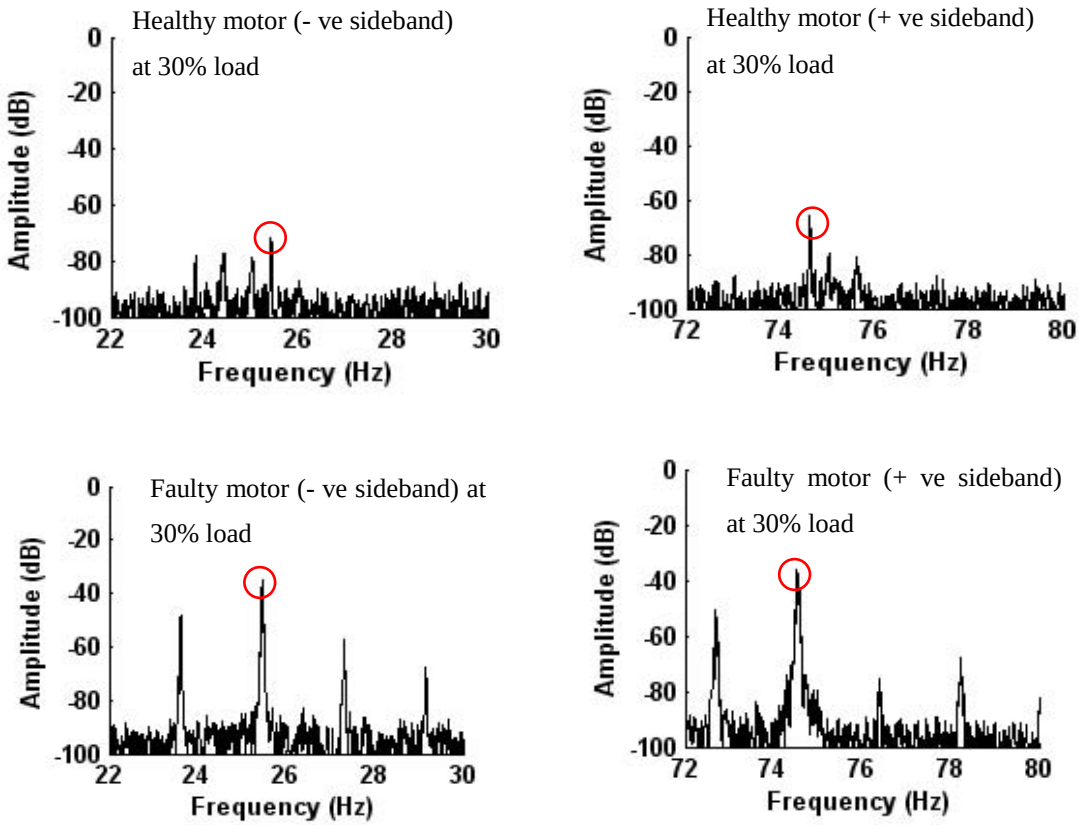

Figure 8.8: Current spectrum from a healthy motor (top) and a faulty motor with eccentricity of +0.3 mm at driving-end (bottom) at 30% load. The circles indicate the sidebands.

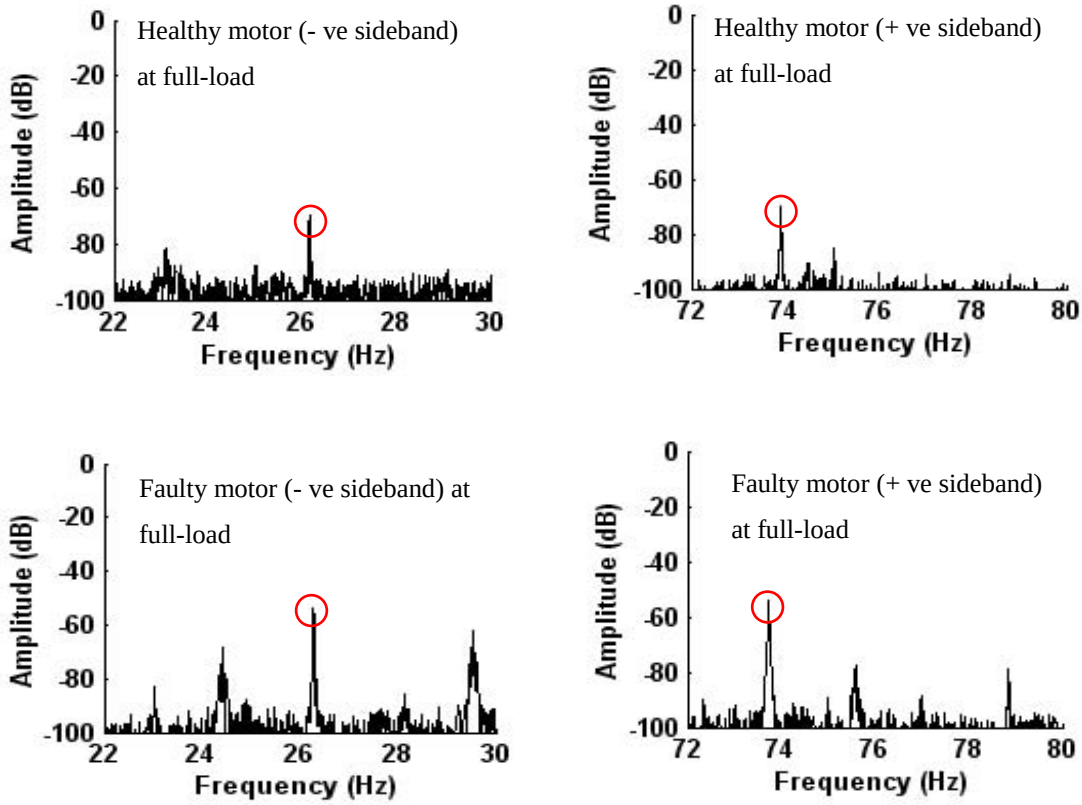

Figure 8.9: Current spectrum from a healthy motor (top) and a faulty motor with eccentricity of +0.3 mm at driving-end (bottom) at full-load. The circles indicate the sidebands.

8.4.1.2 Eccentricity Fault Frequencies from Current Spectra

The variations in the amplitude of eccentricity sideband components ($f_1 \pm f_r$) in the current spectrum as a function of load for healthy motor and faulty motors are clearly shown in the Figure 8.10.

Variations in the amplitude of sideband components at any level of loading are clearly visible, when compared to the healthy motor. Differences in the sideband amplitude of faulty motor were found to be more than 25 dB up to 50% of rated load and about (>10 dB) at or over 75% of rated load.

The current spectrum produced reliable results for detecting the combination of multiple faults (broken bars and eccentricity) using eccentricity fault frequencies at any level of load tests.

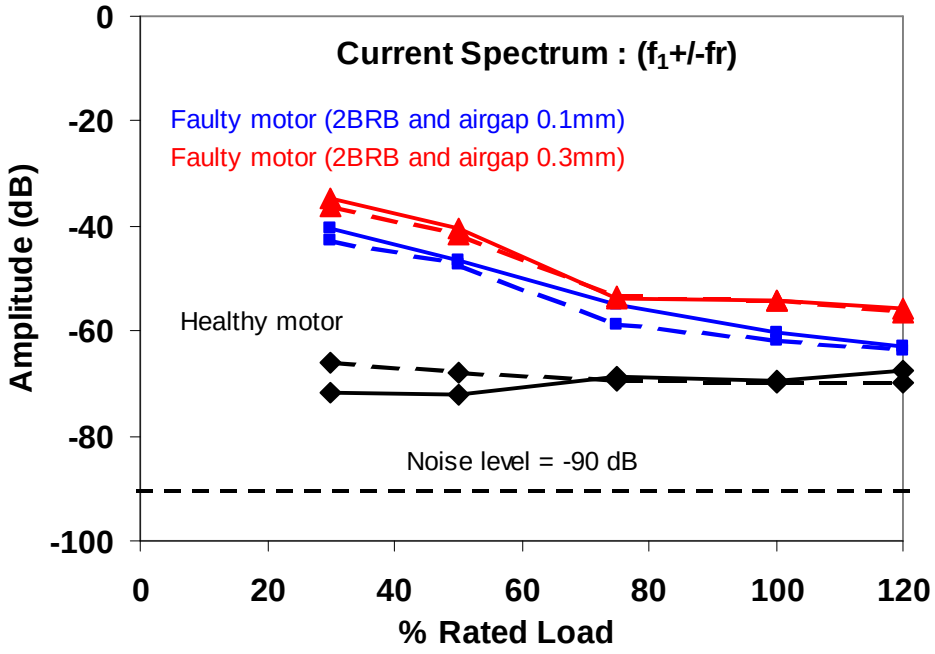

Figure 8.10: Comparison of variation in sidebands amplitudes versus % of rated load of a healthy motor with faulty motors (combination of two broken bars and eccentricity of +0.1mm and +0.3 mm at driving-end) from current spectrum.

8.4.2 Multiple Fault Detection using Eccentricity Fault Frequencies from Flux Spectra

8.4.2.1 Comparison of Healthy and Faulty Motors from Flux Spectra

It has been observed from the Figure 8.11, variations in the amplitude of the eccentricity fault frequencies of a faulty motor at 30% load and at full-load are clearly visible in than flux spectrum at the same level of loading.

Even in the presence of other peaks in the frequency spectrum, variations in the amplitude are clearly visible because of significant variations in the healthy motors as the load on the motor increases. However, a significant decrease in the amplitude of faulty motor was found when the motor operates at higher loads. The noise level is over or about –65 dB.

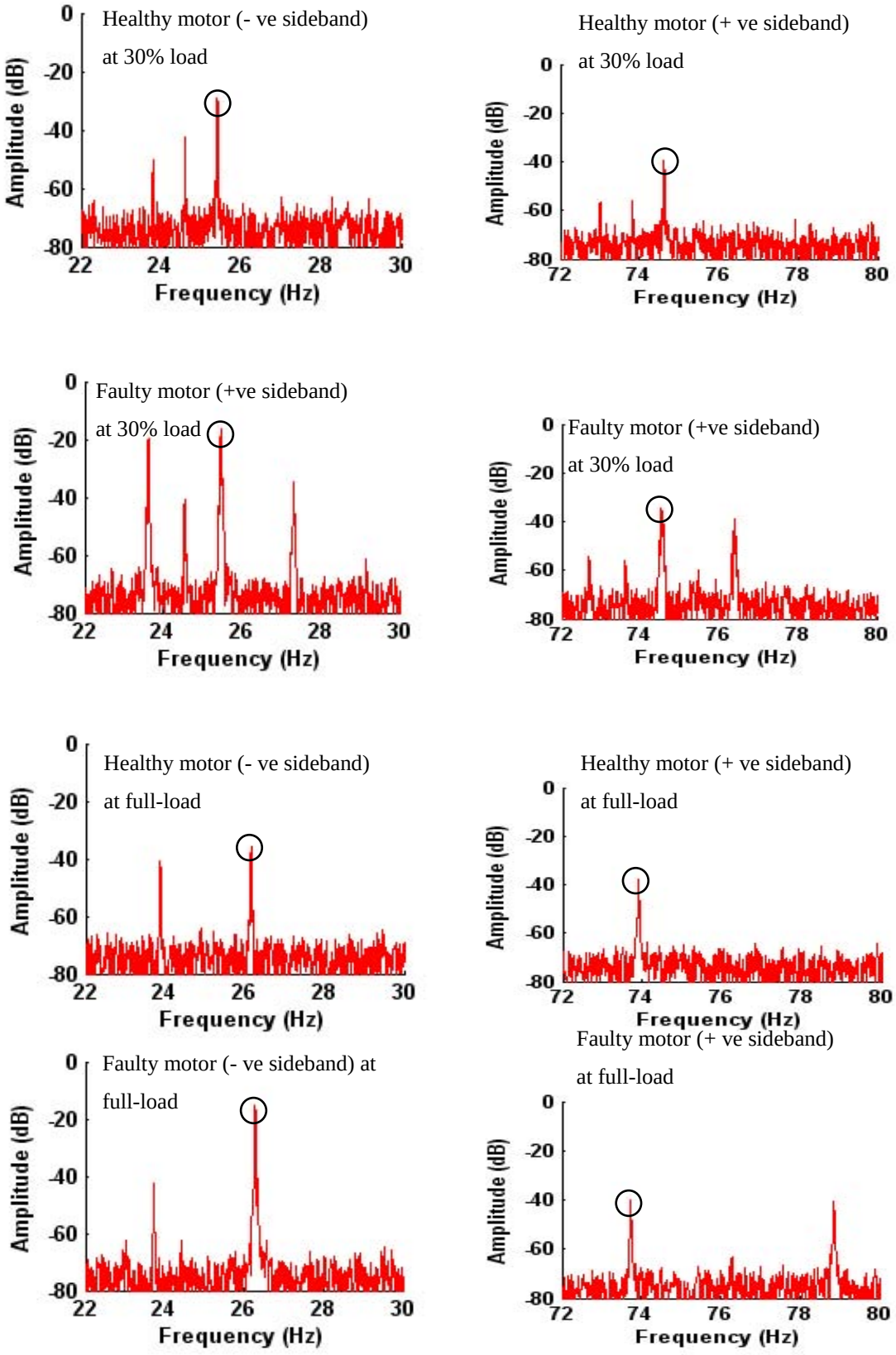

Figure 8.11: Flux spectrum from a healthy motor (row 1 and 3) and a faulty motor with eccentricity of +0.3 mm at driving-end (row 2 and 4) at 30% load and full-load. The circles indicate the sidebands.

8.4.2.2 Eccentricity Fault Frequencies from Flux Spectra

Eccentricity fault frequency components ($f_1 \pm f_r$) of the healthy and faulty motors are shown in Figure 8.12. The results indicate that variation in the amplitude of negative sideband of the faulty motor was found to be (> 15 dB) at any level of loading condition to the healthy motor, which is significant. However, variation in the amplitude of the faulty motor of positive sideband component is about (< 4 dB) up, which is very small. Therefore, the results from the flux spectrum showed that it is not suitable for detecting the multiple faults (i.e. combination of broken rotor bars and eccentricity faults) using eccentricity fault frequencies sideband components.

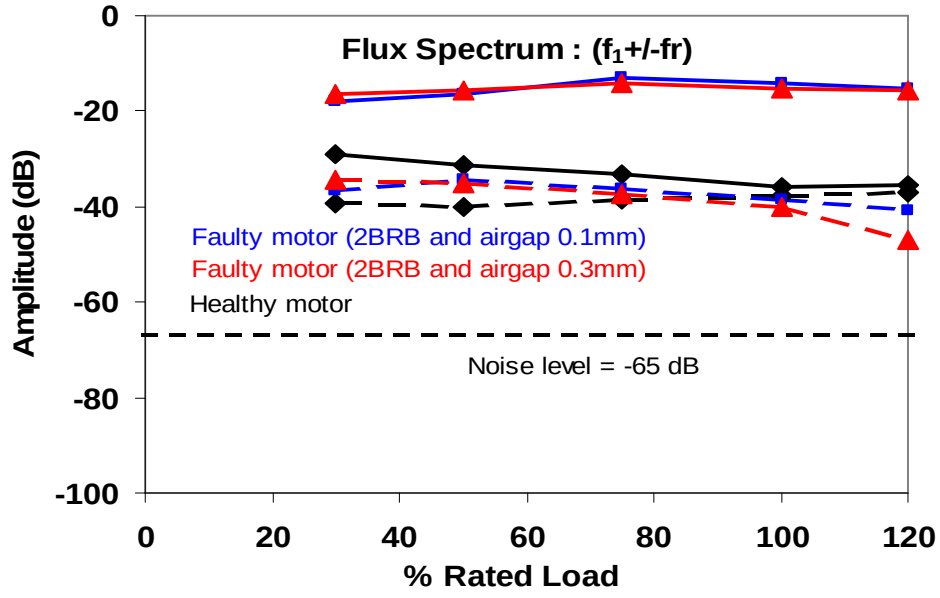

Figure 8.12: Comparison of variation in sidebands amplitudes versus % of rated load of a healthy motor with faulty motors (multiple faults) from flux spectrum.

8.4.3 Multiple Fault Detection using Eccentricity Fault Frequencies from Instantaneous Power Spectra

8.4.3.1 Comparison of Healthy and Faulty Motors from Instantaneous Power Spectra

According to Figure 8.13, changes in the amplitude of sideband components for a faulty motor at 30% load are significant for the healthy motor and are clearly visible in the spectra. The noise level is about –80 dB with eccentricity of +0.3 mm at the driving-end.

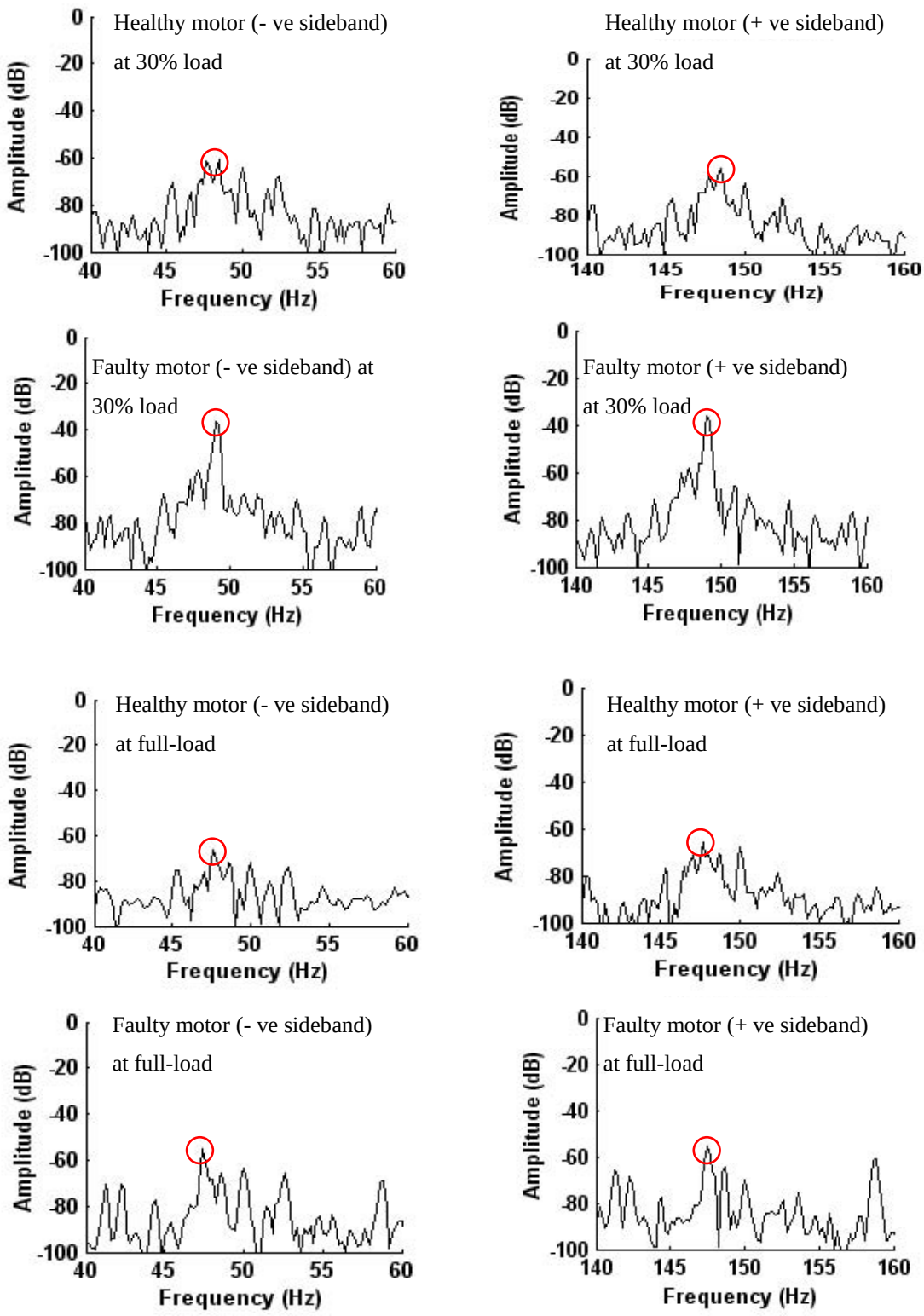

Figure 8.13: Instantaneous power spectrum from a healthy motor (row 1 and 3) and a faulty motor (row 2 and 4) at 30% load and full-load respectively.

8.4.3.2 Eccentricity Fault Frequencies from Instantaneous Power Spectra

The results emerging from the instantaneous power spectra indicate inconsistent increase/decrease in the sideband amplitude of faulty motors under different load tests as shown in Figure 8.14. This makes it difficult to detect the multiple faults. Therefore, instantaneous power is not suitable for detecting multiple faults.

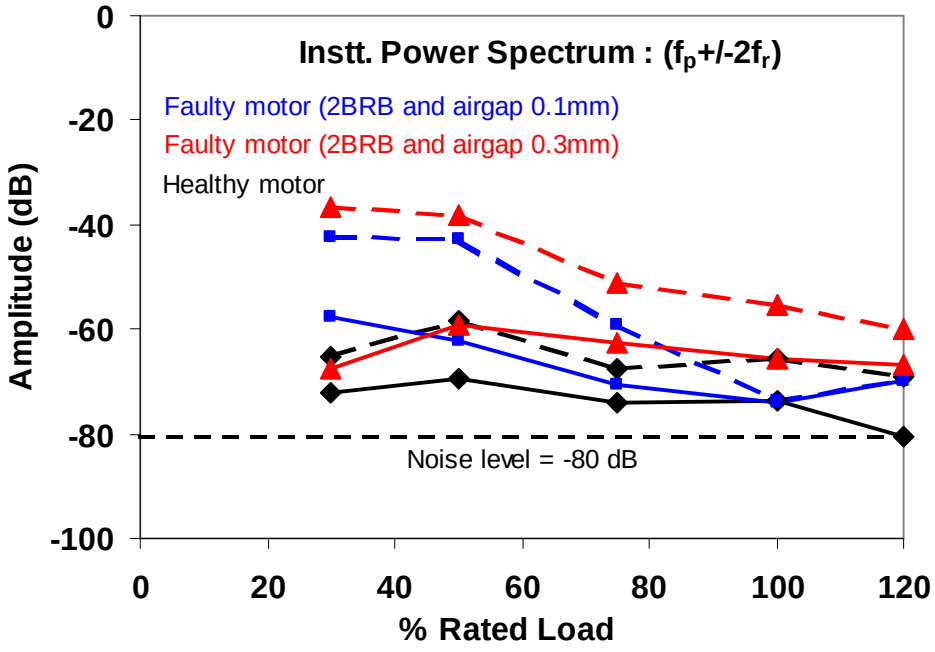

Figure 8.14: Comparison of variation in sidebands amplitudes of a healthy motor with faulty motors (combination of two broken bars and eccentricity of +0.1mm and +0.3 mm at driving-end) from instantaneous power spectrum.

8.5 Analysis of Eccentricity Fault Frequencies

We examined the current, flux and instantaneous power spectra in order to detect multiple faults using eccentricity fault frequency components in the presence of broken rotor bar under different loading conditions. A summary of the results obtained is shown in Table 8.2.

The current spectrum showed reliable results for detecting the combination of multiple faults (broken bars and eccentricity) using classical eccentricity fault frequency components ($f_1 \pm f_r$) at any levels of load (specifically light loads). The results for the flux

spectrum showed that it is not suitable for finding multiple faults in the machines using eccentricity fault frequency components.

The instantaneous power spectrum also proved not to be suitable for detecting the multiple faults and nor for estimating severities of faults. The results obtained from the instantaneous power spectra indicated inconsistent increase/decrease and small variations in the amplitudes of faulty motors under different load tests. This makes it difficult to detect multiple faults accurately under any level of load tests.

Table 8.2: Comparison of healthy and faulty motors to detect the multiple faults in the presence of broken rotor bars using ($f_1 \pm f_r$).

Sensor Signal	**Minimum load when the variations between the healthy and faulty motor is >20 dB**	**Negative sideband Amplitude**	**Positive sideband Amplitude**	**Comments**
Current	30%	38	30	Suitable for detecting multiple faults i.e. combination of BRB and eccentricity at light loads.
Flux	Not found	Not found	Not found	Not applicable.
Instt. Power	Not found	Not found	Not found	Not reliable for detecting multiple faults under any level of loading.

8.6 Summary

The analyses carried out in this chapter showed that the current spectra is able to detect multiple faults i.e. a combination of broken rotor bars and eccentricity faults either by using broken rotor bars fault frequency components $(1\pm2s)f_1$ or using eccentricity fault frequency components ($f_1 \pm f_r$) at any levels of loading.

The results from the instantaneous power spectra using modified broken rotor bar fault frequency components ($f_p \pm 4f_2$) showed that it is preferable for estimating either the machines having multiple faults or those that are not only at the higher levels of load. However, is not preferable when compared to the current signal.

It can be concluded that from the results, flux signal is also not a useful source to detect multiple faults using both broken rotor bar and eccentricity fault frequency components.

It is proposed that using both current and instantaneous power signals simultaneously will detect multiple faults reliably, specifically using broken rotor bar fault frequencies in the presence of eccentricity faults under various load conditions.

Chapter 9

Conclusions and Recommendations

Condition monitoring of induction machines relies on being able to detect differences between healthy and faulty machines. An accurate interpretation of a motor's condition requires knowledge of the effects of different operating conditions (including level of loading, non-ideal supplies), and typical variability between machines and test repeatability.

For the detailed investigation of fault detection in particular type of induction machine we selected a number of 2.2 kW, four-pole machines (highest rating which can be tested using available laboratory facilities in the University of Adelaide). Some of them were used for introducing faults i.e. broken rotor bar (by milling rotor-end), shorted turns (stator rewound with tap), misalignment (introduce control misalignment using shims) and static eccentricity (developed custom test-rig for rotor eccentricity adjustment) of varying severity.

We also developed an experimental set-up based on hardware tools and a software programme. In the hardware set-up, a precision laser alignment tool and a torque were used to ensure the accuracy and repeatability of the experimental set-up.

For software section we developed two programmes. First is the data acquisition programme, which is used for data collection from different multiple types sensors i.e. current, axial flux, voltage and vibration (in earlier work generally used single sensor type e.g. broken rotor bar detection using current sensors) and the second one is the custom-written programme which used for the analysis of raw sensor data and produce frequency spectrum of current, flux and instantaneous power spectra that helps us to

locate the appropriate peaks in the spectra of different signals simultaneously. These programmes are based on the experimental set-up developed for this research in order to provide the necessary technology for accurate and reliable effective fault detection and prediction of incipient failures in induction motors.

The purpose of this study is to investigate the different factors, that make it possible to overcome any shortcoming concerning the detection of different faults i.e. broken rotor bar, eccentricity, shorted turn and misalignment in the machines using the fault frequency components from the current, flux and instantaneous power signals for different levels of loading. Therefore, an extensive series of tests and analyses were carried out on different healthy and faulted induction motors to investigate changes in the amplitudes of the fault frequency components in the current, flux and instantaneous power spectra to detect different faults under varying load conditions.

Unlike previous studies that generally used single sensor type, for example eccentricity fault detection using current sensor at full-load conditions, or limited number of load cases, this work examines the use of multiple type sensors to detect the different fault (broken rotor bar, eccentricity, stator, misalignment, etc) using standard fault frequencies. The effect of load variations on fault detection showed that load has a substantial influence on fault detection, particularly the difficulty in detecting faults at light loads. The key results related to the different faults are as follows:

Broken Rotor Bar Faults

We investigated the detection of partial, two and four broken rotor bar faults over a wide range of loading conditions, using the sideband components $(1\pm2s)f_1$ for the current and axial flux signals, and modified sideband components $(f_p\pm4f_2)$ for the instantaneous power signal.

Since the detection of broken rotor bar based on the changes in current distribution were due to changes in bar resistance. These changes in current under different loading conditions in the case of partial broken rotor bar were small. Therefore to estimate the partial broken rotor bar fault on the basis of variations in the amplitudes of fault frequency components using current, flux or instantaneous power spectra is difficult because these small variations either represent the cracked rotor bars or other source of high resistance.

The current spectrum showed clearly visible and reliable variations of more than 25 dB in the amplitudes of fault frequency components between the healthy and faulty motor for more than one broken rotor bar when the minimum load on the machine is ≥ 75% of rated load. However, detecting the broken rotor bars at light load is difficult because of the small currents in the rotor bars and the low slip frequency.

The result from the flux spectrum showed reasonable variations of more than 25 dB between the healthy and faulty motor, only when the load on the machine is around 100% and the number of broken bars is ≥ 4. Therefore, flux signal is not a suitable medium to detect the broken rotor bar faults.

We also investigated the instantaneous power as a diagnostic medium to detect the broken rotor bar faults under varying load conditions. The variations in the amplitudes of the fault frequency components between the healthy and faulty motor were found to be ≥ 25 dB when the minimum load on the machine is 30% of rated load. The result obtained from instantaneous power signal showed the best features over the full range of loads tested to detect the broken rotor bar faults when compared to the current and flux spectra. Therefore on the basis of the features extracted from the instantaneous power signal it has been suggested to detect and estimate the severity of broken rotor bar faults over a wide range of loading using modified characteristic fault frequency components ($f_p \pm 4f_2$) of instantaneous power signal.

Eccentricity Faults

We investigated the characteristic fault frequencies, ($f_1 \pm f_r$), and $f_1[(R\backslash p)(1-s) \pm k]$ from current and flux signals and modified characteristic fault frequencies ($f_p \pm 2f_r$), $f_p[(R\backslash p)(1-s) \pm k]$ from instantaneous power signal, in order to detect eccentricity faults over a wide range of loads.

Previous studies used variations in the amplitudes of the fault frequency components ($f_1 \pm f_r$), between the healthy motor and faulty motor versus % of rated load of the motor to detect eccentricity faults. In comparison, this work examines variations in the amplitudes of the fault frequency components between the healthy motor and faulty motor versus average eccentricity level over a wide range of loading conditions, which is calculated by using formula "Average Eccentricity" $=[(E_1+E_2)/2]$, which is introduced in this work. The selected range for average eccentricity level is from 0 to 0.3 mm (because

the maximum airgap between the stator and rotor is 0.4 mm at both sides of the machine).

The results from current and instantaneous power signals showed an ability to detect eccentricity faults at light loads. It has been suggested that both current and instantaneous power can detect eccentricity faults. However, current spectra are preferable because they showed consistent variations in the sideband amplitudes when compared to the instantaneous power signals.

This work also examines the use of fault frequencies components $f_1[(R\backslash p)(1-s)\pm k]$ and $f_p[(R\backslash p)(1-s)\pm k]$ to detect eccentricity faults using current, flux and instantaneous power signals for different values of k at different levels of load tests. The results were found to have inconsistent increase/decrease in the amplitudes of the faulty motors, because these fault frequency components heavily depend on the values of k. It is difficult to estimate the appropriate values of k, which is suitable for detecting eccentricity faults under varying load conditions.

Finally, it is suggested to use fault frequencies components $(f_1\pm f_r)$ and $(f_p\pm 2f_r)$ to detect eccentricity with variations in the amplitudes of the fault frequency components versus average eccentricity level over a wide range of loading conditions. That is, from current and instantaneous power signal under varying loading conditions instead of using the variations in the amplitudes of the fault frequency components versus % of rated load of the motor from current and instantaneous power signal.

Shorted Turn Faults

We investigated the use of current, flux and instantaneous power signals to detect the shorted turn faults using standard fault frequencies over wide range of varying loads. The use of fault frequency components to detect the faults and estimate fault severity in the machines heavily depends upon the variations in the amplitudes of sideband components. The results from flux signal showed useful features to detect the shorted turn faults at light loads. However, flux signal is not able to provide useful information which helps to detect the shorted turn faults at higher loads because at higher loads the variations in the amplitudes of sideband components between the healthy and faulty motor is small.

Instantaneous power displays the enough separation between the healthy and faulty motors in the frequency spectra at full-load. However, results at light loads showed small variations in the amplitudes of fault frequency components.

The use of single signal, which is obtained by adding together the flux and instantaneous power signals to detect the shorted turns fault showed much clearer variations between healthy and faulty motors over a wide range of loads. Therefore, it is suggested to detect the shorted turns fault using combined single signal over a wide range of loadings.

Misalignment Faults

We investigated the effect on healthy motors in the presence of misalignment faults using current, flux and instantaneous power signals under varying load conditions. The results showed visible variations in the sideband amplitudes at different levels of loads in the flux and instantaneous power spectra, which are sufficient to detect the misalignment.

However, because the misalignment normally develops eccentricity faults (which are best detected by flux signals), it is more accurate to detect misalignment in the machines by using eccentricity fault frequencies ($f_1 \pm f_r$) from the flux signal. This will increase the accuracy and reliability of the test results, when considering the fault frequencies' sideband components for finding different faults in machines.

Multiple Faults

The results from the current spectrum indicated the ability to detect multiple faults, using broken rotor bar fault frequencies in the presence of eccentricity faults over a wide range of loading. In addition, significant variations in the sideband amplitudes (>27 dB) between healthy and faulty machines, at any level of loads, can be readily distinguished from healthy motors in the current spectra. Similarly, instantaneous power can detect multiple faults at higher level of loads.

However, the investigation into detecting multiple faults using eccentricity fault frequencies in the presence of broken rotor bar faults only worked in the current spectra under varying load conditions. Therefore, it is proposed to detect multiple faults in the machines under the wide range of loading.

It can be concluded that from the results that flux signal is a useful source for discovering multiple faults at high loads. However, variations in the sideband amplitudes are occurred less when compared to the current spectra at the same level of loadings.

The above investigation confirmed that the current and instantaneous power spectra are useful signals for detecting multiple faults i.e. combination of broken rotor bars and eccentricity faults by using broken rotor bars fault frequencies of $(1\pm2s)\ f_1$ and eccentricity $(f_p\pm2f_2)$ at any levels of loading. The selected range of sideband amplitudes on the basis of results estimated the severity of multiple faults from the current and instantaneous power spectrums. Instantaneous power as a diagnostic medium to detect the different single and multiple faults in induction motor has proved to be another useful and tool for detecting different faults in induction motors in this research.

Recommendations

- The most important recommendation refers to instantaneous power; instead of using traditional stator current and flux as diagnostic medium to detect different type of single and multiple faults, instantaneous power is providing accurate and reliable results to detect the different faults in machines.
- In this study the “slip-speed” method is used to determine the percentage of rated load of the motor due to its simplicity and safety advantages. However, the use of “direct-read” power measurements to determine the percentage of rated load of the motor (as discussed in Chapter 3) may increase the reliability and accuracy of instantaneous power.
- The use of multiple sensors to detect both single and multiple faults in induction motors with advanced computerized data processing and acquisition will provide significant improvement in the field of condition monitoring of induction machines.

References

[1] W. T. Thomson and M. Fenger, “Current Signature Analysis to Detect Induction Motor Faults”, IEEE Industry Applications Magazine, pp. 26-34, July/August 2001.

[2] Ahmed, R. Supangat, J. Grieger, J, N. Ertugrul, and W.L Soong, "A Baseline Study for On-Line Condition Monitoring of Induction Machines." Australian Universities Power Engineering Conference, Brisbane, Australia 2004,

[3] M.L. Sin, W.L. Soong and N. Ertugrul, "Induction Machine On-Line Condition monitoring and Fault diagnosis- A Survey" AUPEC 2003, Christchurch, New Zealand.

[4] H. A. Toliyat et al., “Condition monitoring and fault diagnosis of electrical machines—A review,” in Conf. Rec. 1999 IEEE-IAS Annual. Meeting, vol. 1, Phoenix, AZ, pp. 197–204.

[5] B. S. Payne, B. Liang and A. D. Ball, “Modern Condition Monitoring Techniques for Electric Machines”, Proceedings of the 1st International Conference on the Integration of Dynamics, Monitoring and Control (DYMAC 99), Manchester, UK, pp. 325-330, September 1999.

[6] M.E.H. Benbouzid, “A Review of Induction motors Signature Analysis as a Medium for Faults Detection”, IEEE Transaction on Industry Electronics, Vol. 47, No. 5, Oct., pp 984 – 993, 2000.

[7] D. M. T. Siyambalapitiya et al., “Reliability improvement and economic benefits of on-line monitoring system for large induction machines”, IEEE Trans. Ind. Applicat, vol. 26, pp. 1018–1025, July/Aug. 1990.

[8] F. J. Discenzo et al., “Motor diagnostics: Technological drivers leading to 21st century predictive diagnostics,” in Proc. 1997 Int. Conf. Maintenance and Reliability, vol. 1, Knoxville, TN, pp. 30.01-30.12.

[9] Stephan J. Chapman, “Electric Machinery Fundamentals,” McGraw-Hill International Editions: Singapore, 1987.

[10] http://www.clrwtr.com/ABB-Motors-Electric-Motor.

[11] Vincent Del Toro, “Basic Electrical Machines,” Prentice-Hall International, Inc. Division of Simon and Schuster, Englewood cliffs, New Jersey 1990.

[12] http:// www.mcsainterpreter.com/bb10 data, Accessed on March 2005

[13] Workshop on hidden Faults in Induction Motors, Condition Monitoring and Future Trends. Delivered by Ertugrul, N., Soong, Department of electrical and electronics Engineering, The university of Adelaide, 4-5 December, 2003 Adelaide.

[14] IAS Motor Reliability Working Group, “Report of large motor reliability survey of industrial and commercial installations—Part I,” IEEE Trans. Ind. Applicat., vol. IA-21, pp. 853–864, July/Aug. 1985.

[15] IAS Motor Reliability Working Group, “Report of large motor reliability survey of industrial and commercial installations—Part II,” IEEE Trans. Ind. Applicat., vol. IA-21, pp. 865–872, July/Aug. 1985.

[16] IAS Motor Reliability Working Group, “Report of large motor reliability survey of industrial and commercial installations—Part III,” IEEE Trans. Ind. Applicat., vol. IA-23, pp. 153–158, Jan. /Feb. 1987.

[17] O.V. Thorsen and M. Dalva, “Methods of Condition Monitoring and Fault Diagnosis for Induction Motors” Eur. Trans. Electr. POWER ETEP 8, pp. 383–395, 1998.

[18] W. R. Finlay et al., “Troubleshooting motor problems,” IEEE Trans. Ind. Applicat., vol. 30, pp. 1383–1397, Sept./Oct. 1994.

[19] J. Siau, A. Graff, W. L. Soong, and N. Ertugrul, "Broken Bar Detection in Induction Motors Using Current and Flux Spectral Analysis,” Australian Universities Power Engineering Conference, Christchurch, New Zealand 2003.

[20] G. Habetler,“On-Line Condition Monitoring and Diagnostics of Electric Machines” Power Electronics and Motor Diagnostics Laboratory, School of Electrical and Computer Engineering Georgia Institute of Technology, USA.

[21] I. Ahmed, N. Ertugrul, and W. L. Soong, "A Study on the Detection of Fault Frequencies for Condition Monitoring of Induction Machines,” Australian Universities Power Engineering Conference, Tasmania, Australia 2005.

[22] R. Fiser and S. Ferkolj, “Application of Finite Element Method to Predict Damaged Induction Motor Performance,” IEEE Trans. on Magnetics, Vol. 37, no 5, Sep. 2001, pp. 3635-3639.

[23] W. T. Thomson and A. Barbour, “On-Line Current Monitoring and Application of a Finite Element Modelling of Induction Motor Faults with Finite Element Method to predict the Level of Static Airgap Eccentricity in Three-Phase Induction Motors,” IEEE Transactions on energy Conversion, Vol. 13, no 4, December 1998, pp. 347-352.

[24] R. J. Tallam, T. G. Habetler and R. G. Harley, “Transient Model for Induction Machines With Stator Winding Turns Faults,” IEEE Transactions on Industry Applications, Vol. 38, no 3, May/June 2002, pp. 632-637.

[25] E. Schaeffer, E. L. Carpentier and M. E. Zaim, “Failure Detection in Induction Machine by Means of Parametric Identification,” CESA’98, IEEE Conference on Computational Engineering in Systems Applications, Nabeul-Hammament, Tunisia, 1-4 April 1998.

[26] R. Beguenane and M.E.H. Benbouzid, “Induction Motors Thermal Monitoring By Means of Rotor-Resistance Identification”, IEEE Transaction on Energy Conversion, Vol. 14, No 3, September 1999, pp 566 – 570.

[27] J. F. Bangura and N. A. Demerdash, “Diagnosis and Charactization of effects of Broken Rotor Bars and Connectors in Squirrel-Cage Induction Motors by a Time-Stepping Coupled Finite Element-State Space Modeling Approach,” IEEE Transactions on energy Conversion, Vol. 15, December 1999, pp. 1167-1176.

[28] R. J. Povinelli, J. F. Bangura, N. A. Demerdash and R. H. Brown, “Diagnostic of Bar and End-Ring Connector Breakage Faults in Poly-phase Induction Motors Through a Novel Dual Track of Time-Stepping Coupled FE-State Space Modelling,” IEEE Transactions on energy Conversion, Vol. 17, no 1, March 2002, pp. 39-46.

[29] F. Filippetti, G. Franceschini, P. Vas and C. Tassoni “Broken Bar Detection in Induction Machines: Comparison between Current spectrum Approach and Parameter Estimation Approach”, IEEE Industry Application Society, Vol. 1, pp. 95-102, 1994.

[30] F. Filippetti, G. Franceschini and C. Tassoni "Neural Networks Aided On-Line Diagnostics of Induction Motor Rotor Faults", IEEE Industry Application Society, Vol. 1, pp. 316-323, 1993.

[31] F. Filippetti, G. Franceschini, C. Tassoni, G. Gentile, S. Meo, A. Ometto and N. Rotondale, "Deterministic Approach and Neural Network Approach for Stator Short Circuits Diagnosis in Induction Motor," 7 Industry Application Society, Vol. 1, pp. 316-323, 1993.

[32] M. Y. Chow, "Methodologies of Using Neural Network and Fuzzy Logic Technologies for Motor Incipient Fault Detection," World Scientific, Singapore, 1997.

[33] M. Y. Chow, S. Altug, and H. J. Trussel, "Set Theoretic Based Neural-Fuzzy Motor Fault Detect", IECon, 1998.

[34] F. Filippetti and M. Martelli, "Development of Expert System Knowledge Base to On-Line Diagnosis of Rotor Electrical Faults of Induction Motors," IEEE Ind. Applicat. Society Annual Meeting, vol. 1, 1992, pp. 92-99.

[35] E. Styvaktakis, M. H. J. Bollen and I. Y. H. Gu. Martelli, "Expert System for Classification Knowledge and Analysis of power System Events," IEEE Trans. on Power Delivery, vol. 17, no 2, April. 2002, pp. 423-428.

[36] S. Big, M. Negrea, A. Arkkio, H. Hyotyniemi and H. Koivo, "Support Vector Classification for Fault Diagnostics of an Electrical Machine," Proceeding of International Conference on Signal Processing (ICSP "02). Beijing, 2002. 26-30.

[37] M. G. Melero, M.F. Cabanas, C. Rojas, G.A. Orcajo, J. M. Cano and J. Solares "Study of an Induction Motor working under Stator Winding inter-Turn Shorted Circuit Condition," IEEE International Symposium on Diagnostics for Electrical Machines, Power Electronics and Drives SDEMPED 2003. Atlanta, USA. 24-36 Aug. 2003.

[38] M. Haji, H. A. Toliyat et al., "Pattern Recognition – A Technique for Induction Machines Rotor Broken Bar Detection," IEEE Transactions on Energy Conversation, vol. 16, no. 4, Dec., pp. 312–317.

[39] A.A. Da Silva et al., "Rotating machinery monitoring and diagnosis using short-time Fourier transform and wavelet techniques," in Proc. 1997 Int. Conf. Maintenance and Reliability, vol. 1, Knoxville, TN, pp. 14.01–14.15.

[40] B. S. Payne, A. Ball and F. Gu, "Detection and Diagnosis on Induction Motor Faults using Statistical Measures", International Journal of Condition Monitoring and Diagnosis Engineering Management, vol. 5, no.2, April 2002, pp. 5-19.

[41] H. Nejjari and M. E. H. Benbouzid, "Monitoring and Diagnosis of Induction Motors Electrical Faults Using a Current Park's Vector Pattern Learning Approach", IEEE Transactions on Industry Applications, Vol. 36, No. 3, May/June 2000, pp. 730-735.

[42] A.J. M. Cardoso et al., "Computer-aided detection of airgap eccentricity in operating three-phase induction motors by Park's vector approach," IEEE Trans. Ind. Applicat, vol. 29, pp. 897–901, Sept./Oct. 1993.

[43] J. M. Cardoso, S. M. A. Cruz and D. S. B. Fonseca, "Inter-Turn Stator Winding Fault Diagnosis in Three-Phase Induction Motors, by Park's Vector Approach", IEEE Transactions on Energy Conversion, Vol. 14, No. 3, September 1999, pp. 595-598.

[44] G. C. Stone, H. G. Sedding and M. J. Costello, "Application of Partial Discharge Testing to Motor and Generator Stator Winding Maintenance", IEEE Transactions on Industry Applications, Vol. 32, No. 2, March/April 1996, pp. 459-464.

[45] A. Bellini, F. Filippetti, G. Franceschini, C. Tassoni and G. B. Kilman, "Quantities Evaluation of Induction Motor Broken Bars by Means of Electrical Signature Analysis," IEEE Trans. On Ind. Appl., vol. 37, no 5, Sep./Oct 2001, pp. 1248-1255.

[46] R.Maier., "Protection of Squirrel of induction motor utilizing instantaneous power and phase information," IEEE Trans. Ind. Applicant, vol, 28, pp 376-380, 1992.

[47] S. F. Legowski et al, "Instantaneous power as a medium for the signature analysis of induction motors," IEEE Trans. Ind, Applicant, vol 32, pp. 904-909, July/Aug. 1996

[48] A.M. Trzynadlowski et al., “Diagnostics of mechanical abnormalities in induction motors using instantaneous electric power,” in Proc. 1997 IEEE Int. Electric Machines and Drives Conf., Milwaukee, WI, pp. MB1-9.1–MB1-9.3.

[49] A.W. Galli et al., “Exploring the power of wavelet analysis”, IEEE Comput. Applicat. Power, vol. 9, pp. 37–41, Oct. 1996.

[50] www.motor.doe.gov “ The energy saving network” Accessed on March 2005.

[51] J. Sottile, J. L. Koher, “An On-Line Method to Detect Incipient Failure of Turn Insulation in Random Wound Motors”, IEEE Transactions on Energy Conversion, Vol. 32, No. 2, December 1993.

Appendix

Experimental Result of Healthy Motor using Developed Custom-Written Programme

Machine Name: CM1

Machine Condition: Healthy

Fault Type: Healthy

Load Percentage: 30.3939 %

Sampling Frequency (fs): 400Hz / 8000Hz

Supply Frequency [f1]: 50.00 Hz

Voltages (rms) at [400Hz]: 405.70 (Vab) 398.59 (Vbc) 396.19 (Vca)

Voltages (rms) at [8000Hz]: 407.55 (Vab) 404.00 (Vbc) 407.03 (Vca)

Currents (rms) at [400Hz]: 2.81 (Ia) 2.79 (Ib) 2.77 (Ic)

Currents (rms) at [8000Hz]: 2.87 (Ia) 2.82 (Ib) 2.81 (Ic)

Real Input Power of the loaded motor (Average Power): 924.12 W

Power Factor: 0.46

Meas. Speed - [400Hz] : 1475.00 rpm

Meas. Speed - [8000Hz]: 1475.00 rpm

Calculated Slip Frequency based on Measured Speed

Calc.Slip Freq [400Hz]: 0.84

Calc.Slip Freq [8000Hz]: 0.84

DATA FROM CURRENT SENSORS:

Supply Frequency [f1] of phase (a) at [400Hz]:

Meas. Freq. (Hz): 50.00

Meas. Ampl. (dB): 0.00

Supply Frequency [f1] of phase (b) at [400Hz]:

Meas. Freq. (Hz): 50.00

Meas. Ampl. (dB): 0.00

Slip Frequency [f2] of phase (a) at [400Hz]:

Meas. Freq. (Hz): 0.65

Meas. Ampl. (dB): -89.72

Slip Frequency [f2] of phase (b) at [400Hz]:

Meas. Freq. (Hz): 0.83

Meas. Ampl. (dB): -89.61

Broken Rotor Bar Frequencies [(1 (+/-) 2s)f1] of Phase (a) at [400Hz] :

Calculated Freq. (Hz): 48.38 51.62

Meas. Freq. (Hz): 48.38 51.62

Meas. Ampl. (dB): -66.64 -67.17

Broken Rotor Bar Frequencies [(1 (+/-) 2s)f1] of Phase (b) at [400Hz]:

Calculated Freq. (Hz): 48.34 51.66

Meas. Freq. (Hz): 48.38 51.62

Meas. Ampl. (dB): -68.30 -66.47

Shorted Turn Frequencies [f1((n/p)(1-s) (+/-) k)] of Phase(a) at [8000Hz]:

Calculated Freq. (Hz): 74.60 174.60 99.19 -25.41 -125.41 -0.81

Meas. Freq. (Hz): 74.59 174.81 100.01 25.41 125.41 0.82

Meas. Ampl. (dB): -63.00 -83.75 -59.37 -58.09 -75.83 -90.42

Shorted Turn Frequencies [f1((n/p)(1-s) (+/-) k)] of Phase(b) at [8000Hz]:

Calculated Freq. (Hz): 74.60 174.60 99.19 -25.41 -125.41 -0.81

Meas. Freq. (Hz): 74.59 174.81 100.01 25.41 125.41 0.83

Meas. Ampl. (dB): -60.76 -77.08 -59.76 -58.70 -71.08 -89.61

Eccentricity Freq (1) [f1((R/p)(1-s) (+/-) k)] of Phase(a) at [400Hz] :

Calculated Freq. (Hz): 935.47 985.47 1035.47 835.46 785.46 735.46

Meas. Freq. (Hz): 936.05 984.85 1034.45 836.04 785.24 734.64

Meas. Ampl. (dB): -68.22 -90.16 -89.09 -69.26 -90.50 -93.89

Eccentricity Freq (1) [f1((R/p)(1-s) (+/-) k)] of Phase(b) at [400Hz]:

Calculated Freq. (Hz): 935.47 985.47 1035.47 835.46 785.46 735.46

Meas. Freq. (Hz): 936.05 986.05 1036.05 836.04 785.84 734.44

Meas. Ampl. (dB): -67.39 -92.83 -93.91 -70.36 -87.68 -86.39

Eccentricity Freq (2) [f1 (+/-) fr] of Phase (a) at [400Hz]:

Calculated Freq. (Hz): 25.41 74.60

Meas. Freq. (Hz): 25.41 74.59

Meas. Ampl. (dB): -58.09 -63.00

Eccentricity Freq (2) [f1 (+/-) fr] of Phase (b) at [400Hz]:

Calculated Freq. (Hz): 25.41 74.60

Meas. Freq. (Hz): 25.41 74.59

Meas. Ampl. (dB): -58.70 -60.76

DATA FROM VOLTAGE SENSORS:

Supply Frequency [f1] of voltage (ab) at [400Hz]:

Meas. Freq. (Hz): 50.00

Meas. Ampl. (dB): 0.00

Supply Frequency [f1] of voltage (bc) at [400Hz]:

Meas. Freq. (Hz): 50.00

Meas. Ampl. (dB): 0.00

Slip Frequency[f2] of Voltage(ab) at [400Hz] :

Meas. Freq. (Hz): 0.71

Meas. Ampl. (dB): -99.46

Slip Frequency[f2] of Voltage(bc) at [400Hz]:

Meas. Freq. (Hz): 0.72

Meas. Ampl. (dB): -99.61

Broken Rotor Bar Frequencies [(1 (+/-) 2s)f1] of voltage(ab) at [400Hz]:

Calculated Freq. (Hz): 48.58 51.42

Meas. Freq. (Hz): 48.99 51.00

Meas. Ampl. (dB): -89.82 -90.37

Broken Rotor Bar Frequencies [(1 (+/-) 2s)f1] of voltage(bc) at [400Hz]:

Calculated Freq. (Hz): 48.56 51.44

Meas. Freq (Hz): 48.49 51.52

Meas. Ampl. (dB): -88.17 -84.66

Shorted Turn Freq[f1((n/p)(1-s) (+/-) k)] of voltage(ab) at [8000Hz]:

Calculated Freq. (Hz): 74.65 174.65 99.29 -25.36 -125.36 -0.71

Meas. Freq. (Hz): 74.70 174.61 100.01 25.33 126.01 0.71

Meas. Ampl. (dB): -92.93 -95.04 -76.38 -100.49 -93.05 -99.46

Shorted Turn Freq [f1((n/p)(1-s) (+/-) k)] of voltage(bc) at [8000Hz]:

Calculated Freq. (Hz): 74.59 174.59 99.17 -25.42 -125.42 -0.83

Meas. (Hz): 74.60 174.81 100.01 25.41 125.41 0.83

Meas. (dB): -97.35 -91.13 -69.47 -96.36 -94.83 -102.18

Eccentricity Freq (1) [f1((R/p)(1-s) (+/-) k)] of voltage(ab) at [400Hz]:

Calculated Freq. (Hz): 937.27 987.27 1037.27 837.26 787.26 737.26

Meas. Freq. (Hz): 937.65 987.65 1038.25 837.64 788.44 738.24

Meas. Ampl. (dB): -89.77 -100.54 -102.78 -77.91 -99.09 -100.05

Eccentricity Freq (1) [f1((R/p)(1-s) (+/-) k)] of voltage(bc) at [400Hz]: Calculated

Freq. (Hz): 935.11 985.11 1035.11 835.10 785.10 735.10

Meas. Freq. (Hz): 934.65 985.65 1034.85 834.64 786.24 734.64

Meas. Ampl. (dB): -95.91 -101.23 100.65 -89.98 -104.59 -98.57

Eccentricity Freq (2) [f1 (+/-) fr] of voltage(ab) at [400Hz]:

Calculated Freq. (Hz): 25.41 74.65

Meas. Freq. (Hz): 25.75 74.70

Meas. Ampl. (dB): -97.34 -92.93

Eccentricity Freq (2) [f1 (+/-) fr] of voltage(bc) at [400Hz]:

Calculated Freq. (Hz): 25.42 74.59

Meas. Freq. (Hz): 25.18 74.66

Meas. Ampl. (dB): -94.67 -94.05

DATA FROM FLUX SENSOR:

Slip Frequency [f2] of Flux at [400Hz] :

Meas. Freq. from FFT (Hz): 0.81

Meas. Ampl. from FFT (dB): -44.13

Broken Rotor Bar Freq [(1 (+/-) 2s)f_1] of Flux at [400Hz] :

Calculated Freq. (Hz): 48.38 51.62

Meas. Freq. (Hz): 48.38 51.62

Meas. Ampl. (dB): -51.47 -55.65

Shorted Turn Freq [f_1((n/p)(1-s) (+/-) k)] of Flux at [8000Hz]:

Calculated Freq. (Hz): 74.60 174.60 99.19 -25.41 -125.41 -0.81

Meas. Freq. (Hz): 74.59 174.61 99.20 25.41 125.41 0.81

Meas. Ampl. (dB): -26.70 -49.29 -47.53 -21.62 -48.75 -44.13

Eccentricity Freq (1) of Flux at [400Hz]:

Calculated Freq. (Hz): 935.47 985.47 1035.47 835.46 785.46 735.46

Meas. Freq (Hz): 935.25 984.45 1036.65 836.64 786.24 734.64

Meas. Ampl. (dB): -52.53 -52.76 -68.56 -53.48 -66.24 -61.48

Eccentricity Freq(2) of Flux at [400Hz]:

Calculated Freq (Hz): 25.41 74.60

Meas.Freq. (Hz): 25.41 74.59

Meas. Ampl. (dB): -21.62 -26.70

DATA FROM VIBRATION SENSORS:

Stator Fault Freq [$2f_1$] of vibration at [400Hz] :

Calculated Freq (Hz): 100.01

Measured DE Vibration. Freq (Hz): 100.01

Measured DE Vibration. Ampl (dB): 7.22

Measured NDE Vibration. Freq (Hz): 100.01

Measured NDE Vibration. Ampl (dB): -5.87

Instantaneous Power Analysis at [8000Hz] :

Broken Rotor Bar Freq [(1 (+/-) 2s)fp] of Inst.Power at [8000Hz] :

Calculated Freq. (Hz): 96.76 103.25

Meas. Freq: 98.63 101.04

Meas. Ampl: -61.09 -58.86

Eccentricity Freq (1) [fpower ((R/p)(1-s) (+/-) k)] of Inst. Power at [8000Hz]:

Calc Freq. (Hz): 1871.50 1971.53 2071.57 1671.42 1571.39 1471.35

Meas. Freq (Hz): 1871.09 1970.50 2070.90 1670.28 1570.68 1471.67

Meas. Ampl (dB): -89.92 -89.84 -91.89 -86.43 -86.99 -86.38

Eccentricity Freq (2) [fpower (+/-) fr] of Inst. Power at [8000Hz]:

Calculated Freq. (Hz): 75.44 124.63

Meas. Freq. (Hz): 75.43 124.64

Meas. Ampl. (dB): -57.15 -61.31

Shorted Turn Freq [fpower ((n/p)(1-s) (+/-) k)] of inst. Power at [8000Hz]:

Calculated Freq. (Hz): 149.24 349.31 198.45 -50.83 -250.90 -1.62

Meas. Freq. (Hz): 150.05 350.12 199.47 50.02 250.09 1.60

Meas. Ampl (dB): -63.60 -77.22 -66.11 -57.07 -63.64 -60.31

List of Publications

1. Ahmed, I., Supangat, R., Grieger, J., Ertugrul, N., and Soong, W. L. "A Baseline Study for On-Line Condition Monitoring of Induction Machines". Australian Universities Power Engineering Conference, Brisbane, Australia, 26-29th September 2004.
2. Ahmed, I., Ertugrul, N., and Soong, W. L. "A Study on the Detection of Fault Frequencies for Condition Monitoring of Induction Machines." Australian Universities Power Engineering Conference, Tasmania, Australia, 26-29th September 2005.
3. Ahmed, I., Ertugrul, N., and Soong, W. L. "A Study of Detection of Broken Rotor Bars in Induction Motors Using Instantaneous power", Energy and Power System International Conference 'EPS 2006' IASTED, Chiang Mai, Thailand, 28-30th March 2006.